NASA/TM–2017-219639

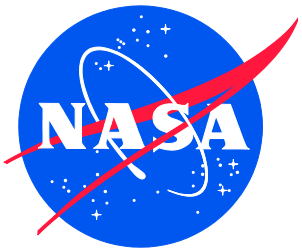

Assessment of a Conceptual Flap System Intended for Enhanced General Aviation Safety

Bryan A. Campbell and Melissa B. Carter
NASA, Langley Research Center, Hampton, Virginia

July 2017

NASA STI Program . . . in Profile

Since its founding, NASA has been dedicated to the advancement of aeronautics and space science. The NASA scientific and technical information (STI) program plays a key part in helping NASA maintain this important role.

The NASA STI program operates under the auspices of the Agency Chief Information Officer. It collects, organizes, provides for archiving, and disseminates NASA's STI. The NASA STI program provides access to the NTRS Registered and its public interface, the NASA Technical Reports Server, thus providing one of the largest collections of aeronautical and space science STI in the world. Results are published in both non-NASA channels and by NASA in the NASA STI Report Series, which includes the following report types:

- TECHNICAL PUBLICATION. Reports of completed research or a major significant phase of research that present the results of NASA Programs and include extensive data or theoretical analysis. Includes compilations of significant scientific and technical data and information deemed to be of continuing reference value. NASA counter-part of peer-reviewed formal professional papers but has less stringent limitations on manuscript length and extent of graphic presentations.

- TECHNICAL MEMORANDUM. Scientific and technical findings that are preliminary or of specialized interest, e.g., quick release reports, working papers, and bibliographies that contain minimal annotation. Does not contain extensive analysis.

- CONTRACTOR REPORT. Scientific and technical findings by NASA-sponsored contractors and grantees.

- CONFERENCE PUBLICATION. Collected papers from scientific and technical conferences, symposia, seminars, or other meetings sponsored or co-sponsored by NASA.

- SPECIAL PUBLICATION. Scientific, technical, or historical information from NASA programs, projects, and missions, often concerned with subjects having substantial public interest.

- TECHNICAL TRANSLATION. English-language translations of foreign scientific and technical material pertinent to NASA's mission.

Specialized services also include organizing and publishing research results, distributing specialized research announcements and feeds, providing information desk and personal search support, and enabling data exchange services.

For more information about the NASA STI program, see the following:

- Access the NASA STI program home page at http://www.sti.nasa.gov

- E-mail your question to help@sti.nasa.gov

- Phone the NASA STI Information Desk at 757-864-9658

- Write to:
  NASA STI Information Desk
  Mail Stop 148
  NASA Langley Research Center
  Hampton, VA 23681-2199

NASA/TM-2017-219639

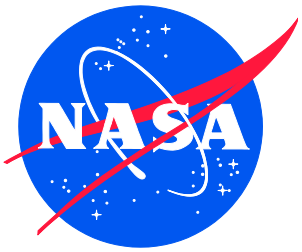

Assessment of a Conceptual Flap System Intended for Enhanced General Aviation Safety

Bryan A. Campbell and Melissa B. Carter
NASA, Langley Research Center, Hampton, Virginia

National Aeronautics and
Space Administration

Langley Research Center
Hampton, Virginia 23681-2199

July 2017

Available from:

NASA STI Program / Mail Stop 148
NASA Langley Research Center
Hampton, VA 23681-2199
Fax: 757-864-6500

Contents

List of Figures

Nomenclature

Symbols

b	wing span, ft
C_D	drag coefficient, Drag/$q_\infty S$
C_L	lift coefficient, Lift/$q_\infty S$
C_l	rolling-moment coefficient, rolling moment/$q_\infty Sb$
C_m	pitching-moment coefficient, pitching moment/$q_\infty S\bar{c}$
C_n	yawing-moment coefficient, yawing moment/$q_\infty Sb$
C_Y	side-force coefficient, side force/$q_\infty S$
$\bar{c}$	mean aerodynamic chord, ft
D	Drag, lb
L	Lift, lb
L/D	lift-drag ratio
q_∞	free-stream dynamic pressure, psf
S	wing reference area, ft^2
Xmc	x location of the moment center
Ymc	y location of the moment center
Zmc	z location of the moment center
α	angle of attack, deg
$\%\Delta C_L$	percent change in lift coefficient
$\%\Delta C_D$	percent change in drag coefficient

Abbreviations

AGL	above ground level
Aux-In	auxiliary flap, inboard
Aux-Out	auxiliary flap, outboard

CFD	computational fluid dynamics
CG	center of gravity
deg	degrees
ft	feet
G	Gurney flap
g	gravitational constant
GA	general aviation
LSS	lower surface spoiler
P	pointed (sharp) leading edge
psf	pounds per square foot
TE	trailing edge
VIA	variable incidence auxiliary

Abstract

A novel multielement trailing-edge flap system for light general aviation airplanes was conceived for enhanced safety during normal and emergency landings. The system is designed to significantly reduce stall speed, and thus approach speed, with the goal of reducing maneuvering-flight accidents and enhancing pilot survivability in the event of an accident. The research objectives were to assess the aerodynamic performance characteristics of the system and to evaluate the extent to which it provided both increased lift and increased drag required for the low-speed landing goal. The flap system was applied to a model of a light general aviation, high-wing trainer and tested in the Langley 12-Foot Low-Speed Wind Tunnel. Data were obtained for several device deflection angles, and component combinations at a dynamic pressure of 4 pounds per square foot. The force and moment data supports the achievement of the desired increase in lift with substantially increased drag, all at relatively shallow angles of attack. The levels of lift and drag can be varied through device deflection angles and inboard/outboard differential deflections. As such, it appears that this flap system may provide an enabling technology to allow steep, controllable glide slopes for safe rapid descent to landing with reduced stall speed. However, a simple flat-plate lower surface spoiler (LSS) provided either similar or superior lift with little impact on pitch or drag as compared to the proposed system. Higher-fidelity studies are suggested prior to use of the proposed system.

1. Introduction

On a per hour basis, general aviation (GA) conducts many more takeoffs and landings than either commercial air carriers or the military. During these takeoff and landing phases, the pilots experience the highest workloads, are subject to the most distractions, and are engaged in maneuvering flight at low altitudes, slow airspeeds, and high angles of attack. Any one of these conditions alone could make a pilot more vulnerable to a stall/spin accident than in other phases of flight. Combining these conditions, especially in instrument meteorological conditions, could result in higher accident rates.

The Joseph T. Nall Report,[1] an annual statistical report based on the National Transportation Safety Board reports of accidents involving fixed-wing GA aircraft weighing less than 12,500 pounds, highlights three pilot-related accident categories accounting for a disproportionate number of fatal accidents: weather, maneuvering flight, and descent/approach. Thus far, GA pilots are still at the mercy of weather. Therefore, detailed weather briefings, with special consideration to airmen's meteorological information and en route updates, via the en route flight advisory service, or Flight Watch, help most GA pilots avoid significant weather hazards.

The Nall report points to maneuvering flight as the category with the largest number of pilot-related fatal accidents, accounting for one out of four such crashes. Maneuvering flight was also the number one fatal accident category for single-engine fixed-gear aircraft, responsible for 30.1

percent of all such mishaps. For single-engine retractable-gear aircraft, maneuvering flight tied with descent/approach accidents for most fatal crashes, accounting for 24.2 percent of all accidents that ended in death.

One reason for the loss of control, and the potential loss of life, during maneuvering flight, has to do with exceeding the critical angle of attack, or stall angle. Jeppesen's Private Pilot Manual[2] summarizes several factors that influence stall. Most pilots and those familiar with aeronautics are familiar with the fact that "if an airplane's speed is too slow, the required angle of attack to maintain lift may exceed the critical angle, causing stall." Additionally,

> as aircraft weight increases, a higher angle of attack is required to maintain the same airspeed since some of the lift must be used to support the increased weight. This causes an increase in the aircraft's stall speed. The distribution of weight also affects the stall speed of an aircraft. For example, a forward center of gravity (CG) creates a situation which requires the tail to produce more downforce to balance the aircraft. This, in turn, causes the wings to produce more lift than if the CG was located more rearward. So, you can see that a more forward CG also increases stall speed … Snow, ice or frost accumulation on the wing's surface not only changes the shape of the wing, disrupting the airflow, but also increases weight and drag, all of which will increase stall speed … Turbulence encounters can significantly and suddenly cause an aircraft to stall at a higher airspeed than the same aircraft in stable conditions. This occurs when a vertical gust changes the direction of the relative wind and abruptly increases the angle of attack. (pp. 3-36, 3-37)

Also, there are accelerated stalls that occur when high maneuver loads are imposed, such as during steep turns and abrupt pull-ups. Such maneuvers frequently occur in the traffic pattern when a pilot overshoots the turn to final approach and rapidly attempts to correct by inducing an abrupt maneuver such as a steep turn. During such conditions the airplane will stall at higher airspeeds. This type of stall tends to be more rapid and severe, and often results in an uncontrolled power-on spin.

Unfortunately, since the majority of GA stall/spins occur at low altitudes, such as in the airport traffic pattern, the chances of recovery are slim. A special report entitled "Stall/Spin; Entry Point for Crash and Burn?"[3] reported that more than 80 percent of the stall/spin accidents that occurred during the period of 1991–2000 began at an altitude of less than 1000 feet above ground level (AGL), the usual GA traffic pattern altitude. For light GA aircraft, the typical altitude loss during recovery from a stall is approximately 100 to 350 feet, assuming proper recovery technique. However, the typical altitude loss during recovery from a spin is approximately 1200 feet. Keeping in mind that the typical traffic pattern altitude is 1000 feet AGL, and the turn from the base leg to final approach is initiated at approximately 500 feet AGL, it becomes clear that a stall/spin during this phase of maneuvering flight is almost certain to result in an accident.

While the addition of parachute recovery systems in some aircraft has provided a means of accident survivability, their deployment time may render them ineffective at traffic pattern altitude. Therefore, enhanced stall/spin prevention, lower stall speeds, slower landing approach speeds and greater pilot situational awareness are essential to minimize the number of GA fatalities.

However, in recent years, the GA trend has been toward higher cruise performance, not lower stall speeds and slower approach landing speeds. Engineers are now designing airplanes with lightweight composites, high-output engines, and low-drag shapes to enable cruise speeds approaching 200+ knots for single engine piston aircraft and 350+ knots for single-engine turboprops. It is anticipated that the arrival and maturation of high-speed very light jets will further increase the GA cruise speeds. This increased cruise performance, coupled with sophisticated flat panel cockpit displays, has resulted in resurgent sales for the GA sector. This raises the question, however, has safety kept pace with performance? Often the very airfoils and wing designs selected to enhance high-speed cruise result in deficiencies for low-speed high lift. This places a high demand on high-lift systems, usually flaps, to minimize these deficiencies.

A novel approach, called the variable incidence auxiliary (VIA) wing, was designed to enhance GA safety. Dr. Roger Nahas originated the flap system.[4,5] One of the objectives of this VIA wing system is to increase lift with an increase in drag for the purpose of providing controlled emergency descents, steep low-speed approaches, reduced stall speed and enhanced short-field landing operations. As such, large peak values of *L/D* are not the goal. Rather than a peak at some discrete angle of attack, the goal of *L/D* for this study is a moderate, sustained plateau over low-to-moderate angles of attack.

The capability of the pilot to select a drag commensurate with the desired dive angle during an emergency descent, or steep glide slope for landing approach opens many operational benefits. These, in part, include the following:

1. The ability to maintain higher-than-normal engine rpms during the short-final portion of the landing approach to facilitate an aborted landing and subsequent go-around
2. A controlled steep glide slope to provide better obstacle clearance during landings at short-field runways, and noise abatement
3. Reduced landing speeds for enhanced accident survivability
4. Significantly reduced landing ground roll via large drag at touchdown for enhanced safety

Dr. Nahas's concept came to the attention of the NASA Langley Aviation Safety Program Office by way of the Aircraft Owners and Pilots Association Air Safety Foundation. It was recommended as a potential means to enhance both low-speed safety and accident survivability through reduced stall speeds and landing approach speeds. This report will discuss the evaluation of this system as applied to a generic light GA high-wing trainer aircraft.

2. Description of Model

Figure 1(a) shows a side-view of the VIA flap system in both the retracted and deflected configurations. The system consists of a lower-surface, full-span auxiliary flap and an inboard conventional trailing-edge split flap. The auxiliary flap chord measures 25 percent of the local main-wing chord, and the split flap chord measures 15 percent of the inboard wing chord. In the stowed configuration, the original cruise airfoil shape is retained, with minimal impact on the cruise wing aerodynamics.

As a preliminary proof-of-concept, the inventor adapted this flap system to a 1/5-scale radio controlled model of a light GA high-wing trainer aircraft and made several flights. While the

results seemed promising, a more controlled environment was needed for verification. Hence, for this investigation, the as-flown model was acquired and mounted in the Langley 12-Foot Low-Speed Wind Tunnel (see fig. 1(b)). The geometric characteristics are shown below:

Wing Span	7.16 ft
Wing Area	6.96 ft^2
$\bar{c}$	0.98 ft
Length	5.43 ft
Xmc	1.54 ft.
Ymc	0.0 ft.
Zmc	–0.15 ft

The full-span auxiliary flap and the inboard trailing-edge split flap, are colored red and white, respectively, in the photograph in figure 1(b). The auxiliary flap was split at approximately the mid-span to allow for independent inboard and outboard deflections of 45° and 90°. The trailing-edge split flap was confined to the inboard half of the wing only, and was tested at deflections up to 60°. Aileron surfaces were locked at 0° for the majority of the test. However, for selected runs, both ailerons were deflected 10°, trailing edge down, to evaluate the impact on the system performance. Elevator and rudder surfaces were locked at 0° for the entire test. Additionally, the engine and propeller were removed, and the holes in the engine cowling were sealed to provide a smooth aerodynamic surface. As such, no power-on propeller wash effects were evaluated.

3. Test Conditions and Instrumentation

Tests were conducted in the Langley 12-Foot Low-Speed Wind Tunnel.[6] The entire test was conducted at a dynamic pressure of 4.0 psf. The model was tested over an angle-of-attack range of –4° to 32° to encompass the linear, stall, and post-stall regions of the flight envelope. All data were acquired at zero sideslip and zero roll. It is believed all of the data was obtained with free transition.

A six-component strain-gauge balance mounted inside the fuselage measured the forces and moments. Appendix A presents the accuracy of this strain-gauge balance and plots of data repeatability. The pitch and height assembly of the model support system set the angle of attack. The angle of attack was measured with an accelerometer installed in the model. The model was leveled in roll via a line level mounted on the balance block.

4. Computational Method and Description

The goals of the computational study were to provide insight into the system flow physics, and to compare the performance of the modified wing to that of the wing with the conventional flap system. Since the exact definition of the wind tunnel model was not available, the computational fluid dynamics (CFD) used a different light GA high-wing aircraft definition. While slight geometric differences exist, insight into the system and comparison of the modifications to the baseline aerodynamic characteristics were obtained.

Seven different flap settings were computed on the computational model. These configurations included baseline (no flaps deflected), conventional Fowler flaps at 10° and 40°, the proposed auxiliary wing at 45° and 90° (with split flap at 60°), the proposed auxiliary wing at 45° (with split flap at 30°), and the proposed auxiliary wing at 45° (with split flap at 0°). The conventional Fowler flap deflections were modeled from measurements of a light GA high-wing airplane. Flap supports and the aircraft's engine were not modeled.

The computational study was conducted using the USM3D CFD code. USM3D is a Navier-Stokes solver for unstructured, tetrahedral meshes. The code uses a Roe upwind, implicit, cell-centered, finite-volume discretization applied to the integral form of the Navier-Stokes equations.[7] This approach provides a consistent approximation to the conservation laws of fluid dynamics. For this study, the code was run with the Spalart-Allmaras turbulence model coupled with a wall function formulation to reduce the grid resolution needed for the sublayer portion of a turbulent boundary layer.[8,9] In order to achieve this, the inner region of the boundary layer is modeled by an analytical function that is matched with the numerical solution in the outer region.

Appendix B contains a detailed CFD discussion including information about the computational grids, analysis conditions, and results.

5. Results and Discussion

Since this flap system consists of several parts working together, an attempt was made to understand the contributions of each individual element. Therefore, the following discussion has been subdivided into sections that look at the effects of these elements in detail.

It should be noted that due to the combined effects of the turbulent flow of this wind tunnel and the poor fit and finish of the model, caution should be exercised in trying to infer detailed performance quantities from this data. Rather, it is advised to use this data to establish performance trends. To assist in this regard, plots of the percent change in lift ($\%\Delta C_L$) and the percent change in drag ($\%\Delta C_D$) are shown for each configuration. These percent change plots show the changes relative to the performance of the cruise (0° flap deflection) configuration.

Appendix C presents photographs of the tuft flow visualization study. These images may also be referred to for greater insight into the relative deflections of the various system elements.

5.1. Trailing-Edge Split Flap

The aerodynamic effects of deflecting the inboard trailing-edge split flap from 0° to 60° are depicted in figure 2. Also shown on these plots are the effects of deflecting both ailerons down 10° to act as flaperons, with the split flap at 60°.

As the split-flap deflection angle is increased from 0° to 60°, the plot of lift coefficient versus angle of attack (figure 2(a)) shows a fairly linear increase in lift for low-to-moderate angles of attack. This is accompanied by an increase in pitching moment stability (more negative slope), and an approximate 5° shift in trim angle. There is also an increase in drag over the same region. This behavior is indicative of increasing trailing-edge flap deflections. However, note that as the $C_{L,max}$ increases from about 1.25 to 1.45, the corresponding stall angle decreases from approximately 14° to 12°. Typically, leading-edge treatment, such as a slat, or deflected leading-edge flap, are used to extend the $C_{L,max}$ to higher angles of attack. However, no such device was used during this investigation. The stall region, though, is well defined, with a gradual reduction in the lift-curve slope prior to the $C_{L,max}$. As such, the pilot will have adequate warning of an impending wing stall.

The addition of both ailerons deflected down 10° as flaperons, with the split flap at 60°, provides further lift over the entire prestall α-range, but with similar drag as the 60° split flap alone (figure 2(a)).

Figure 2(b) shows the effects on the lateral aerodynamics. As shown, symmetrically deflecting the trailing-edge split flap has very little effect on yawing moment or side force in the prestall region. It is expected that nonzero values of roll angle and/or yaw angle, will yield different results. While these minimal effects are typical for all of the elements of the VIA wing system discussed herein, such plots will continue to be presented for data completeness.

The combined effects of increased lift and increased drag are shown in the plots of the lift-to-drag ratios presented in figure 2(c). The upper format allows for a quick configuration assessment at a constant C_L, which is typically used for overall flap design considerations. The lower format provides an assessment at a fixed angle of attack, which is typically used for a more detailed study of the configuration performance, stability, and control. This dual presentation of lift-to-drag ratio will be used throughout this report. In both cases, however, it can be seen that maximum *L/D* benefits will result from a scheduling of the flap deflection as a function of either α or C_L. However, keep in mind that one of the objectives of this VIA wing system is to increase lift with an increase in drag for the purpose of providing controlled emergency descents, steep low-speed approaches, reduced stall speed, and enhanced short-field landing operations. As such, large peak values of *L/D* are not the goal. Rather than a peak at some discrete angle of attack, the goal of *L/D* for this study is a moderate, sustained plateau over low-to-moderate angles of attack. This will be discussed in more detail when the effects of the auxiliary-flap element are analyzed.

Figure 2(d) shows the percent changes in lift and drag relative to the cruise-wing baseline[1]. Clearly, increasing the deflection of the inboard trailing-edge split flap, with or without the added enhancement of the aileron deflection, provides both lift and drag increases at shallow to moderate angles of attack. As more elements of the system are deployed, it is anticipated that large increases in lift will be accompanied by very large increases in drag over low-to-moderate angles of attack.

5.2. Auxiliary Flap Independent 45° Deflections

Figure 3 shows the effects of deploying the inboard and outboard auxiliary-flap elements to 45°, both individually and in unison, with all other elements at zero degrees. The benefits of deflecting both together are depicted in figure 3(a). When compared to the best split flap (60°) in figure 2(a), the auxiliary flap yields both higher sustained lift over low-to-moderate angles of attack, and a similar $C_{L,max}$. The higher sustained lift comes at the price of a slightly lower stall angle (~11° compared to ~12° for the split flap).

Also, note the prestall behavior of the inboard auxiliary flap compared to that of the outboard. The effects on lift and drag are fairly linear. The inboard auxiliary flap produces the same pitching moment as the combined inboard and outboard, while the outboard alone follows the same level as the cruise wing. On closer examination, the pitching moment curves are grouped according to whether the inboard auxiliary flap is deployed or not. As a result, it is highly recommended that a careful three-dimensional study of tail placement and wake flow-field interactions be done to establish tail effectiveness when the VIA wing system is deployed. Such a study was beyond the scope of this investigation.

The *L/D* curve for the combined inboard and outboard deflections in figure 3(c) show the trend toward the expected sustained plateau mentioned earlier. While this configuration produces higher lift, it also generates much higher drag than the split flap alone (compare 2(d) and 3(d)).

5.3. Auxiliary Flap 45° Deflections with Split Flap

The effects of the split-flap deflections when both inboard and outboard auxiliary flaps are deployed at 45° are shown in figure 4. Clearly the combination of 60° split flap and 45° auxiliary flap produces the highest lift and drag. Also, it appears that the addition of the split-flap deflections produce no change in the stall angle, relative to the 0° split flap, 45° auxiliary-flap case. However, note the grouping of the split flap 0° and 60° deflections compared to the split-flap 15°, 30°, and 45° deflections. The latter group is producing significantly less prestall lift and drag. Figure 4(d) further emphasizes these group effects on the changes in lift and drag, relative

[1] Note that for these plots, the circle symbol does not represent the cruise wing condition. Refer to the symbol key for clarification.

to the cruise wing. As shown in Appendix B, figures B-12–17, these group differences in lift and drag are a product of changes in the system flow physics. Those figures show CFD predicted changes in the nature of the separated flow associated with the split flap at 0° and 30°, and the weak vortical flow on the auxiliary wing with the split flap at 60°. Due to their flow variations, it is recommended that additional tests be conducted on a higher fidelity model, with both pressure data and detailed flow visualization. Figure 5 presents the effects of holding the split-flap deflection at 60°, while deploying the inboard and outboard auxiliary-flap elements to 45°, both individually and in unison. When comparing these effects to those of figure 3, some significant points are highlighted. The presence of the 60° split flap eliminates the linear and additive nature of the auxiliary flap deflections seen earlier with the 0° split flap. Now, the outboard 45° auxiliary flap produces almost similar prestall lift as the combined inboard/outboard auxiliary-flap deflections, but with a slightly higher $C_{L,max}$ and a higher stall angle. Since the outboard 45° auxiliary flap provides most of the performance gains, an airplane with just that element may benefit by less weight and system complexity. Also, note that higher lift is produced at 0° angle of attack, and that it is sustained all the way up to the stall angle of about 10.5°. As a result, two significant benefits can now be realized. The first is an increase in usable lift. At an angle of attack of about 7°, the 60° split flap alone configuration produces a C_L of ~1.2, while the 45° auxiliary flap with the 60° split-flap configuration produces a C_L of ~1.4. Another way of looking at this is if the 60° split flap alone configuration was called on to produce a C_L of ~1.4, it would be dangerously close to stalling, while the 45° auxiliary flap with the 60° split-flap configuration would not. The second benefit has to do with the deck angle for high-lift operations. When compared to the 60° split flap alone configuration, for a given lift coefficient, the 45° auxiliary flap with the 60° split-flap configuration flies at a greatly reduced angle of attack. These two benefits translate into several high-lift operational enhancements, including the following, the desire for which was mentioned in the introduction of this report:

- The ability to carry an increased payload due to the available increase in usable lift.
- Enhanced prevention of accelerated stalls during maneuvers in the airport traffic pattern via greater lift per angle of attack.
- Enhanced power-off stall prevention during landing approach maneuvers with turbulent and/or gusting winds due to the ability to achieve the necessary lift at lower angles of attack.
- Enhanced forward visibility during final approach for landing due to the low deck angles while generating high lift.

Also, the high lift, when combined with the sustained high drag of the combined inboard/outboard 45° auxiliary flap deflections, seen in figures 5(a) and 5(d), should allow for steep final approach glide slopes in excess of the typical 3°, while maintaining low speeds. These performance benefits of the VIA wing will need to be reassessed in the presence of varying propeller wash effects. If the system still yields comparable performance, the elevator and rudder control authority will need to be investigated for the potential very-low-speed landing operations, with and without the propeller wash effects.

5.4. Auxiliary Flap 45° Deflections with Split Flap and Aileron

A comparison of the plots of C_L vs. α, $\%\Delta C_L$, and $\%\Delta C_D$ in figures 5 and 6 indicate that the addition of the 10° aileron/flaperon to the 45° auxiliary flap with the 60° split-flap configuration serves to increase lift for shallow angles of attack, with little impact on drag. However, it also reduces the lift-curve slope and the magnitude of $C_{L,max}$. Hence, the benefits of the aileron with this system are limited to the shallow angle-of-attack range.

5.5. Emergency Descent Configuration / Auxiliary Flap Independent 90° Deflections

Another intended goal of the flap system is to provide the capability of safe, controlled descents during perceived emergencies requiring immediate landing, such as onboard fires, electrical, structural, or mechanical failures, or human factors. Ideally, such descents would allow maneuvering flight while obtaining the maximum loss of altitude with the least traversed horizontal distance. While a steep dive would accomplish this, maneuvering at the ensuing high indicated airspeeds may lead to structural loads that exceed the design limits.

Additionally, this flap system should be capable of providing safe descents during the unintentional dive. This type of dive may stem from pilot spatial disorientation, and can be accompanied by unrecognized rapidly increasing dive speeds. If the pilot recognizes the dive, he or she is trained to reduce the throttle, level the wings, and pull back on the yoke to arrest the dive. Depending on the indicated airspeed, this maneuver can easily exceed structural limits.

Thus, the need exists to rapidly descend, but without exceeding the FAA regulated limiting speeds (FAA FR Part 23, Airworthiness standards: Normal, Utility, Acrobatic, and Commuter Category Airplanes). To ensure rapid deceleration from an unintentional dive, or controlled emergency descents during a perceived emergency, without exceeding structural limits, the auxiliary flap in this study can be deployed to 90°. It is anticipated that the large drag increase will arrest the rapidly rising speeds, much like a dive brake, and simultaneously generate the high lift required for a very steep, low-speed, final approach for landing.

The effects of the 90° deflection without the addition of the split flap are shown in figure 7. When compared with the 45° auxiliary flap shown in figure 3, it can be seen that the trends are the same, but the magnitudes are larger. For example, the inboard/outboard variations show the same linear and additive effects in lift and drag, but the 90° deflection yields higher lift over the prestall angle-of-attack range. Note however, that the 90° $C_{L,Max}$ remains unchanged relative to the 45° case, but the stall angle has decreased to about 8°. This once again highlights the need for leading-edge treatment, which typically extends the $C_{L,Max}$ to higher magnitudes and higher angles of attack. In addition, when the 90° inboard auxiliary flap is deployed, the same nose-up pitching moment trend results, but to a greater extent. This would indicate a greater wing downwash field, and hence, greater tail influence. Thus, once again, it is highly recommended that tail effectiveness, buffet, and position studies be conducted when considering the use of this system.

The most notable differences, however, can be seen when comparing figures 3(d) and 7(d). Clearly, the 90° auxiliary flap produces not only a significant increase in lift, but also a tremendous increase in drag. The combined effect is the desired high lift with high drag for use in emergency descents, intentional or unintentional.

5.6. Emergency Descent Configuration / Auxiliary-flap 90° Deflections with Split Flap

Figure 8 shows that the addition of the deployed split flap has no appreciable effects on lift once the 90° auxiliary flap has been deployed. However, as seen in figure 8(d), there is a trend of increasing drag with increasing split-flap deflection.

Figure 9 presents the effects of holding the split-flap deflection at 60°, while deploying the inboard and outboard auxiliary-flap elements to 90°, both individually and in unison. The trends are similar to those of the 45° auxiliary flap highlighted in figure 5, especially the fact that the outboard auxiliary-flap deployment yields most of the performance gains attributed to both deployed.

However, a few significant differences do exist. First, note that the lift-curve slope is slightly reduced relative to the cruise wing and the 60° split-flap-only configurations, in the prestall region. As a result, the 90° deflections are more effective at producing lift at the shallow angles of attack. Also note that the individual outboard 90° auxiliary flap not only generates a higher $C_{L,Max}$, but it also generates a higher stall angle. Once again, this points to the possibility of designing a simpler device, which acts on the outboard wing segments only, while retaining the existing inboard flap system.

5.7. Emergency Descent Configuration / Auxiliary-flap 90° Deflections with Split Flap and Aileron

A comparison of the plots of C_L vs. α, $\%\Delta C_L$, and $\%\Delta C_D$ in figures 9 and 10 indicate that the addition of the 10° aileron to the 90° auxiliary flap with the 60° split-flap configuration serves to increase the magnitude of lift coefficient with no significant impact on drag. However, unlike the 45° auxiliary flap case (fig, 6), there is no significant change in the lift-curve slope. Hence, the benefits of adding the aileron with the 90° auxiliary flap are observed up to stall.

5.8. Preliminary Deflection Optimization

With a fixed aileron setting of 0° and a fixed split-flap setting of 60° the auxiliary-flap deflections of 45° and 90° were mixed on the inboard and outboard wing segments in an attempt to identify the beginning of any significant optimization trends. Figure 11 depicts two significant results. First, it can be seen in figure 11(a), and especially in figure 11(d), that lift is relatively insensitive to variations of the chosen auxiliary-flap deflections. Second, figures 11(c) and 11(d) show that for a given lift coefficient, various levels of drag can be achieved. This provides the capability of high lift with controlled drag on demand, although each lift coefficient will require a retrim of the aircraft.

As mentioned in the introduction, the capability of the pilot to select a drag commensurate with the desired dive angle during an emergency descent, or steep glide slope for landing approach opens many operational benefits. These, in part, include the following:

1. the ability to maintain higher-than-normal engine rpms during the short-final portion of the landing approach to facilitate an aborted landing and subsequent go-around.
2. a controlled steep glide slope to provide better obstacle clearance during landings at short-field runways, and noise abatement.

3. reduced landing speeds for enhanced accident survivability.
4. significantly reduced landing ground roll via large drag at touchdown for enhanced safety.

5.9. Auxiliary-flap Leading-edge Modification

It was postulated that the strength of the weak vortical flow that exists on the 45° auxiliary flap may be enhanced for increased lift benefits. One method tried during this investigation was to reduce the leading-edge radius of the auxiliary flap to a sharp leading edge and force separation. This was accomplished via a small thin strip of sheet metal attached to the lower surface leading edge of the auxiliary flap (picture 1). The leading edge of the sheet metal extended well beyond the leading edge of the auxiliary flap. The results of this modification are seen in figure 12. With the exception of a slight variation in rolling moment, sharpening the leading-edge of the auxiliary flap had no effect on overall performance.

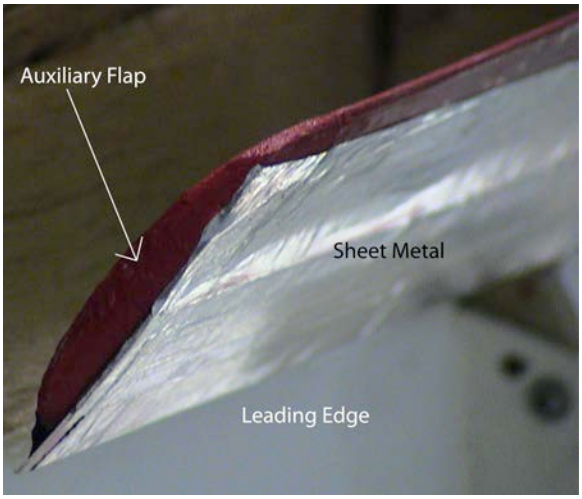

Picture 1. Auxiliary-flap leading-edge modification

5.10. Auxiliary-flap Trailing-edge Modification

Seeing that the leading-edge modification produced no change, an attempt was made to reduce the magnitude of separation on the auxiliary flap. To accomplish this, a simple device used frequently in auto racing, called a Gurney flap was used. Invented by Dan Gurney, the Gurney flap (or wickerbill) is a right-angle piece of metal rigidly bolted to a wing, lower surface, trailing edge. Its presence causes a lower pressure region, or vacuum, just behind the wing trailing-edge. As a result, the higher-pressure separated flow tries to fill that void, thereby reducing the size of the separated flow field and enabling the wing to work harder at higher angles of attack. As expected, such a device should also produce additional drag. The results of adding a 5-percent Gurney flap to the auxiliary flap are shown in figure 13.

A comparison of figure 13 with figure 5 shows that the addition of the Gurney flap to the deployed 45° outboard-only auxiliary flap now matches the lift performance of the 45°

inboard/outboard combination over the linear angle-of-attack range, and produces a slightly higher $C_{L,Max}$.

A comparison of figure 13 with figure 11 also shows that the addition of the Gurney flap to both the 45° inboard / 45°outboard combination, and the 45° inboard / 90° outboard combination has now allowed the 45° inboard / 45° outboard combination to match the lift performance of the 45° inboard / 90° outboard combination, and produce a slightly higher $C_{L,Max}$. Also, as expected, there is a significant, and beneficial increase in drag. This highlights that the VIA wing still has much room for improvement.

5.11. Auxiliary-flap Simplification

This section discusses an attempt to simplify the auxiliary-flap system by use of a lower surface spoiler (LSS). A graphical comparison of the LSS to the original auxiliary flap is shown in sketches A, B and C. It should be noted that the LSS (Sketches B and C) used the same chord length, section span, and deflection angles as the original auxiliary flap (Sketch A). The chordwise attachment point was aft of the stowed auxiliary flap leading edge by a distance measuring 20 percent of the auxiliary flap chord (approximately 0.5 inches). The main differences are the elimination of the gap between the auxiliary flap and the main wing, and the use of a flat plate (similar to a conventional upper-surface spoiler) instead of a contoured airfoil shape. The LSS was tested at 45° and 90° deflections, with the split flap at 0° and 60° for comparison with the original VIA wing configurations.

The aerodynamic results of these modifications are shown in figures 14–19.

Figure 14 compares the configuration of both inboard and outboard 45° auxiliary flaps with 0° split flap to the configuration of both inboard and outboard 45° LSS with 0° split flap. As shown, the LSS produces higher lift over the entire angle-of-attack range. It also produces a significantly higher $C_{L,Max}$ and a slight increase in stall angle. Prestall pitching moments are similar and drag levels remain high.

The effects of adding the deployed 60° split flap to configurations mentioned above, are shown in figure 15 (a). This addition brings the lift of the original auxiliary wing up to a similar level as the LSS (see figure 14). It also allows the original auxiliary flap to generate slightly more drag. Pitching moments are similar.

Figure 16 shows the comparison for the deployed 45° outboard-only auxiliary flap and the LSS. Once again, the LSS generates higher lift over the entire angle-of-attack range. Stall angle and prestall pitching moment remain the same.

Adding the 60° split flap to the deployed 45° outboard-only configurations yield the data shown in figure 17. As shown, the LSS continues to generate higher lift than the auxiliary flap over the full angle-of-attack range with no significant changes in pitching moment or drag.

Figure 18 compares the configuration of both inboard and outboard 90° auxiliary flaps with 0° split flap to the configuration of both inboard and outboard 90° LSS with 0° split flap. Here, too, the LSS generates higher lift and a larger $C_{L,Max}$, with no significant changes to pitching moment or drag.

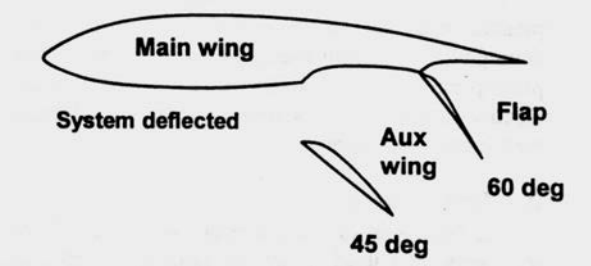

Sketch A. Original 45° Auxiliary-flap configuration.

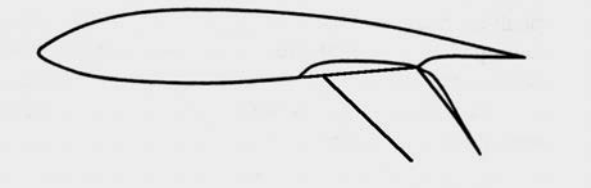

Sketch B. Lower surface spoiler (LSS) with 60° split-flap.

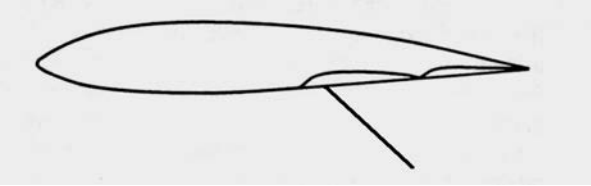

Sketch C. Lower surface spoiler only.

The final comparison, shown in figure 19, is for the inboard 90° auxiliary flap and LSS, with 0° split flap. This comparison shows similar lift and pitching moment for the entire angle-of-attack range. However, the original auxiliary flap produces higher drag.

While the 90° LSS outboard-only configuration was not tested, based on the previous comparisons, it is expected that its performance trends will be similar to those of the outboard 90° auxiliary-flap-only configuration, perhaps with slightly more lift.

In all of the comparisons, the LSS provides either similar or superior lift performance, with little impact on pitch. This suggests several enhances can be made to the original system including the following:

1. The complex hinges required to both deflect the auxiliary flap and to open the necessary gap between it and the main wing element may be replaced with a simple hinge. This should reduce the system weight fraction.
2. The use of a simple flat plate instead of a contoured airfoil saves weight, simplifies production, and recovers useable internal volume for additional fuel.

6. Summary of Results

A novel multielement trailing-edge flap system for light general aviation airplanes was conceived for enhanced stall/spin safety during normal and emergency landings. The system was designed to reduce stall speed, and thus approach speed, with the goal of reducing maneuvering-flight accidents and enhancing pilot survivability in the event of an accident. Wind tunnel tests were conducted to investigate the impact of this device on a typical general aviation high-wing trainer aircraft. The results of this investigation are summarized as follows:

1. The system with 45° auxiliary-flap deflections produced sustained high lift from 0° angle of attack up to stall. While this provided higher $C_{L,Max}$ values than the cruise wing or the best split-flap configuration, there was a reduction in stall angle.
2. The deployed inboard auxiliary flap produced variations in pitching moment, regardless of the deflection angle.
3. The overall lift performance with the inboard 45° auxiliary flap is very sensitive to the deflection angle of the split flap.
4. The deployed outboard auxiliary flap, whether at 45° or 90°, with the inboard 60° split flap, produced almost all of the lift enhancements, and most of the desired drag increase, of the uniformly deployed inboard/outboard auxiliary flaps.
5. The beneficial increase in $C_{L,Max}$ and the trend of sustained high lift was relatively unaffected by increasing the auxiliary-flap deflection from 45° to 90°. However, drag was substantially increased. This provides a capability for scheduled high drag on demand.
6. When the auxiliary flaps are deflected to 90°, variations in split-flap deflection have little effect on system performance.
7. Reducing the leading-edge radius of the auxiliary flap to a pointed leading edge had no effect on system performance.
8. Adding a Gurney flap to the auxiliary flap increased both lift and drag.
9. The simple flat-plate lower surface spoiler provided either similar or superior lift with little impact on pitch or drag as compared to VIA.
10. While this system appears to have beneficial descent and landing characteristics, the drag needs to be considered for all cases to verify the aircraft can handle the increase.

7. Recommendations for System Maturation

While this flap system demonstrated the ability to enhance low-speed safety via increasing the useable lift, providing the capability for very steep glide-slopes, and providing a means for safe recovery from unintentional dives, there are still a number of recommendations that will enhance the understanding of the flow physics and the potential usefulness of this system, as follows, in no particular order:

1. Due to the poor fit and tolerances of the model tested for this investigation, a higher fidelity wing-only investigation may yield greater insight into the flow physics and system sensitivities. The airfoil shape should be selected to maximize the anticipated low-speed flow characteristics, while maintaining the desired high-speed cruise. In addition to acquiring force and moment data, detailed pressure data and flow visualization data are needed, particularly within the channel created by the upper surface of the auxiliary flap and the lower surface of the split flap.
2. Due to the large drag produced by this configuration, the aircraft's performance and tolerance of these conditions needs to be evaluated.
3. Since the system yields large dynamic wakes, computational fluid dynamics predictions will benefit from a grid convergence study and unsteady CFD analysis.
4. Since this system was designed to act mainly on the flow around the trailing-edge, increases in lift resulted in decreases in stall angle. Therefore, it is recommended that some form of leading-edge treatment be added to the system to further increase $C_{L,max}$ and further increase the stall margin.
5. A detailed performance comparison of the current VIA wing system needs to be made with the existing trailing-edge Fowler Flap system. This should be done for the following three configurations: the conventional as-is Fowler Flap; the Fowler Flap used in place of the split flap on the VIA system; and the auxiliary wing on the outboard wing section, with the conventional Fowler Flap only on the inboard trailing edge.
6. Detailed systems analysis needs to be done to assess things like flap-system weight, wing torsional and bending loads, wing spar and rib modifications, hinge moments, flight envelop trade-offs, impact on internal fuel capacity, tail loading, etc.
7. Investigate the influence of both wing sweep and system element sweep, on system performance.
8. Obtain an understanding of the influence of prop-wash (or power-on effects), sideslip, bank angle, and ground effects during landing on system performance.
9. When using this system, obtain an understanding of tail placement, trim and rudder effectiveness for high-wing, mid-wing, and low-wing configurations. Also, investigate the system usefulness on canard and multilifting surface configurations.

8. References

1. Airplane Owners and Pilots Association (AOPA), Air Safety Foundation (ASF): 2004 Joseph T. Nall Report, Accident Trends and Factors for 2003, copyright, 2005
2. Jeppesen Sanderson, Inc.: Private Pilot Manual, 2002
3. Airplane Owners and Pilots Association (AOPA), Air Safety Foundation (ASF): Special Report: Stall/Spin: Entry Point for Crash and Burn?, 2003
4. United States Patent—4,881,703 - Aircraft Flap Assembly - Roger Nahas, Nov. 21, 1989

5. Papadakis, M., Wong, S. C., and Yeong. H. W., "Aerodynamic Performance of an Innovative Flap Design," AIAA 99-0539, January 1999.
6. D. Bruce Owens, Jay M. Brandon, Mark A. Croom, C. Michael Fremaux, Eugene H. Heim , and Dan D. Vicroy, "Overview of Dynamic Test Techniques for Flight Dynamics Research at NASA LaRC," AIAA_2006_3146 Ground Test Conference, San Francisco 2006.
7. Frink, N.T: "Tetrahedral Unstructured Navier-Stokes Method for Turbulent Flows," AIAA Journal, Volume 36, Number 11, November 1998.
8. Spalart, P., and Allmaras, S.A., "One-equation turbulence model for aerodynamic flows," AIAA 92-0439, January 1992.
9. Pirzadeh, S., "Three-Dimensional Unstructured Viscous Grids by the Advancing-Layers Method," *AIAA Journal*, Vol. 34, No. 1, January 1996, pp.43–49.
10. Parikh, P.C., "Application of a Scalable, Parallel, Unstructured-Grid-Based Navier-Stokes Solver," AIAA 2001-2584, June 2001.
11. Pandya, M. J., Frink, N. T., Abdol-Hamid, K. S., and Chung, J. J., "Recent Enhancements to USM3D Unstructured Flow Solver for Unsteady Flows." AIAA Paper 2004-5201.

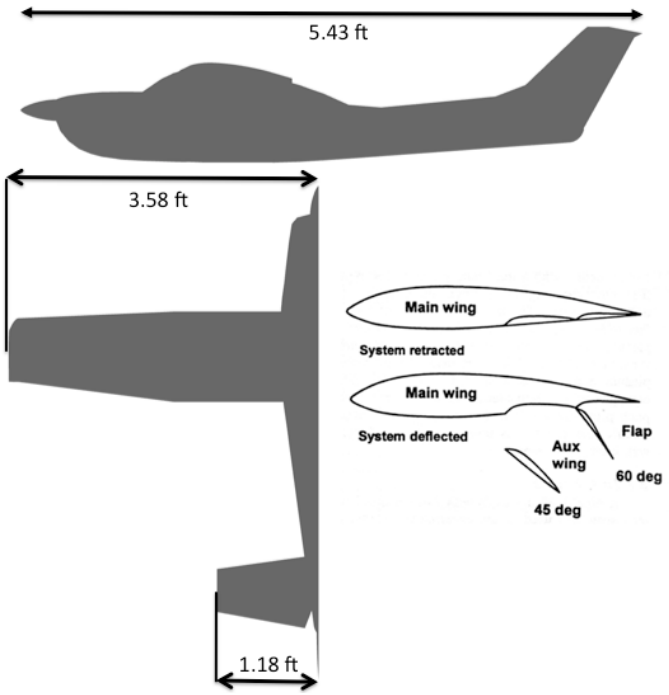

(a)

(b)

Figure 1. (a) Plan view, side view, and sketch of variable incidence auxiliary (VIA) wing; (b) Photograph of model mounted in the 12-Foot Wind Tunnel. (Shown are both inboard and outboard auxiliary flaps (red) deflected at 45°, and the split flap (white) deflected at 60°.

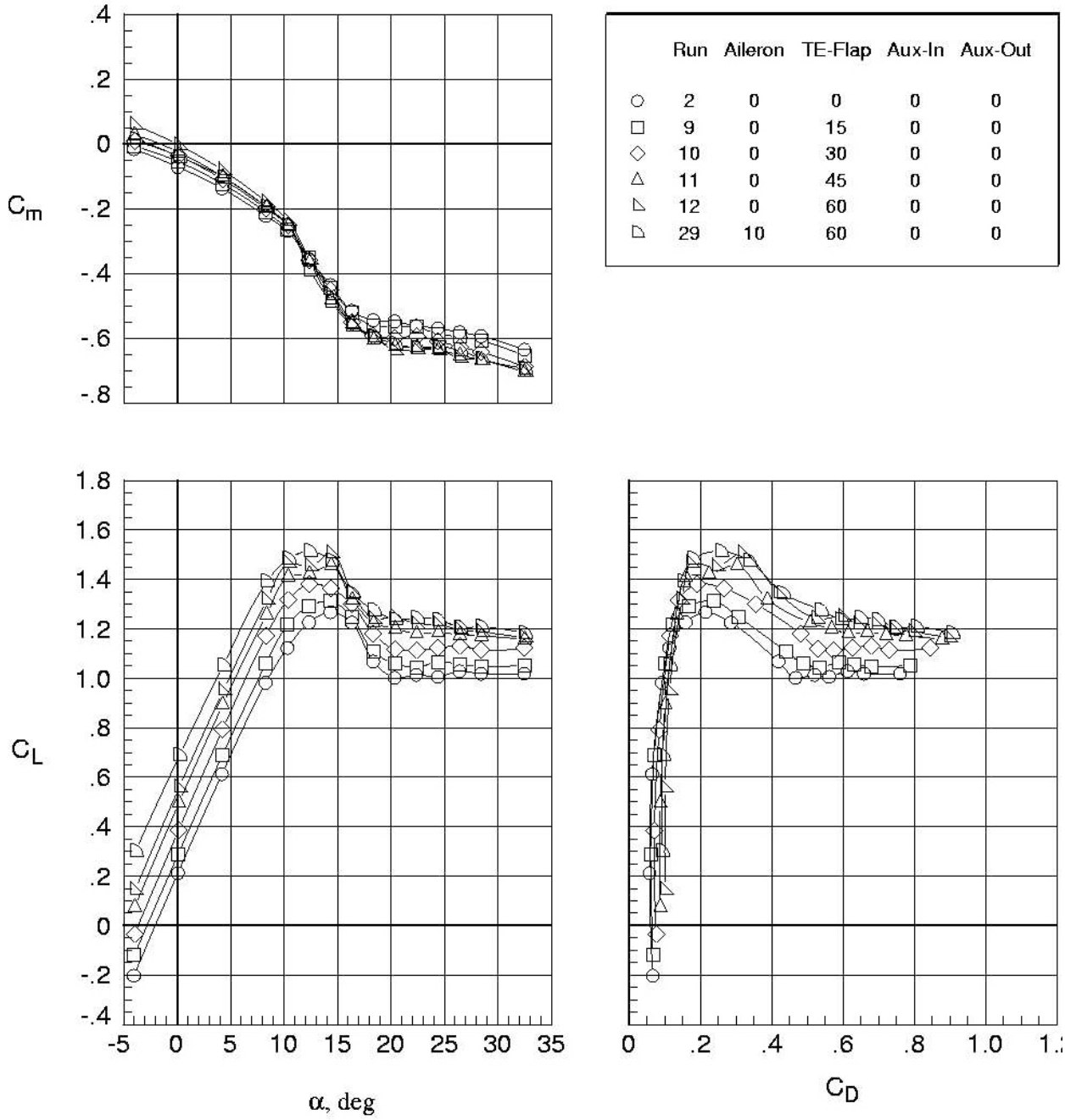

(a) Longitudinal aerodynamics.

Figure 2. Comparison of trailing-edge split-flap deflections: q = 4.0 psf.

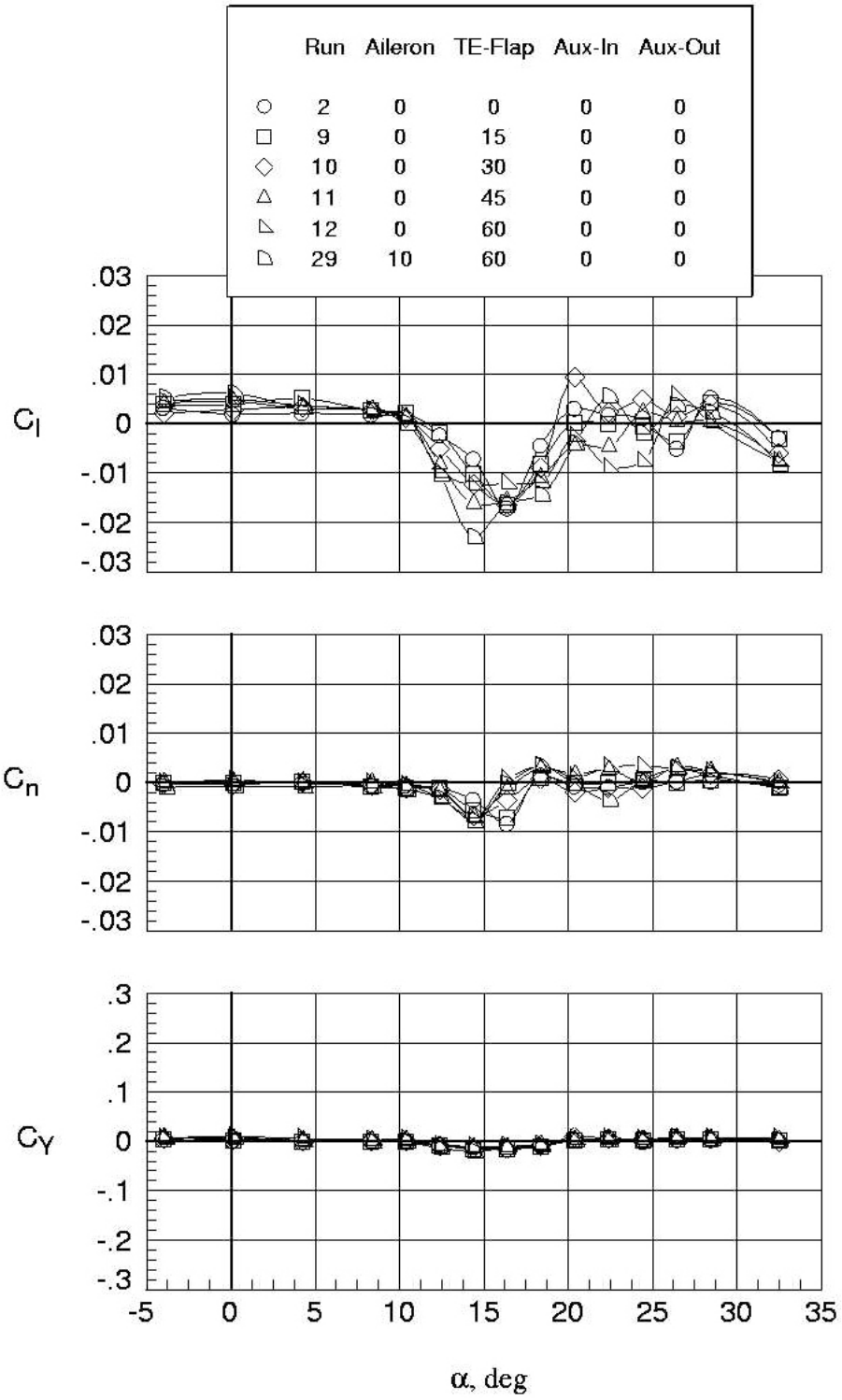

(b) Lateral aerodynamics.

Figure 2. Continued.

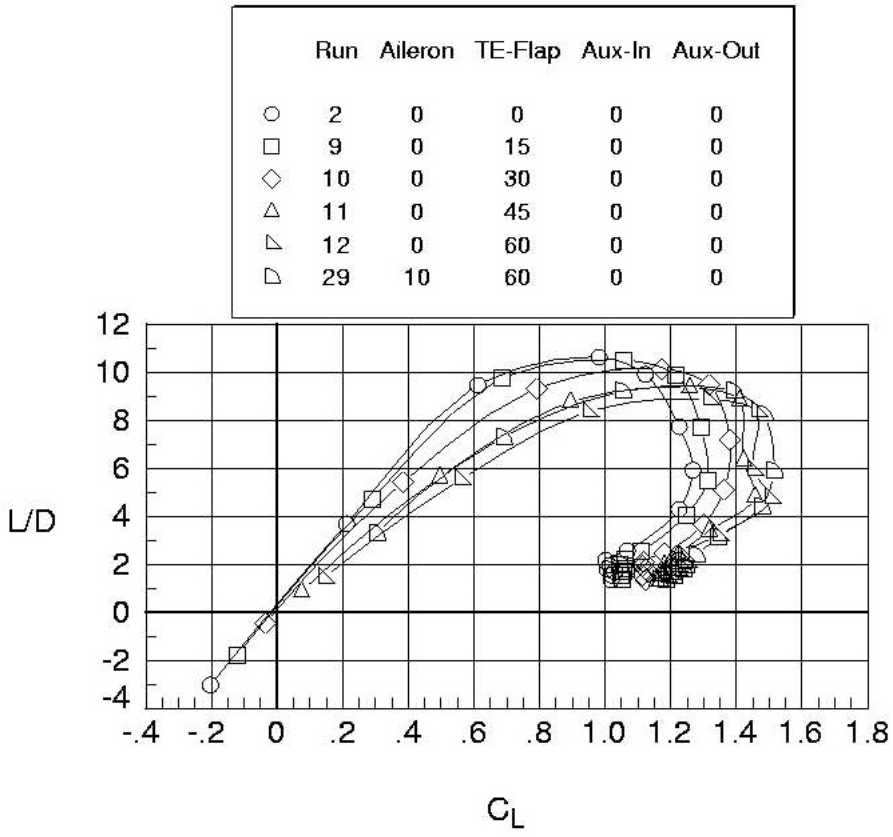

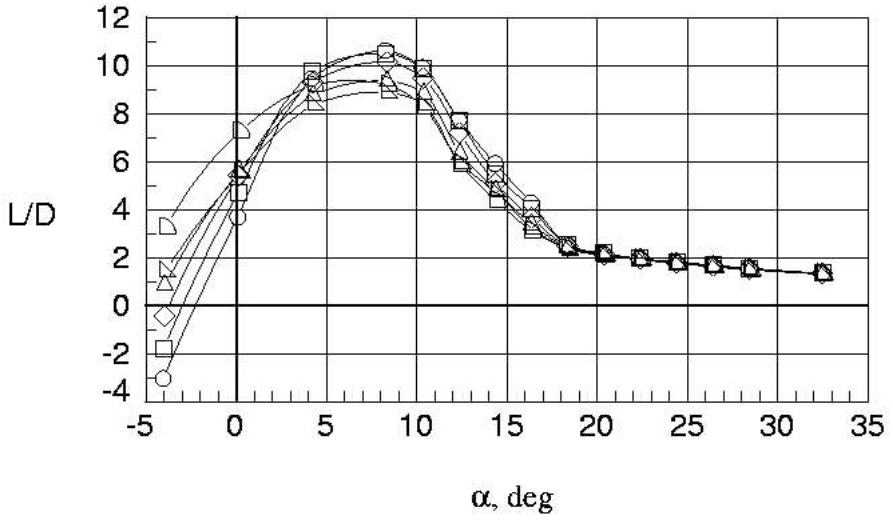

(c) Lift-to-drag ratios.

Figure 2. Continued.

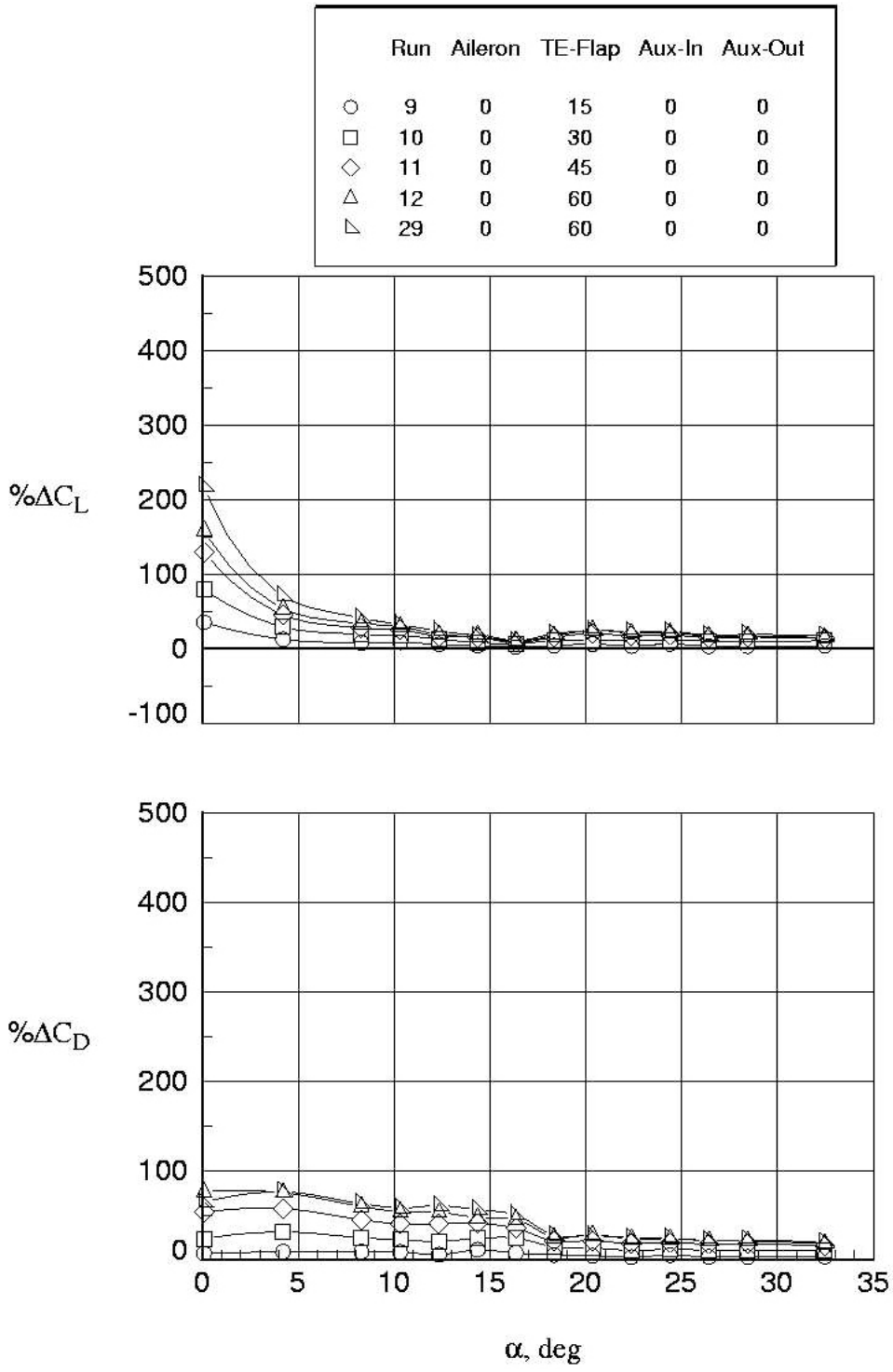

(d) Percent delta changes; baseline = run 2 (aileron deflection = 0°, TE-flap deflection = 0°, aux-in deflection = 0°, aux-out deflection = 0°).

Figure 2. Concluded.

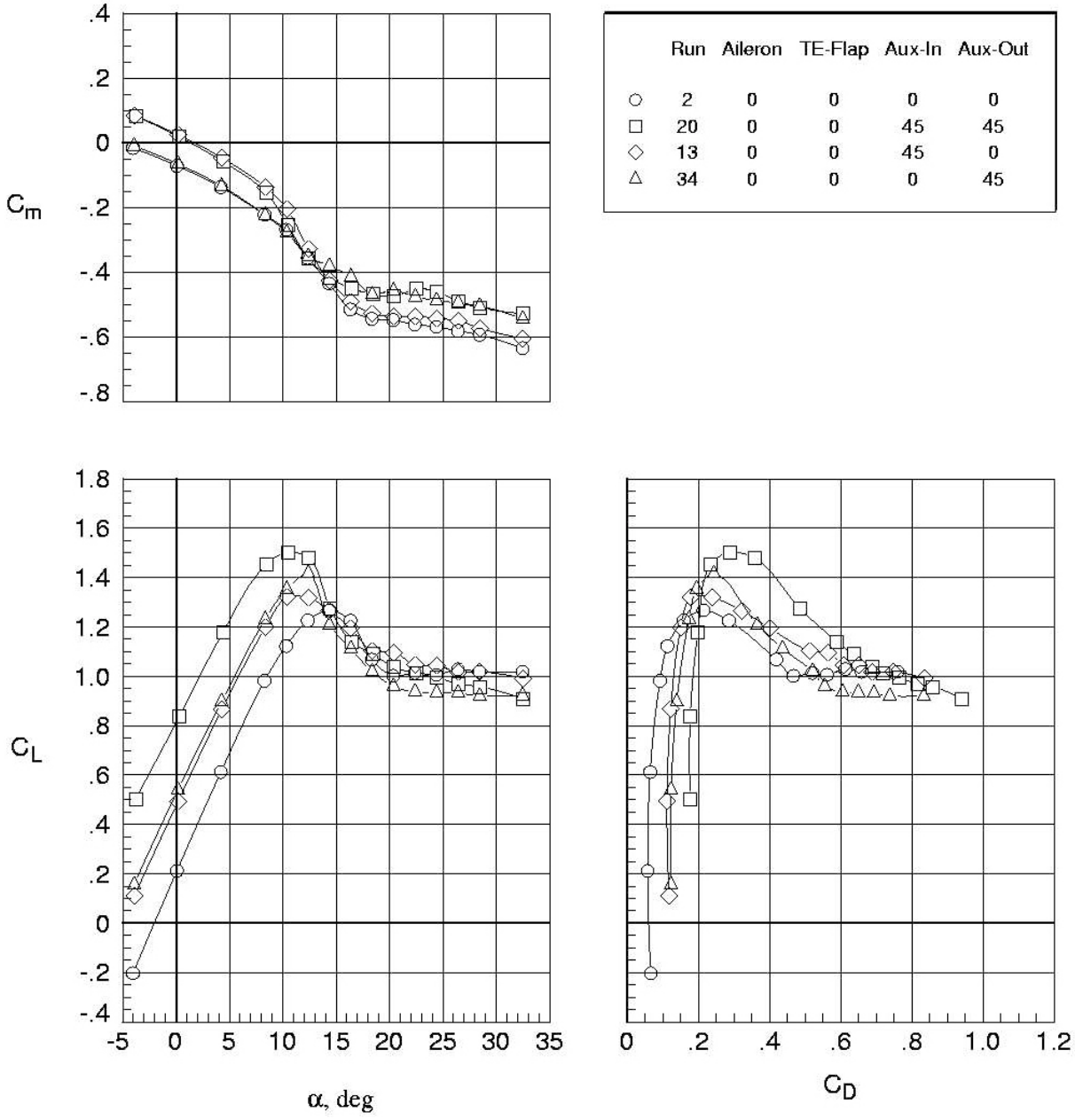

(a) Longitudinal aerodynamics.

Figure 3. Comparison of 45° auxiliary flap deflections; q = 4.0 psf.

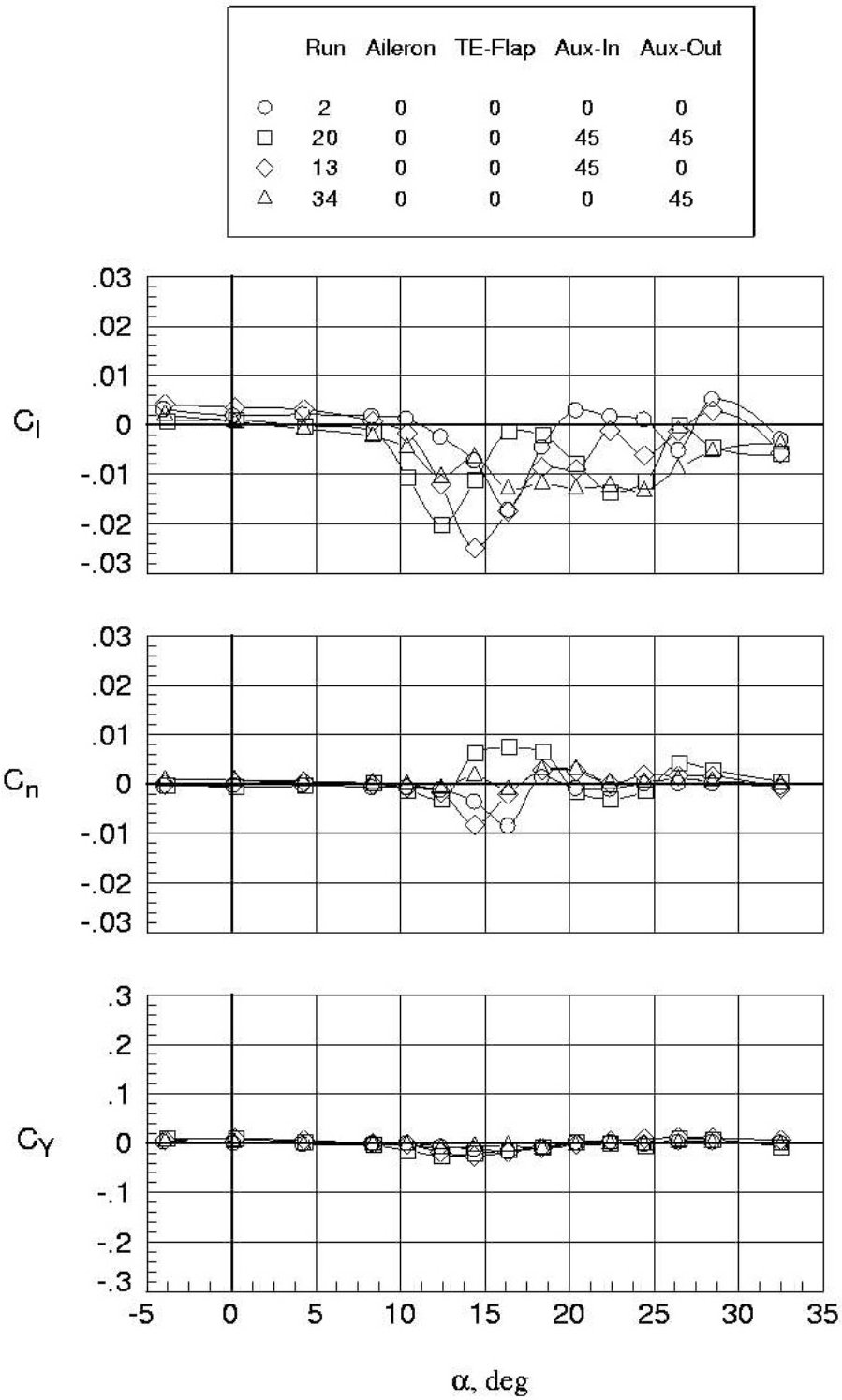

(b) Lateral aerodynamics.

Figure 3. Continued.

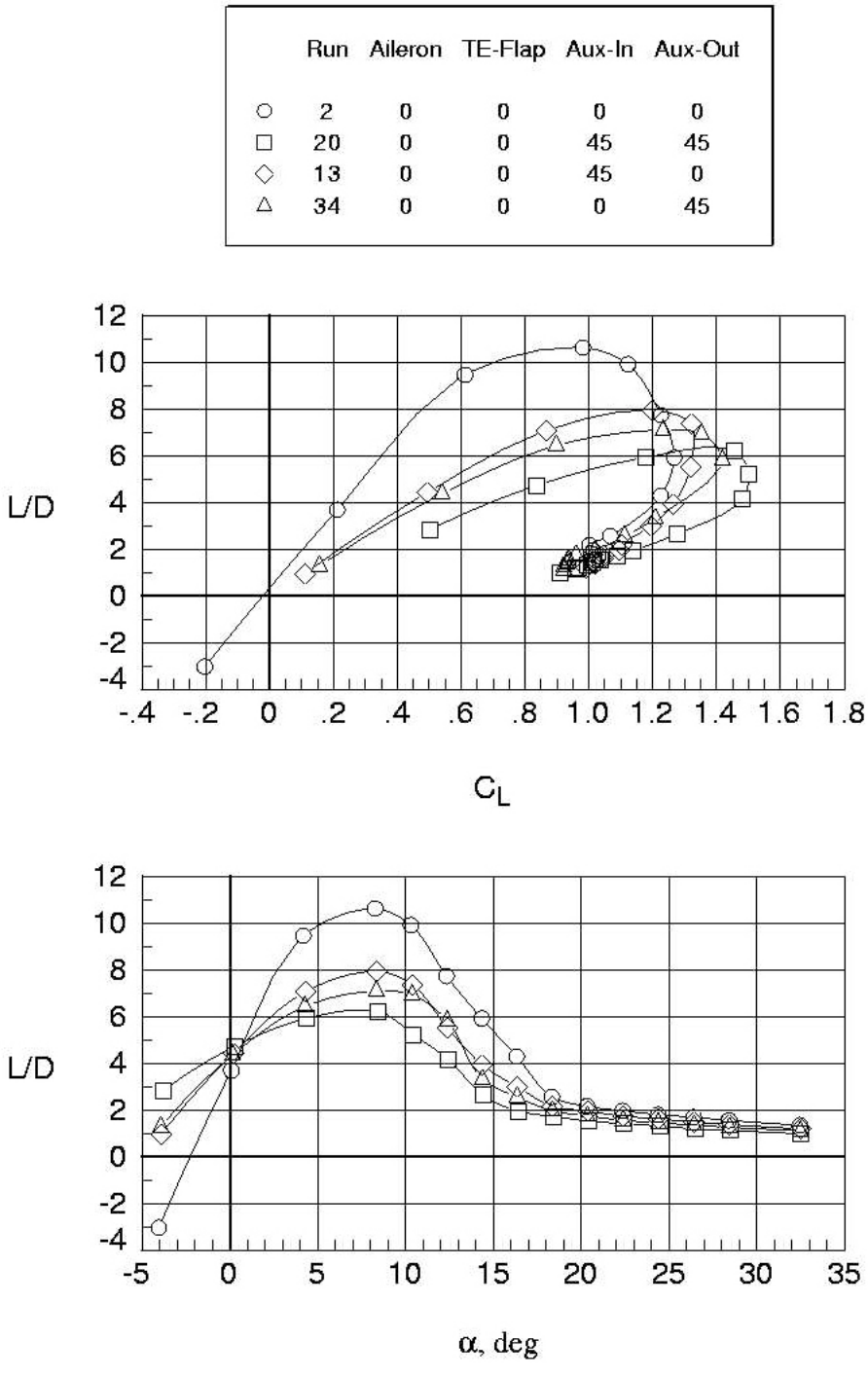

(c) Lift-to-drag ratios.

Figure 3. Continued.

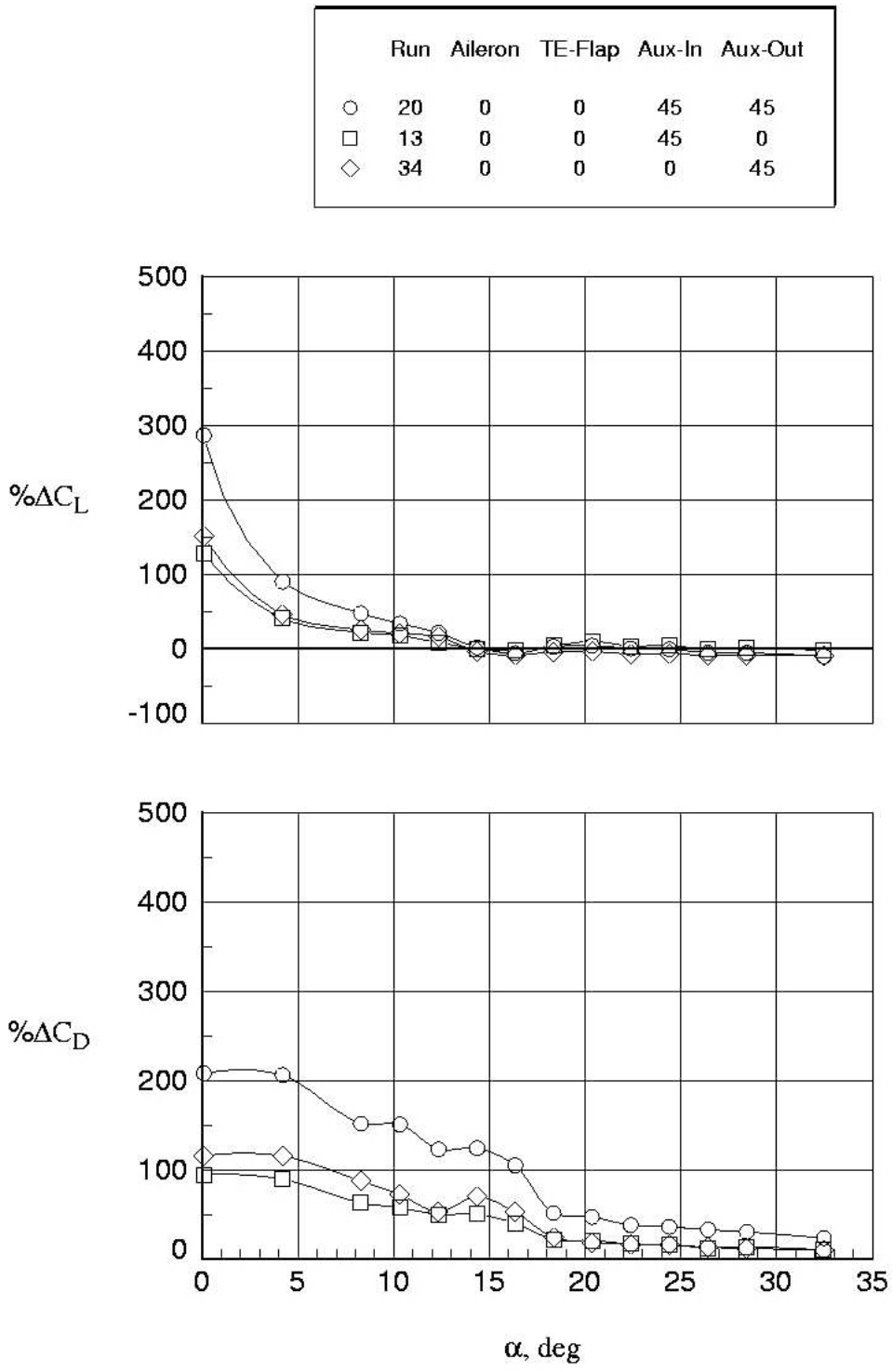

(d) Percent delta changes; baseline = run 2 (aileron deflection = 0°, TE-flap deflection = 0°, aux-in deflection = 0°, aux-out deflection = 0°).

Figure 3. Concluded.

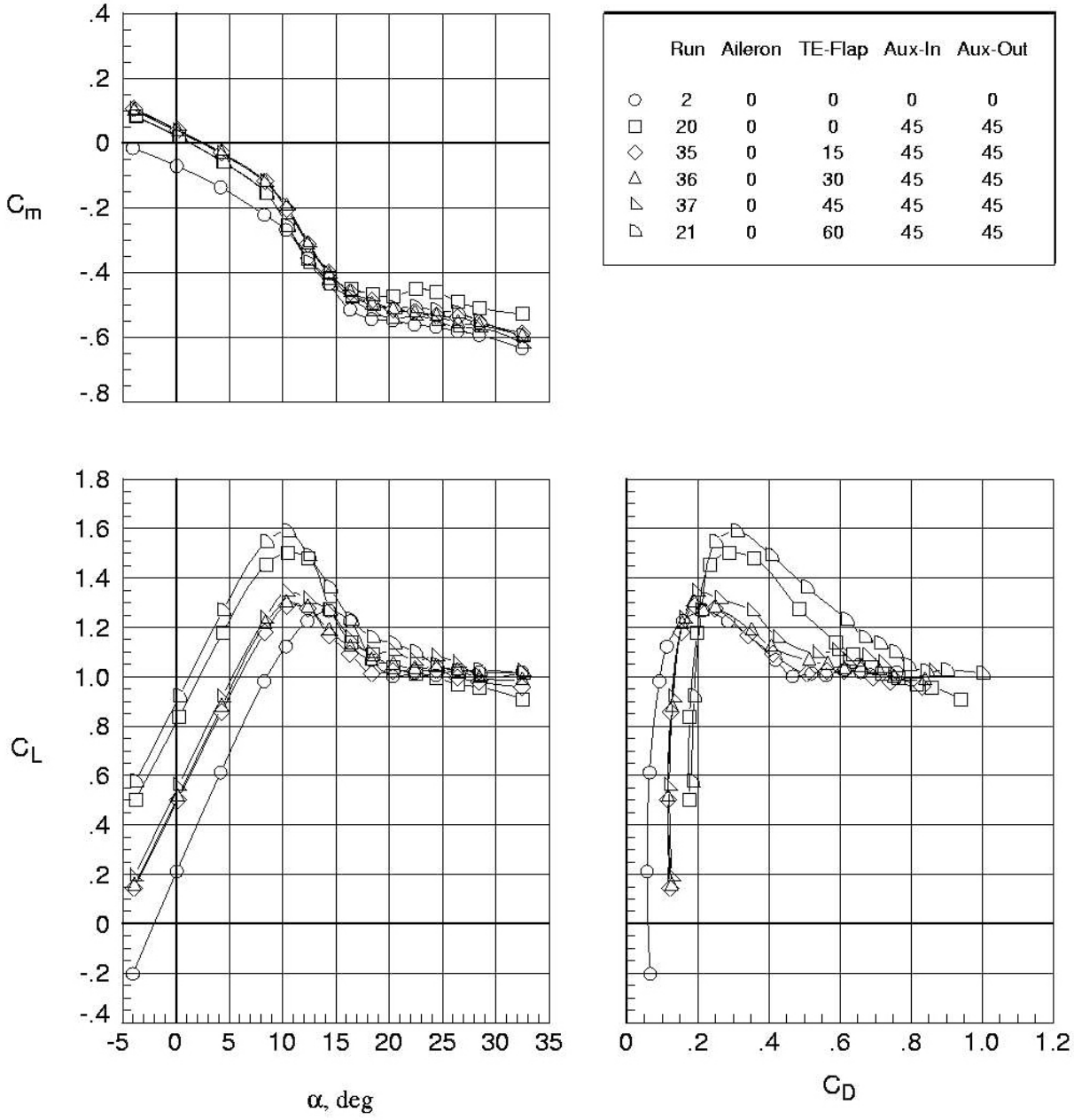

(a) Longitudinal aerodynamics.

Figure 4. Effect of split-flap deflections on 45° auxiliary flap performance; q = 4.0 psf.

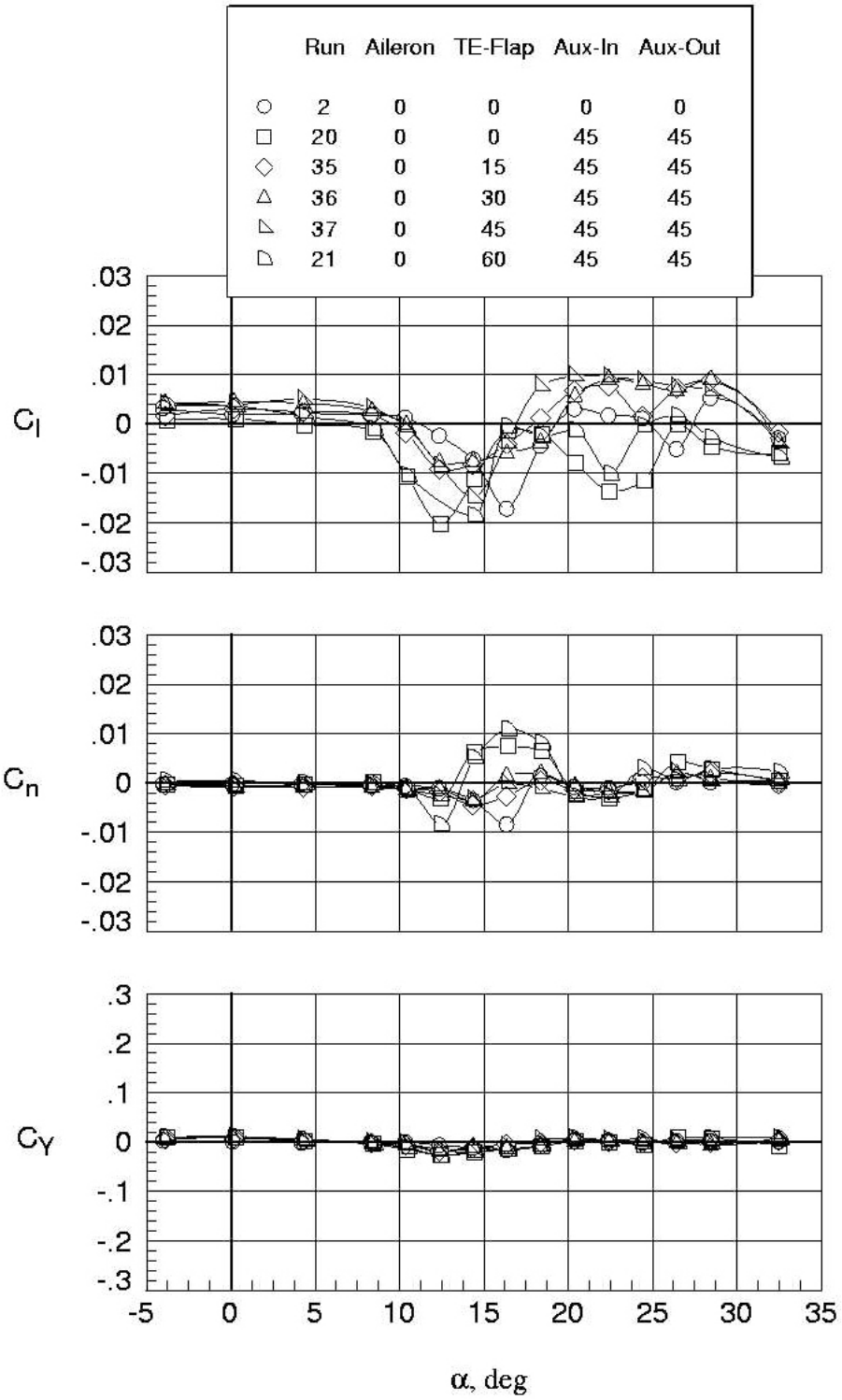

(b) Lateral aerodynamics.

Figure 4. Continued.

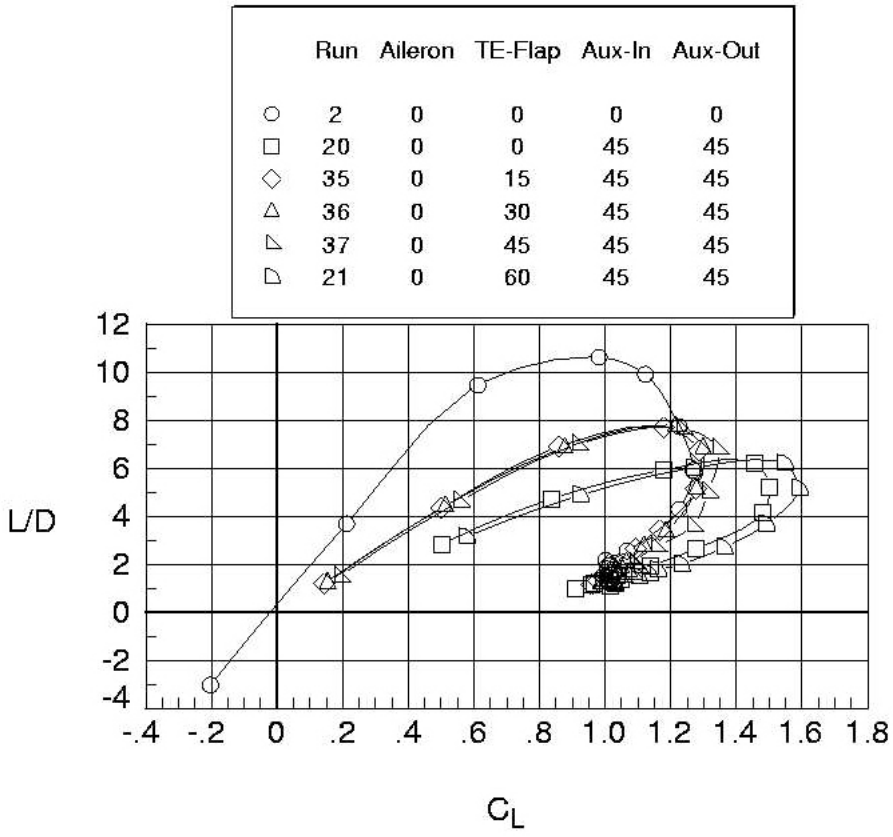

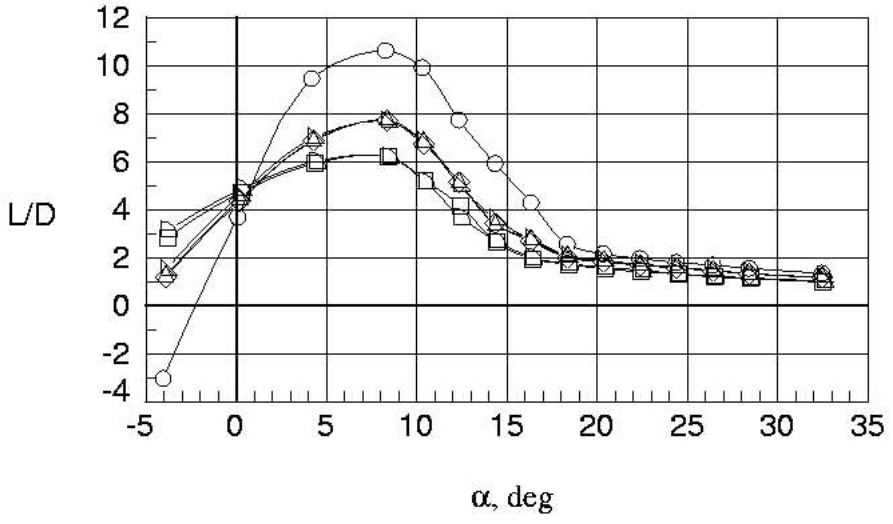

(c) Lift-to-drag ratios.

Figure 4. Continued.

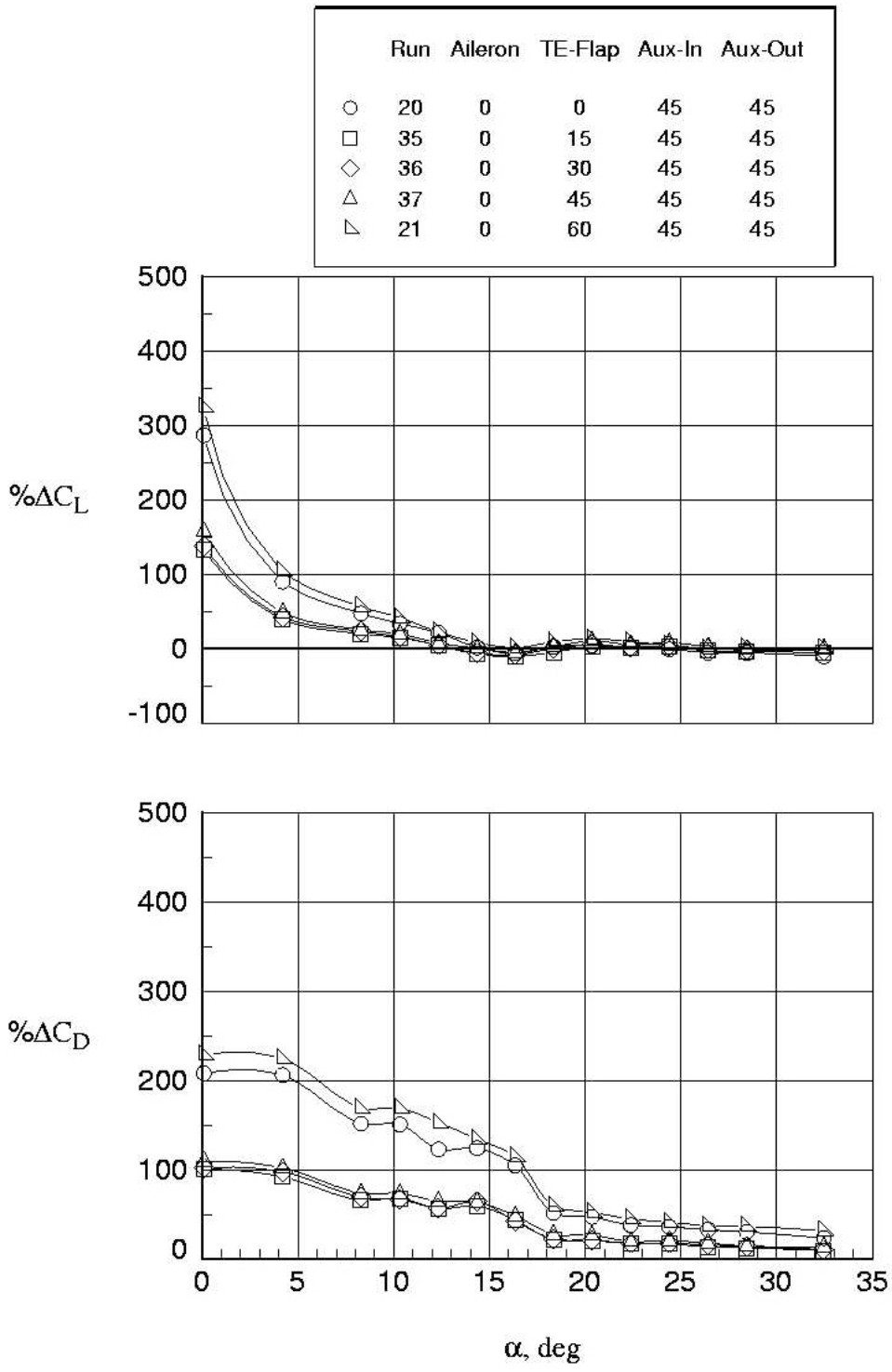

(d) Percent delta changes; baseline = run 2 (aileron deflection = 0°, TE-flap deflection = 0°, aux-in deflection = 0°, aux-out deflection = 0°).

Figure 4. Concluded.

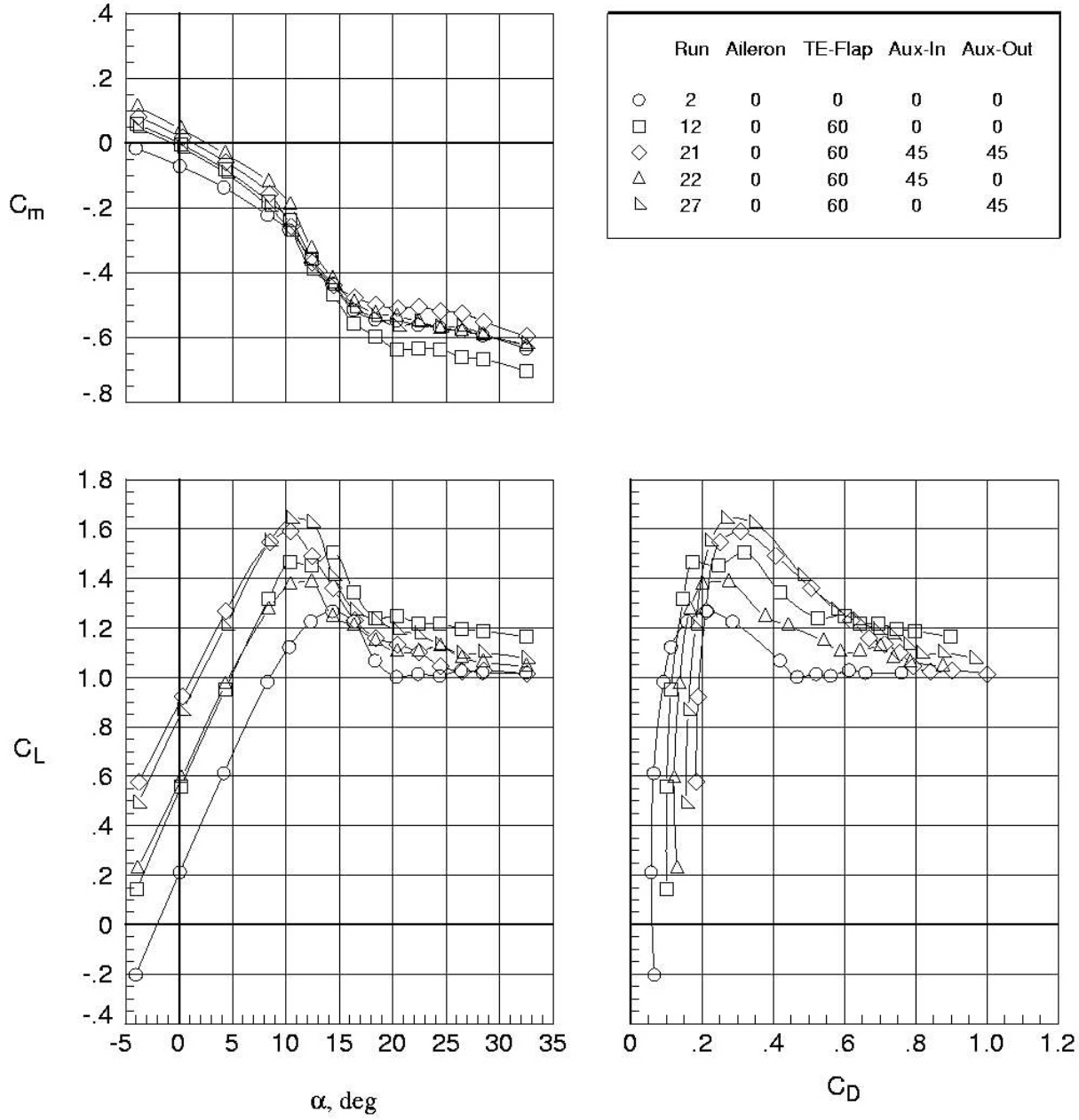

(a) Longitudinal aerodynamics.

Figure 5. Effect of 60° split-flap deflection on 45° auxiliary flap performance; q = 4.0 psf.

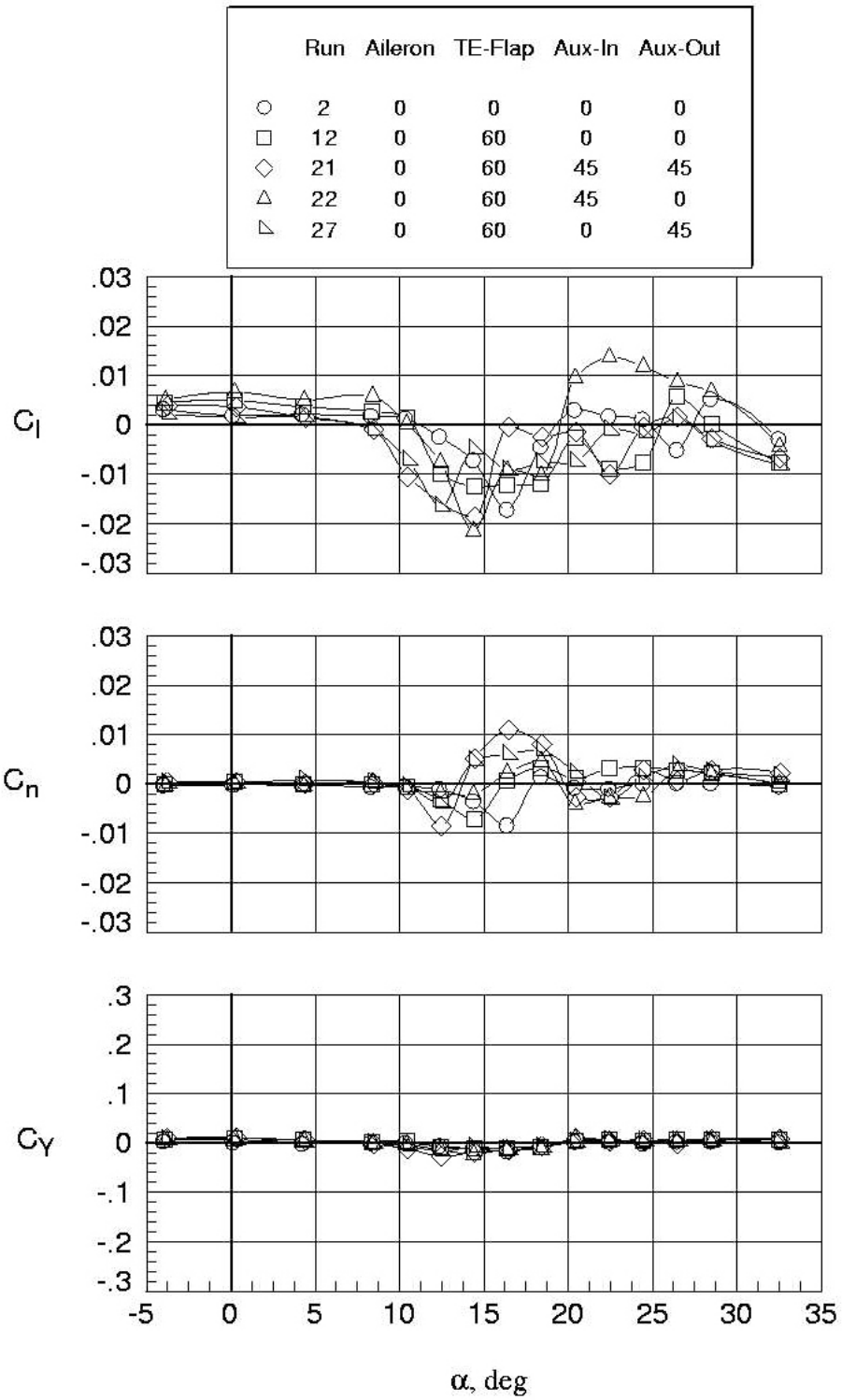

(b) Lateral aerodynamics.

Figure 5. Continued.

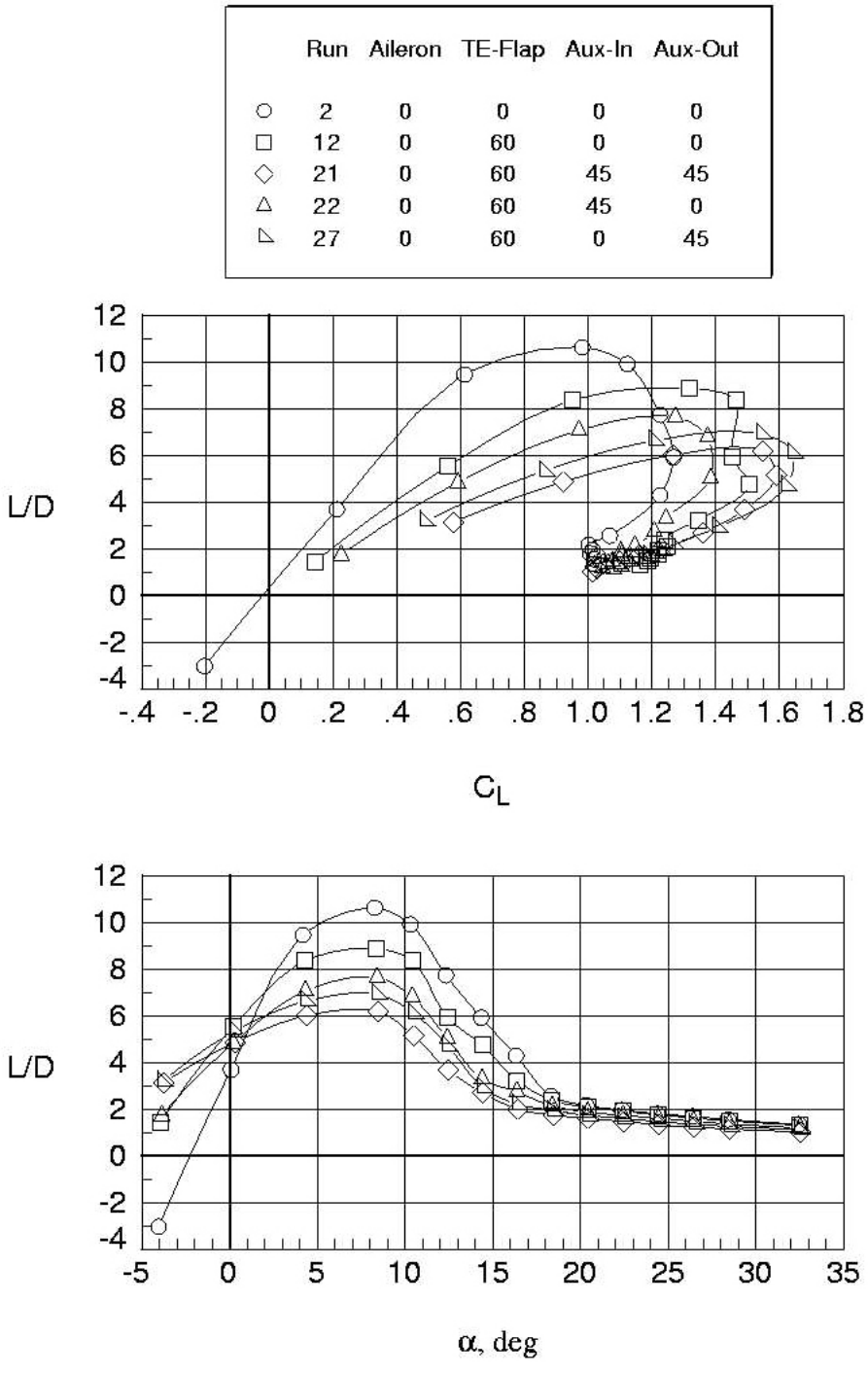

(c) Lift-to-drag ratios.

Figure 5. Continued.

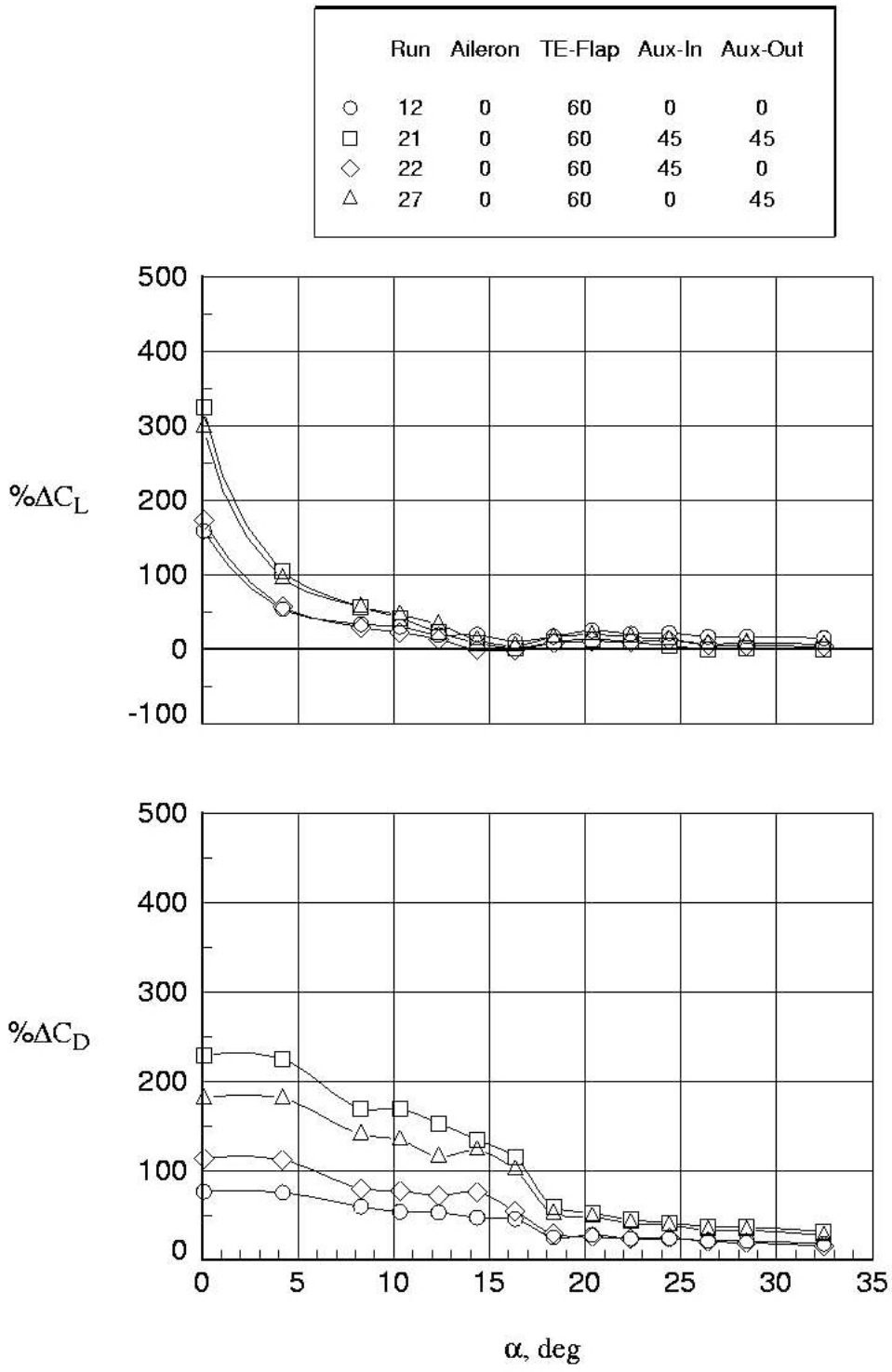

(d) Percent delta changes; baseline = run 2 (aileron deflection = 0°, TE-flap deflection = 0°, aux-in deflection = 0°, aux-out deflection = 0°).

Figure 5. Concluded.

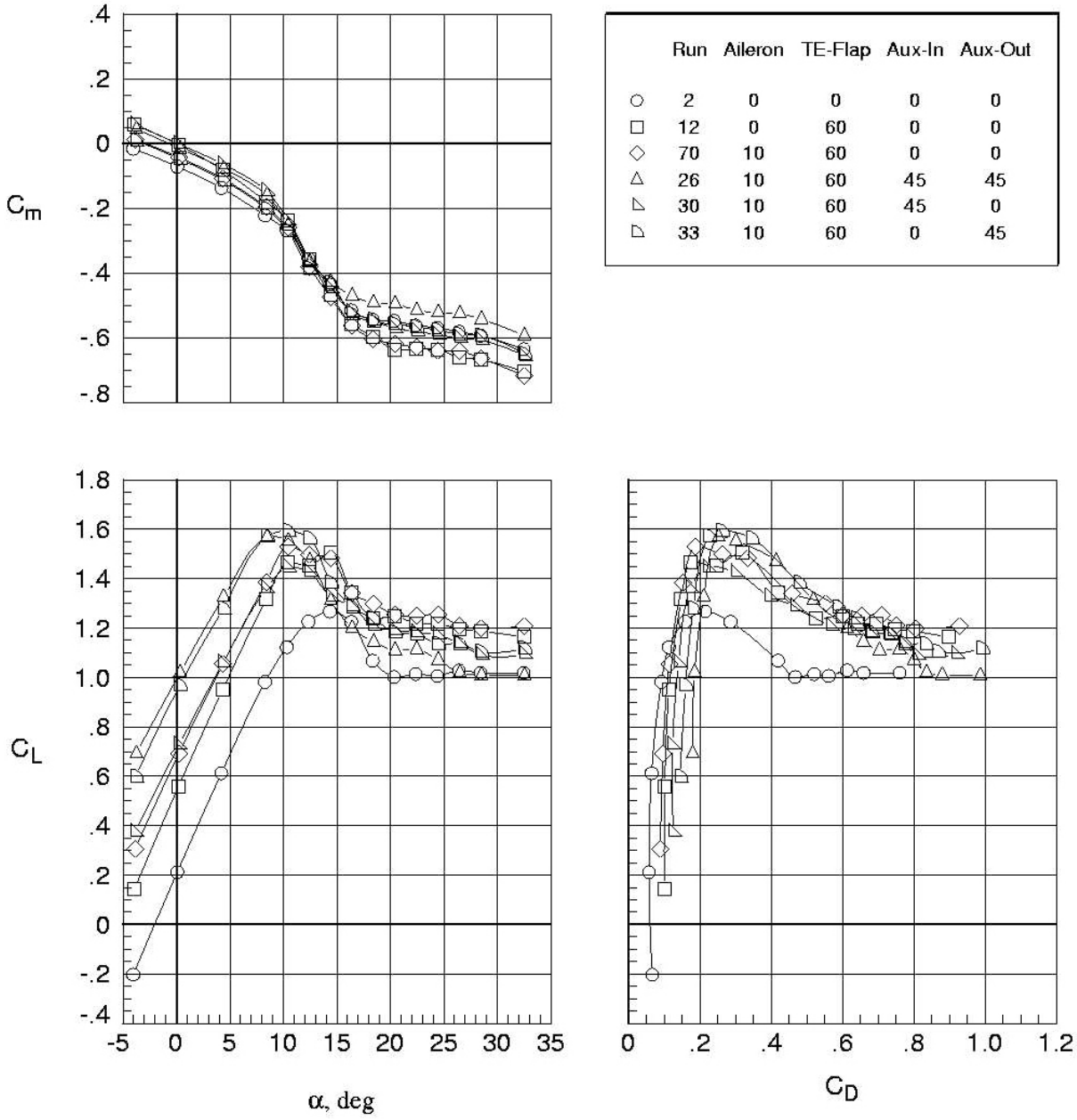

(a) Longitudinal aerodynamics.

Figure 6. Use of aileron as flap with 45° auxiliary flap; q = 4.0 psf.

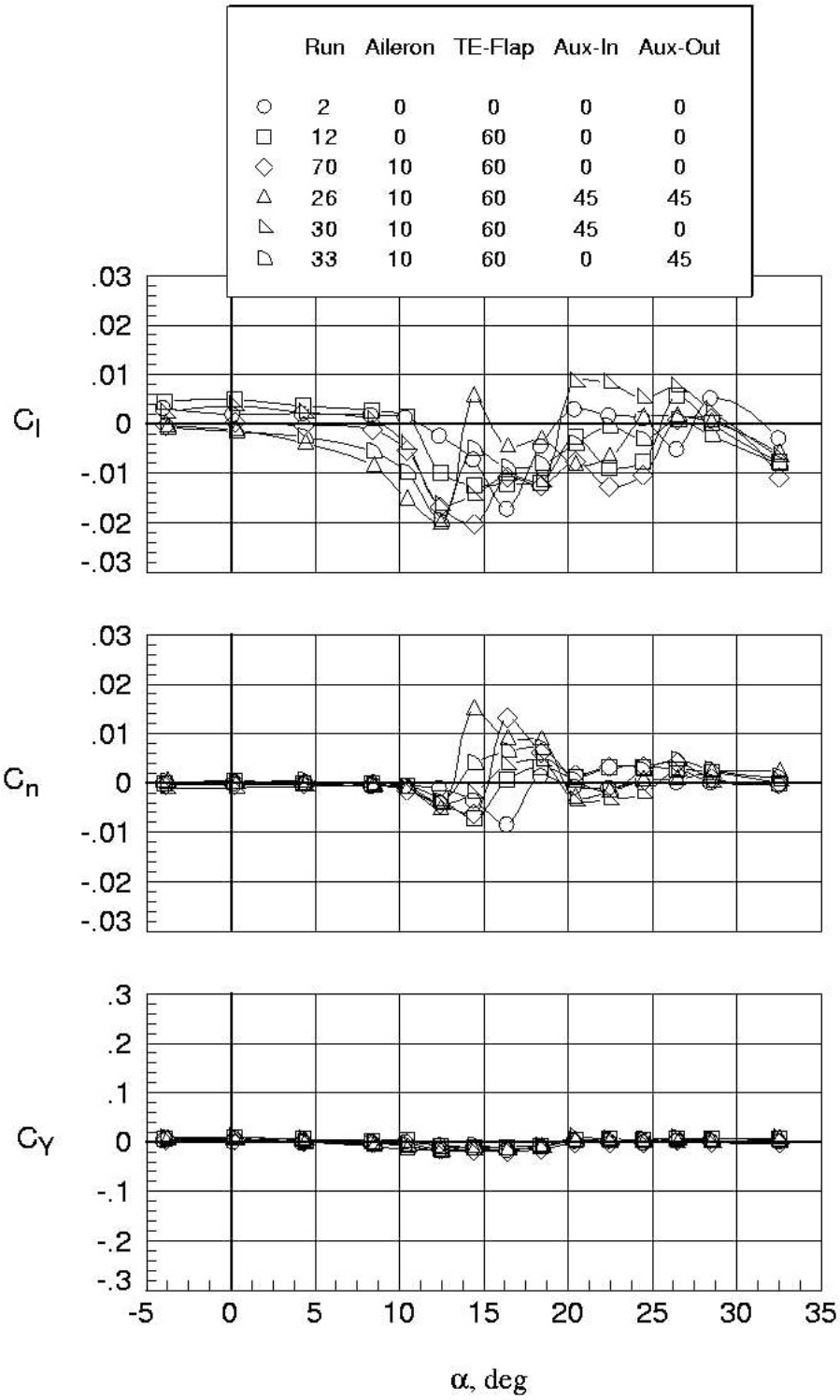

(b) Lateral aerodynamics.

Figure 6. Continued.

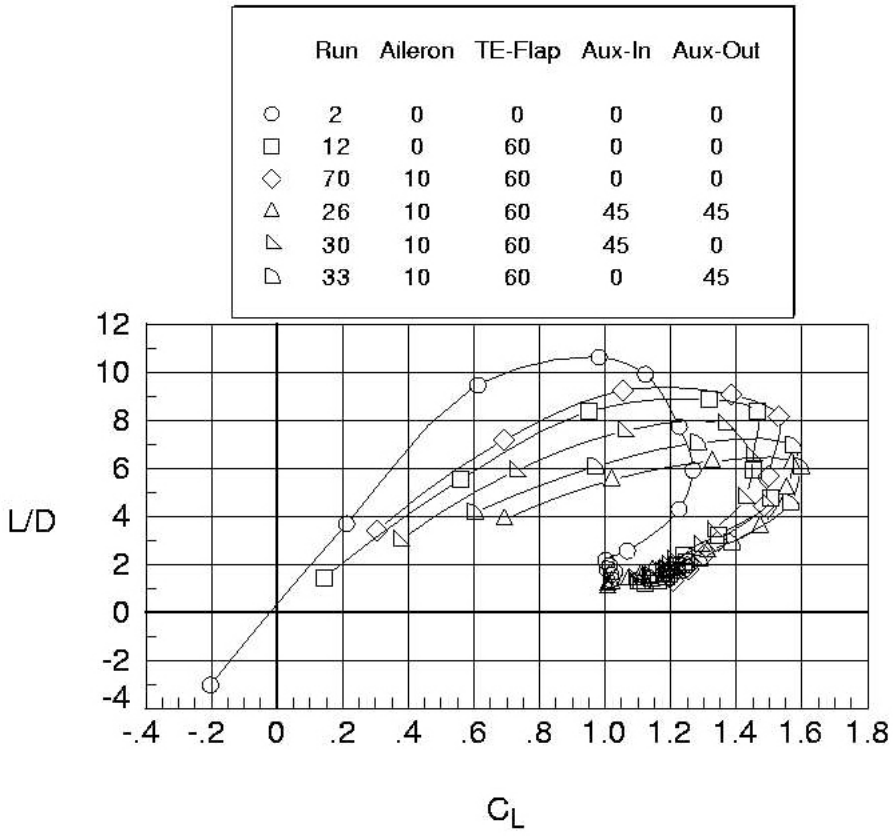

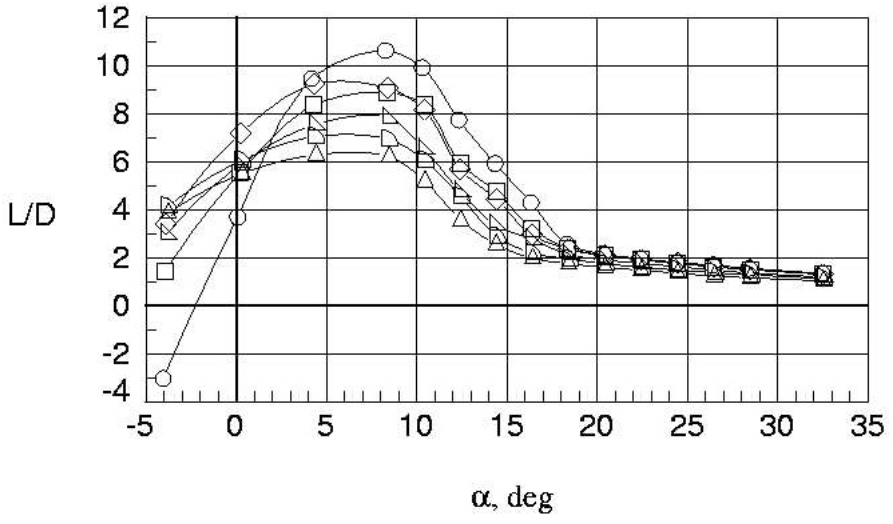

(c) Lift-to-drag ratios.

Figure 6. Continued.

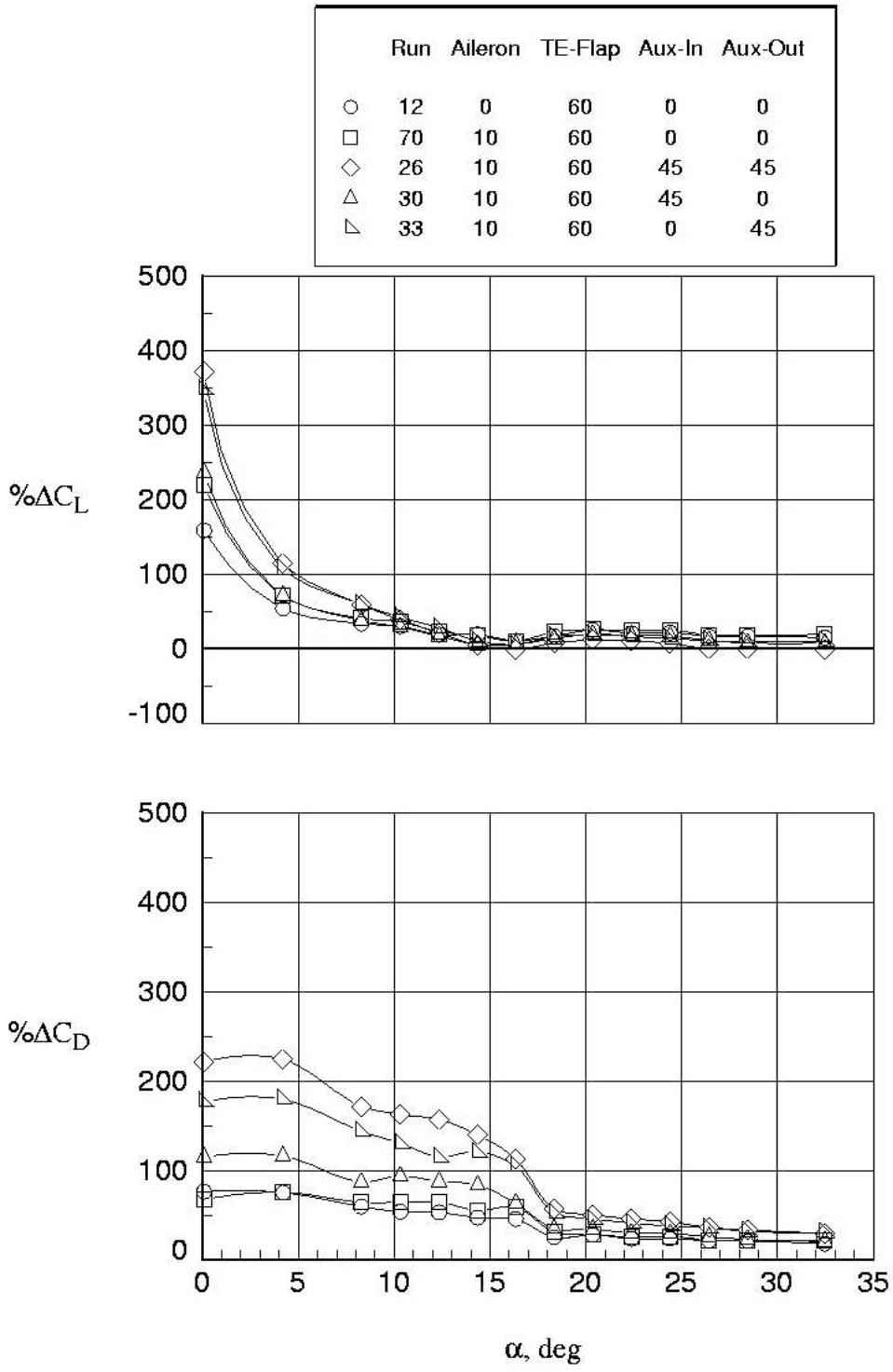

(d) Percent delta changes; baseline = run 2 (aileron deflection = 0°, TE-flap deflection = 0°, aux-in deflection = 0°, aux-out deflection = 0°).

Figure 6. Concluded.

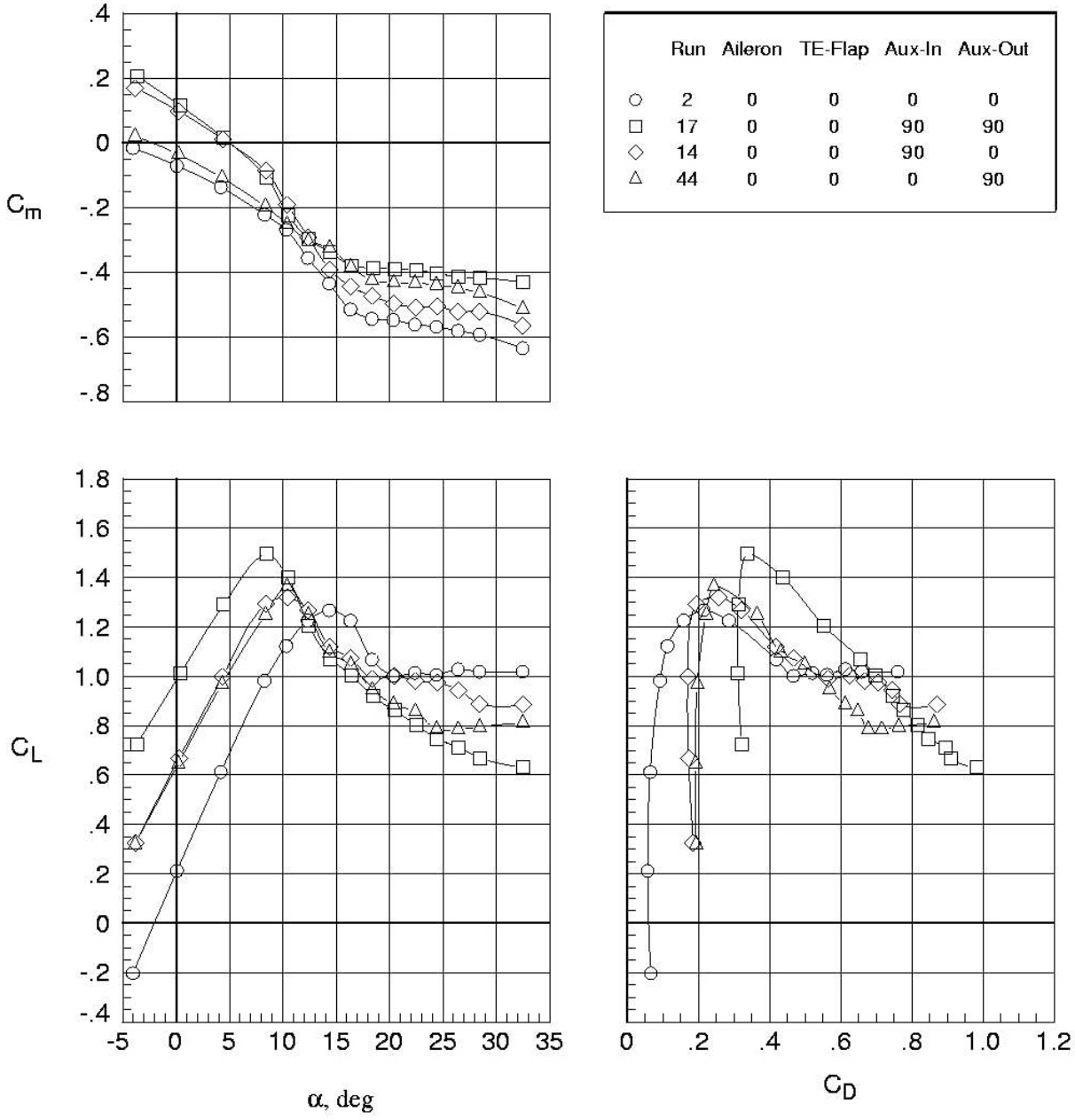

(a) Longitudinal aerodynamics.

Figure 7. Comparison of 90° auxiliary flap performance; q = 4.0 psf.

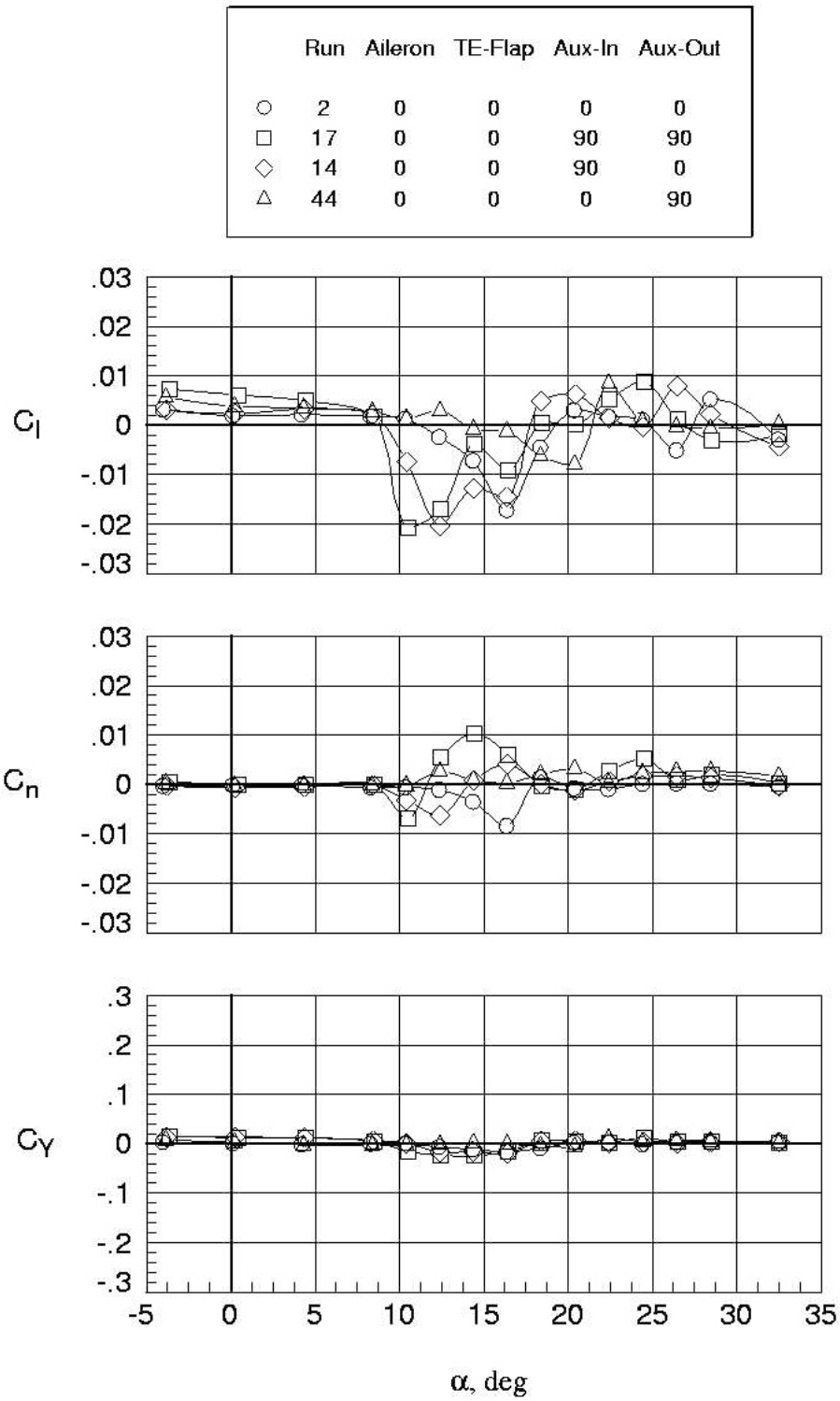

(b) Lateral aerodynamics.

Figure 7. Continued.

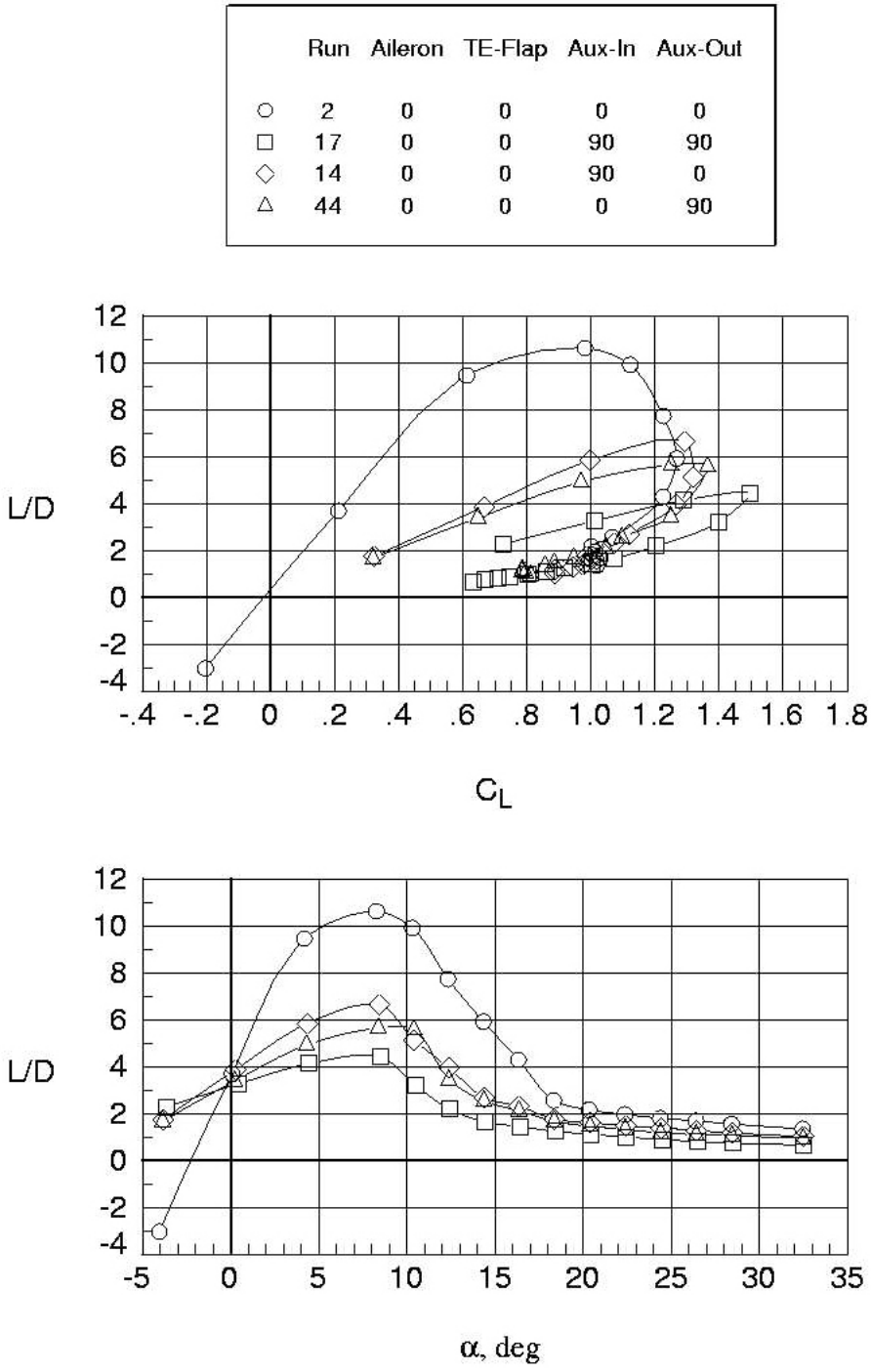

(c) Lift-to-drag ratios.

Figure 7. Continued.

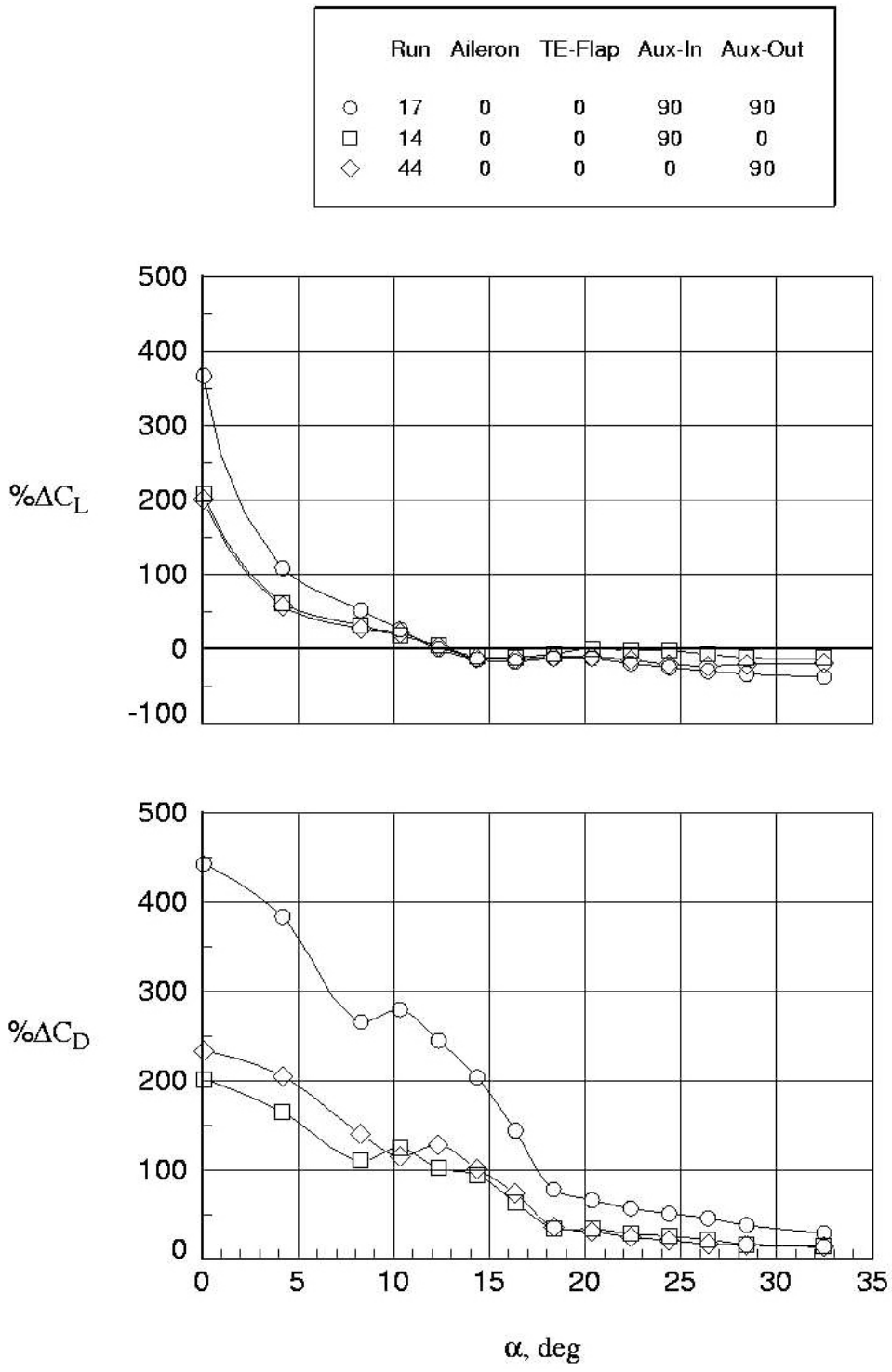

(d) Percent delta changes; baseline = run 2 (aileron deflection = 0°, TE-flap deflection = 0°, aux-in deflection = 0°, aux-out deflection = 0°).

Figure 7. Concluded.

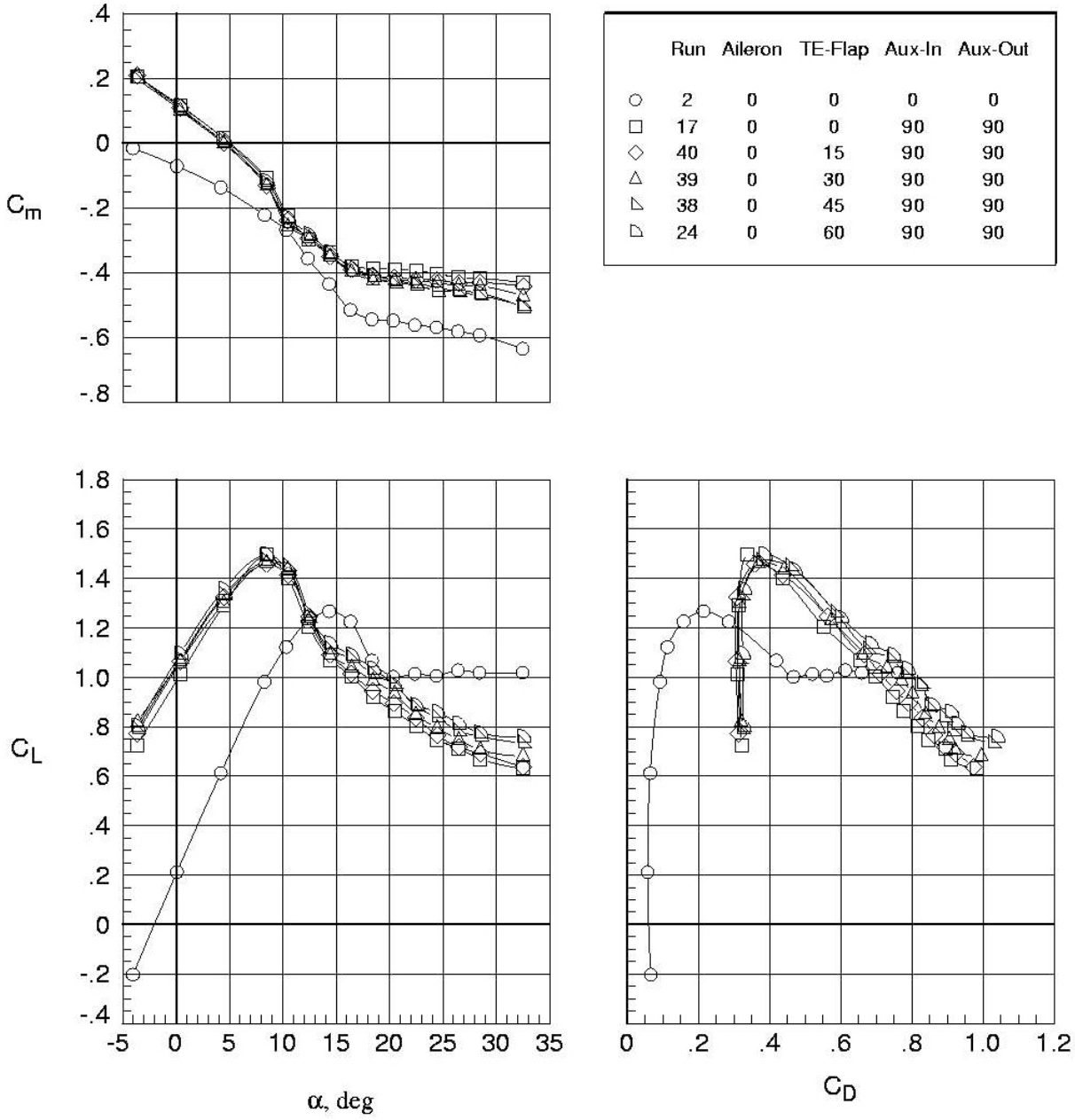

(a) Longitudinal aerodynamics.

Figure 8. Effect of split flap deflections on 90° auxiliary flap performance; q = 4.0 psf.

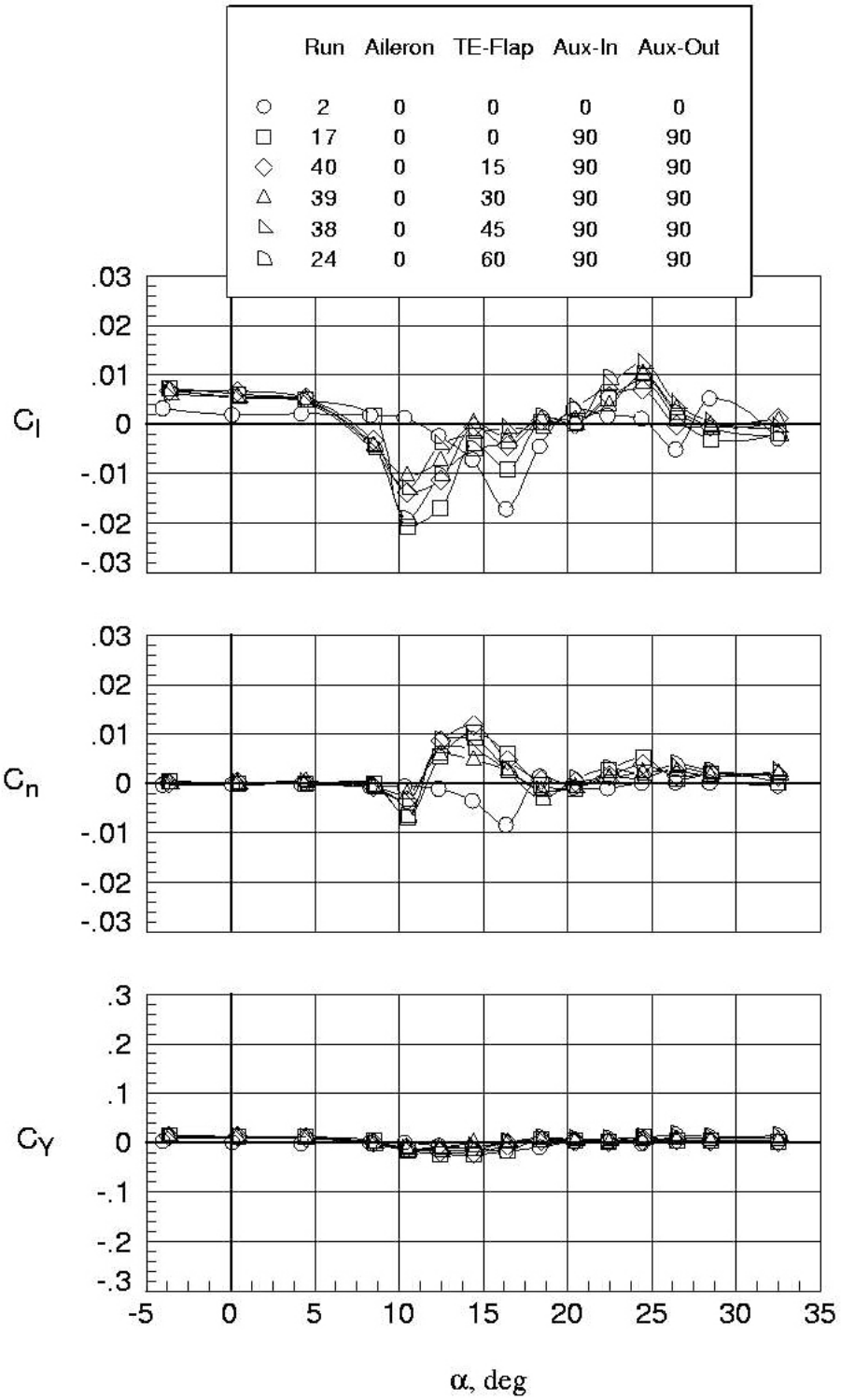

(b) Lateral aerodynamics.

Figure 8. Continued.

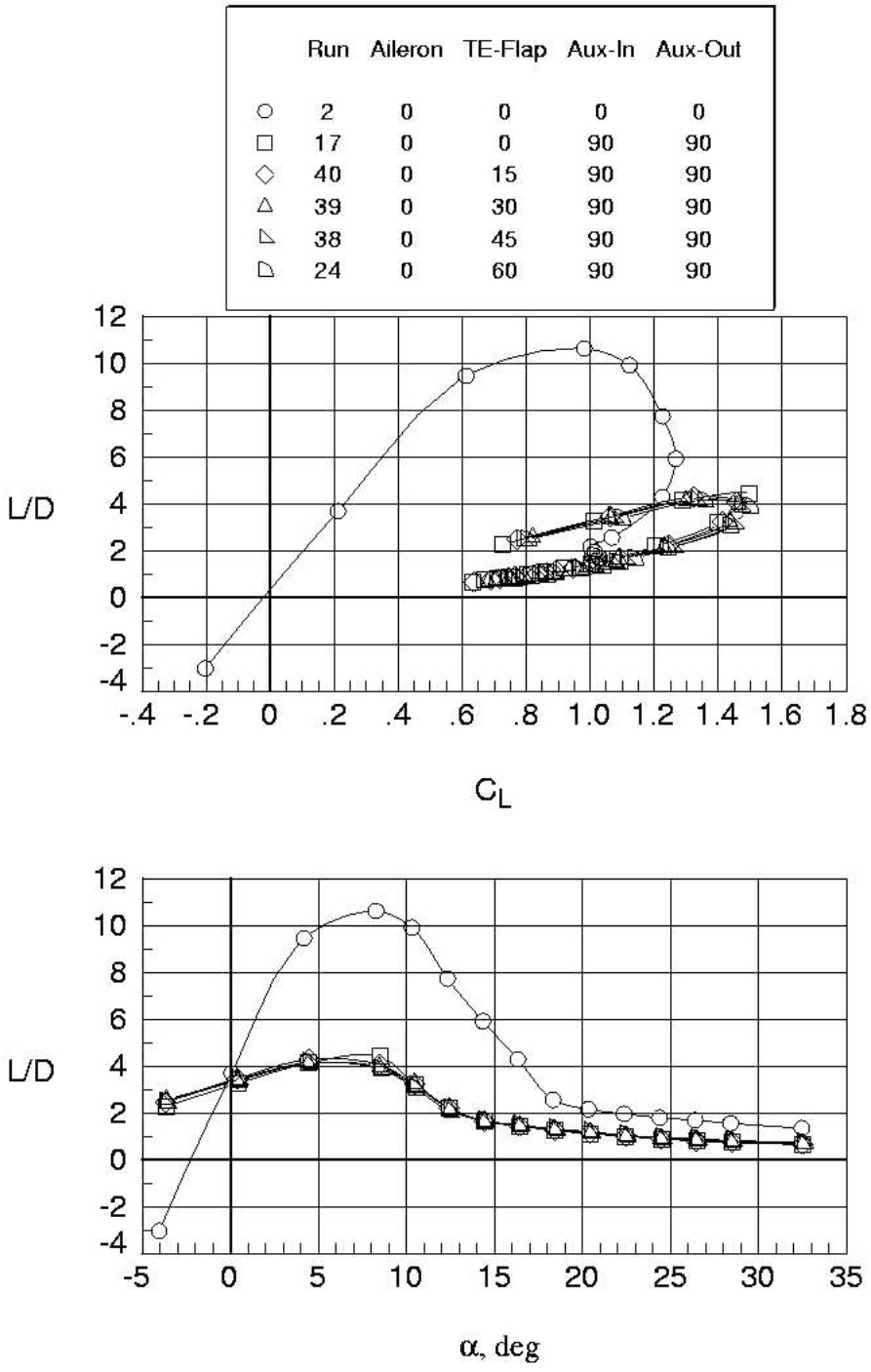

(c) Lift-to-drag ratios.

Figure 8. Continued.

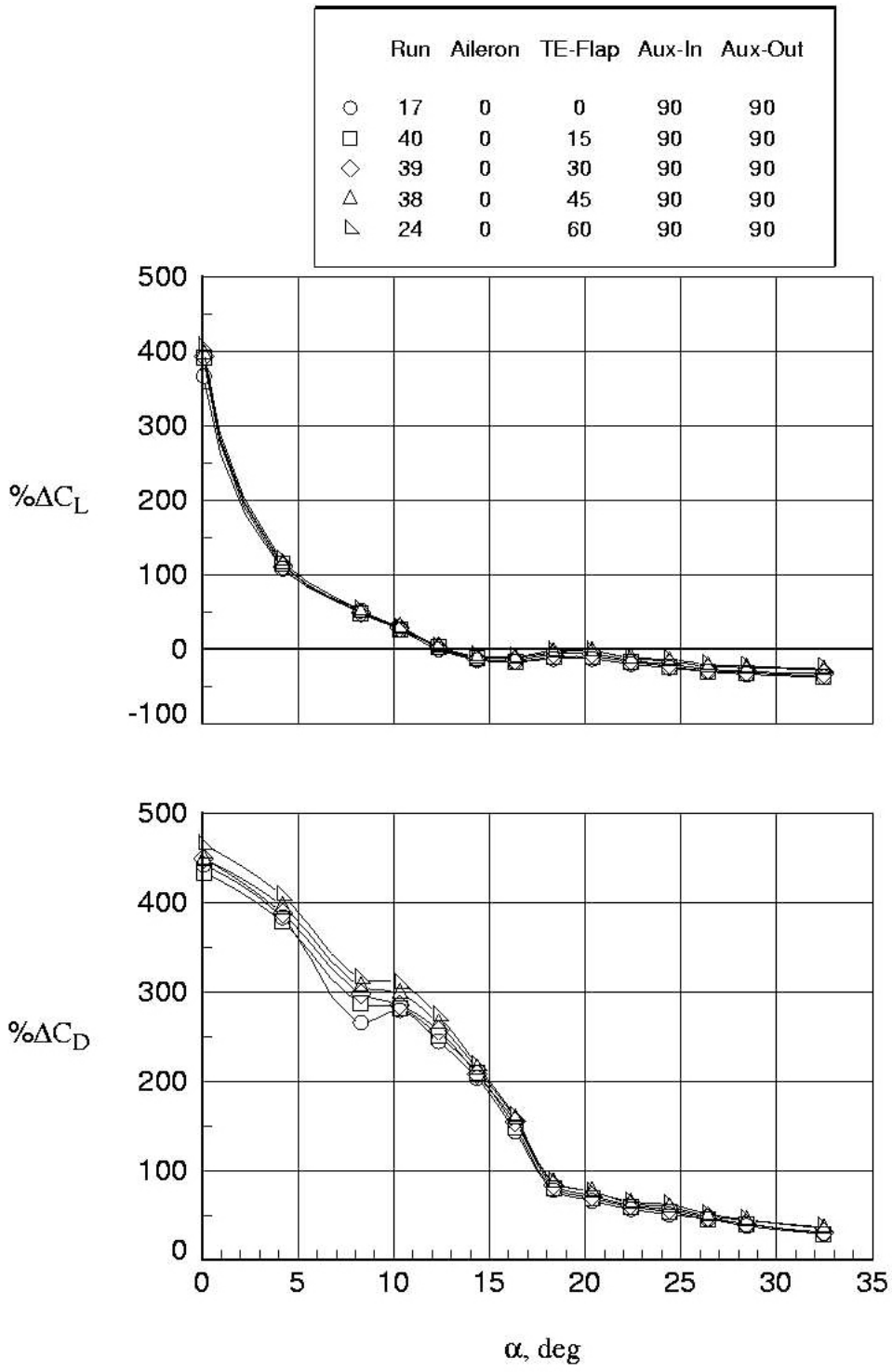

(d) Percent delta changes; baseline = run 2 (aileron deflection = 0°, TE-flap deflection = 0°, aux-in deflection = 0°, aux-out deflection = 0°).

Figure 8. Concluded.

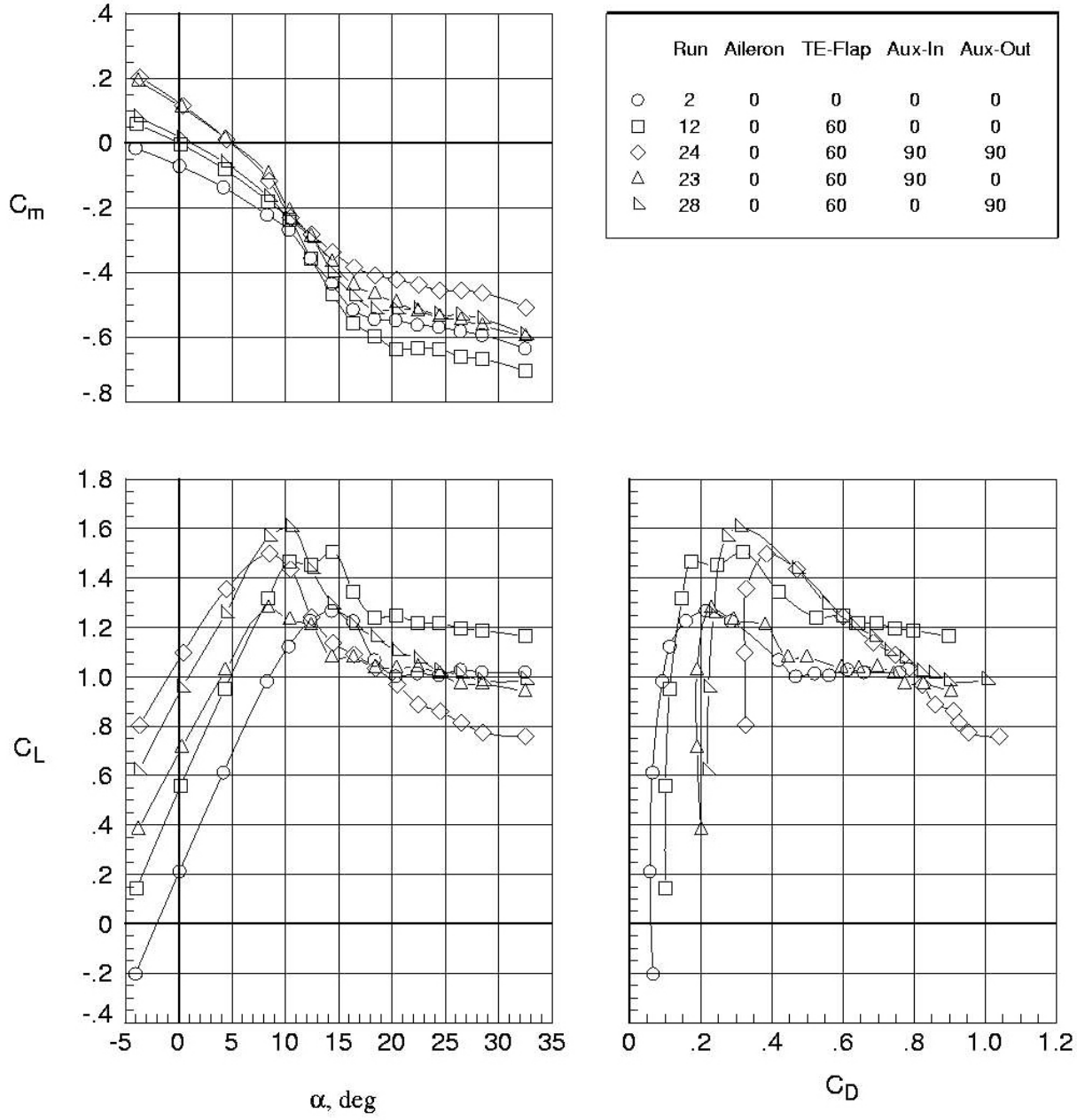

(a) Longitudinal aerodynamics.

Figure 9. Effect of 60° split flap deflection on 90° auxiliary flap performance; q = 4.0 psf.

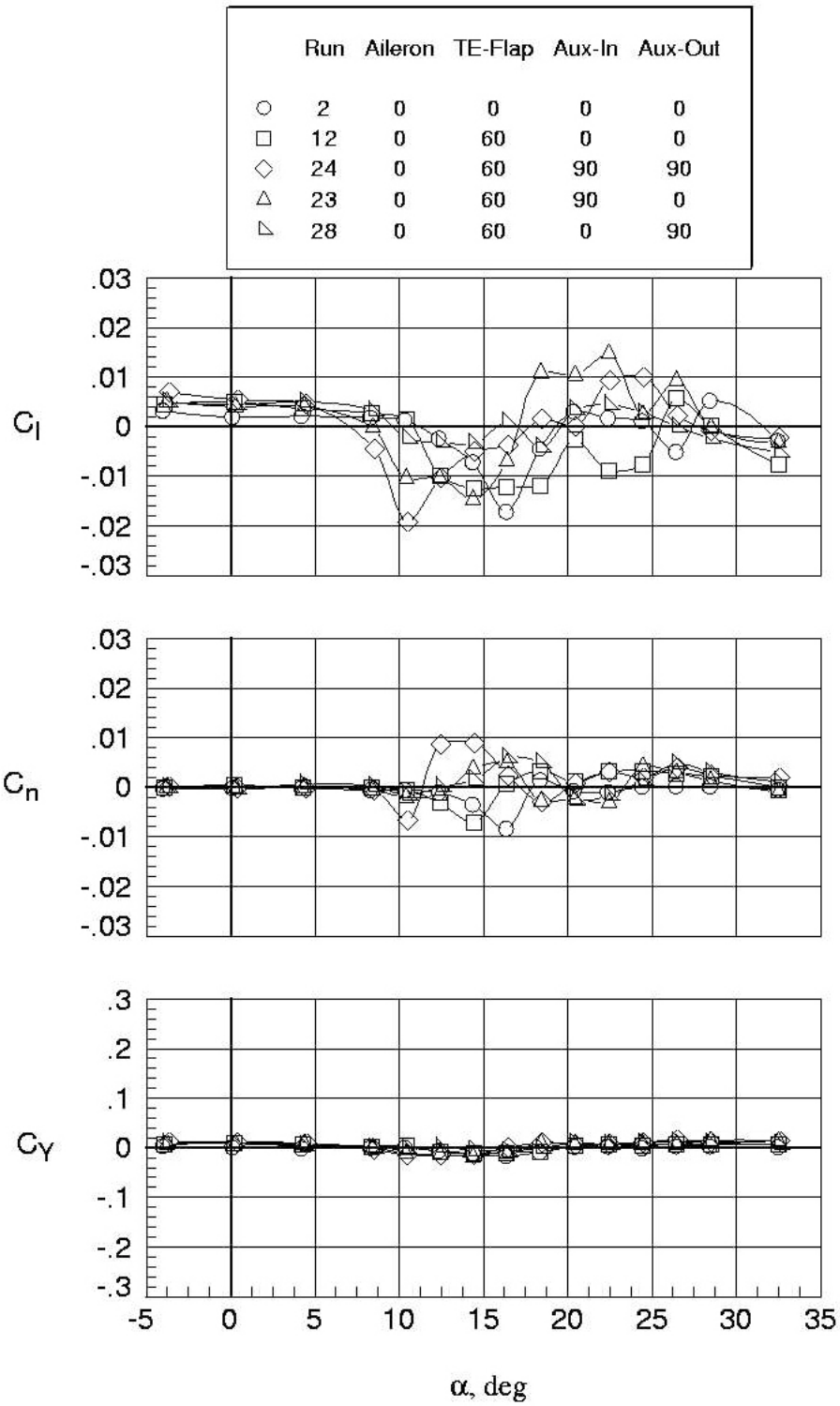

(b) Lateral aerodynamics.

Figure 9. Continued.

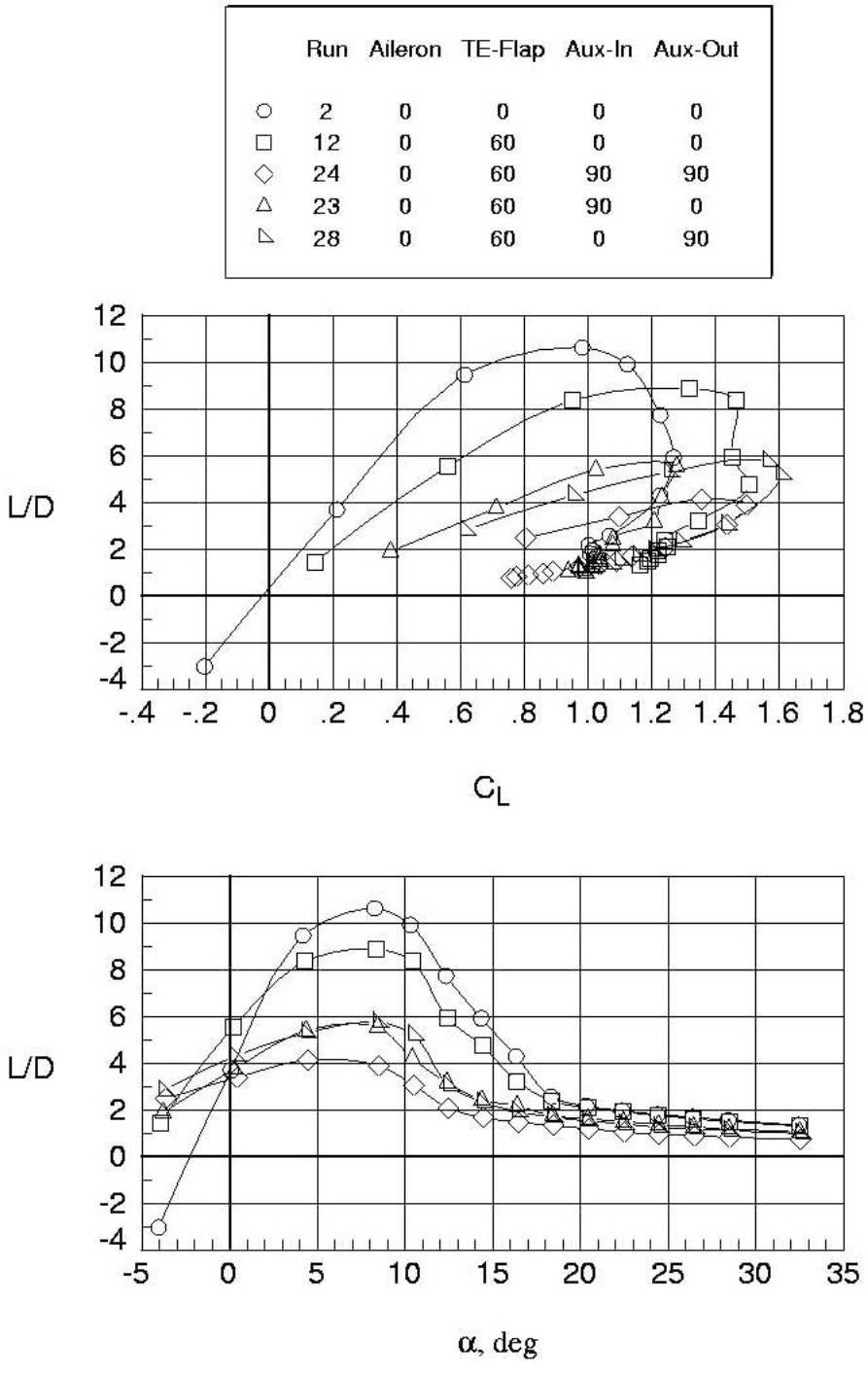

(c) Lift-to-drag ratios.

Figure 9. Continued.

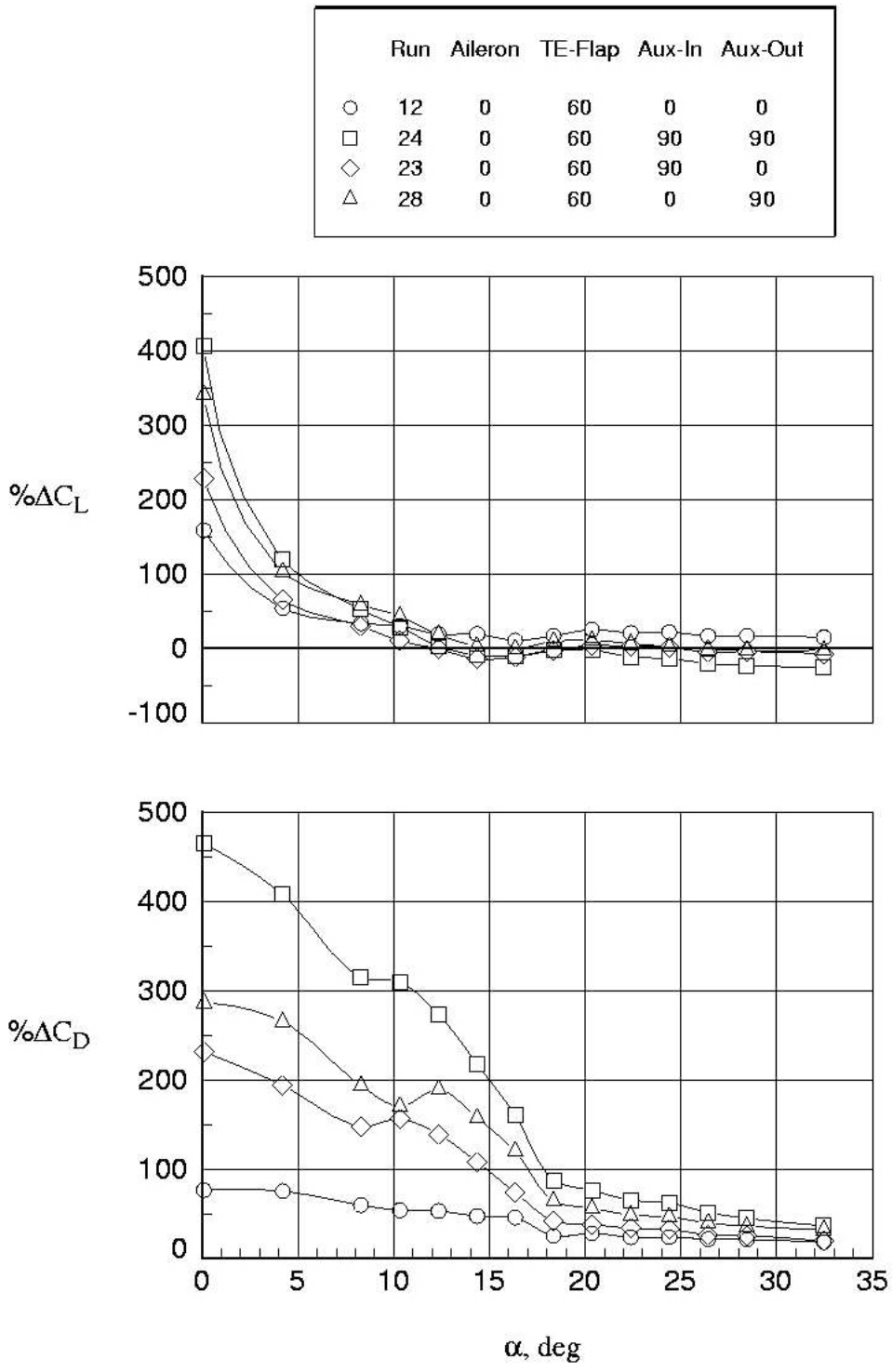

(d) Percent delta changes; baseline = run 2 (aileron deflection = 0°, TE-flap deflection = 0°, aux-in deflection = 0°, aux-out deflection = 0°).

Figure 9. Concluded.

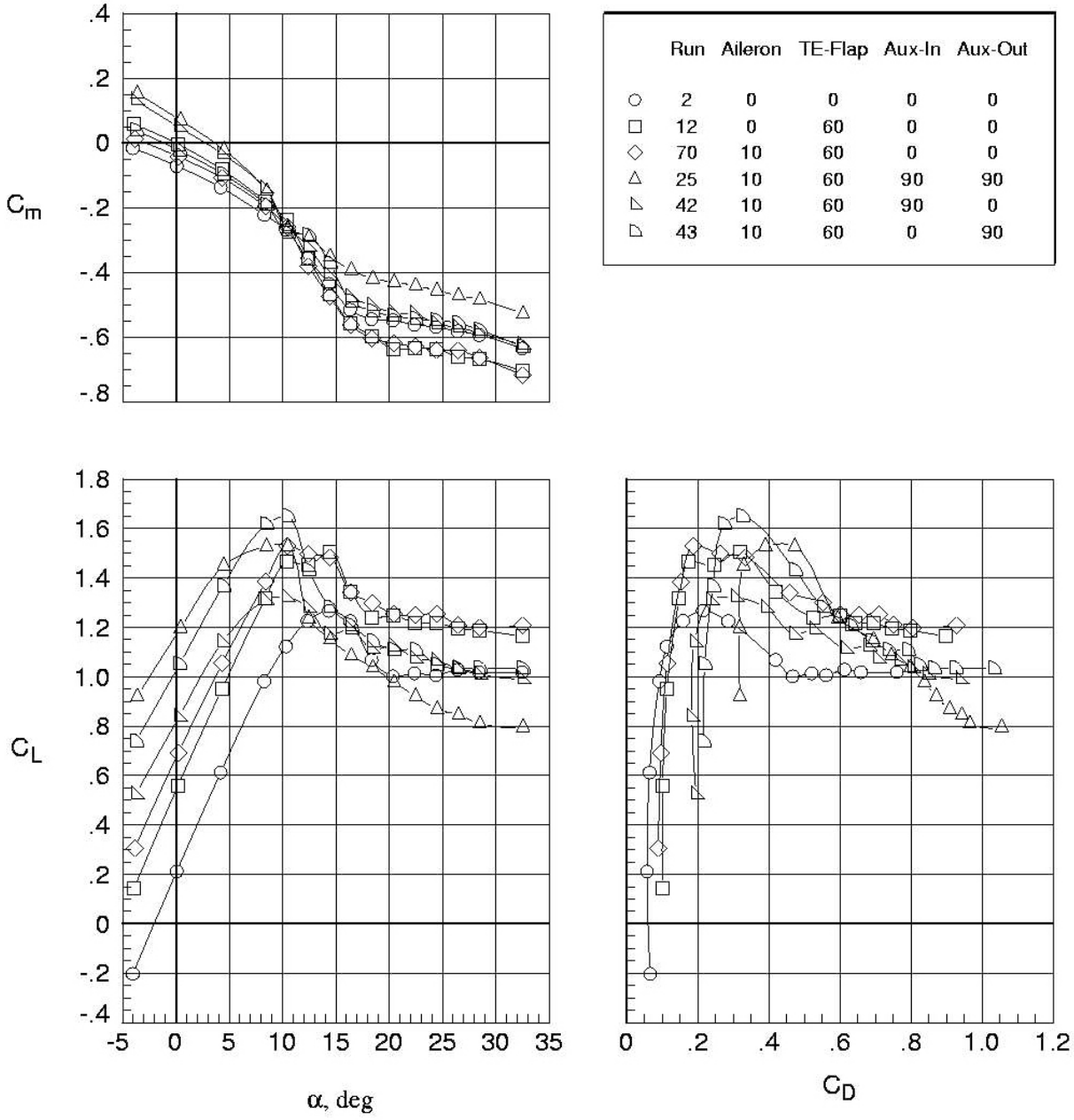

(a) Longitudinal aerodynamics.

Figure 10. Use of aileron as flap with 90° auxiliary flap; q = 4.0 psf.

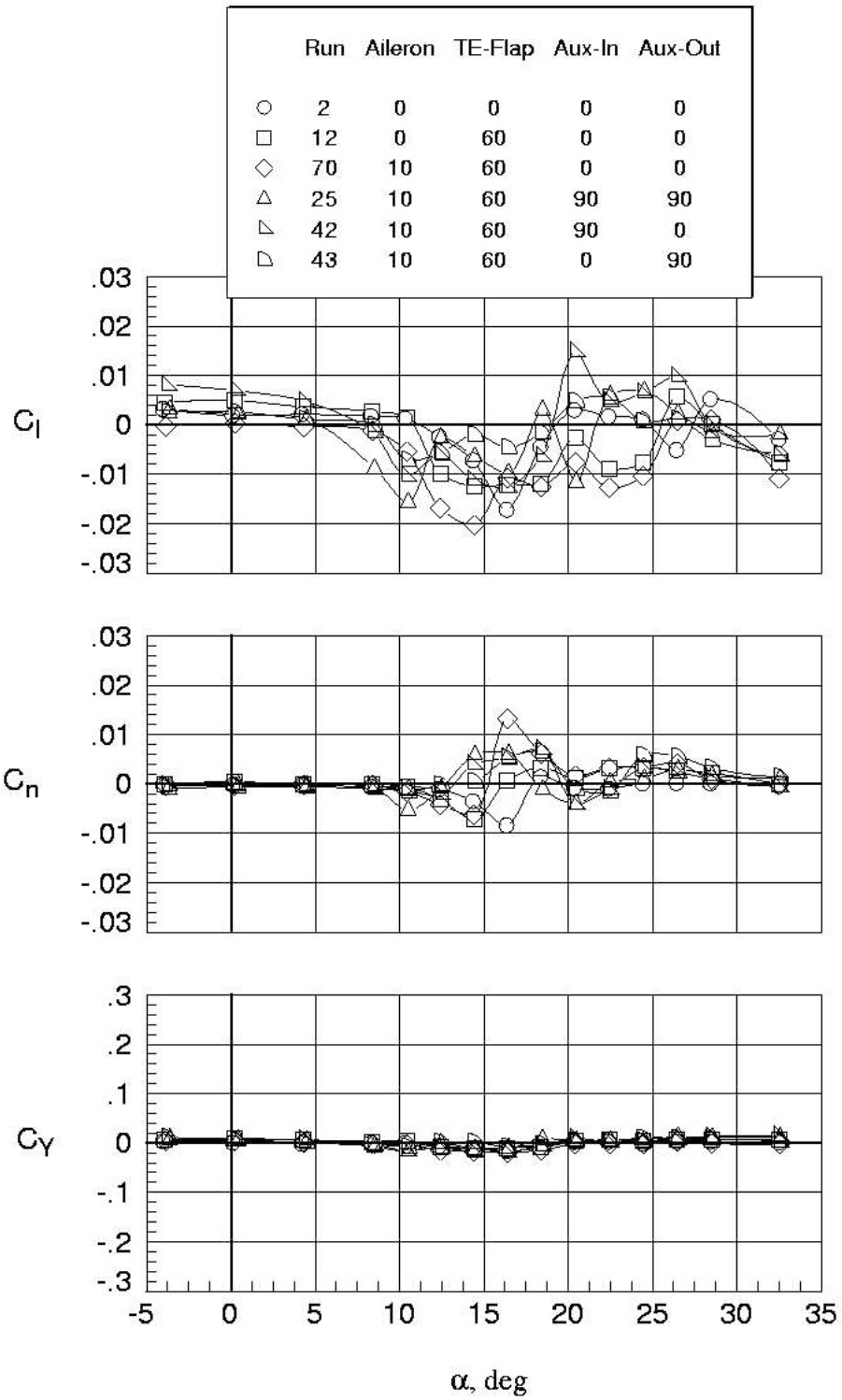

(b) Lateral aerodynamics.

Figure 10. Continued.

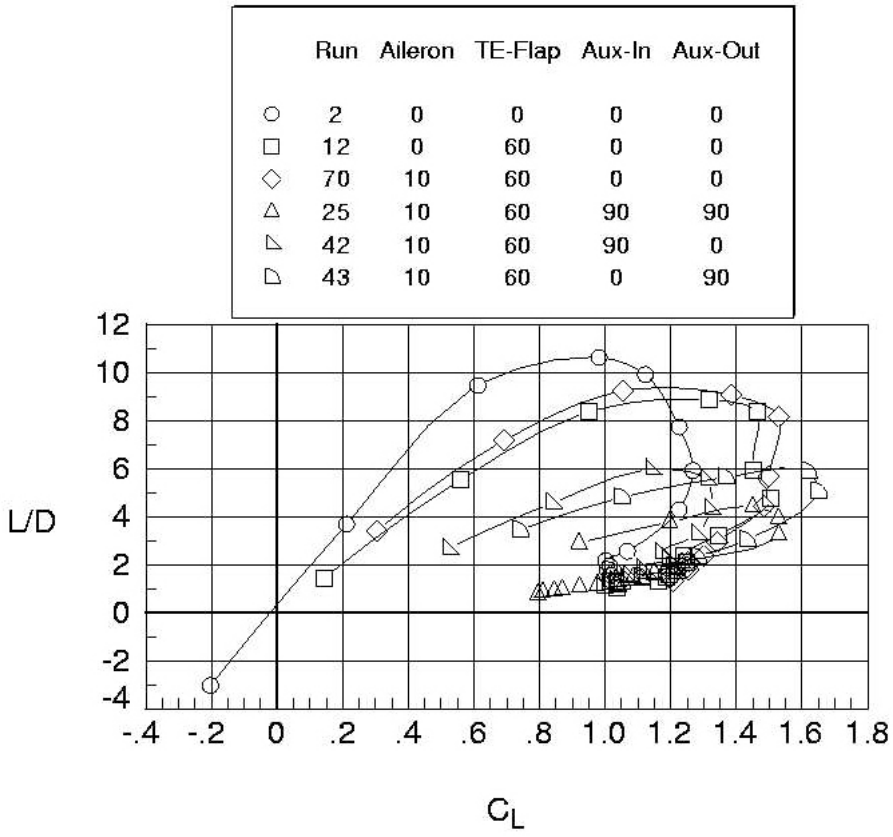

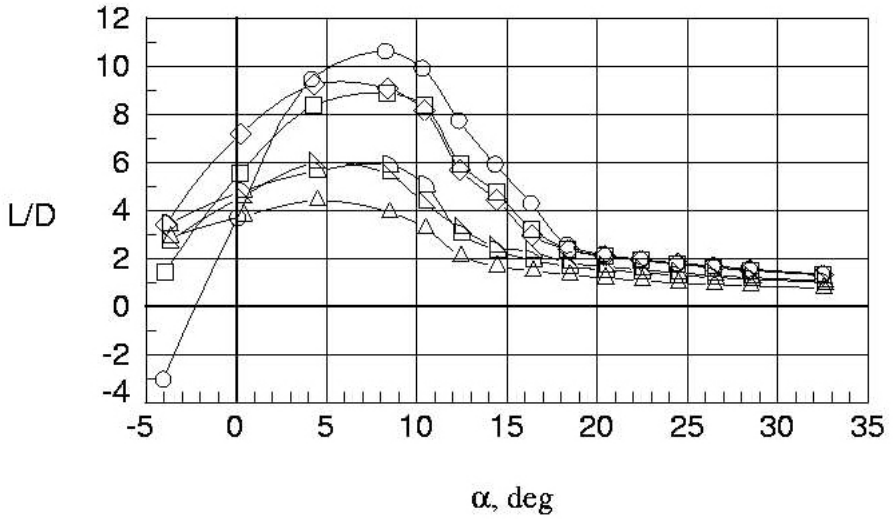

(c) Lift-to-drag ratios.

Figure 10. Continued.

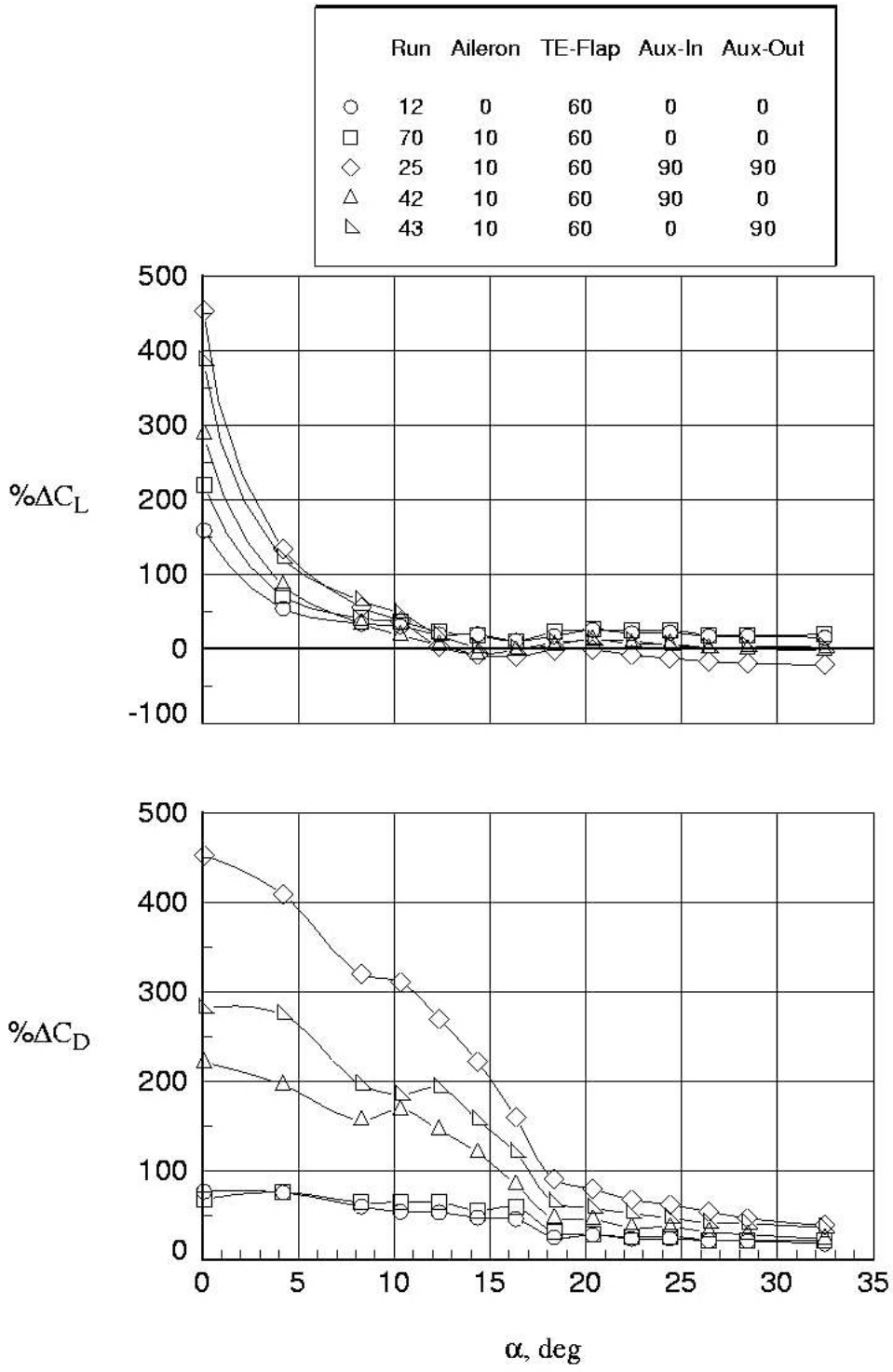

(d) Percent delta changes; baseline = run 2 (aileron deflection = 0°, TE-flap deflection = 0°, aux-in deflection = 0°, aux-out deflection = 0°).

Figure 10. Concluded.

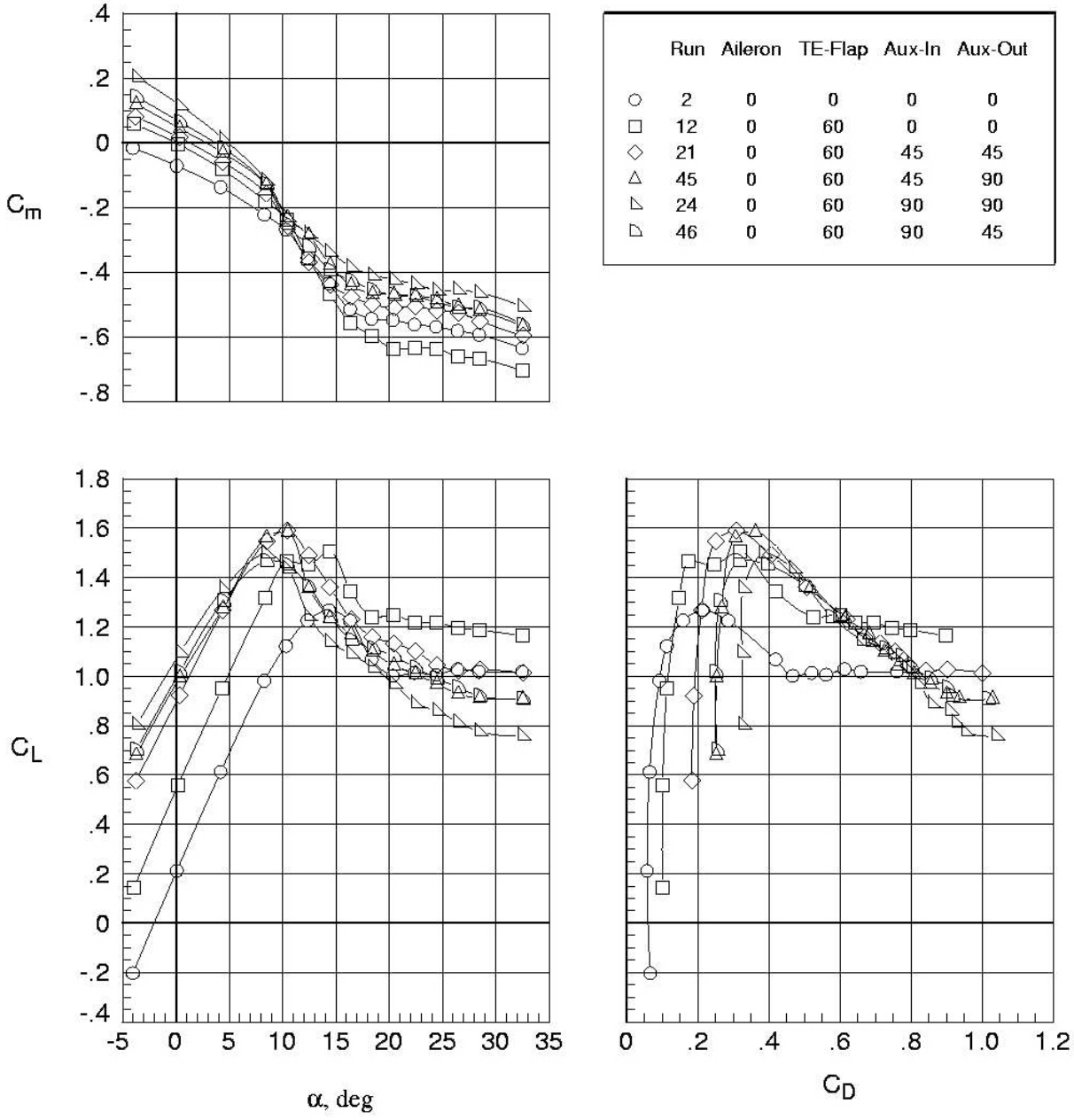

(a) Longitudinal aerodynamics.

Figure 11. Effects of mixing 45° and 90° auxiliary flaps; q = 4.0 psf.

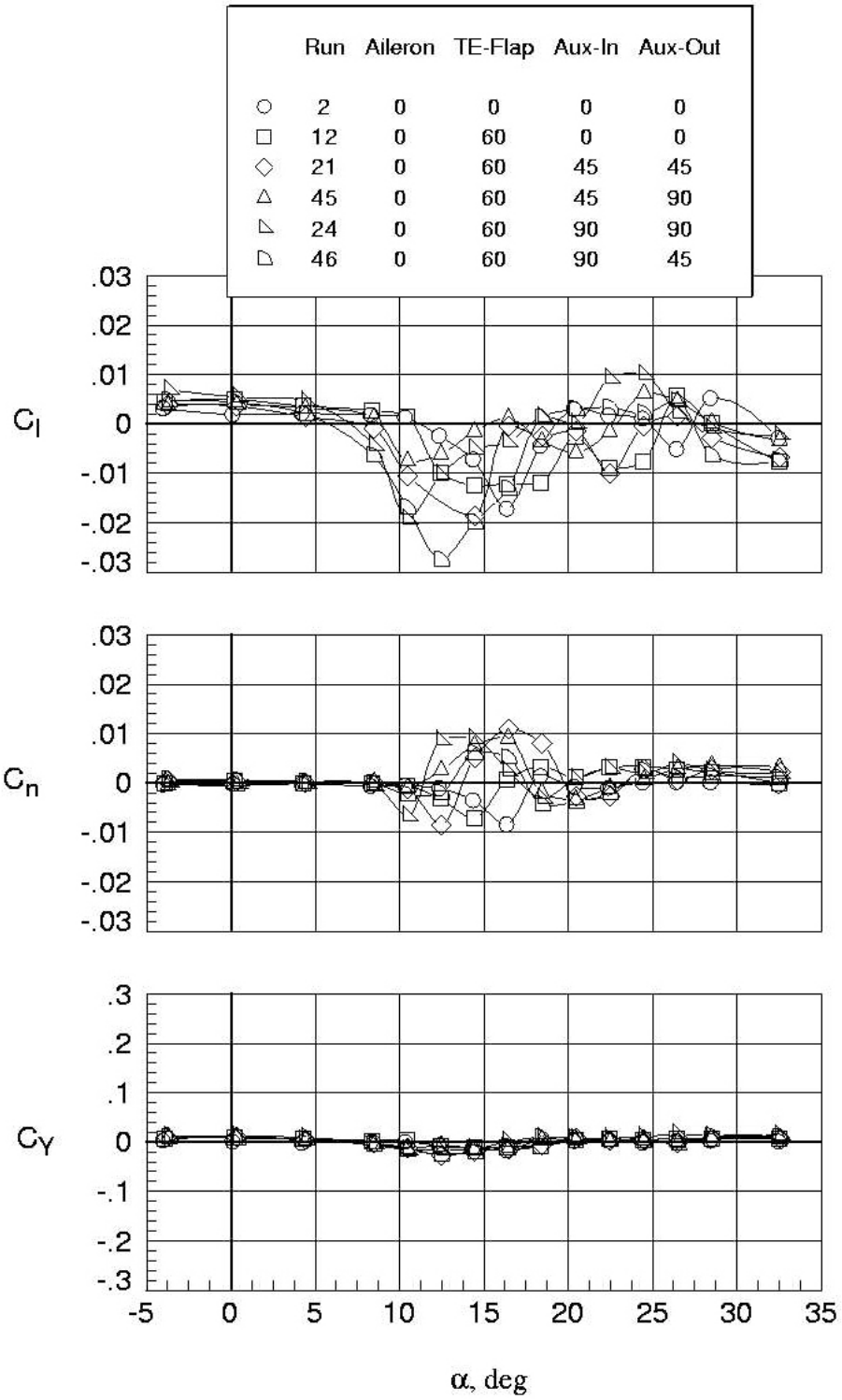

(b) Lateral aerodynamics.

Figure 11. Continued.

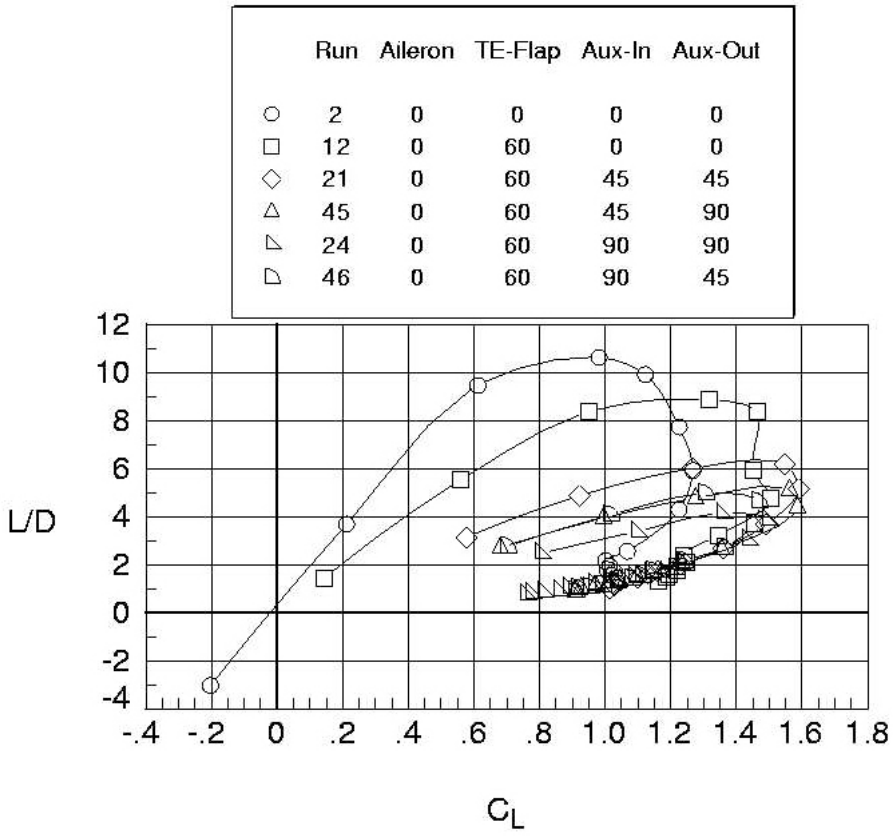

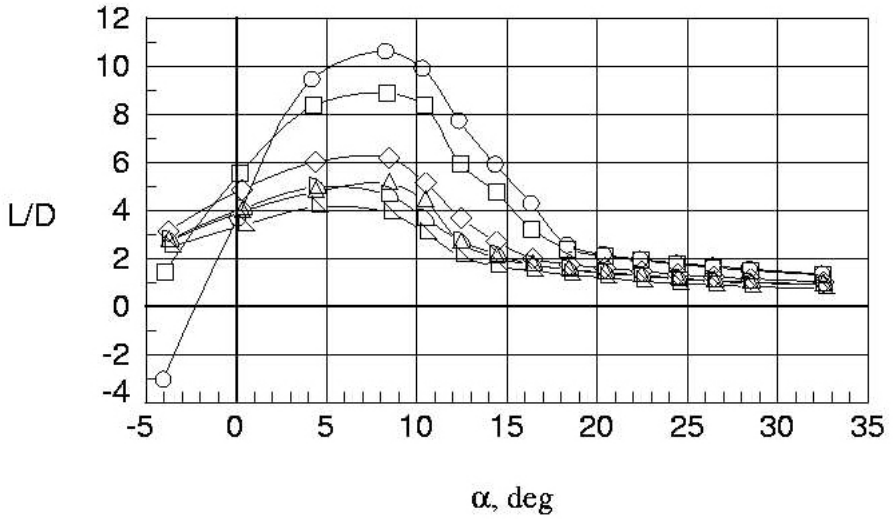

(c) Lift-to-drag ratios.

Figure 11. Continued.

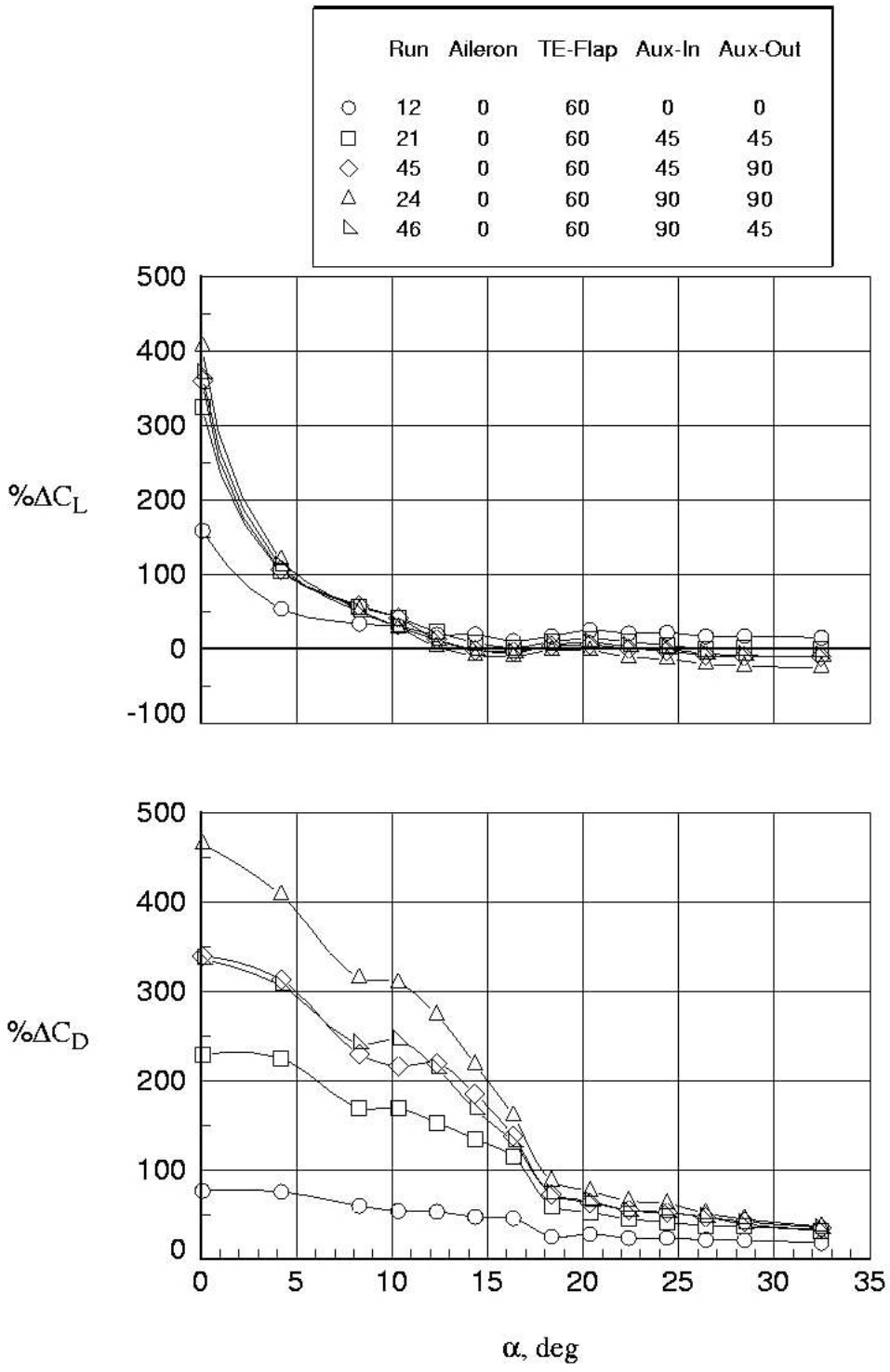

(d) Percent delta changes; baseline = run 2 (aileron deflection = 0°, TE-flap deflection = 0°, aux-in deflection = 0°, aux-out deflection = 0°).

Figure 11. Concluded.

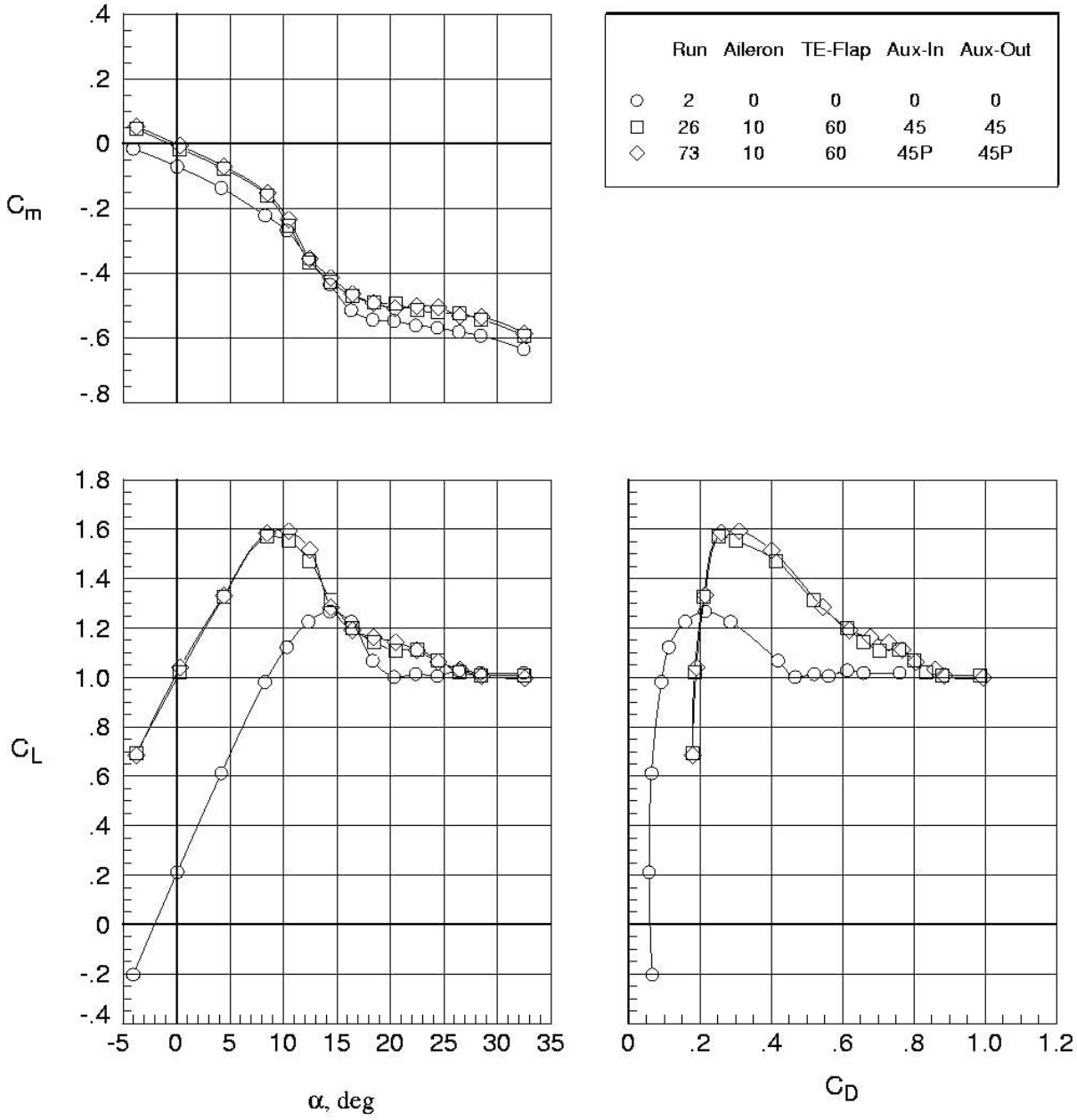

(a) Longitudinal aerodynamics.

Figure 12. Comparison of baseline and sharpened leading edge auxiliary flaps; q = 4.0 psf.

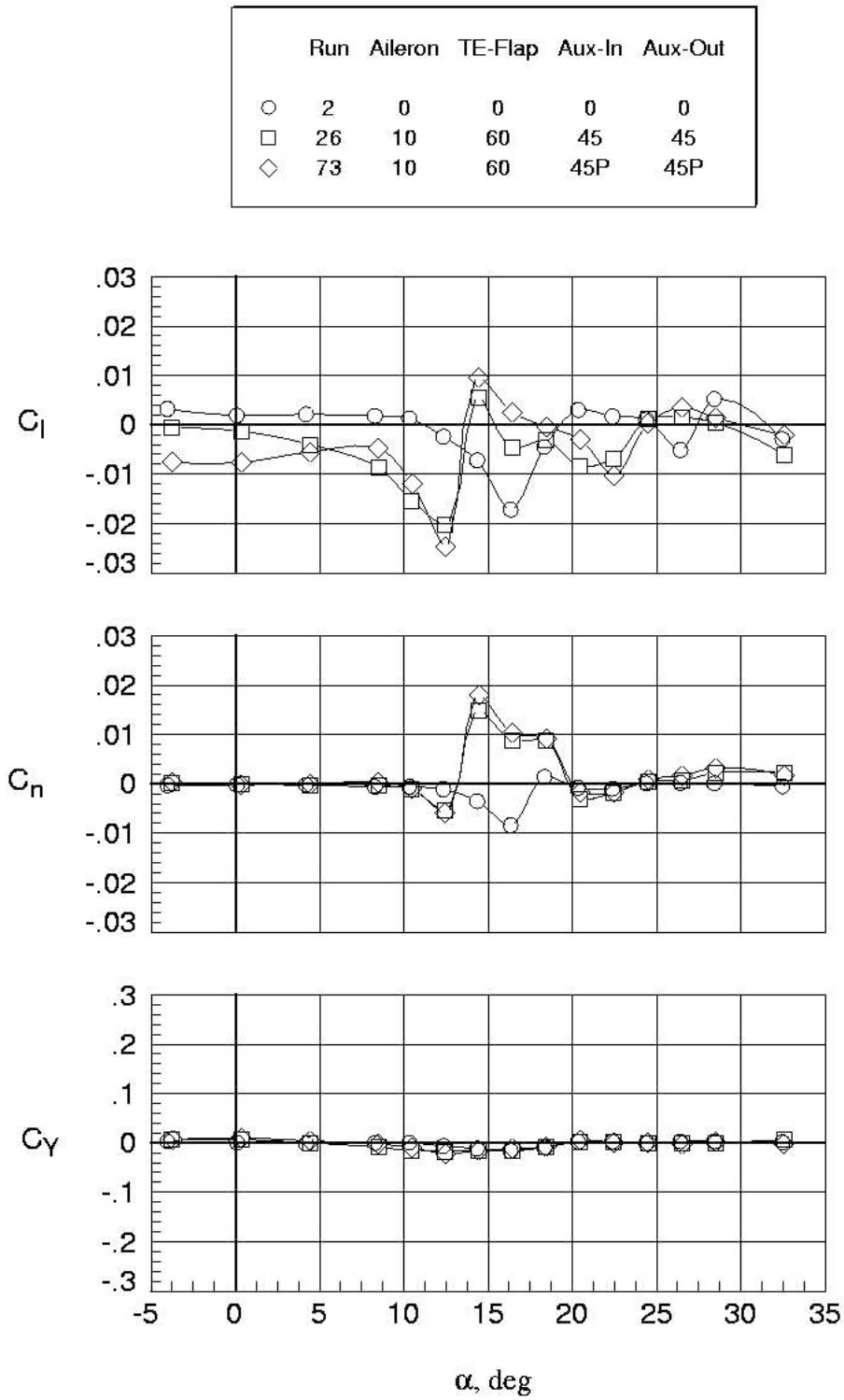

(b) Lateral aerodynamics.

Figure 12. Continued.

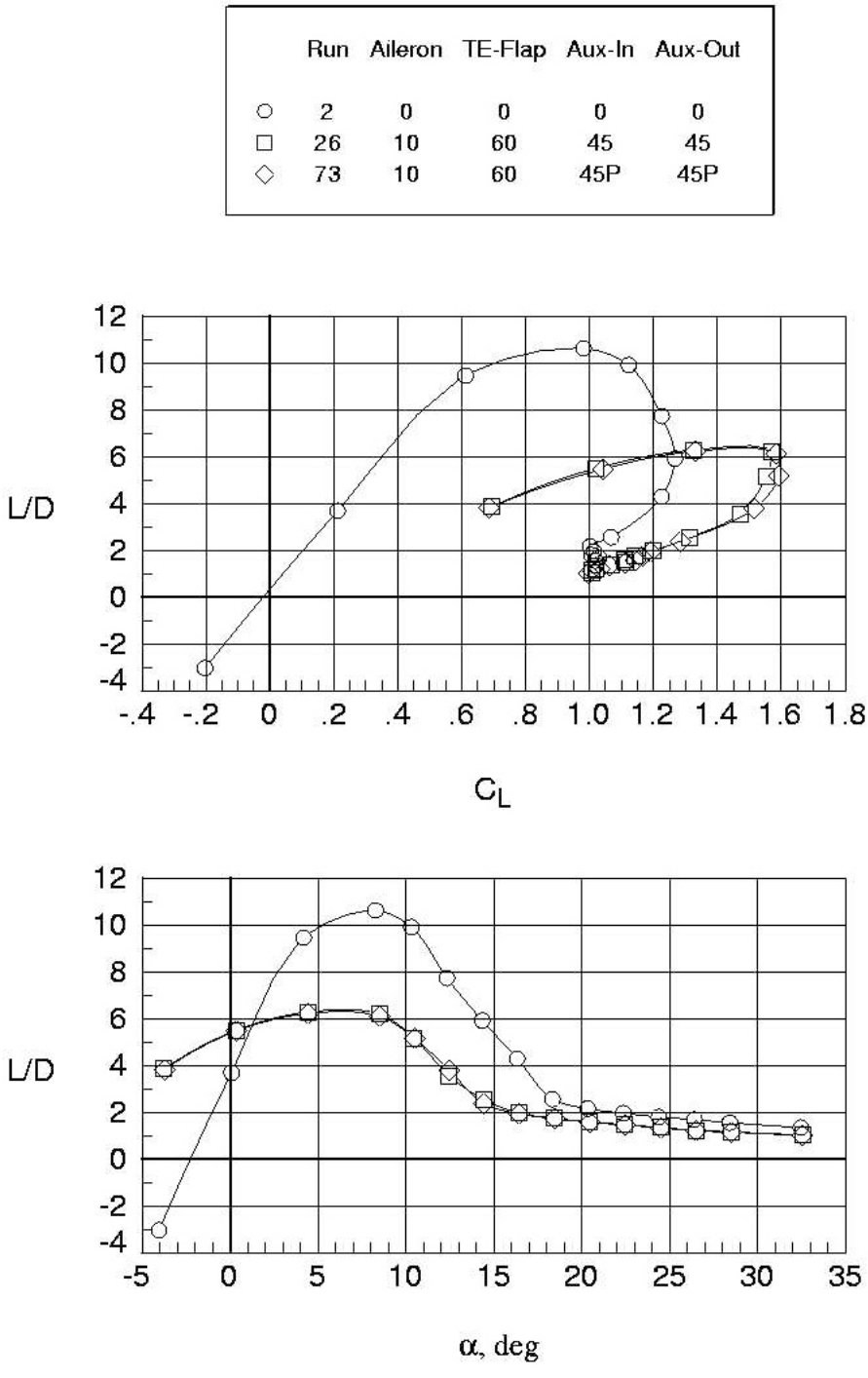

(c) Lift-to-drag ratios.

Figure 12. Continued.

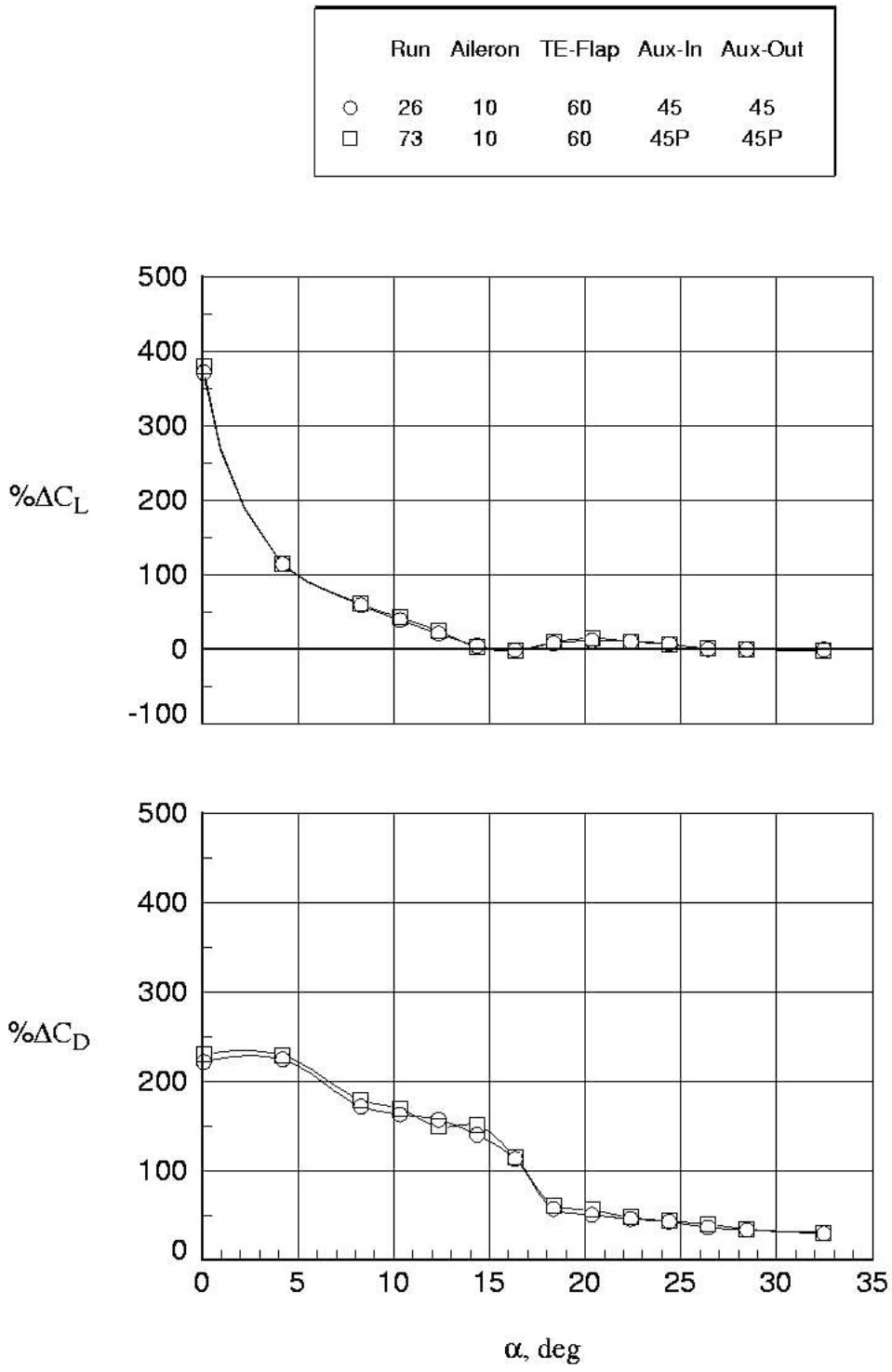

(d) Percent delta changes; baseline = run 2 (aileron deflection = 0°, TE-flap deflection = 0°, aux-in deflection = 0°, aux-out deflection = 0°).

Figure 12. Concluded.

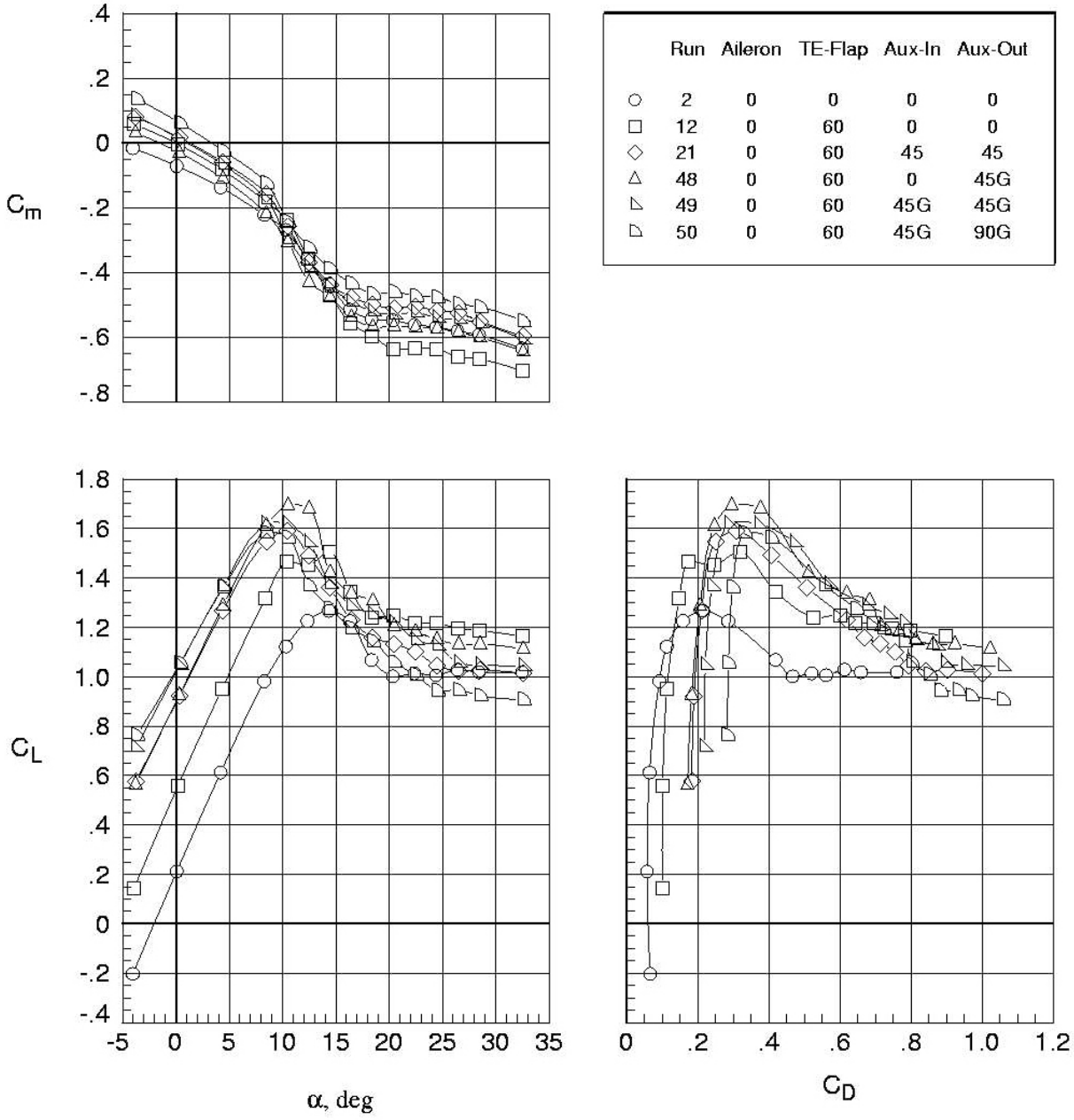

(a) Longitudinal aerodynamics.

Figure 13. Comparison of auxiliary flaps with Gurney labs; q = 4.0 psf.

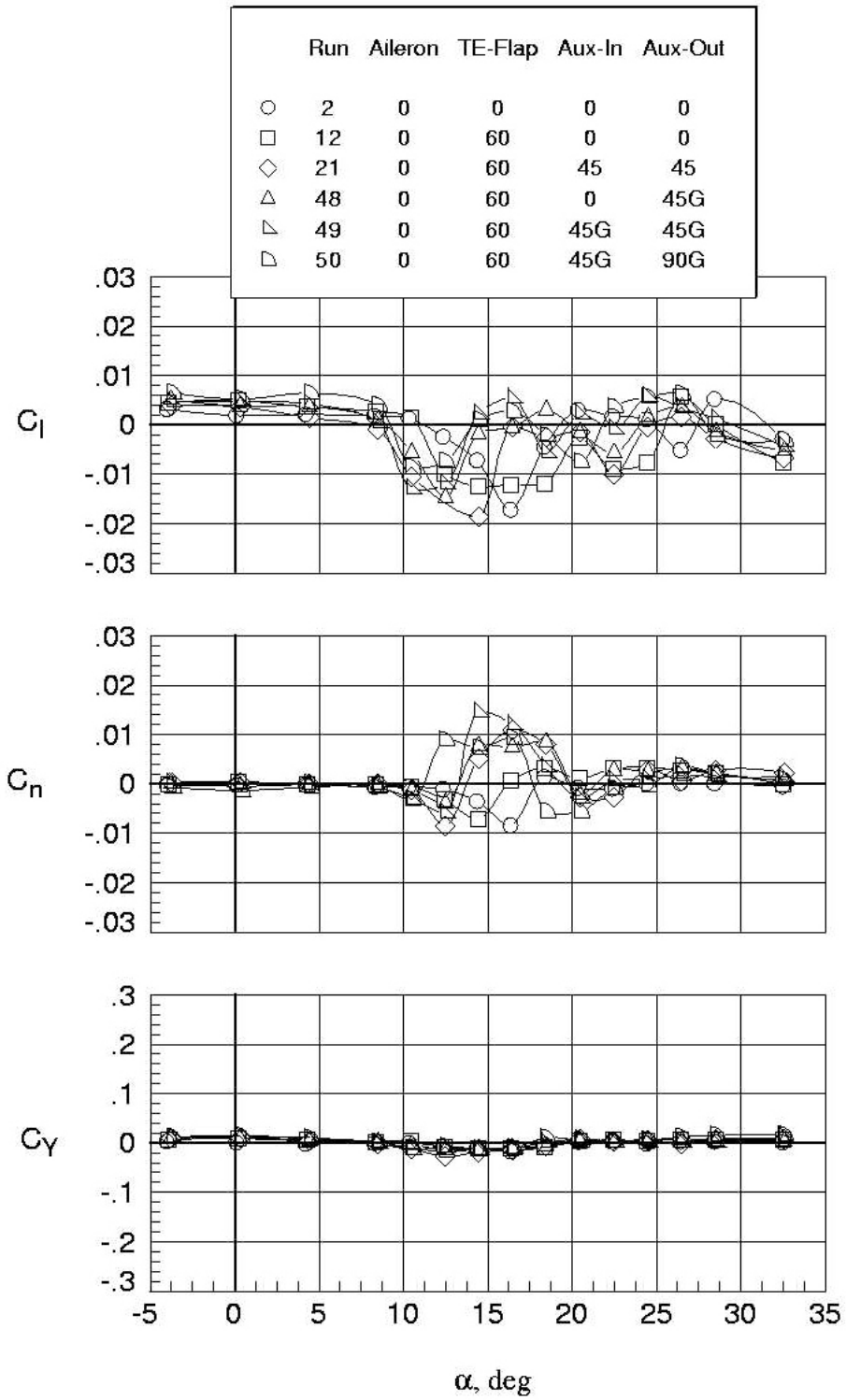

(b) Lateral aerodynamics.

Figure 13. Continued.

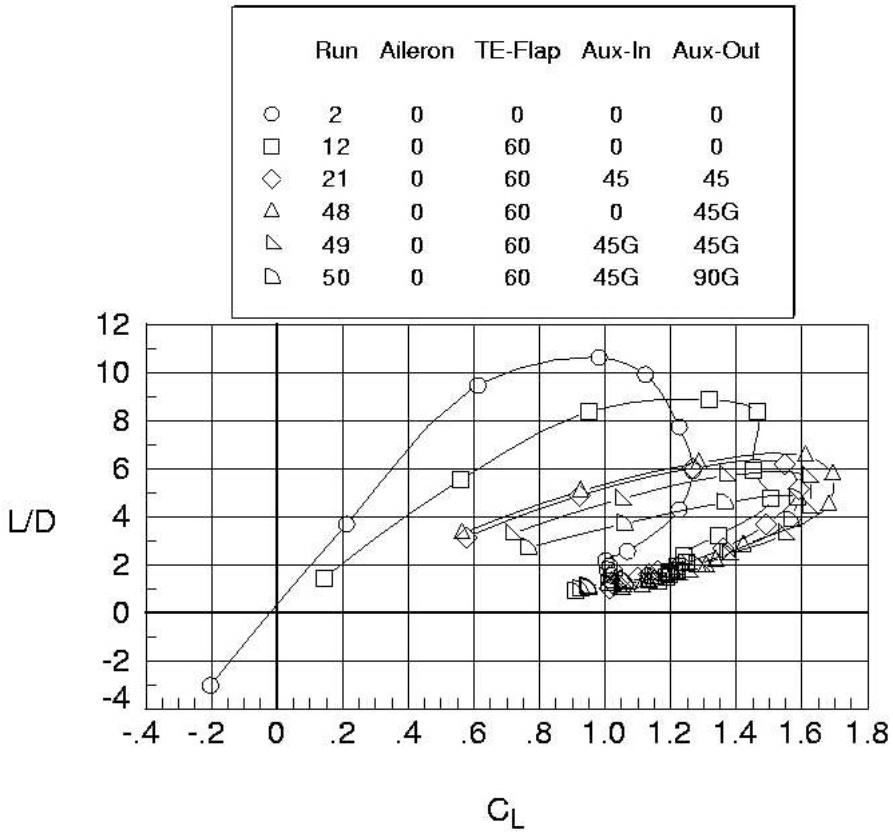

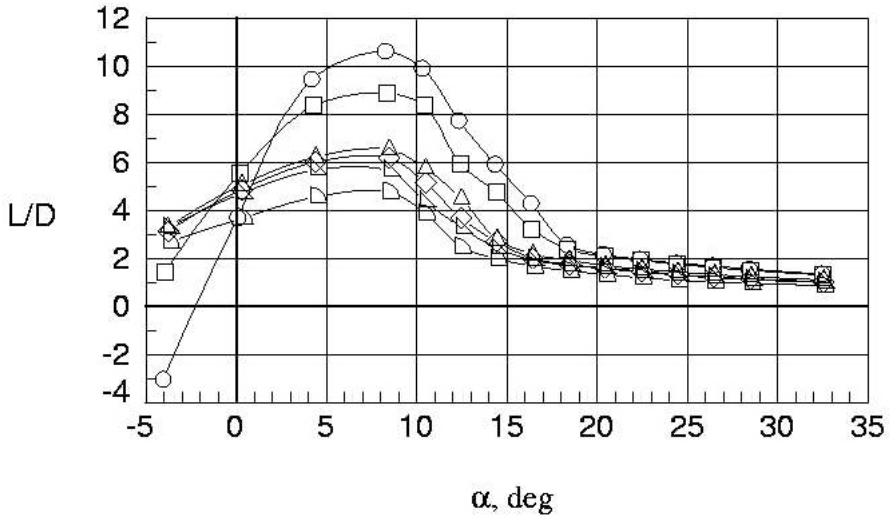

(c) Lift-to-drag ratios.

Figure 13. Continued.

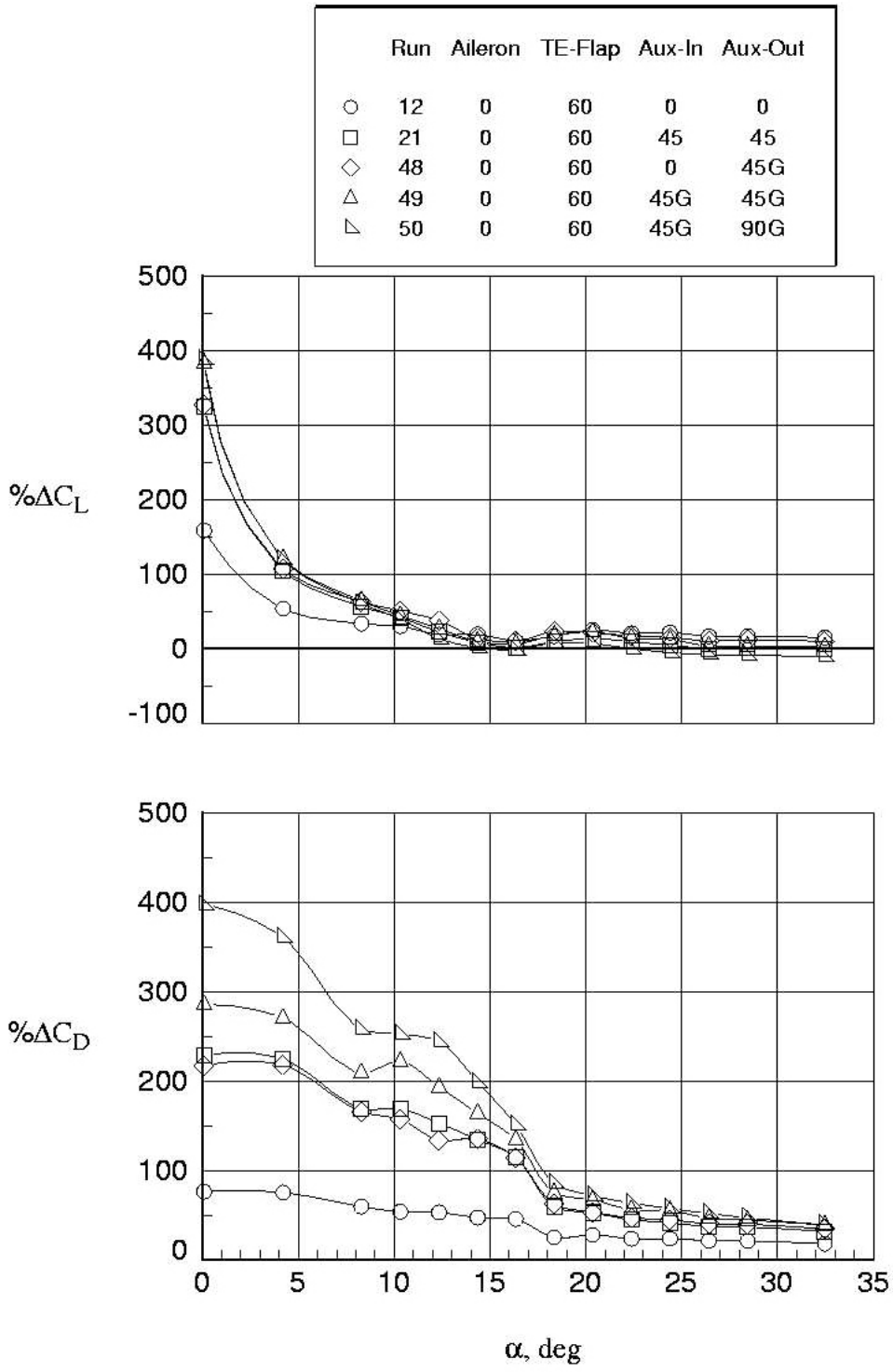

(d) Percent delta changes; baseline = run 2 (aileron deflection = 0°, TE-flap deflection = 0°, aux-in deflection = 0°, aux-out deflection = 0°).

Figure 13. Concluded.

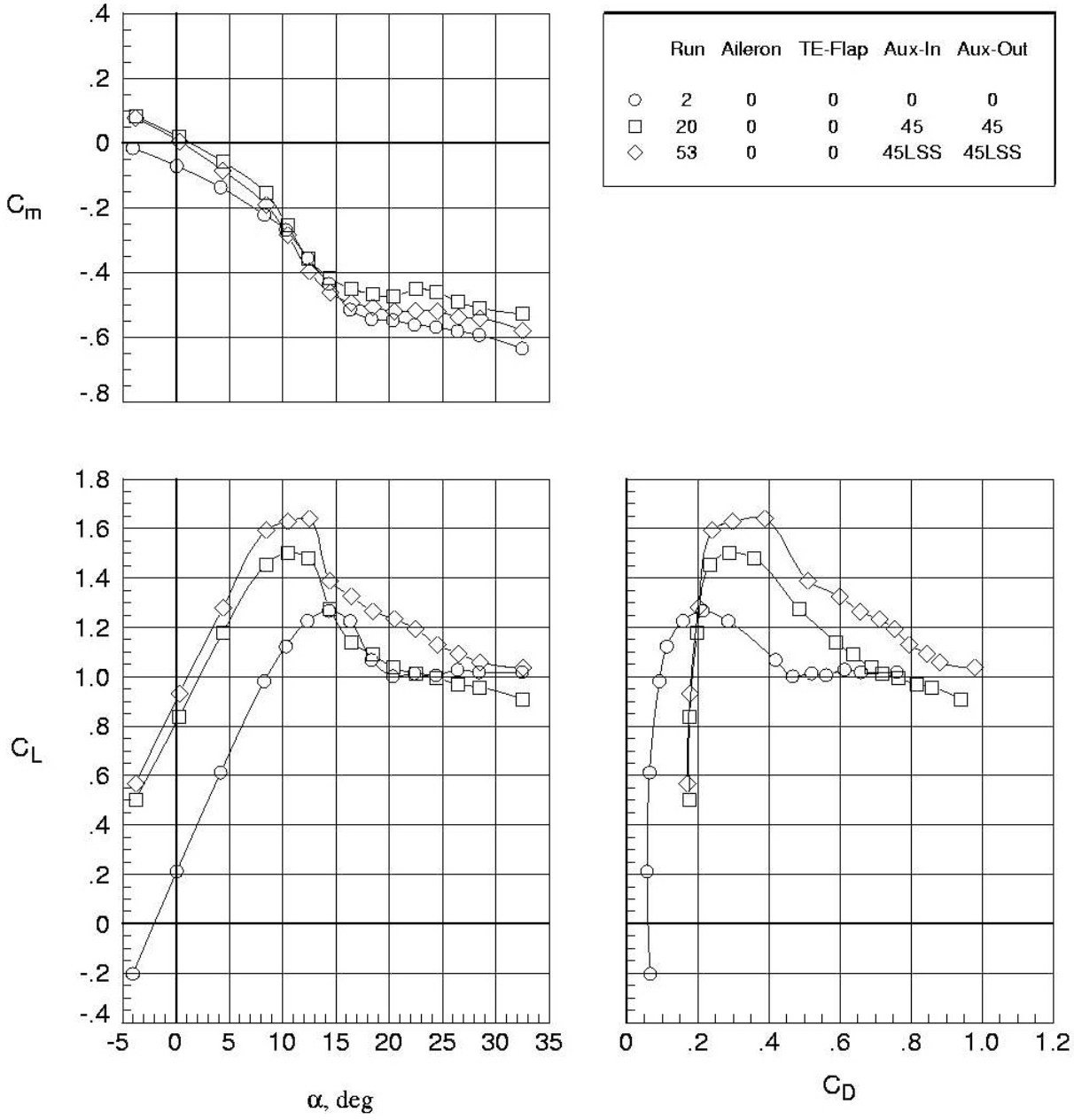

(a) Longitudinal aerodynamics.

Figure 14. Comparison of 45° auxiliary flap with lower surface spoiler; q = 4.0 psf.

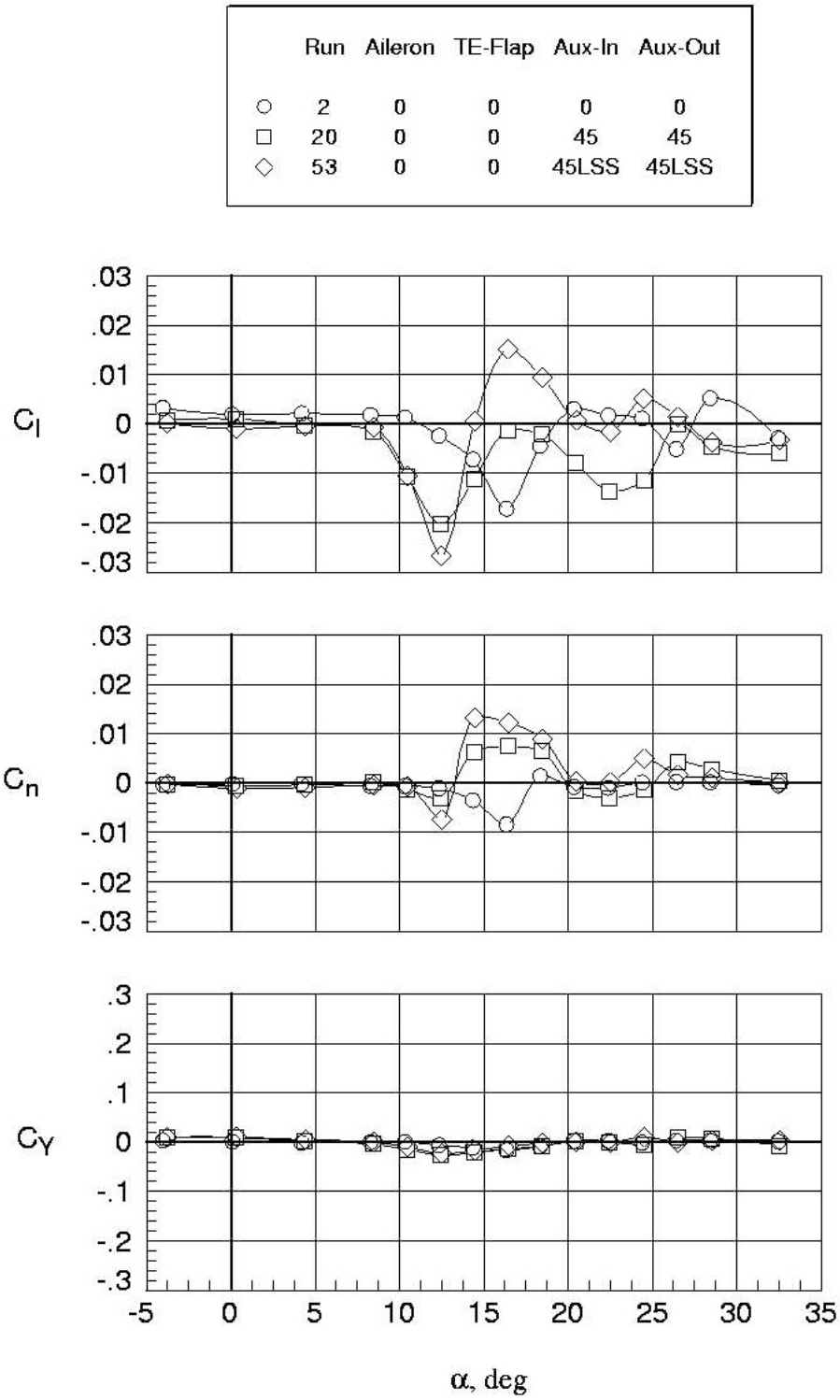

(b) Lateral aerodynamics.

Figure 14. Continued.

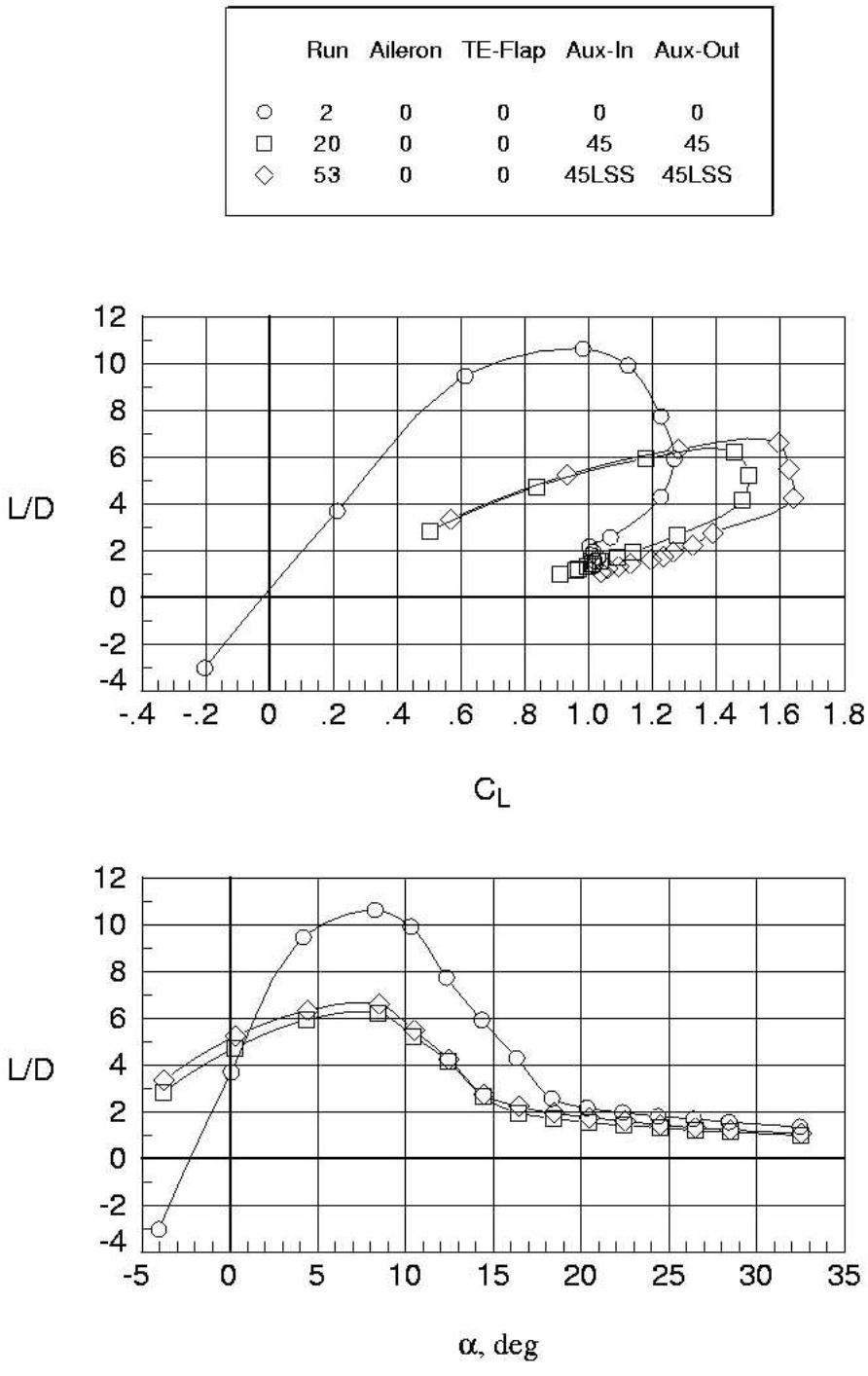

(c) Lift-to-drag ratios.

Figure 14. Continued.

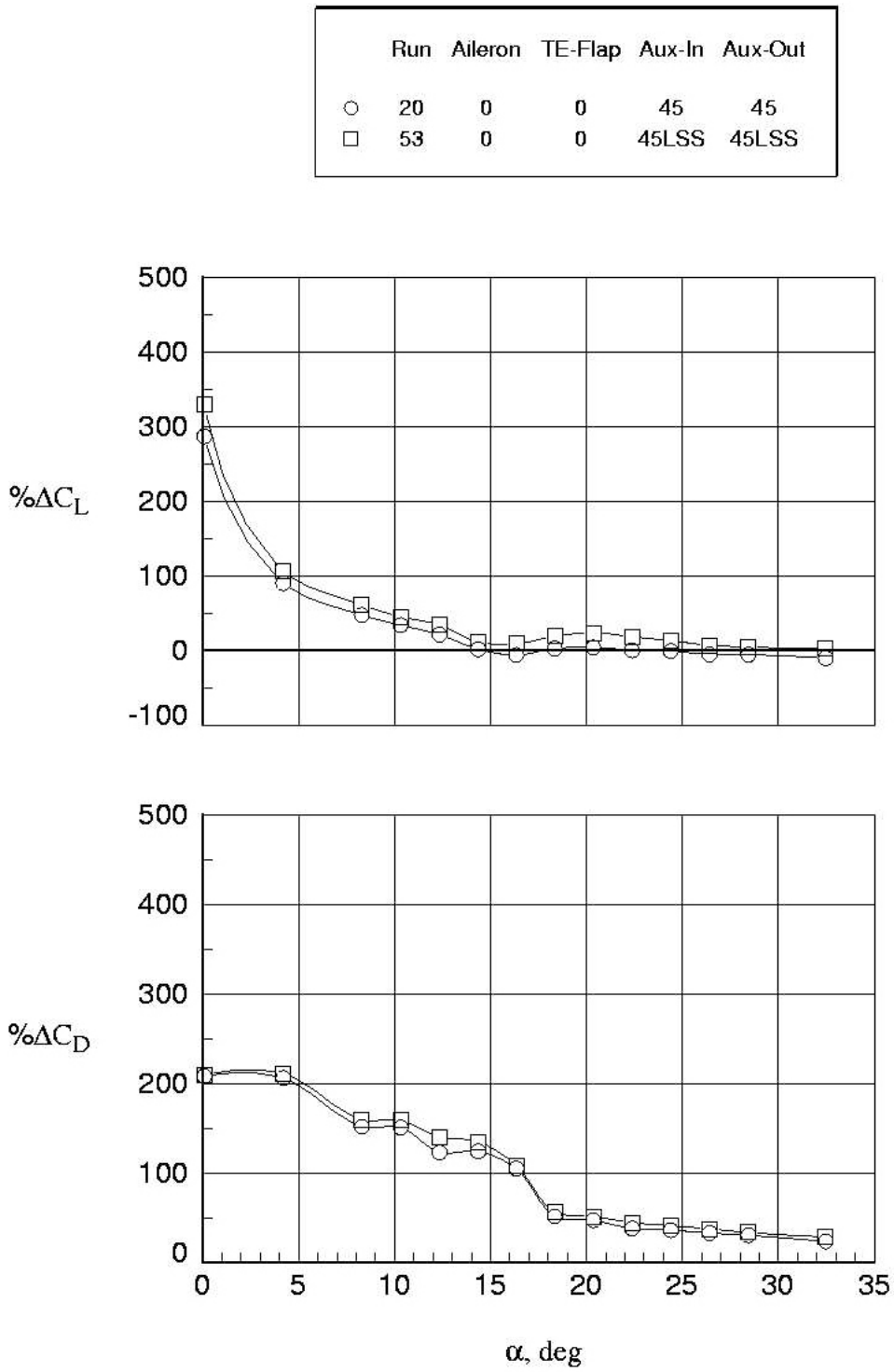

(d) Percent delta changes; baseline = run 2 (aileron deflection = 0°, TE-flap deflection = 0°, aux-in deflection = 0°, aux-out deflection = 0°).

Figure 14. Concluded.

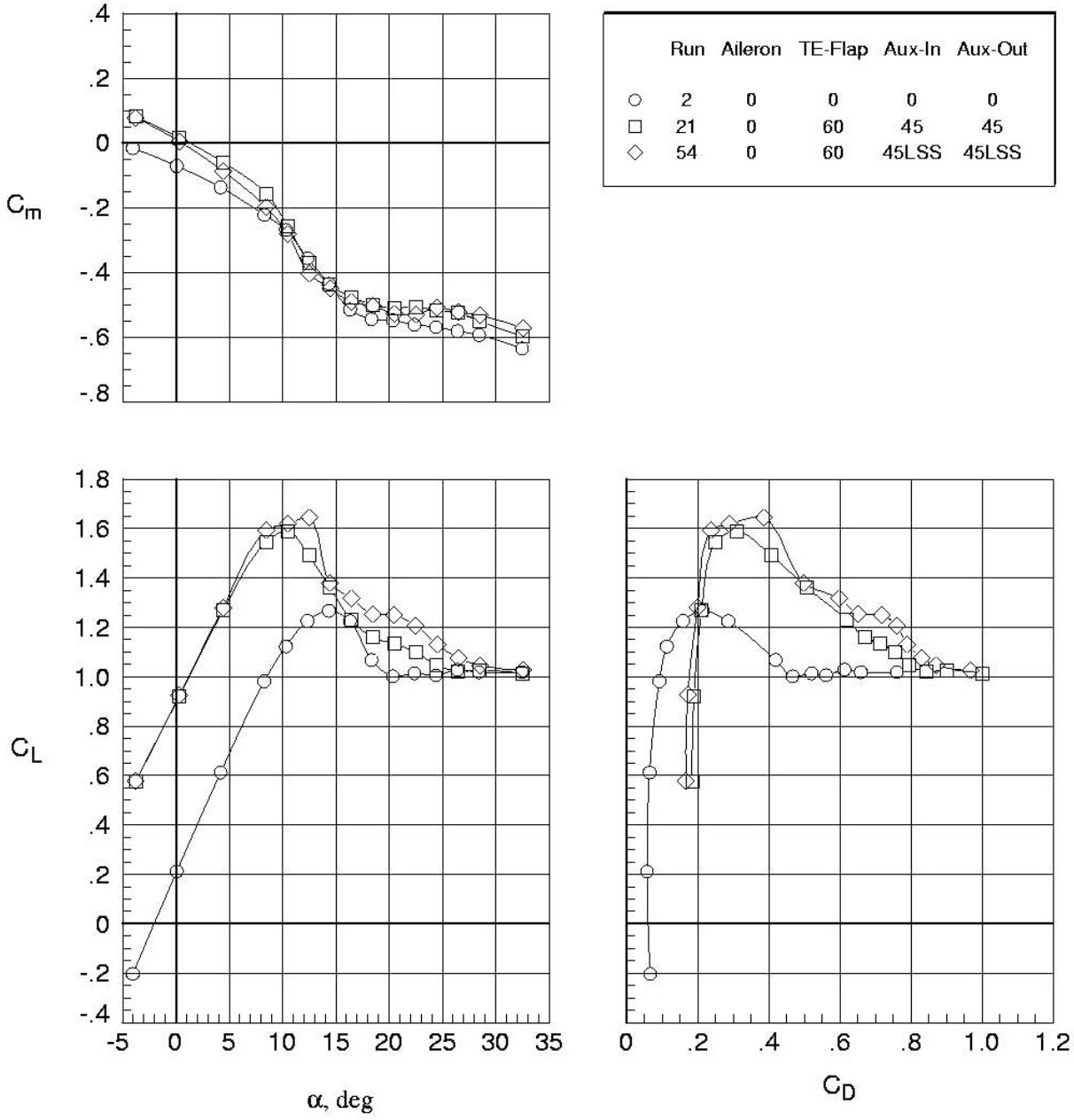

(a) Longitudinal aerodynamics.

Figure 15. Comparison of 45° auxiliary flap with lower surface spoiler; TE flap deflection = 60°, q = 4.0 psf.

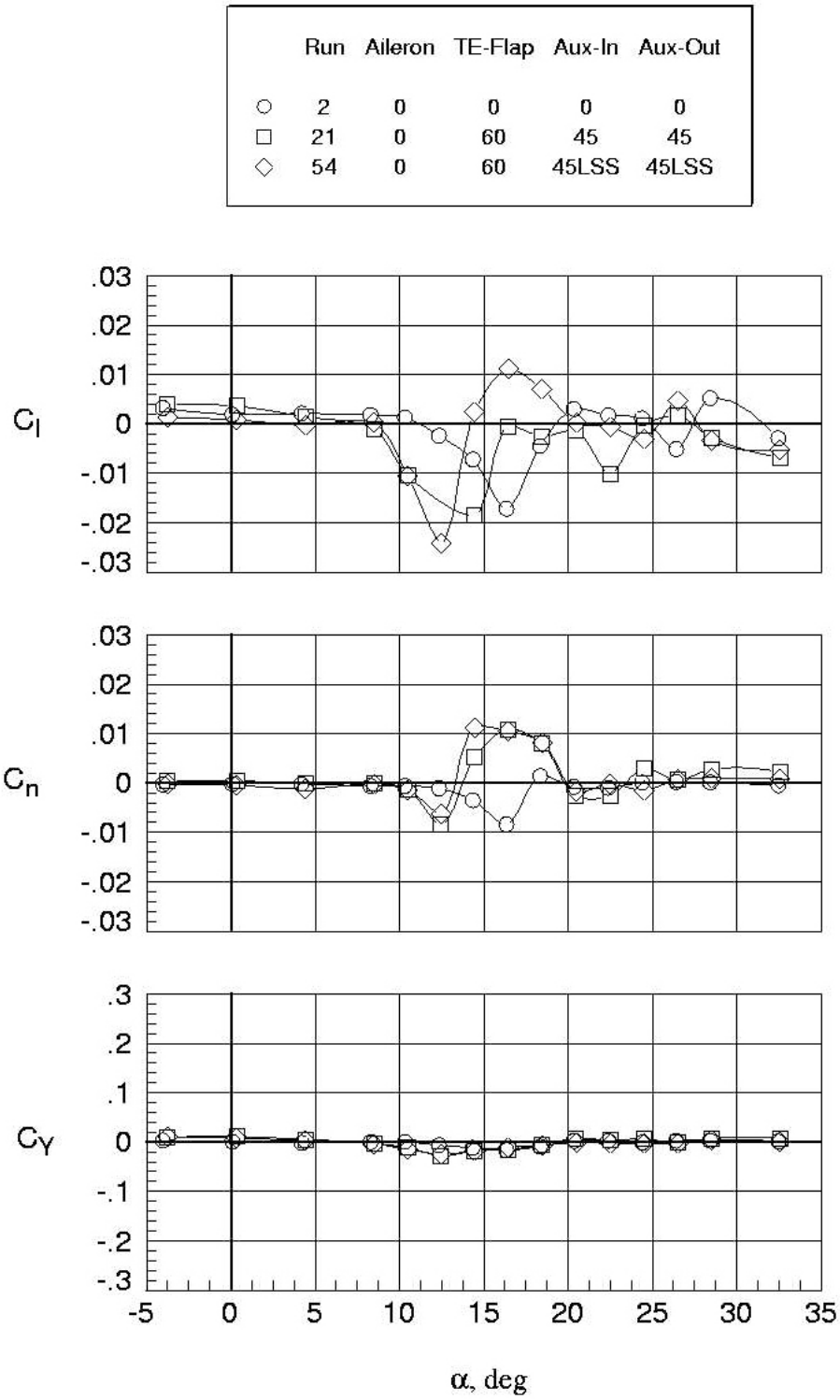

(b) Lateral aerodynamics.

Figure 15. Continued.

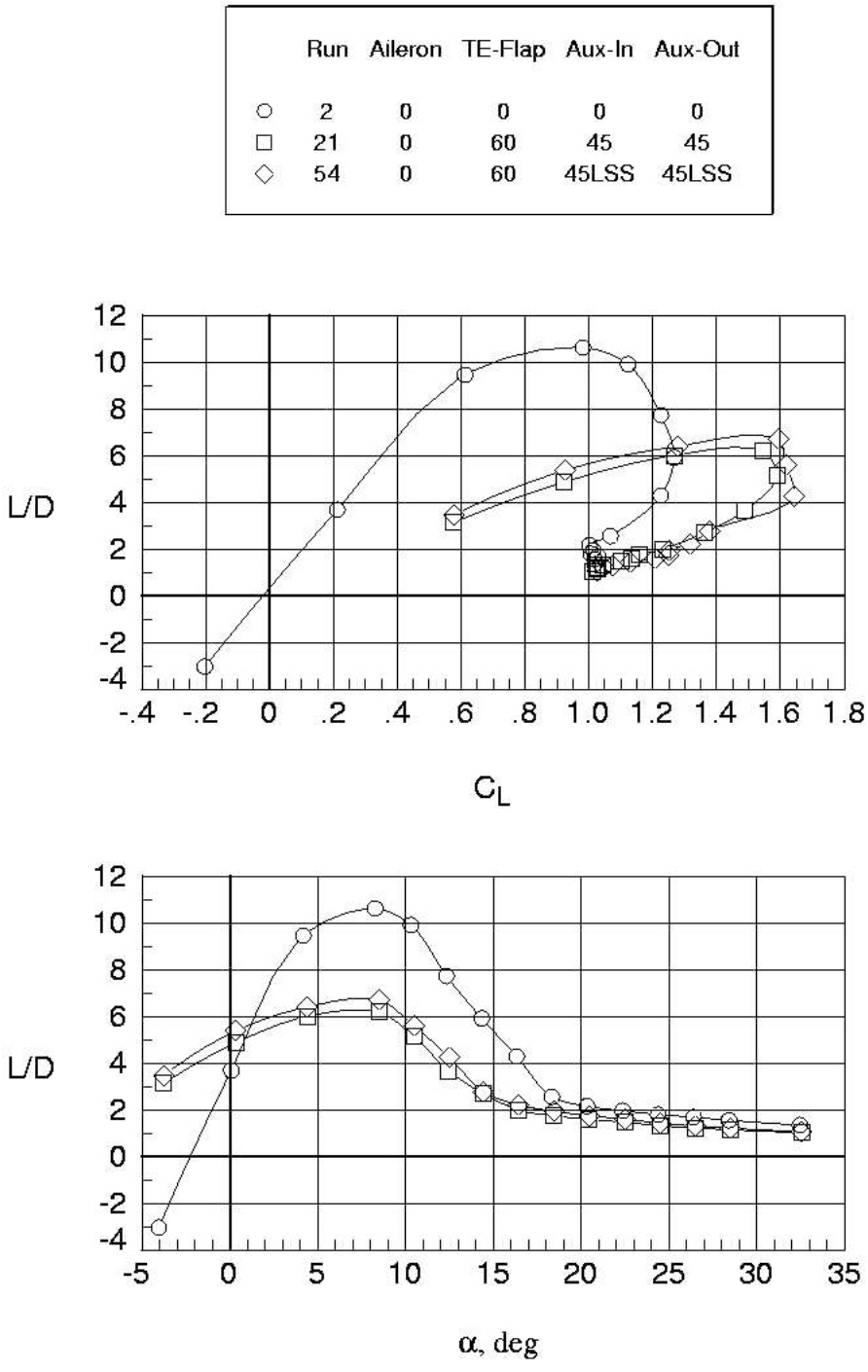

(c) Lift-to-drag ratios.

Figure 15. Continued.

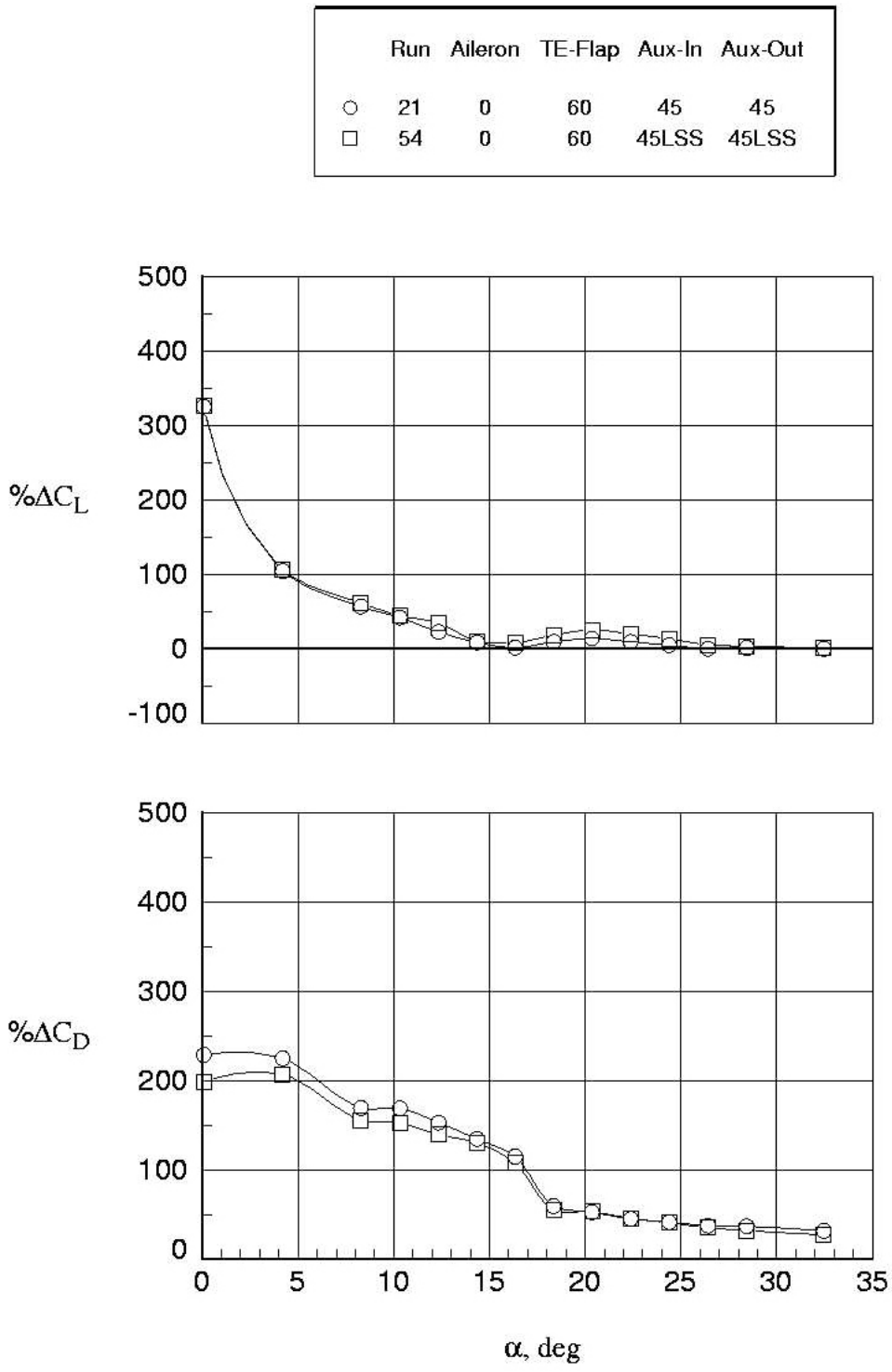

(d) Percent delta changes; baseline = run 2 (aileron deflection = 0°, TE-flap deflection = 0°, aux-in deflection = 0°, aux-out deflection = 0°).

Figure 15. Concluded.

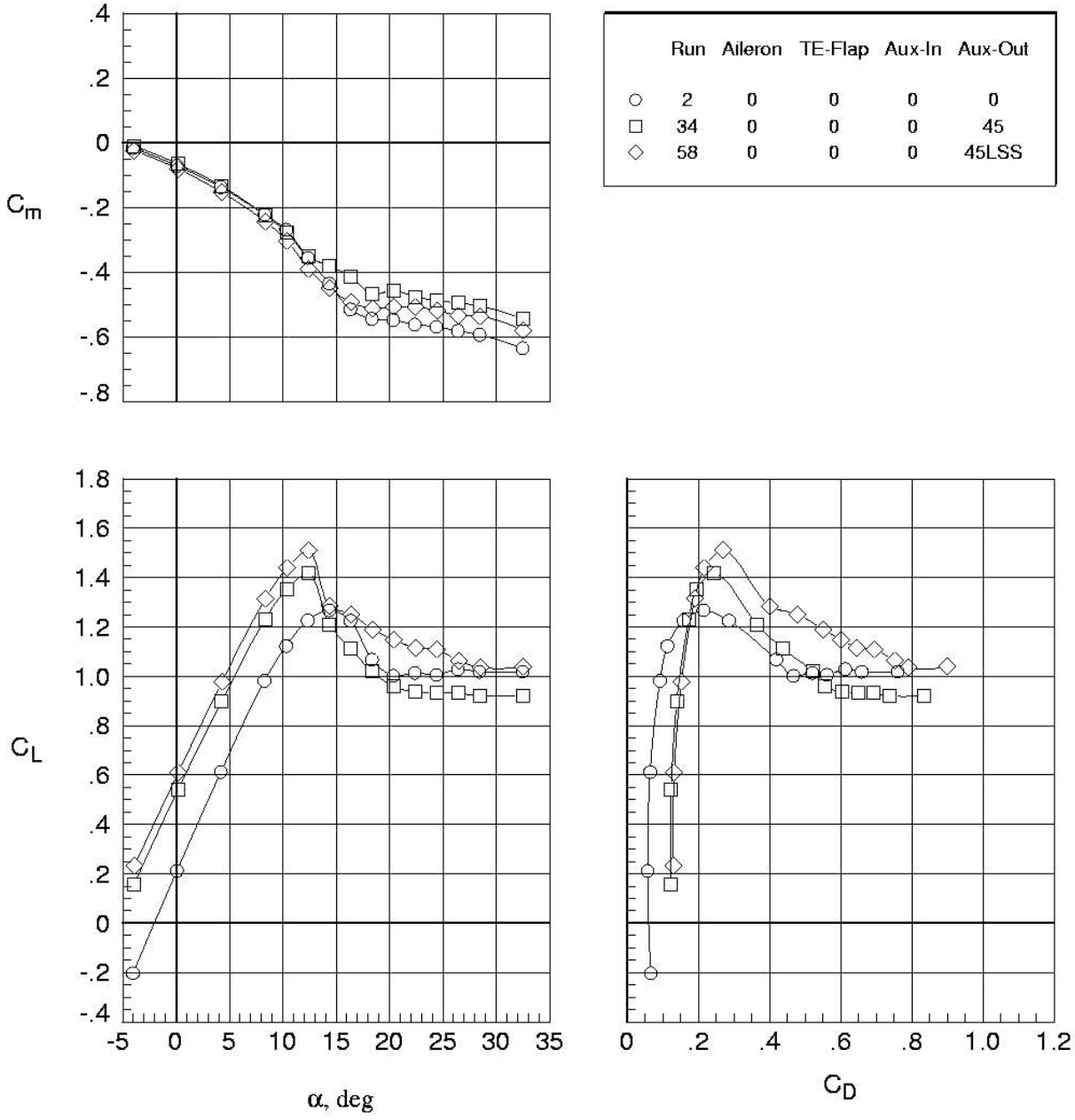

(a) Longitudinal aerodynamics.

Figure 16. Comparison of 45° outboard auxiliary flap with lower surface spoiler; q = 4.0 psf.

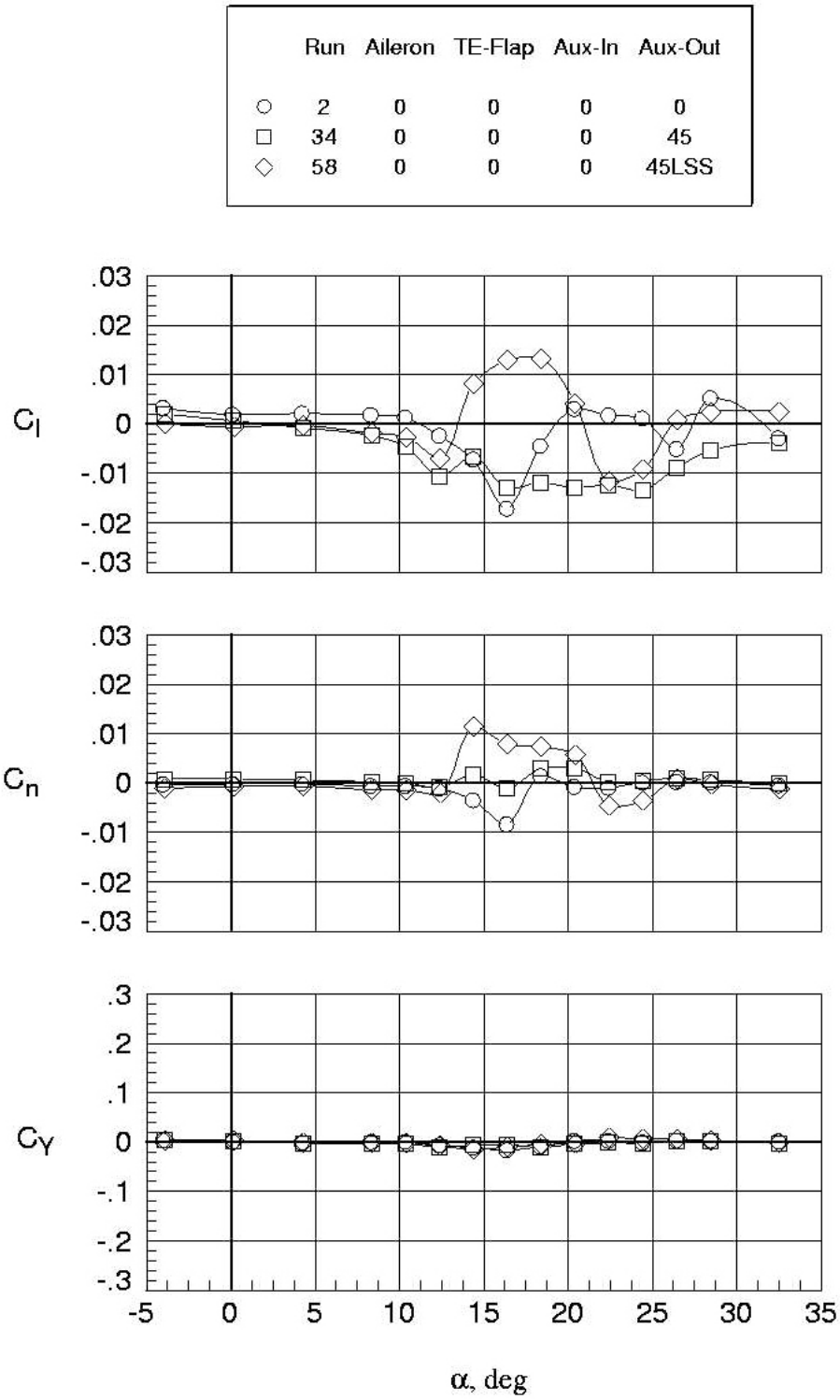

(b) Lateral aerodynamics.

Figure 16. Continued.

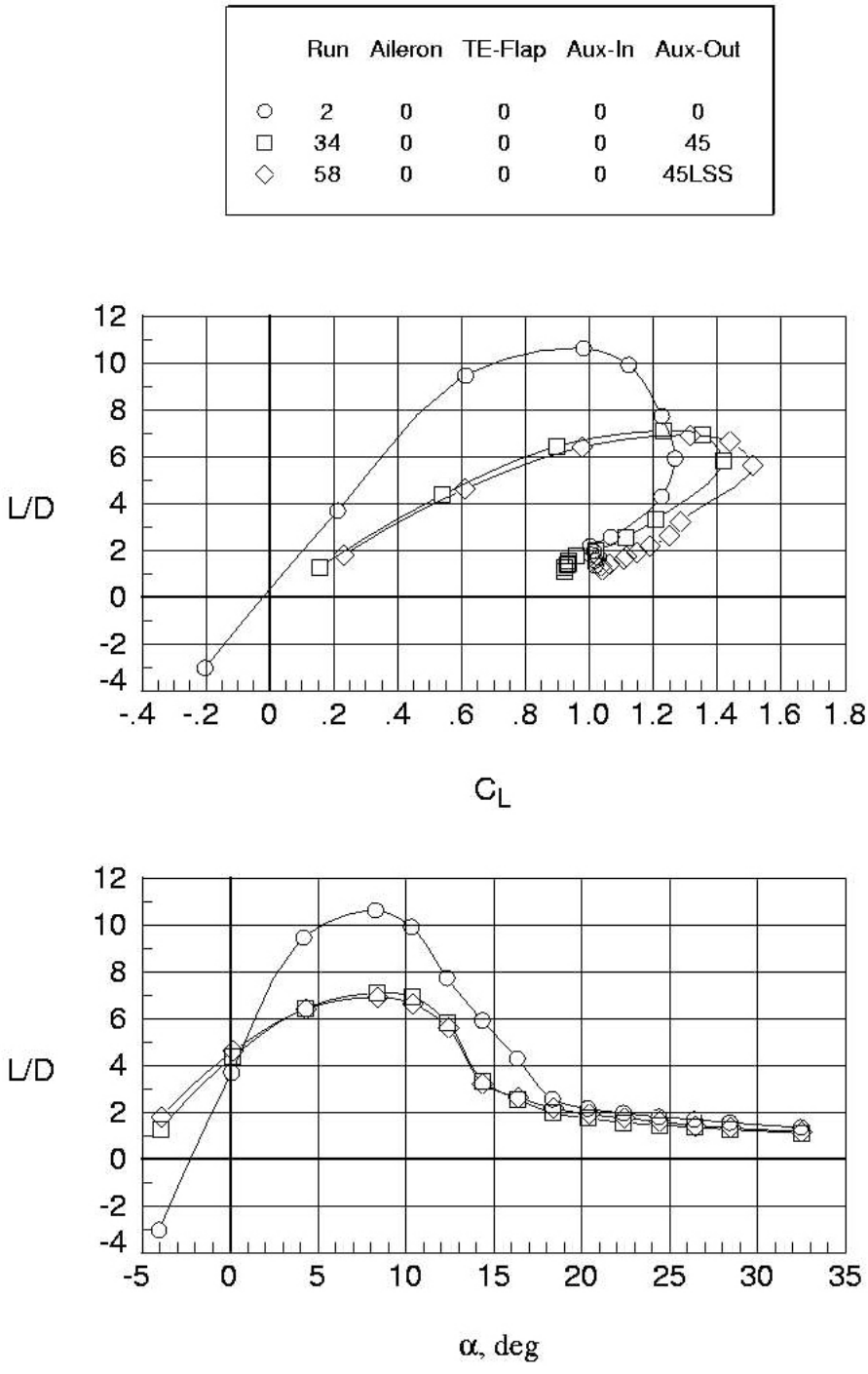

(c) Lift-to-drag ratios.

Figure 16. Continued.

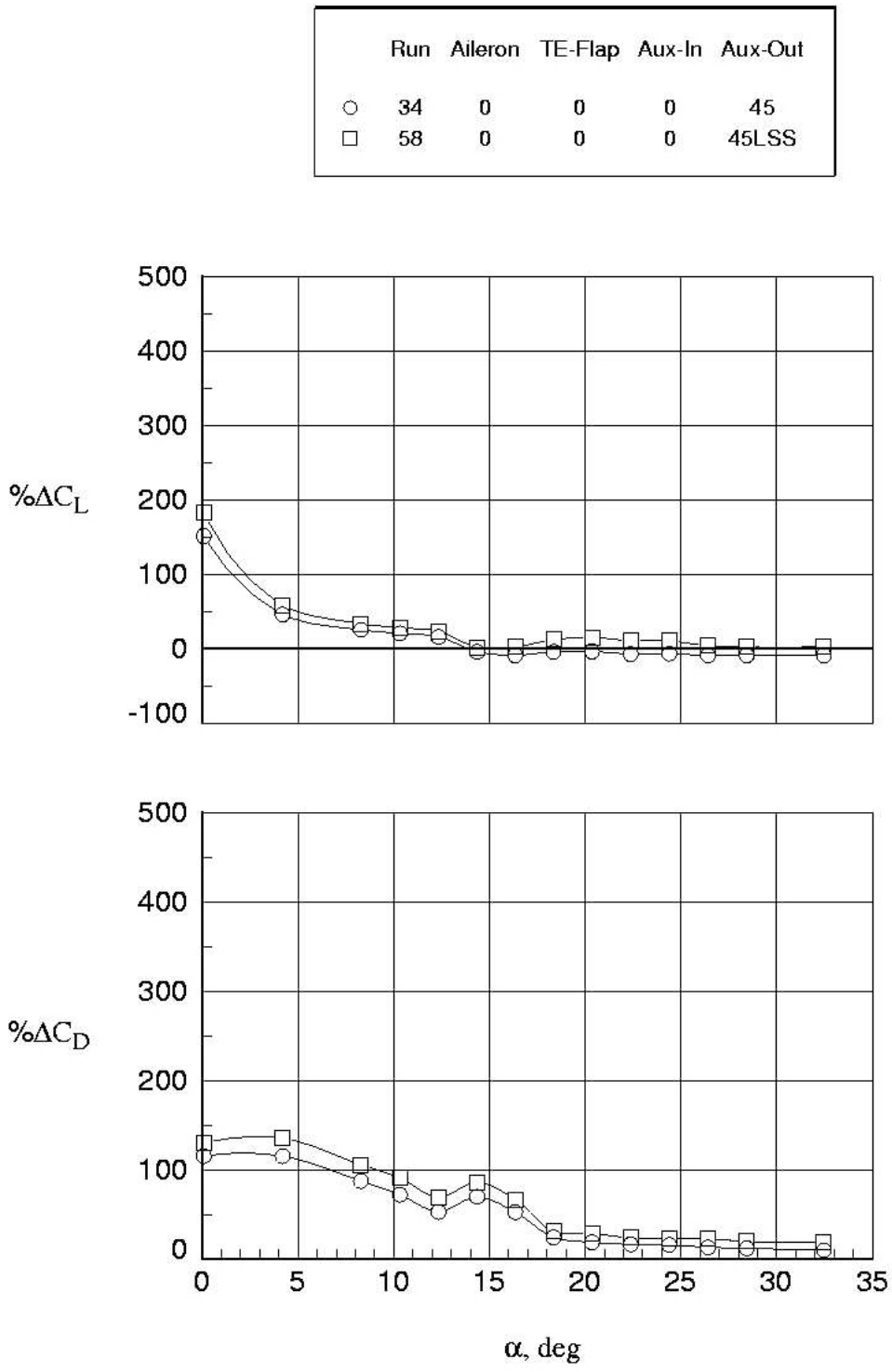

(d) Percent delta changes; baseline = run 2 (aileron deflection = 0°, TE-flap deflection = 0°, aux-in deflection = 0°, aux-out deflection = 0°).

Figure 16. Concluded.

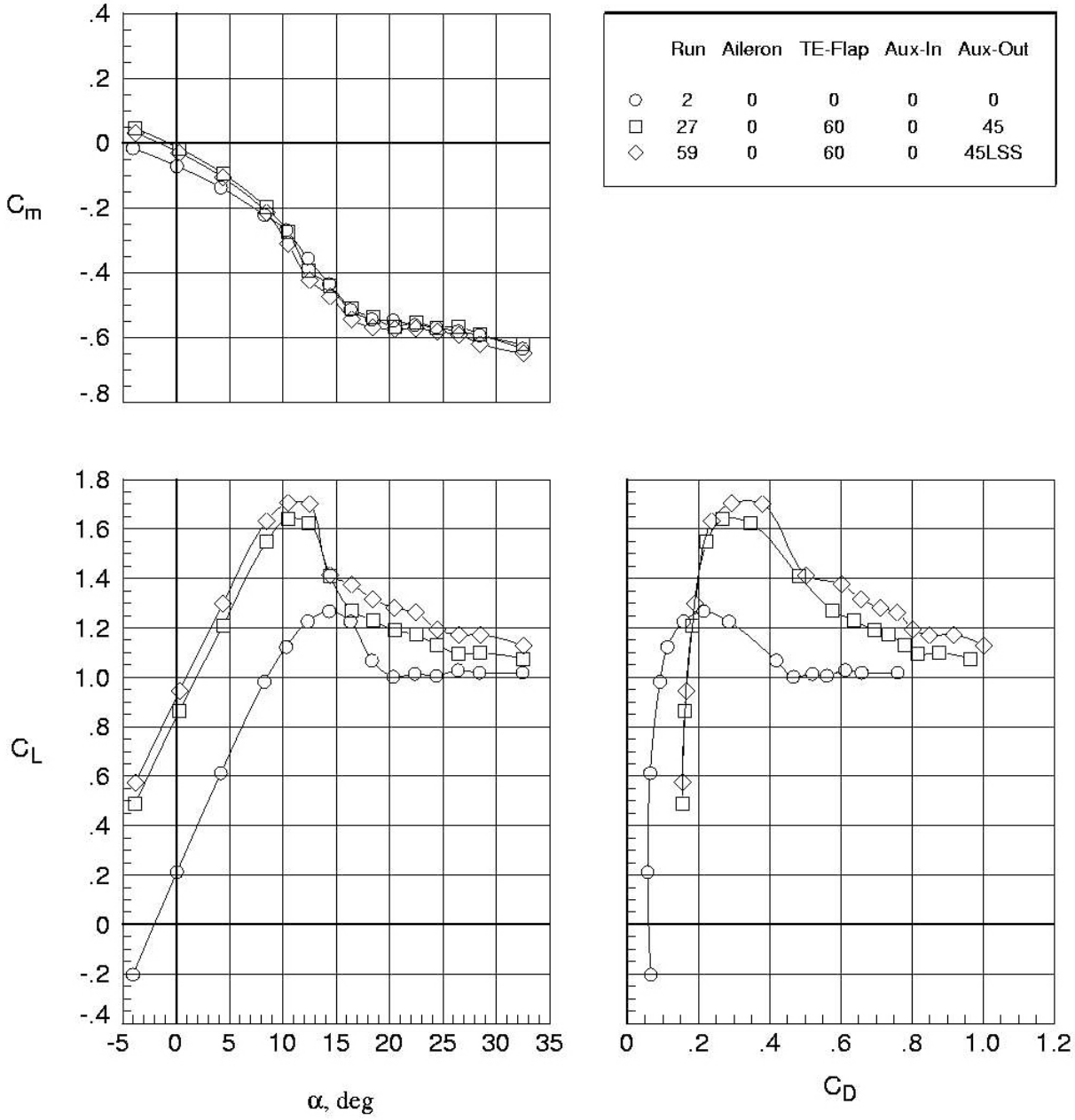

(a) Longitudinal aerodynamics.

Figure 17. Comparison of 45° outboard auxiliary flap with lower surface spoiler; TE-flap deflection = 60°, q = 4.0 psf.

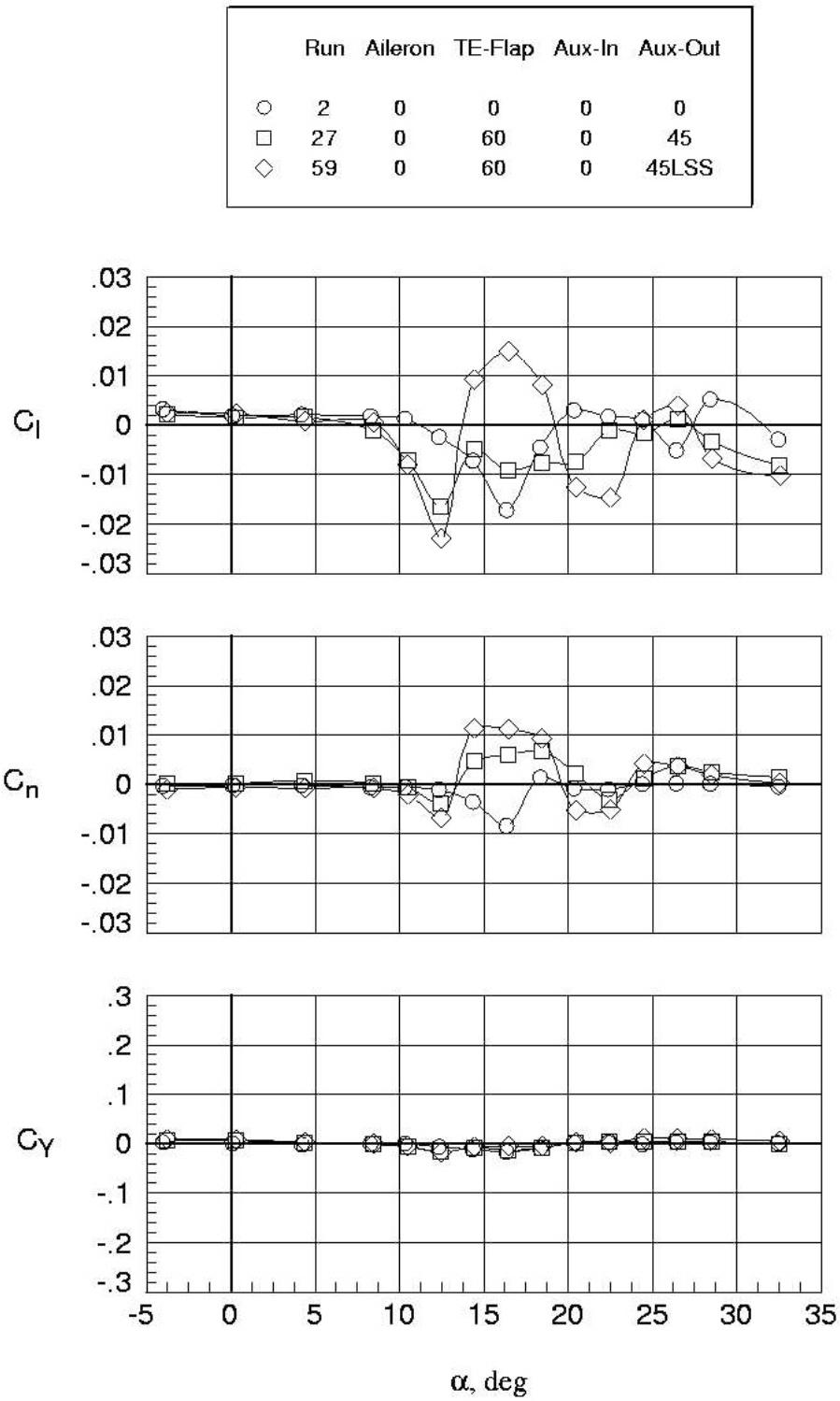

(b) Lateral aerodynamics.

Figure 17. Continued.

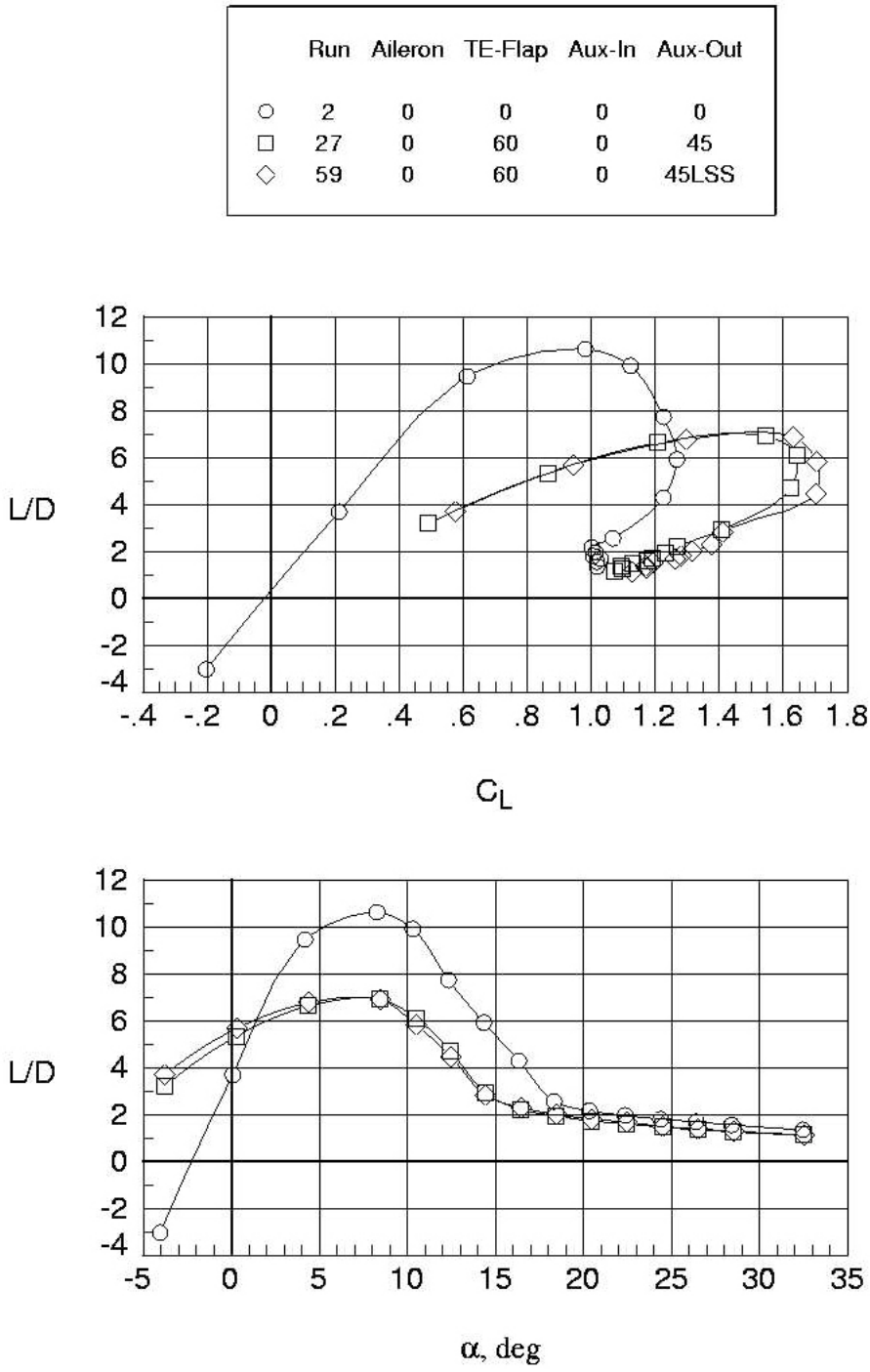

(c) Lift-to-drag ratios.

Figure 17. Continued.

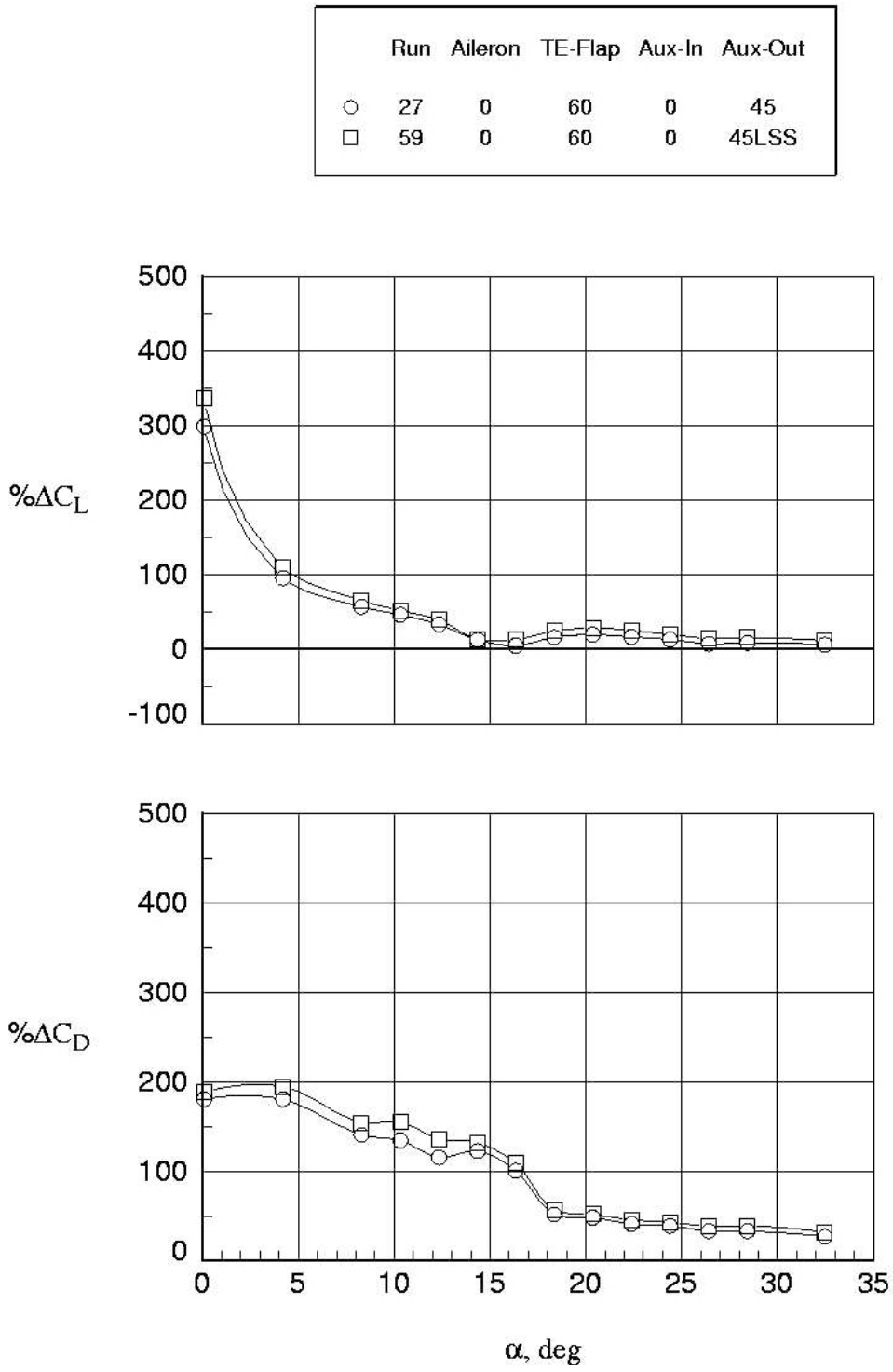

(d) Percent delta changes; baseline = run 2 (aileron deflection = 0°, TE-flap deflection = 60°, aux-in deflection = 0°, aux-out deflection = 45°).

Figure 17. Concluded.

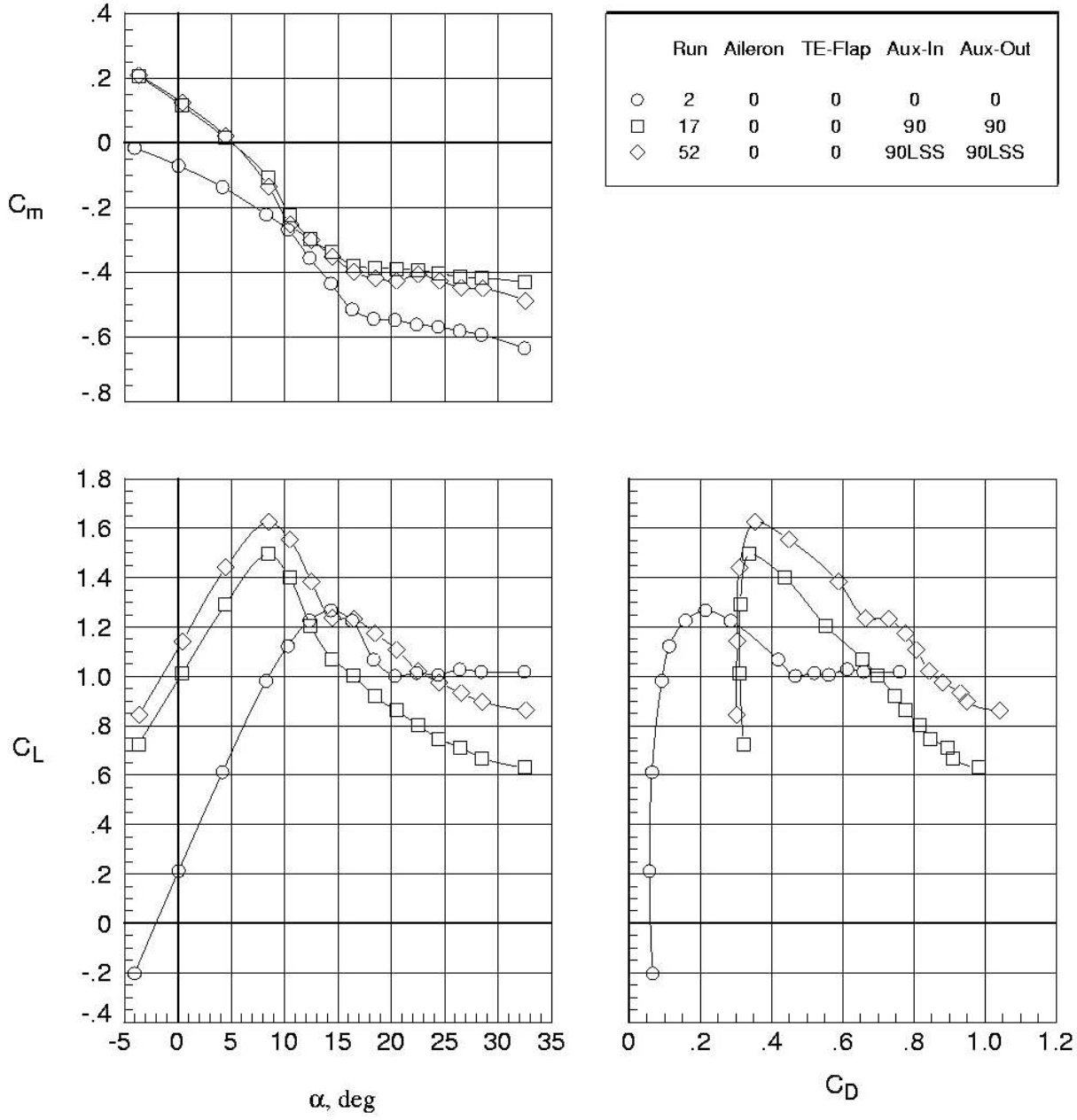

(a) Longitudinal aerodynamics.

Figure 18. Comparison of 90° auxiliary flap with lower surface spoiler; q = 4.0 psf.

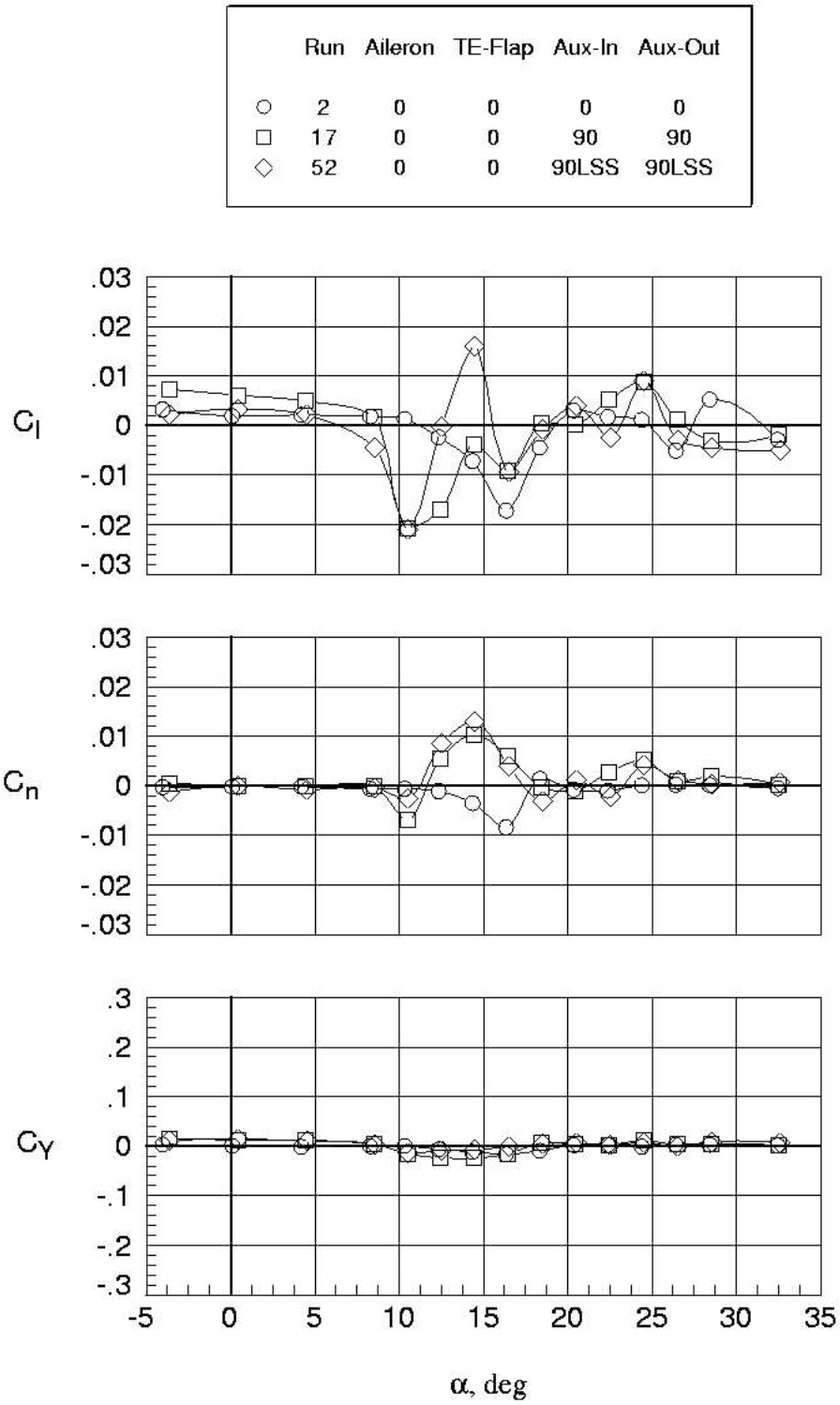

(b) Lateral aerodynamics.

Figure 18. Continued.

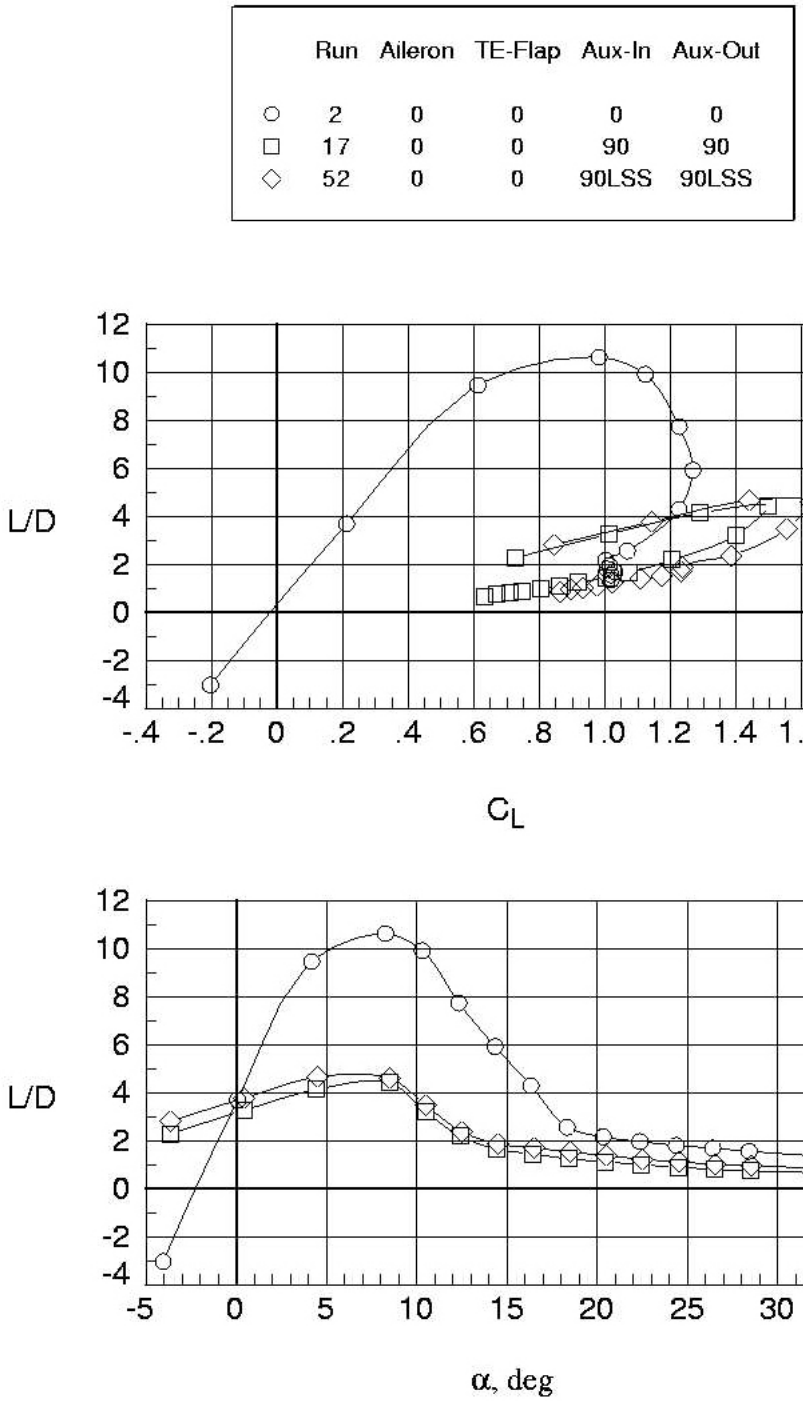

(c) Lift-to-drag ratios.

Figure 18. Continued.

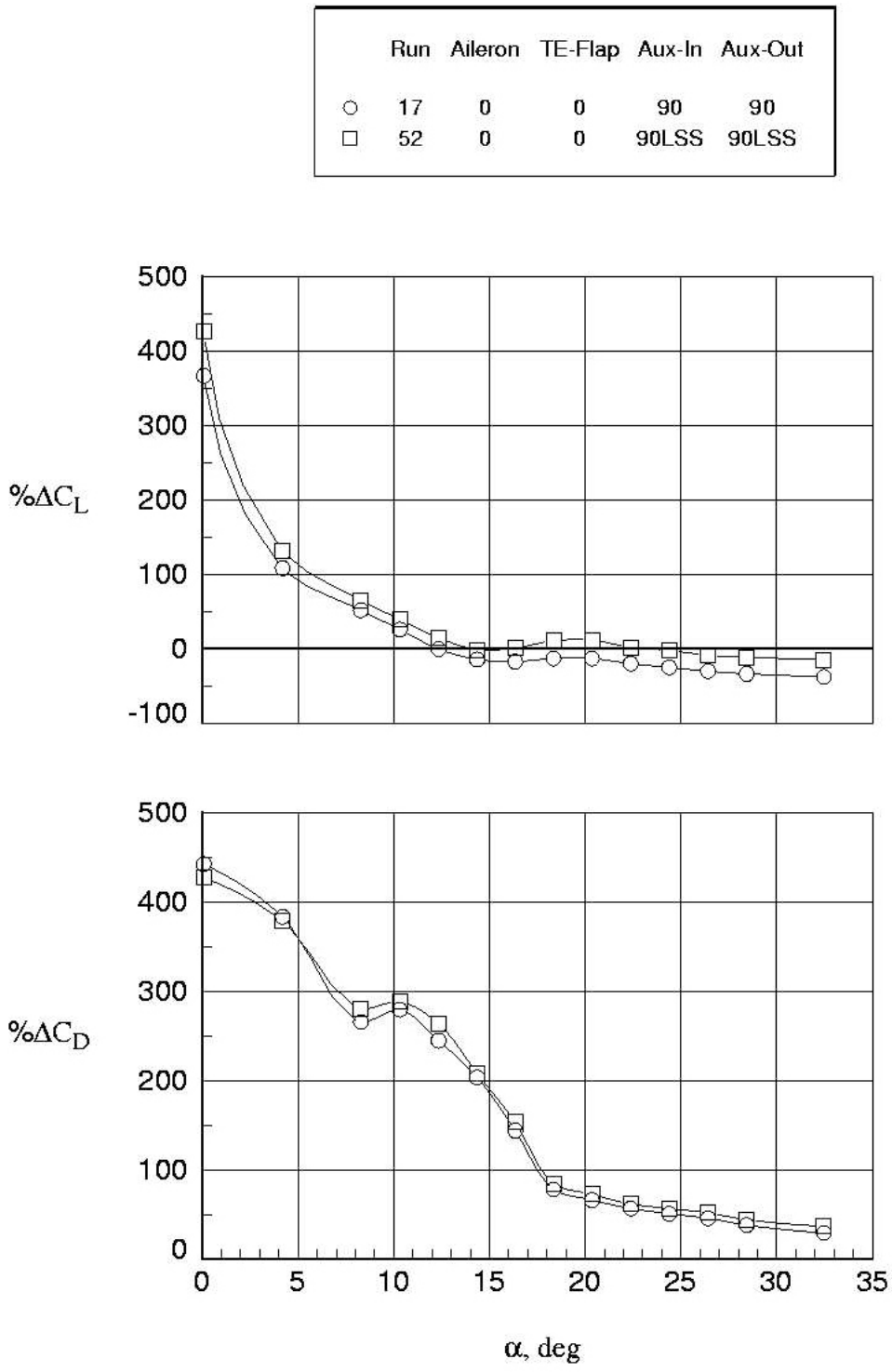

(d) Percent delta changes; baseline = run 2 (aileron deflection = 0°, TE-flap deflection = 0°, aux-in deflection = 90°, aux-out deflection = 90°).

Figure 18. Concluded.

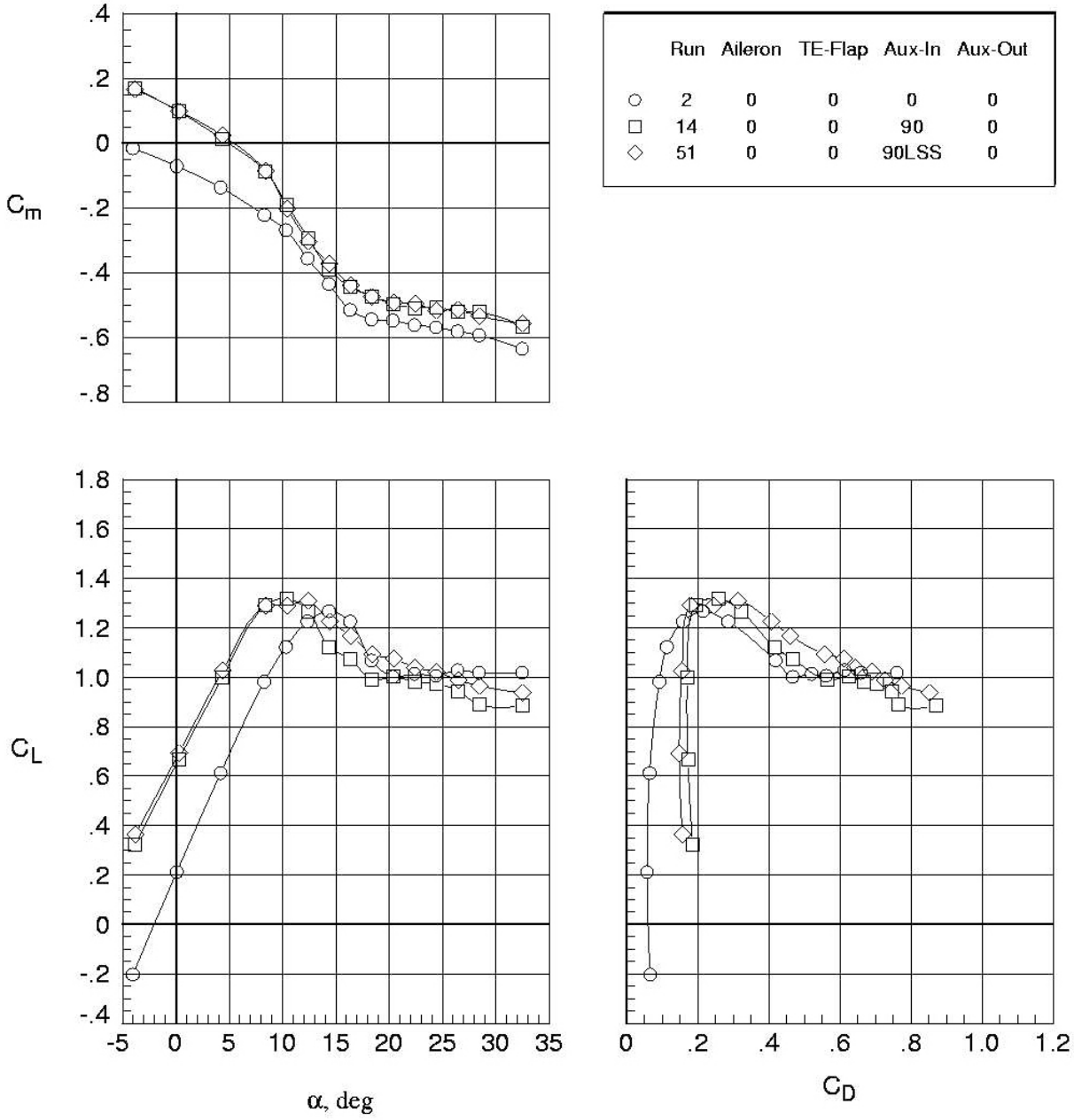

(a) Longitudinal aerodynamics.

Figure 19. Comparison of inboard 90° auxiliary flap with lower surface spoiler; q = 4.0 psf.

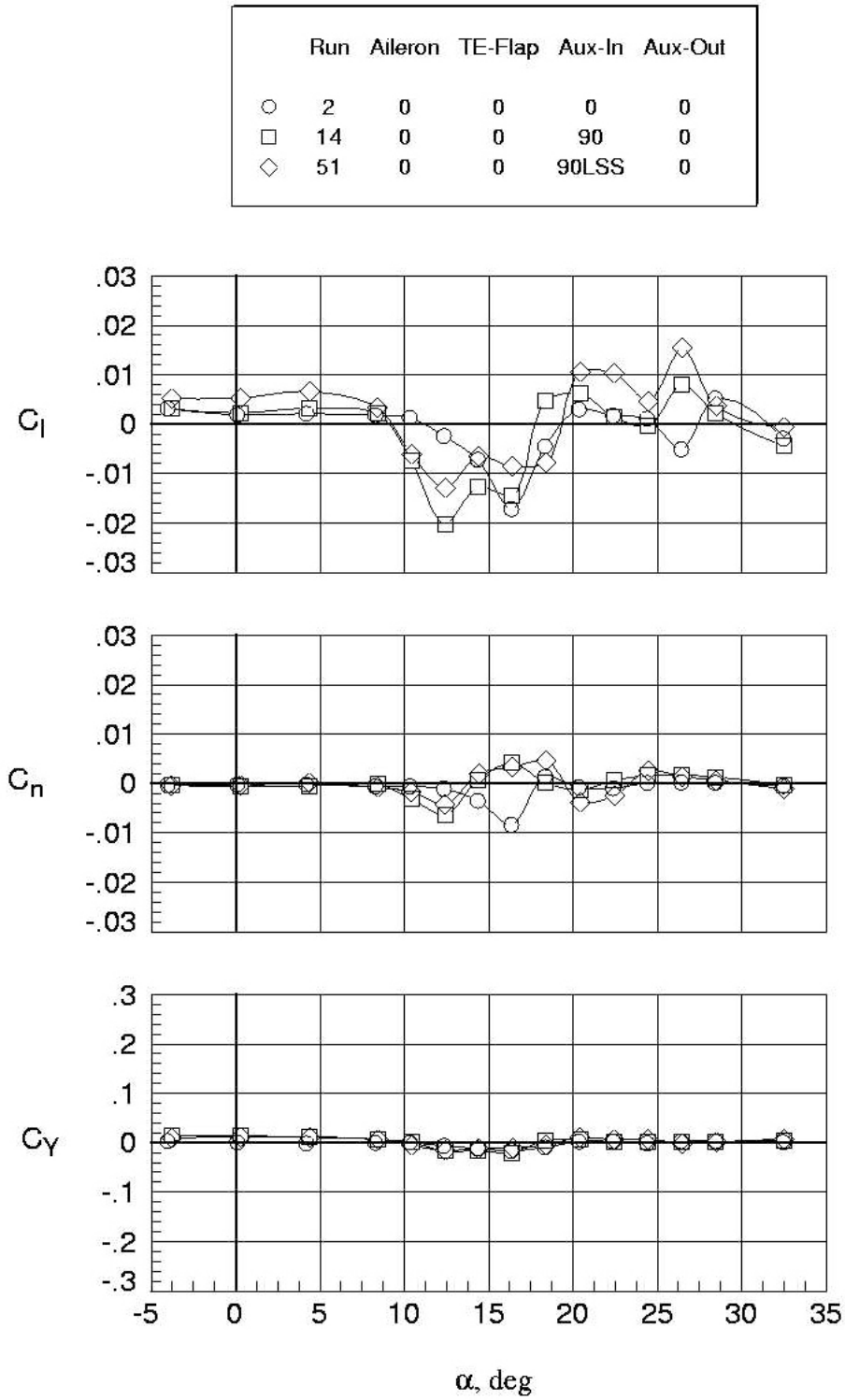

(b) Lateral aerodynamics.

Figure 19. Continued.

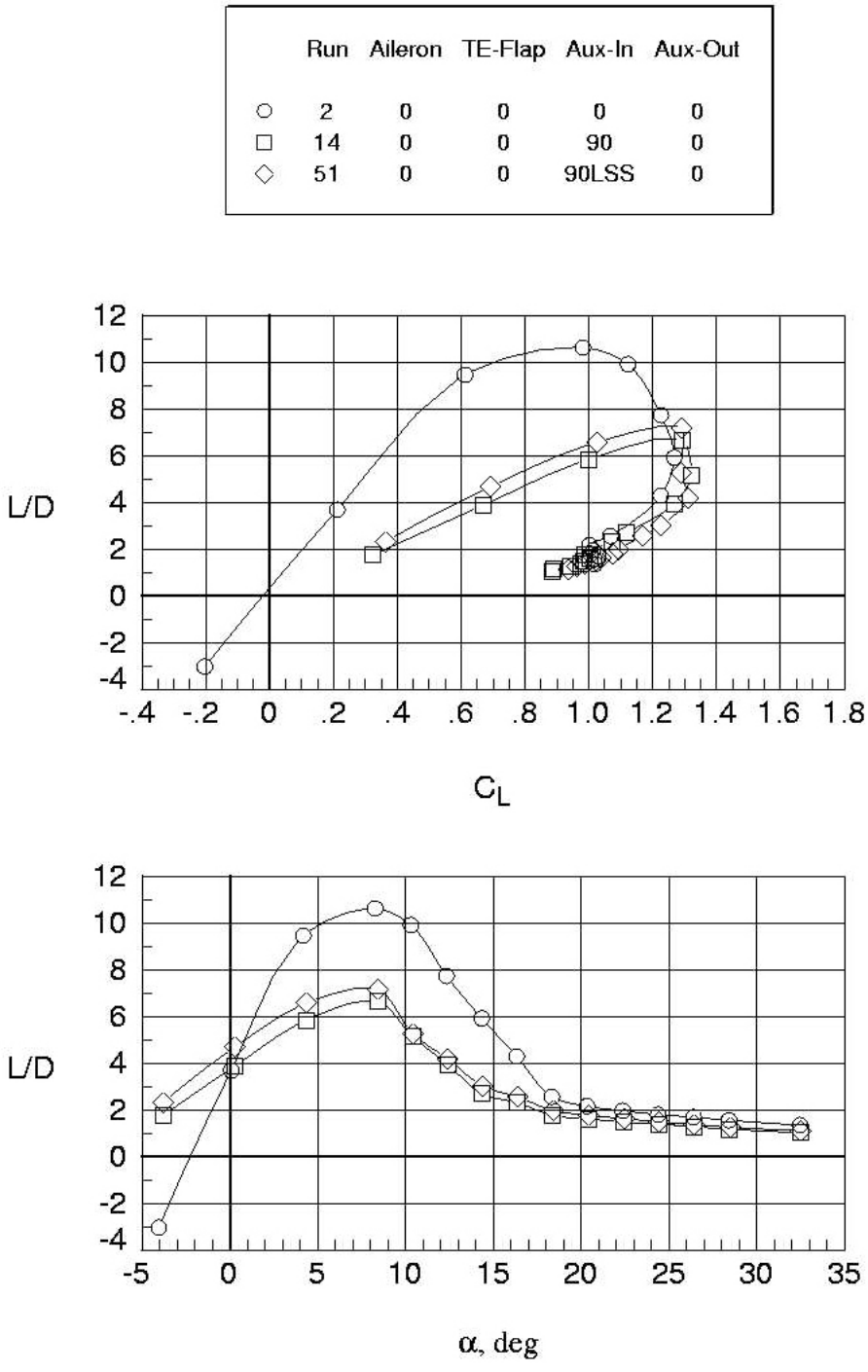

(c) Lift-to-drag ratios.

Figure 19. Continued.

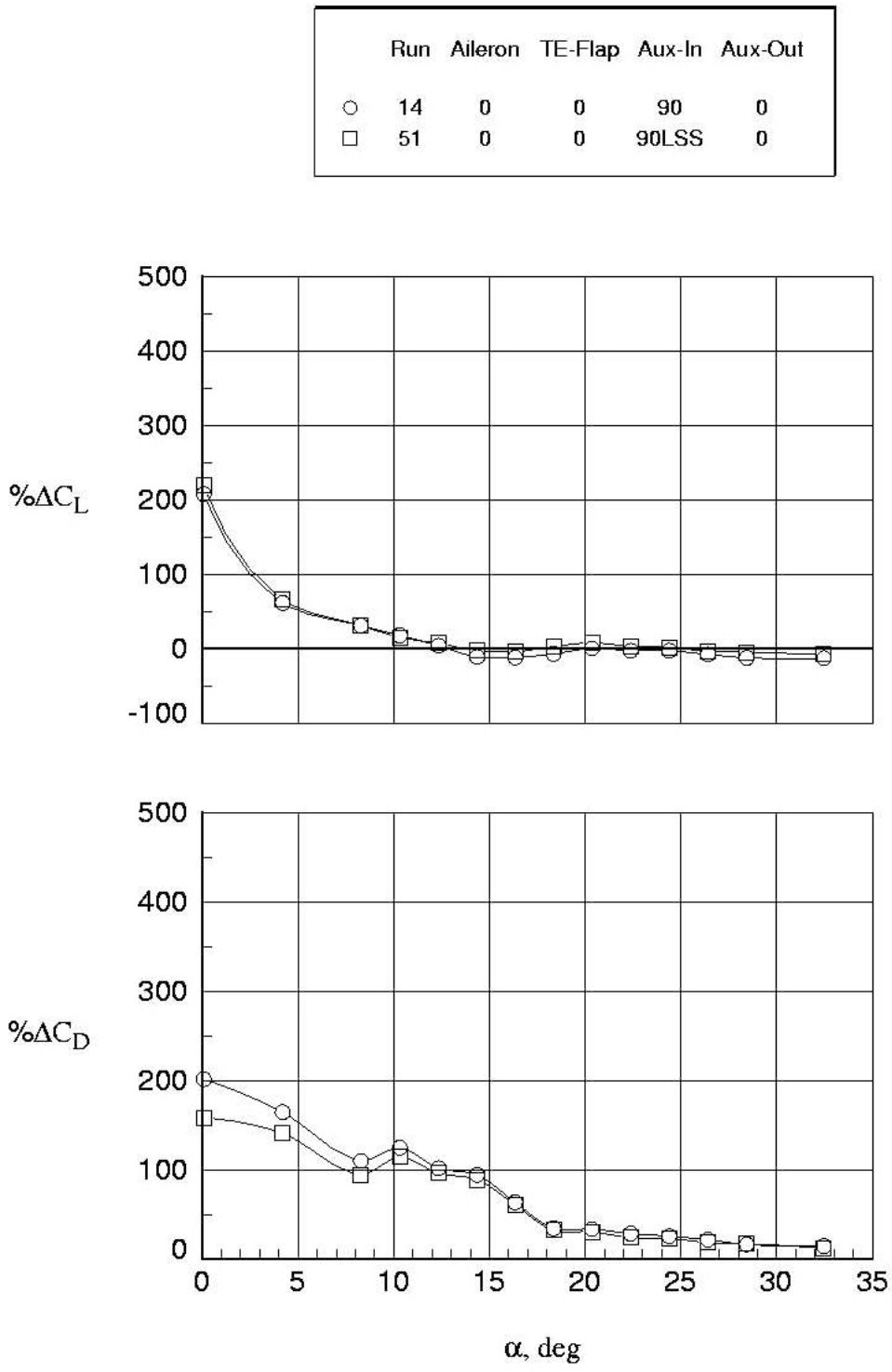

(d) Percent delta changes; baseline = run 2 (aileron deflection = 0°, TE-flap deflection = 0°, aux-in deflection = 90°, aux-out deflection = 0°).

Figure 19. Concluded.

Appendix A: Instrumentation Accuracy and Data Repeatability

Instrumentation Accuracy

Forces and moments were measured with a six-component strain-gauge balance identified as NASA LaRC FF11A. The load limit and error range for each component are listed in table A-1.

Table A-1. Load limits and error ranges for balance components.

Component	Max load range	Accuracy, percent full-scale
Normal Force	120 lb	0.18
Axial Force	120 lb	0.14
Pitching Moment	1200 in-lb	0.13
Rolling Moment	372 in-lb	0.19
Yawing Moment	1200 in-lb	0.05
Side Force	120 lb	0.10

The angle-of-attack sensor had an accuracy of ±0.01°.

Plots of Repeat Runs

Plots of repeat runs for selected key configurations are presented in figures A-1–A-5. In general, the data are fairly repeatable over the prestall angles of attack. The largest nonrepeat errors are seen at stall and beyond. This is especially true for the original auxiliary flap deflected at 45° (fig. A-2), and to a slightly lesser extent for the cruise wing (fig. A-1). Also to be noted is the large repeat error of the 45° auxiliary-flap pitching moment (fig. A-2). Interestingly, the back-to-back repeat runs of the lower surface spoiler (LSS), shown in figures A-4 and A-5, exhibit very good repeatability with the exception of rolling moment.

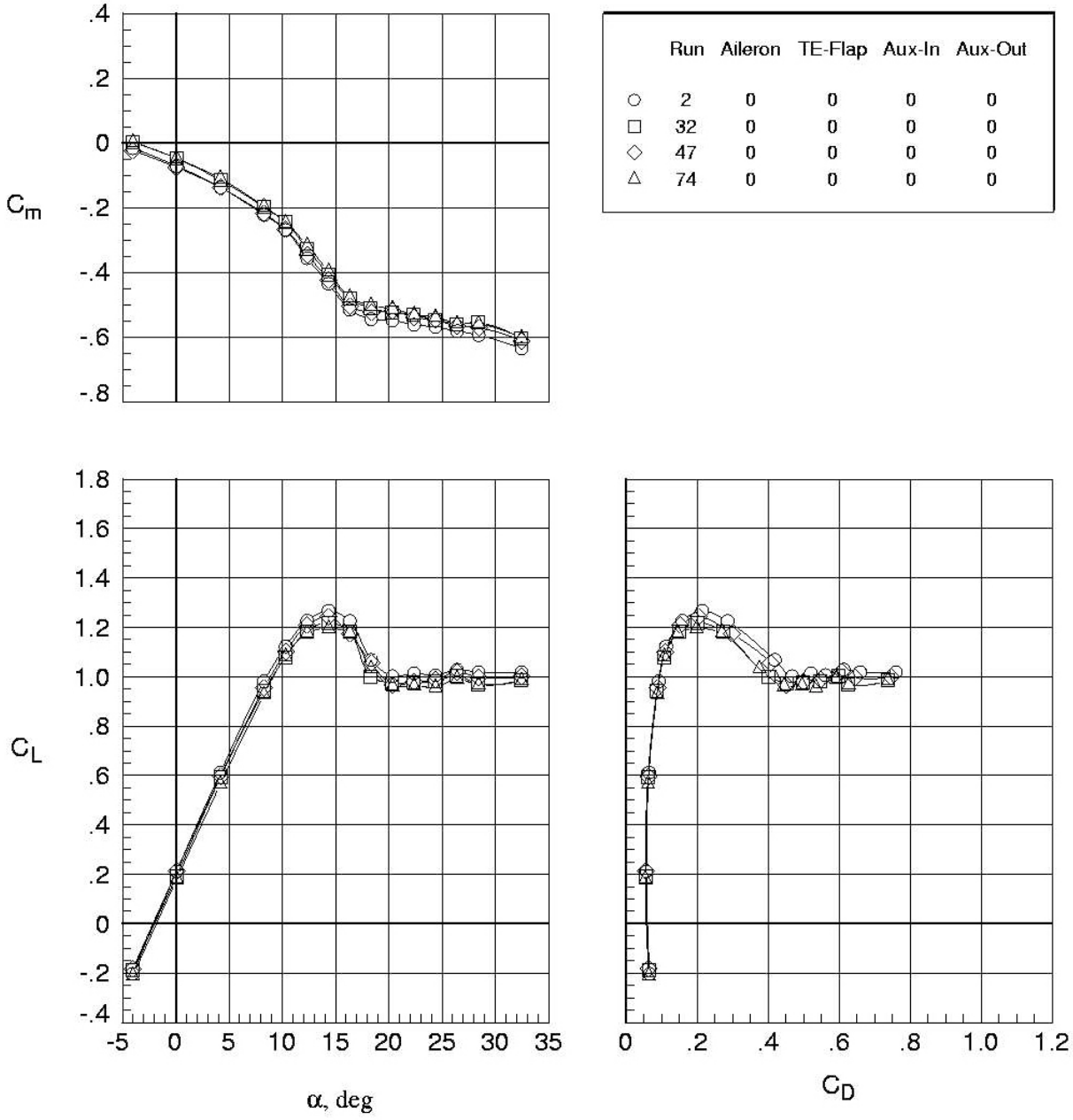

(a) Longitudinal aerodynamics.

Figure A-1. Repeat runs, cruise configuration; q = 4.0 psf.

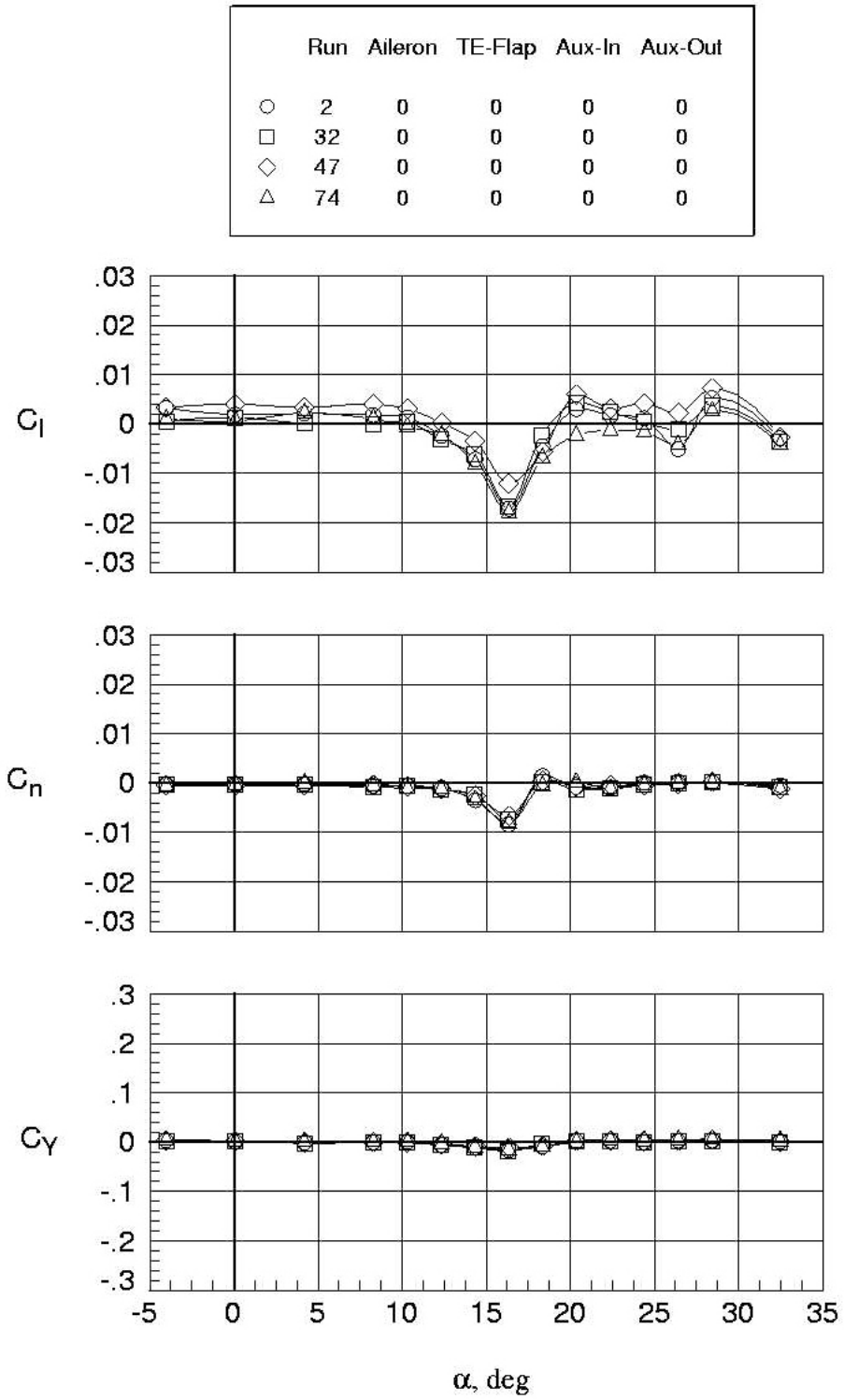

(b) Lateral aerodynamics.

Figure A-1. Continued.

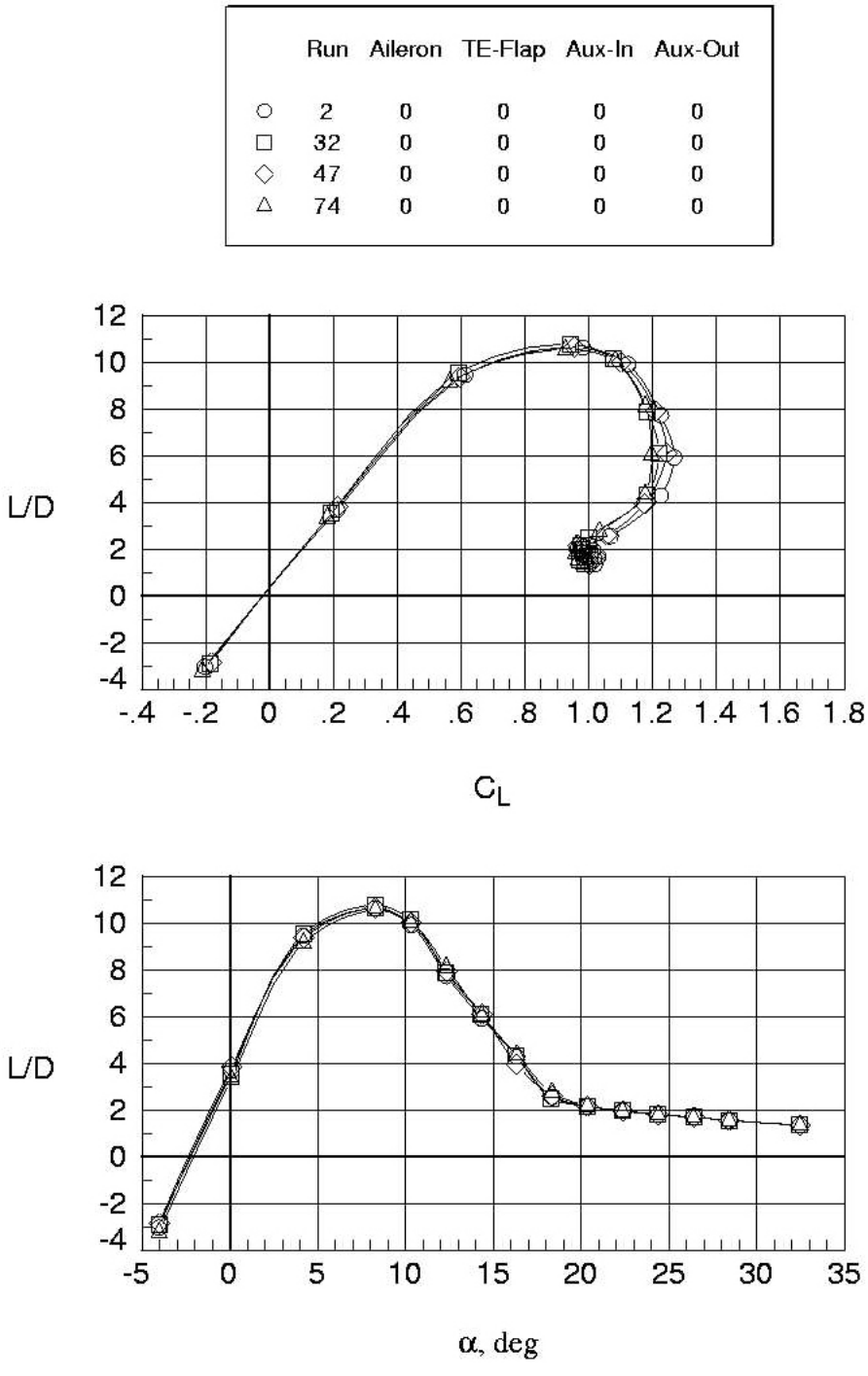

(c) Lift-to-drag ratios.

Figure A-1. Concluded.

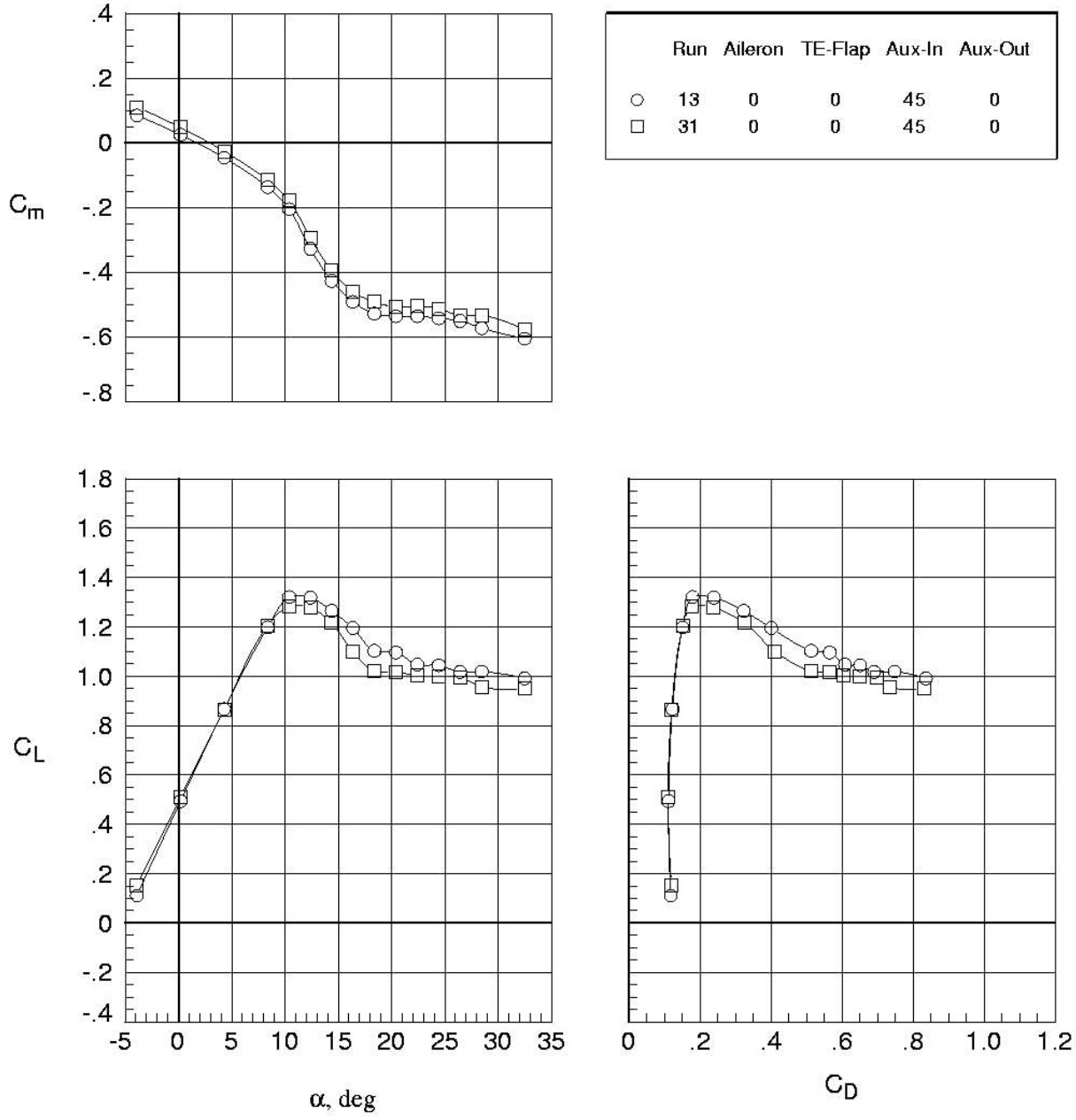

(a) Longitudinal aerodynamics.

Figure A-2. Repeat runs, take-off with only inboard auxiliary flap; q = 4.0 psf.

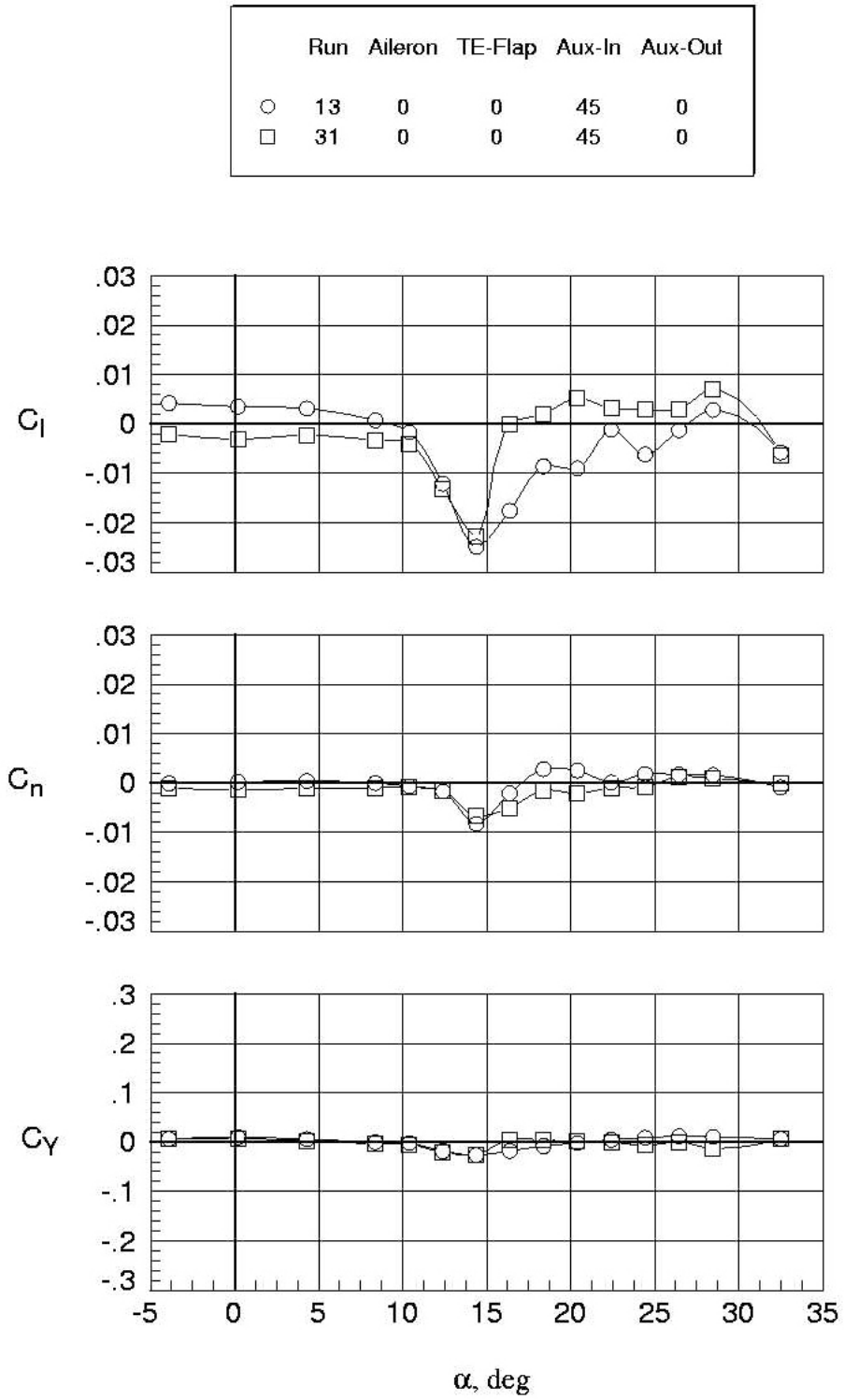

(b) Lateral aerodynamics.

Figure A-2. Continued.

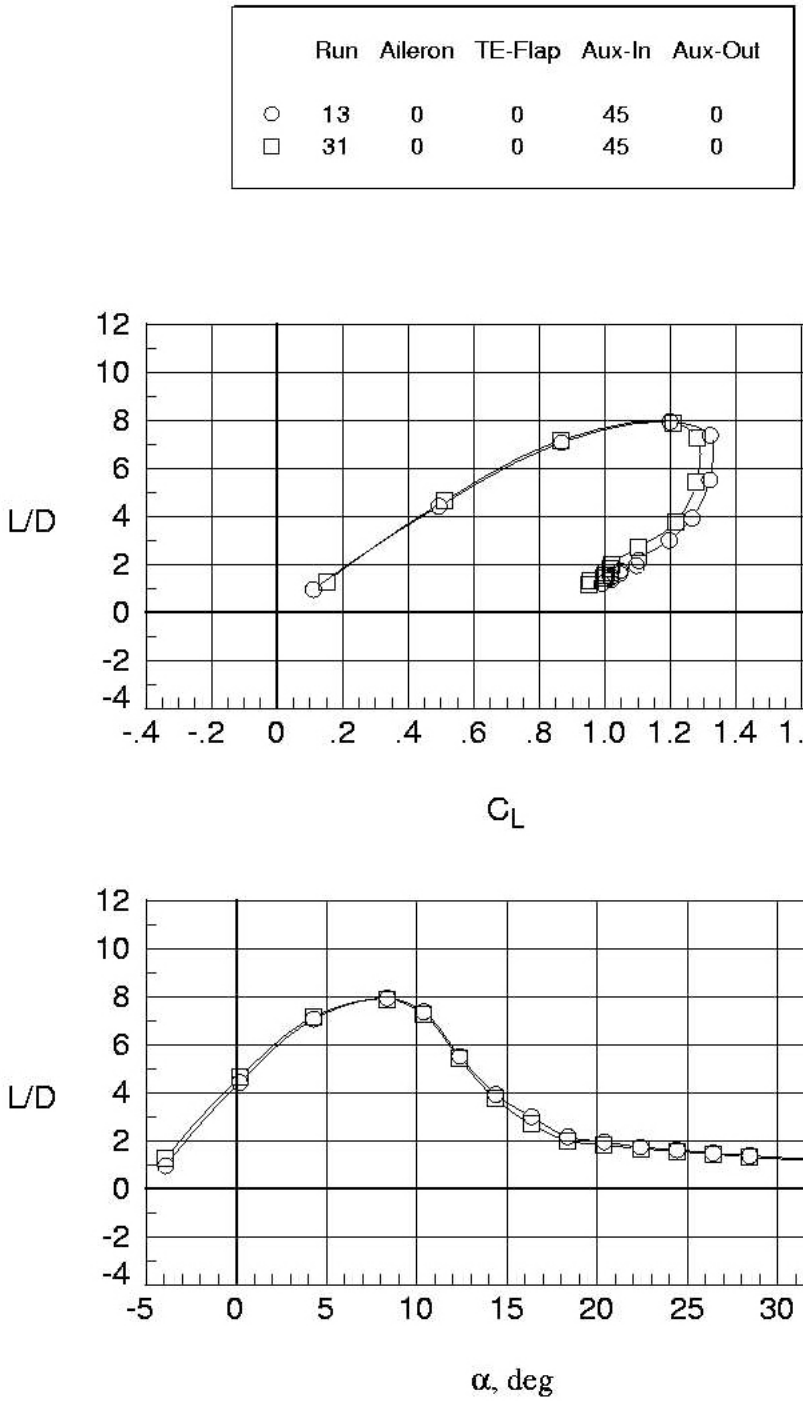

(c) Lift-to-drag ratios.

Figure A-2. Continued.

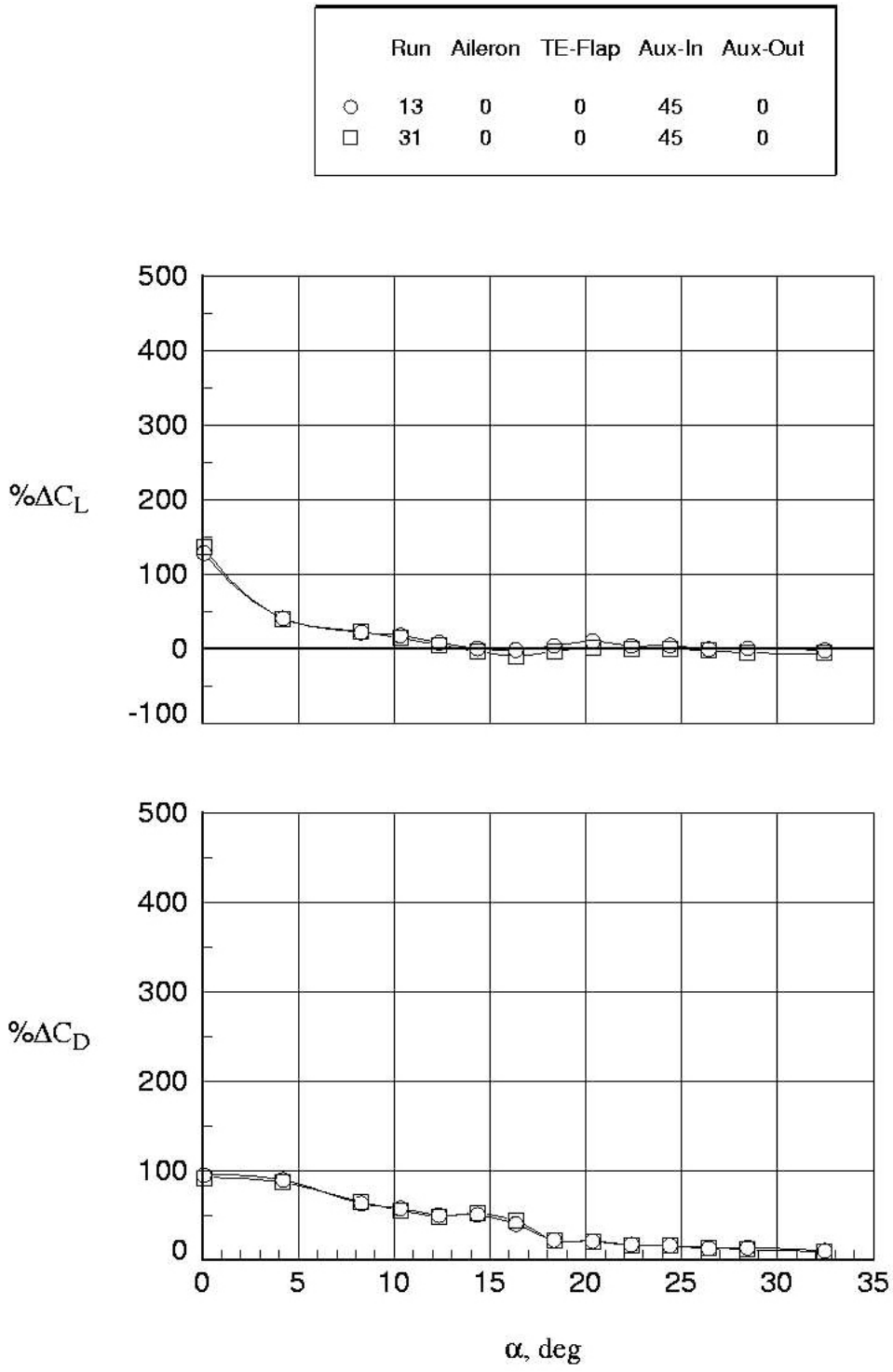

(d) Percent delta changes; baseline = run 2 (aileron deflection = 0°, TE-flap deflection = 0°, aux-in deflection = 45°, aux-out deflection = 0°).

Figure A-2. Concluded.

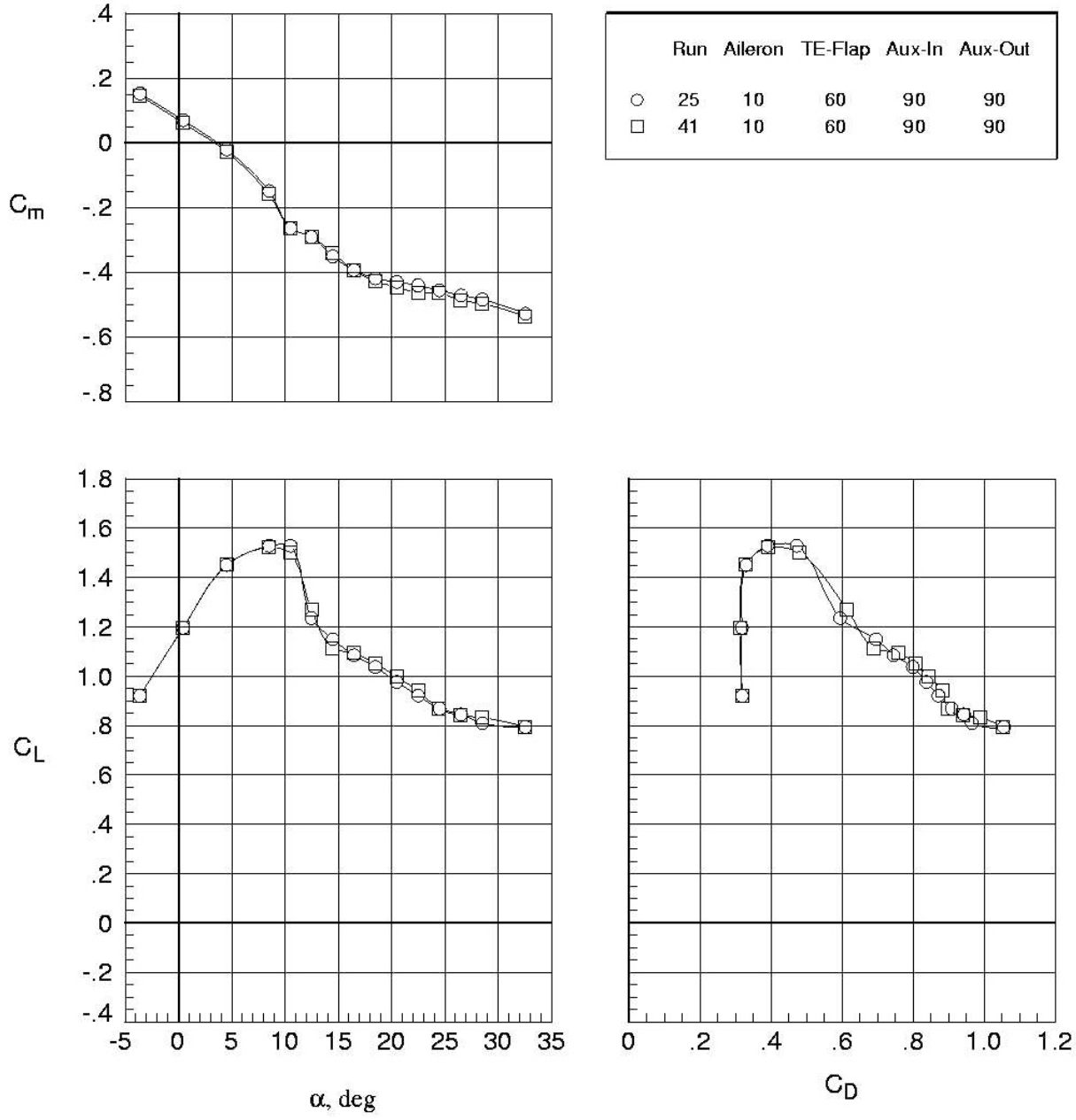

(a) Longitudinal aerodynamics.

Figure A-3. Repeat runs, maximum drag landing configuration; q = 4.0 psf.

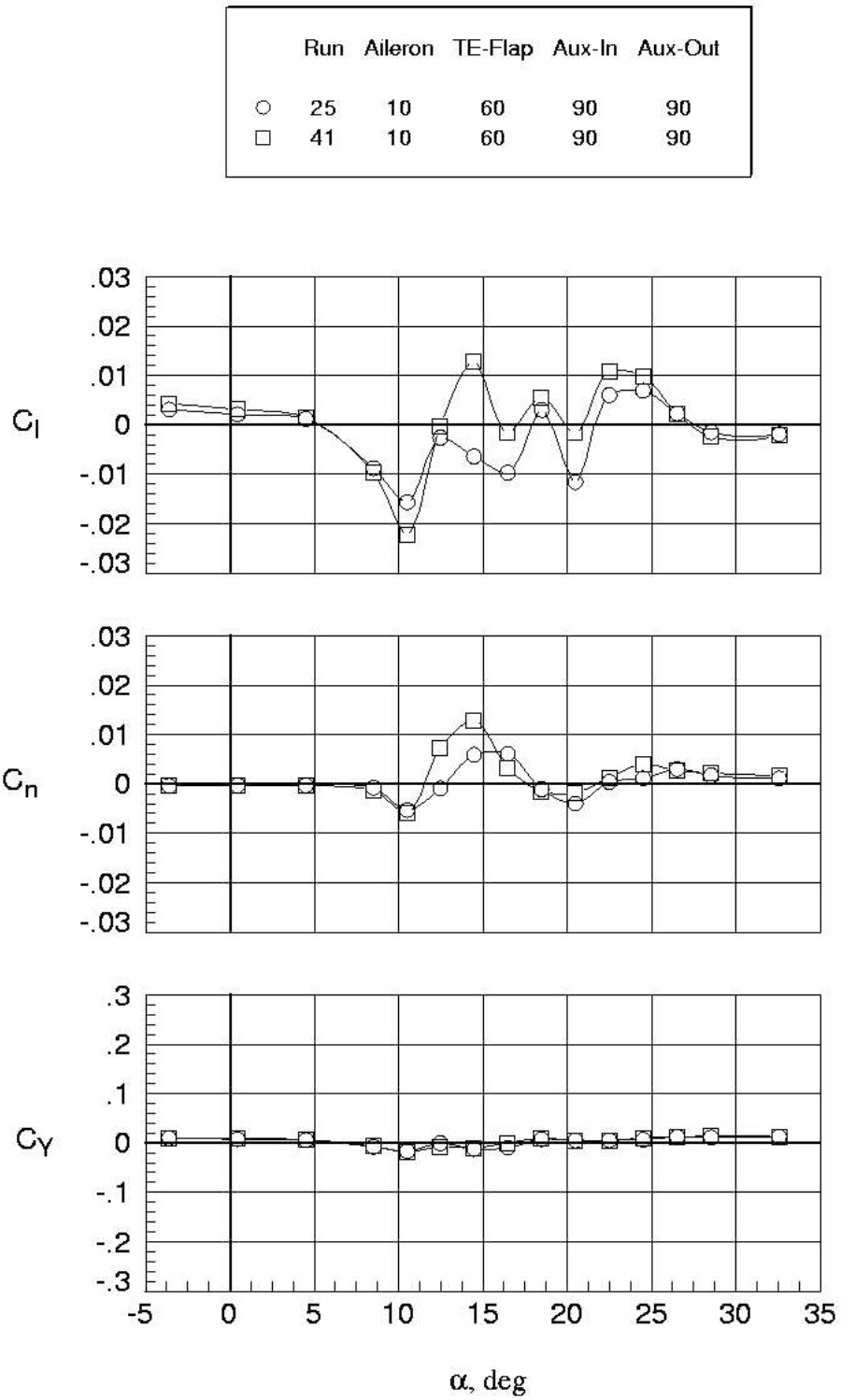

(b) Lateral aerodynamics.

Figure A-3. Continued.

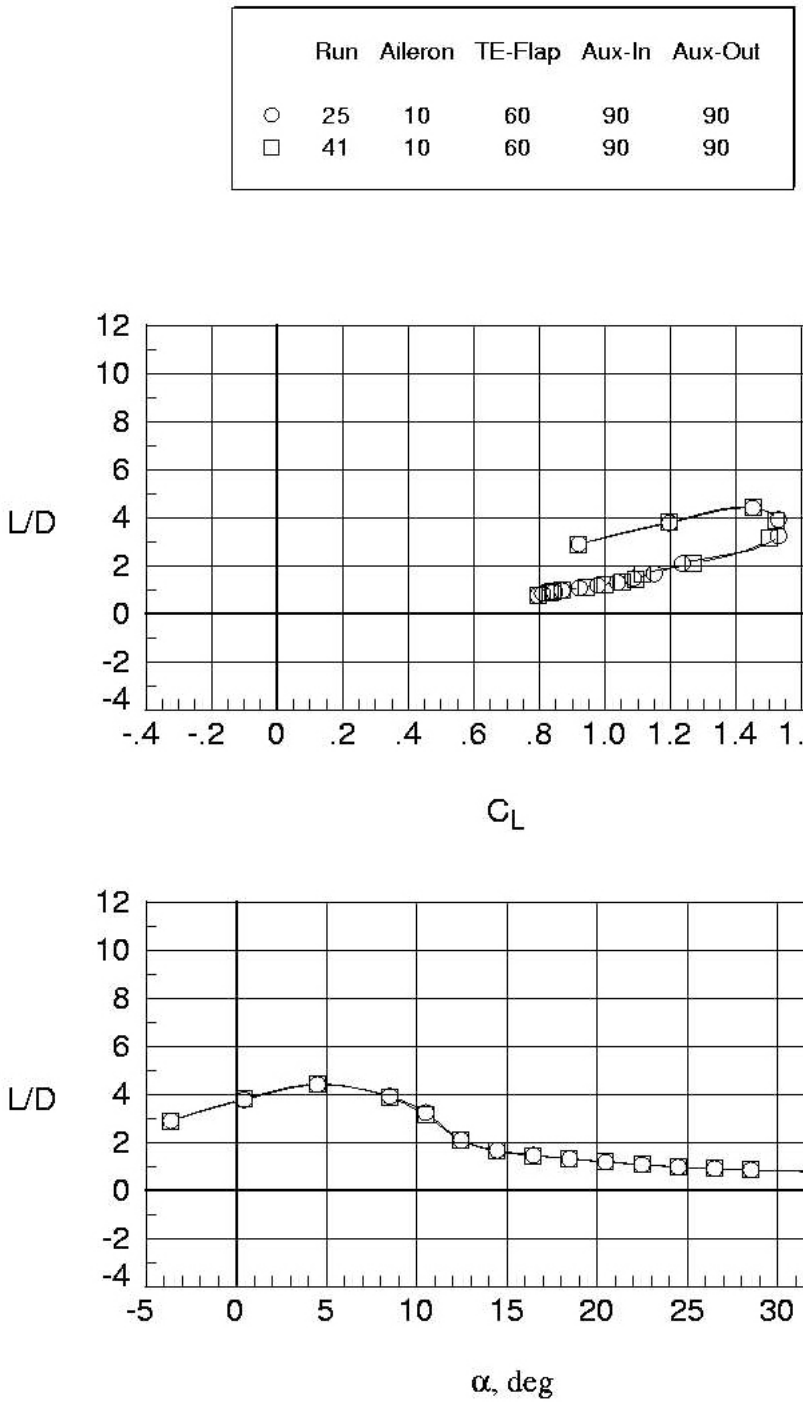

(c) Lift-to-drag ratios.

Figure A-3. Continued.

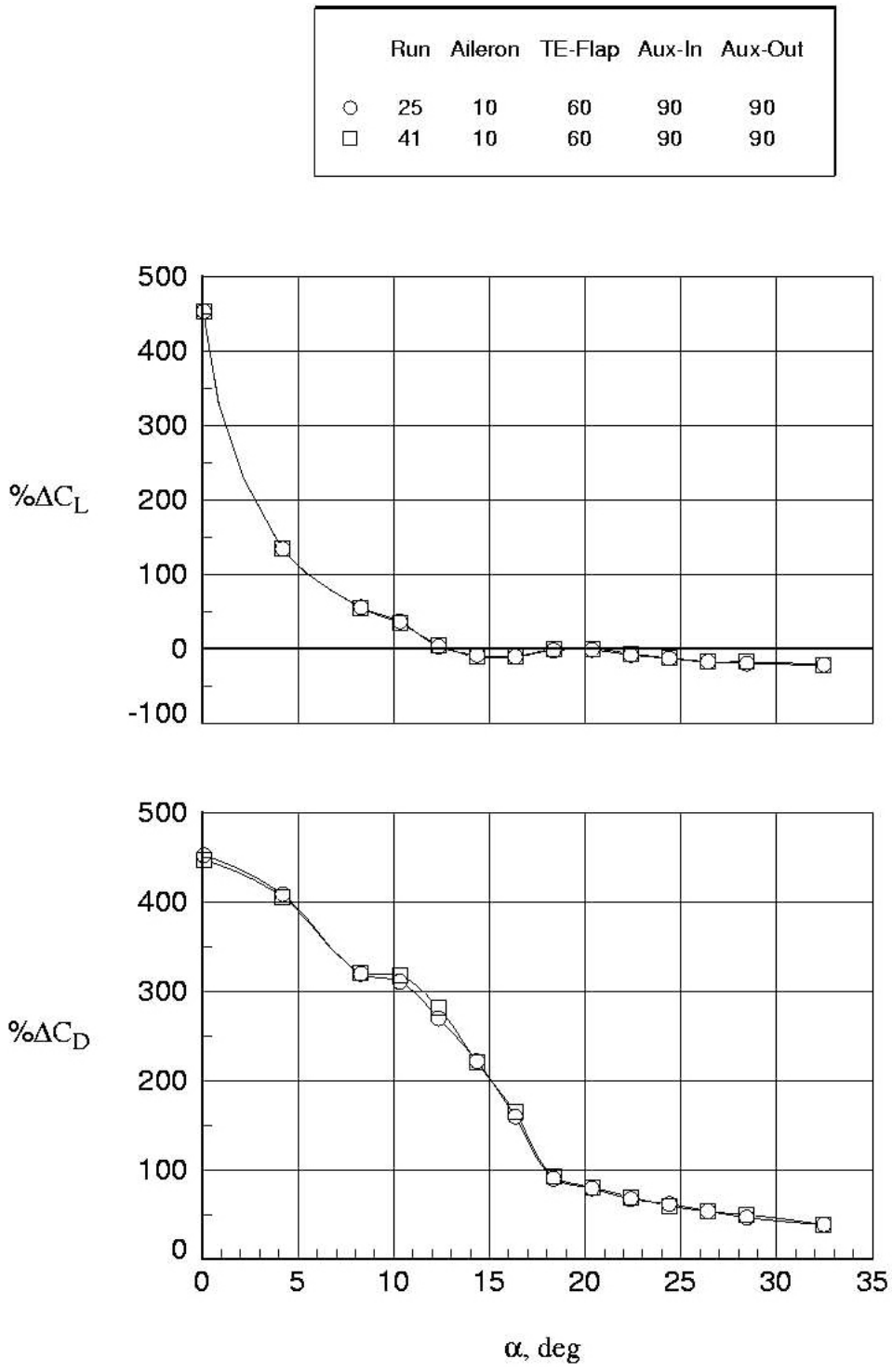

(d) Percent delta changes; baseline = run 2 (aileron deflection = 10°, TE-flap deflection = 60°, aux-in deflection = 90°, aux-out deflection = 90°).

Figure A-3. Concluded.

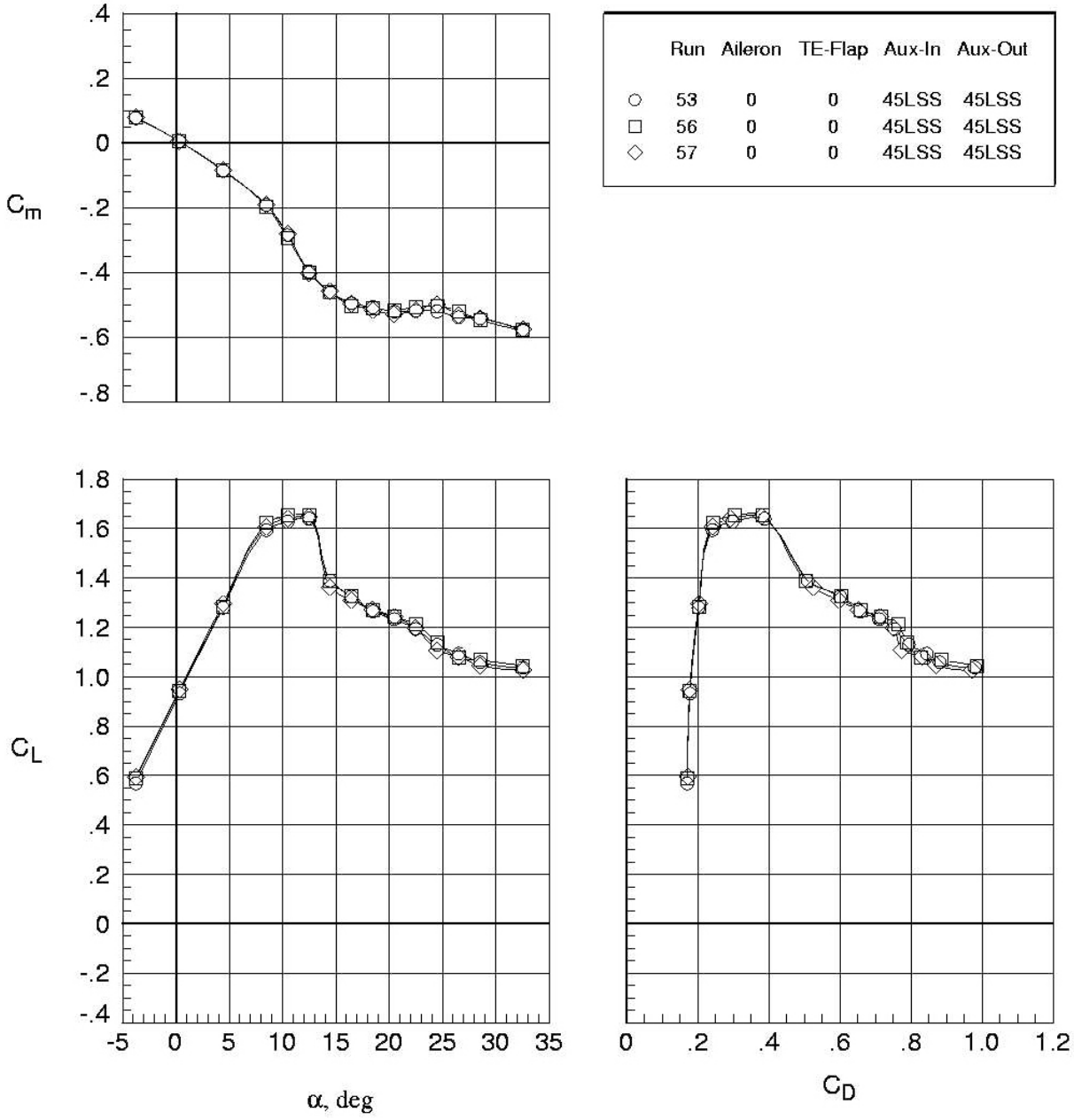

(a) Longitudinal aerodynamics.

Figure A-4. Repeat runs, take-off with lower surface spoilers; q = 4.0 psf.

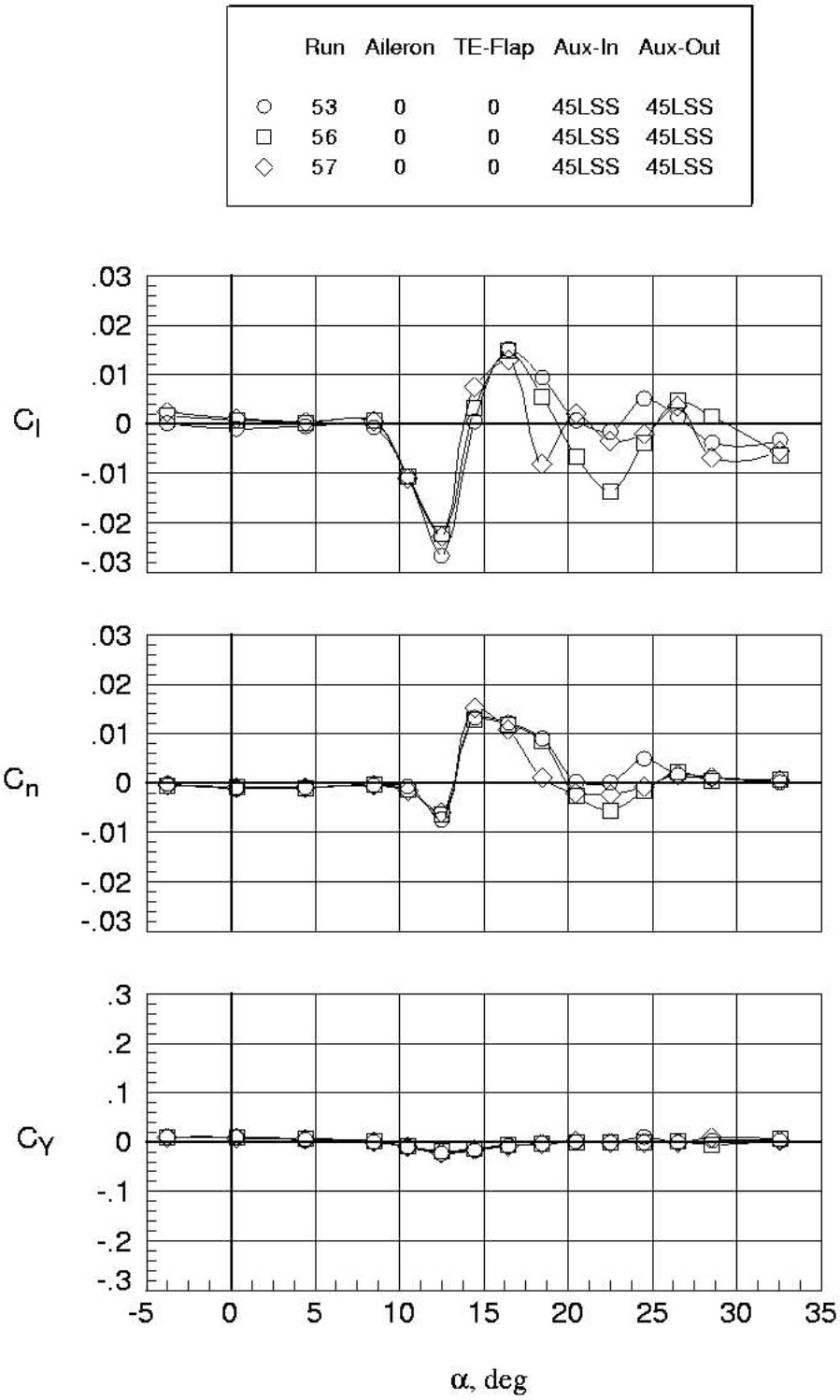

(b) Lateral aerodynamics.

Figure A-4. Continued.

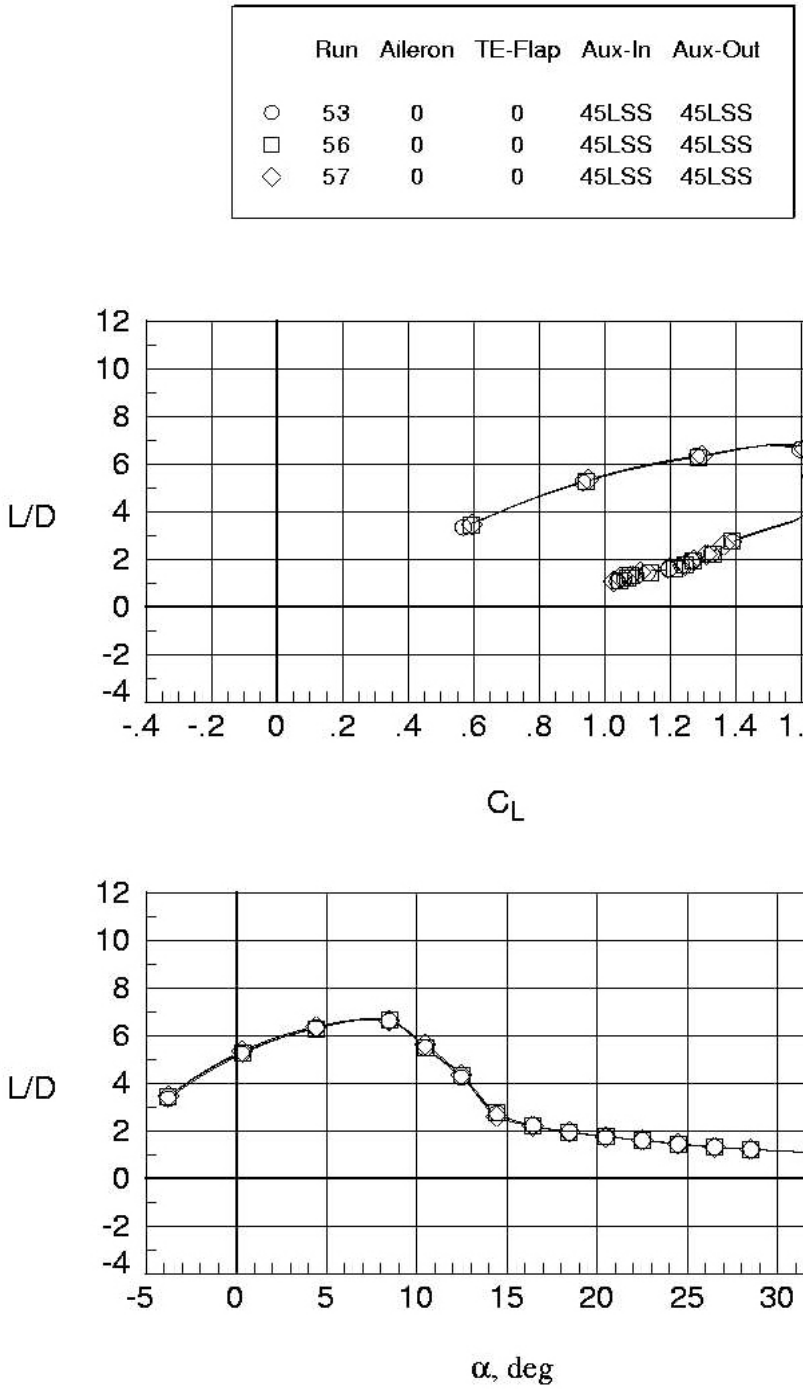

(c) Lift-to-drag ratios.

Figure A-4. Continued.

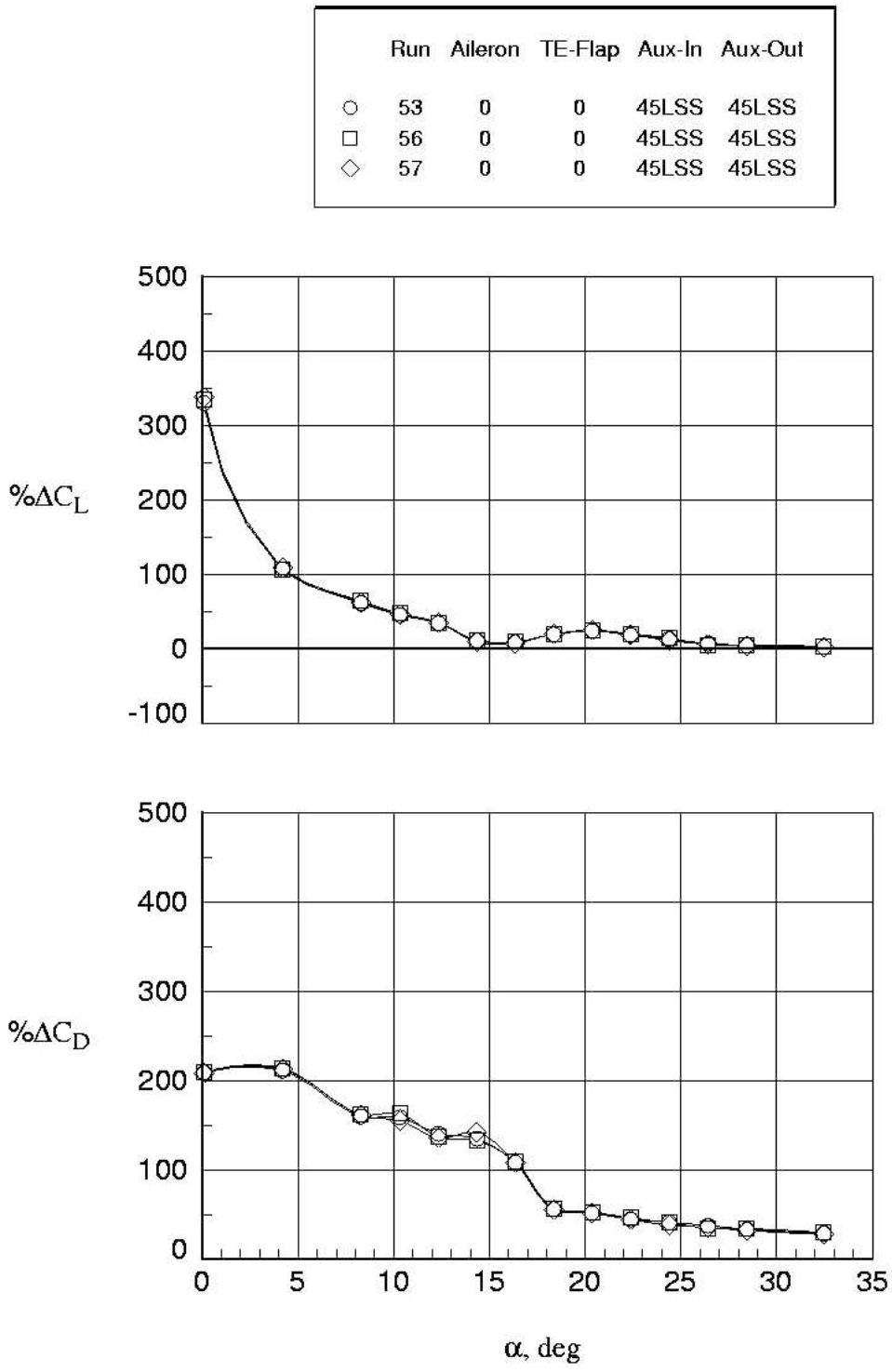

(d) Percent delta changes; baseline = run 2 (aileron deflection = 0°, TE-flap deflection = 0°, aux-in deflection = 45°, aux-out deflection = 45°).

Figure A-4. Concluded.

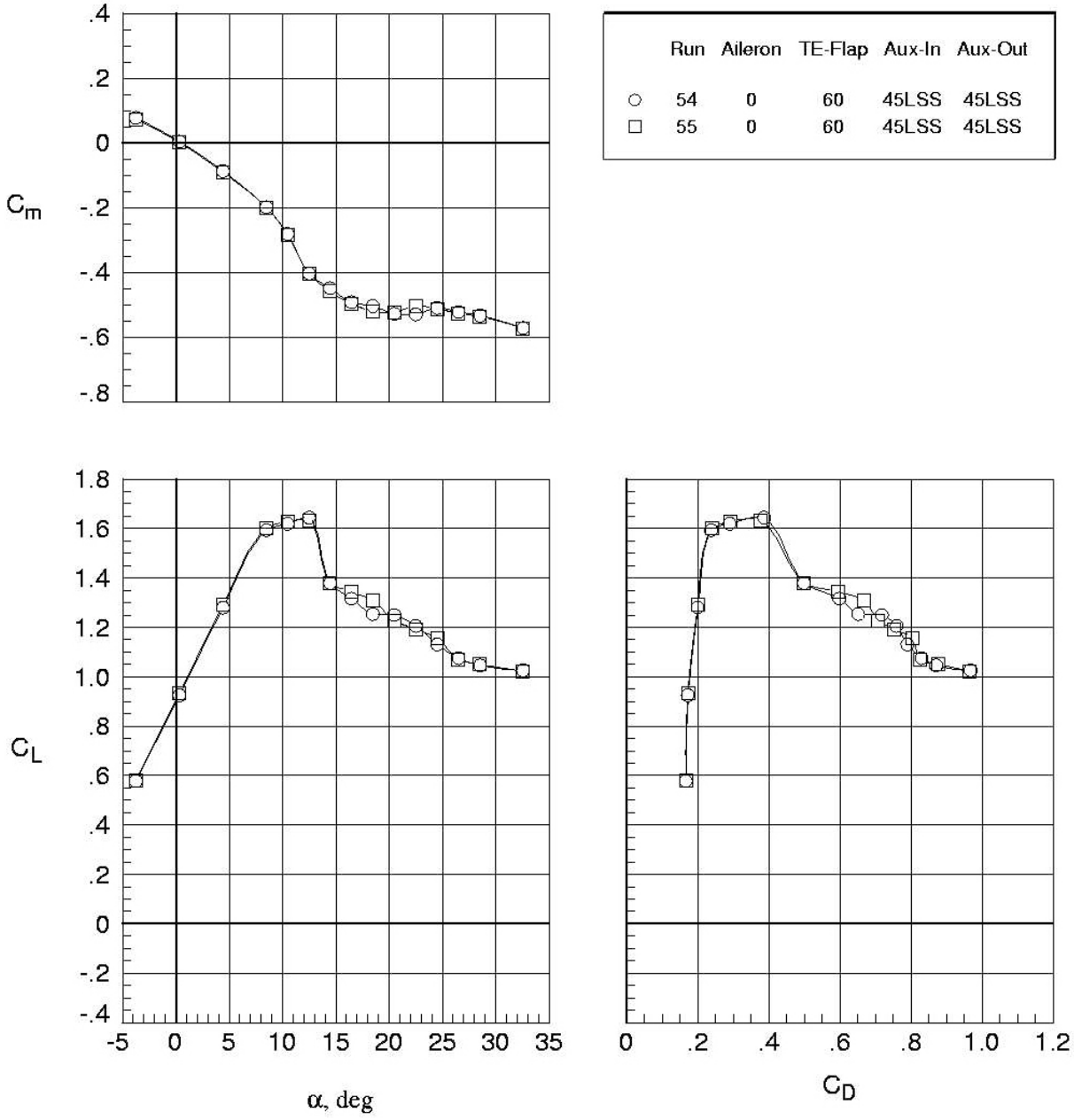

(a) Longitudinal aerodynamics.

Figure A-5. Repeat runs, approach with lower surface spoilers; q = 4.0 psf.

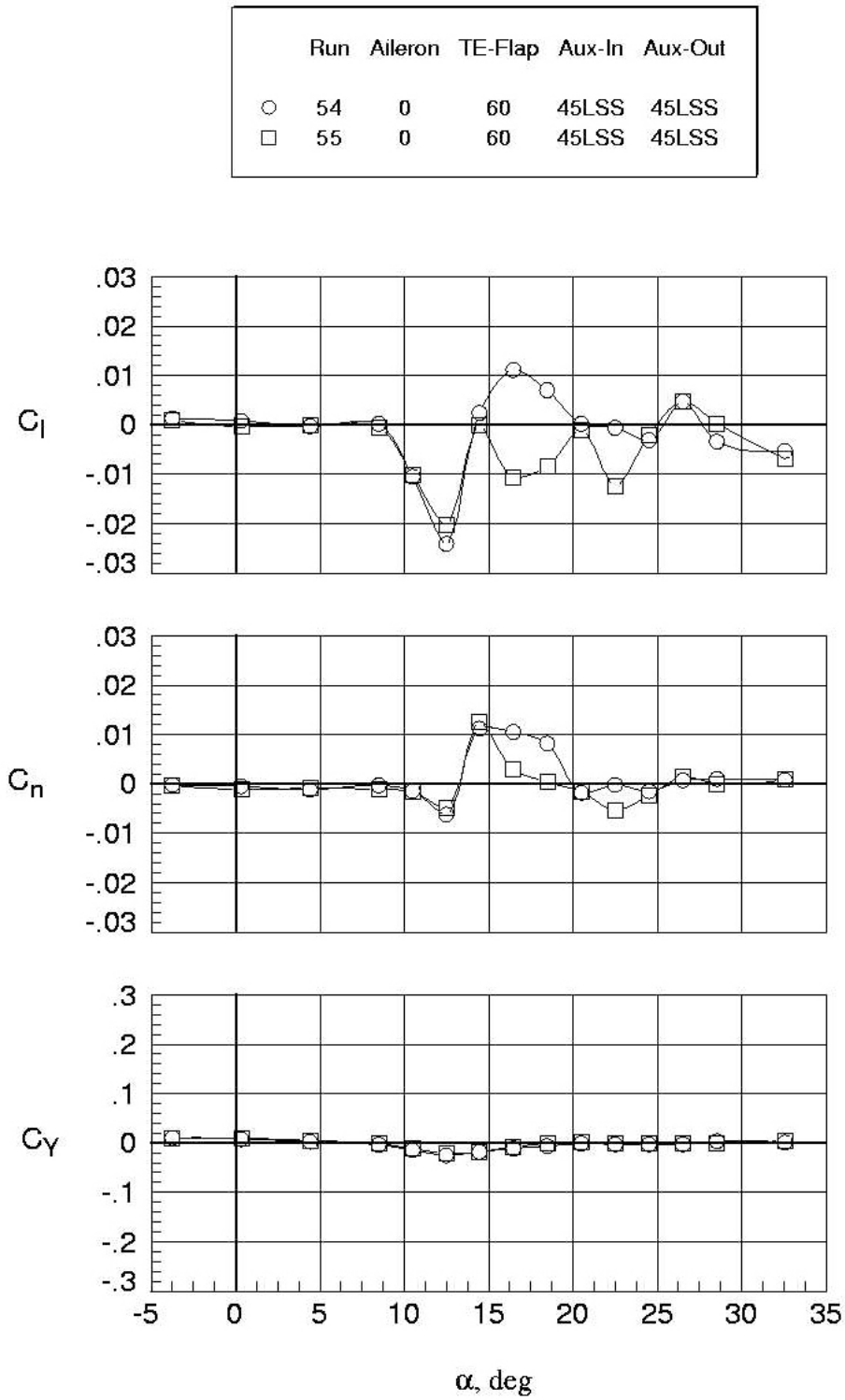

(b) Lateral aerodynamics.

Figure A-5. Continued.

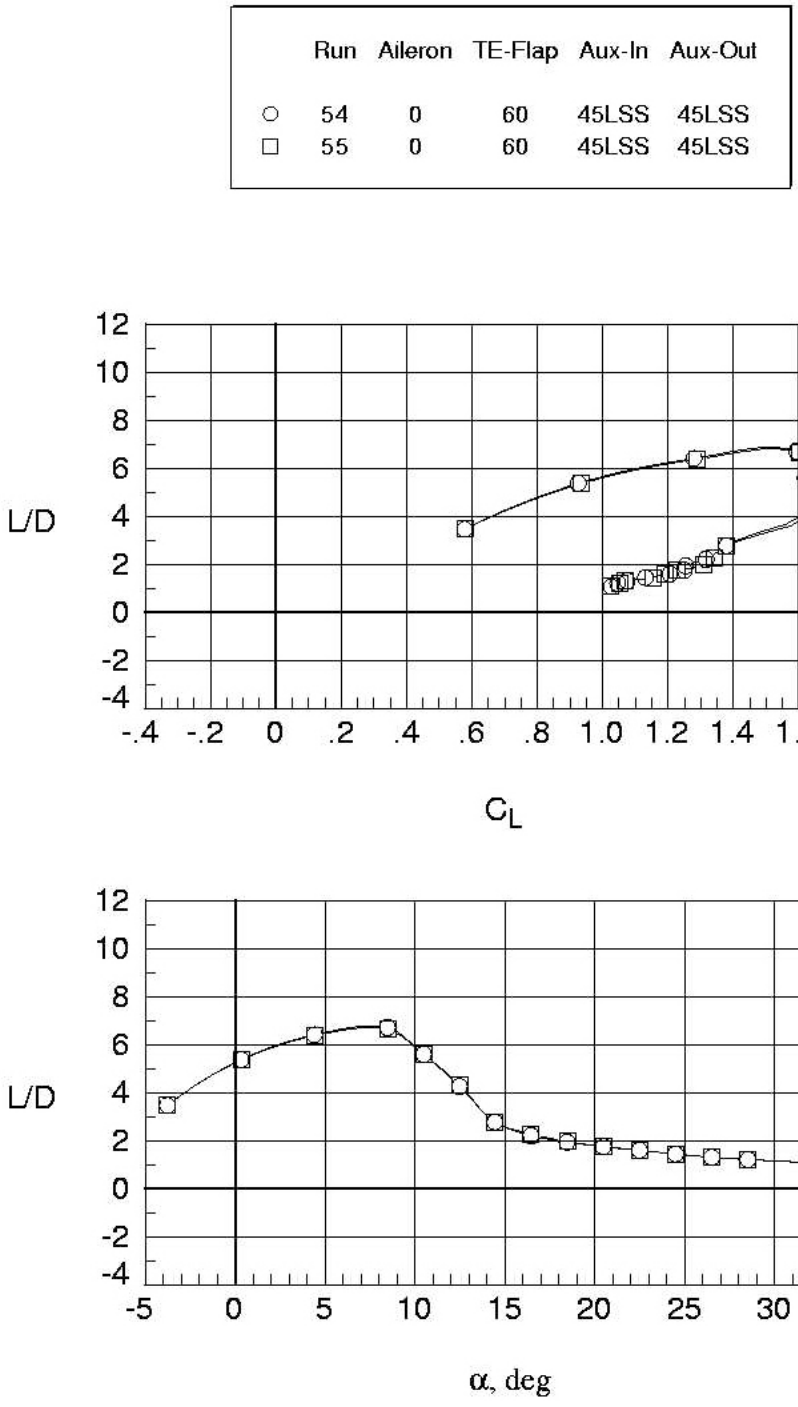

(c) Lift-to-drag ratios.

Figure A-5. Continued.

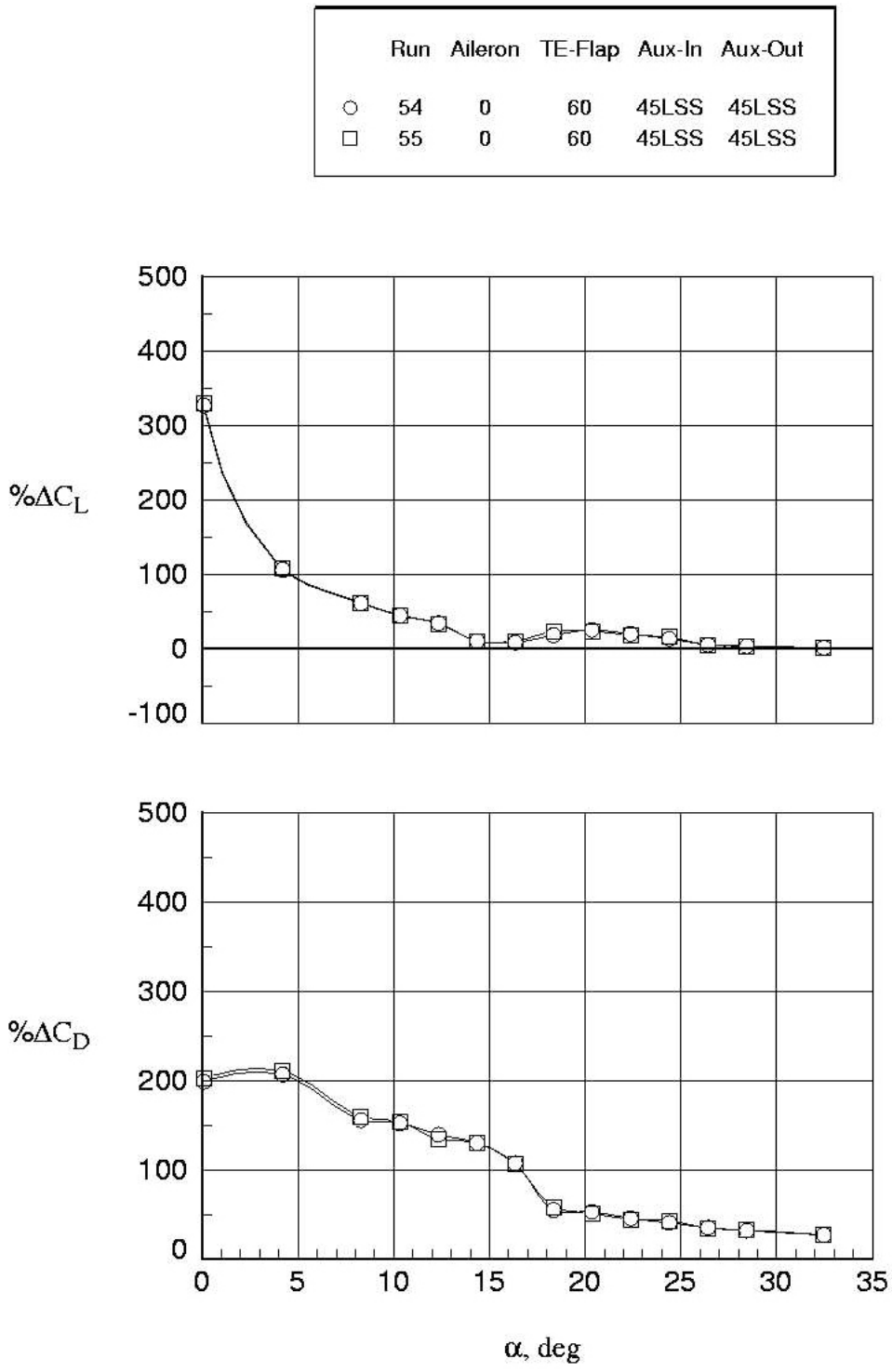

(d) Percent delta changes; baseline = run 2 (aileron deflection = 0°, TE-flap deflection = 60°, aux-in deflection = 45°, aux-out deflection = 45°).

Figure A-5. Concluded.

Appendix B: Computational Fluid Dynamics Discussion and Results

The goals of the computational study were to provide insight into the system flow physics and to give preliminary performance trend comparisons of the modified wing to that of the wing with the conventional flap system.

Grid Generation

In order to develop the computational model of the aircraft, a surface definition needed to be created. The exact definition of the wind tunnel model was not available, so the CFD used a different light GA high-wing aircraft definition. While geometric differences exist, it was determined that the wings are similar enough to have little impact on the wing flow physics, with and without the variable incidence auxiliary (VIA) system installed. The airplane was modeled as a semispan, with the centerline being defined within the CFD as a symmetry plane (fig. B-1).

Six different flap settings were computed on the computational model. These configurations included baseline (no flaps deflected), conventional Fowler flaps at 10° and 40°, the proposed auxiliary flap at 45° and 90° (with split flap at 60°), and the proposed auxiliary flap at 45° (with split flap at 0°). The conventional Fowler flap deflections were modeled from measurements of a light GA high-wing airplane. Flap supports and the aircraft's engine were not modeled. Please note that the reference area remained constant for all of the force and moment calculations, i.e., the additional wing area from the Fowler or auxiliary flap was not added to the reference area.

The computational grids were generated using the grid generation components of NASA Langley's TetrUSS CFD Package.[7] Due to the complex flows expected, each grid was refined around and behind the flaps and resulted in fairly large grids. Table B-1 lists each configuration and its grid size.

Table B-1. Grid sizes for each configuration.

Configuration	Grid Size (number of cells)
Baseline	4,605,418
Conventional Flap, 10°	11,963,457
Conventional Flap, 40°	15,536,347
Auxiliary Flap, 45°	27,881,994
Auxiliary Flap, 45° (Split Flap 30°)	19,377,022
Auxiliary Flap, 45° (Split Flap 60°)	8,395,500
Auxiliary Flap, 90° (Split Flap 60°)	8,420,991

USM3D Flow Solver

The computational study was conducted using the USM3D computational fluid dynamics (CFD) program. USM3D is a Navier-Stokes solver for unstructured, tetrahedral meshes. The code uses a Roe upwind, implicit, cell-centered, finite-volume discretization applied to the integral form of

the Navier-Stokes equations.[7] This approach provides a consistent approximation to the conservation laws of fluid dynamics. For this study, the code was run with the Spalart-Allmaras turbulence model coupled with a wall function formulation to reduce the grid resolution needed for the sublayer portion of a turbulent boundary layer.[8,9] In order to achieve this, the inner region of the boundary layer was modeled by an analytical function that was matched with the numerical solution in the outer region.

For this study, the USM3D parallel program was utilized in order to run on local computer clusters. The grid was partitioned into smaller subsections so that each computer node had approximately the same load. This enabled these complex configurations to be run on Linux machines with only a gigabyte of memory each.[10]

Conditions Analyzed

The six configurations were all run at a Reynolds number of 3.8 million, and a Mach number of 0.113. Under these conditions, the aircraft's speed is equal to 85 miles per hour or 74.7 knots, the approximate airport traffic pattern speed for a light GA high-wing airplane. An alpha sweep was conducted for each configuration and included 5 to 7 angles of attack, which varied by configuration. The details of these alpha sweeps are shown in Table B-2.

Table B-2. Angles of attack computed for each configuration.

Configuration	Angles of Attack (degrees)
Baseline	0, 8, 12, 16
Conventional Flap, 10°	0, 4, 8, 12, 16
Conventional Flap, 40°	0, 4, 8, 12, 16
Auxiliary Flap, 45°	0, 4, 8, 9, 10, 12, 16
Auxiliary Flap, 45° (SF 30°)	0, 4, 8, 9, 10, 12, 16
Auxiliary Flap, 45° (SF 60°)	0, 4, 8, 9, 10, 12, 16
Auxiliary Flap, 90° (SF 60°)	0, 4, 8, 12, 16

Unsteady Conditions

This computational study was conducted using the unsteady state version of USM3D,[11] since numerous unsteady conditions were encountered. In order to obtain accurate results, each condition was run for 2000 iterations in steady-state mode. Then, using the steady state as a starting point, the code was then run to approximately 30,000 total iterations in unsteady mode. Fifteen subiterations for each second-order time-accurate computation were computed.

Computational Results

The results of the computational study are presented graphically in figures B-2–B-19. In order to graph values from the unsteady runs, the last iterated data points were used. However, since these conditions were unsteady, the corresponding values did vary slightly over the computational iterations.

Figure B-2 compares the lift curves of the six configurations. The overall slope remains the same, but the level of lift increases as the flaps and then the auxiliary flaps are deployed. All of the auxiliary flaps coupled with a split flap deflection differed from the rest of the results. These cases reached their maximum lift coefficient by an angle of attack of 12°. Similarly, figures B-3 and B-4 show that the levels of drag increase as flaps and auxiliary flaps are deployed. In the drag versus angle of attack plot (fig. B-3), the auxiliary flap cases produced significantly more drag then the conventional and baseline configuration with the auxiliary flap at 90°, split flap at 60° producing significantly more drag then the baseline configuration. In figure B-4 the lift-versus-drag results show that all of the configurations with the auxiliary flap are almost completely above the entire curve of not only the baseline but the conventional-flap deflection cases. Finally, the pitching moment curves (fig. B-5) show that the auxiliary-flap deflection has become nonlinear in the curves while the remaining cases' results remain relatively linear.

Figures B-6–B-19 show the flow around the wing and flaps. This data was cut from the computational grids 78 inches out from the centerline of the full-scale aircraft (15.6 inches on the model) and graphed using Tecplot. The pressure coefficient is plotted in color with stream traces shown in black. The angles of attack shown are 0° and 8° for each configuration. As shown, the stream traces change only slightly between the two angles of attack.

One of the main questions going into the CFD study was whether the rotational flow seen between the auxiliary flap and the split flap is a trapped separation bubble or a weak trapped vortex. The combination of the pressure and stream traces answers this question. The stream traces follow the flow from a given starting point to the end of the computational grid. In figures B-6–B-9, clean lines around the airfoil were traced. However, starting with the conventional flap deflected at 40°, rotational flow appears near the upper surface of the flap. In each case, there is an upper, clockwise rotational flow and a lower, counter-clockwise rotational flow. In order to determine what type of rotational flow each one is, the pressures within the flow must be examined by referring to the pressure contour color scale. The flow on the conventional flap at 40° (figs. B-10 and B-11) and the split flap (figs. B-12 and B-13) all show the stream traces going through a change of pressure. Keeping the auxiliary flap at 45° and deflecting the split flap to 30°, as shown in figures B-14 and B-15, serves to contain the rotational separation on the auxiliary flap. However, in figures B-16–B-17, with the split flap at 60°, the upper rotational flow on the auxiliary flap creates its own pressure region with a circular pattern leading to low pressure in the middle of the flow. This indicates the presence of a weak trapped vortex. However, the small lower rotational flow on the auxiliary flap does not appear to develop a low-pressure field within the center of rotation and is assumed to be a small trapped separation bubble. The 90° auxiliary flap depicted in figures B-18 and B-19 shows large rotational separation bubbles.

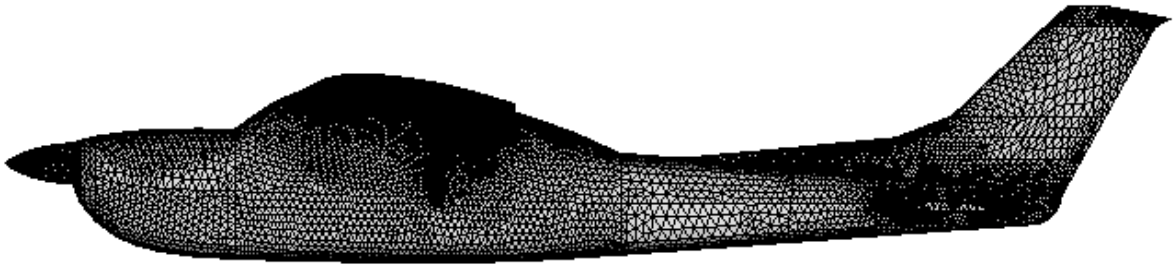

Figure B-1. Computational grid definition of aircraft.

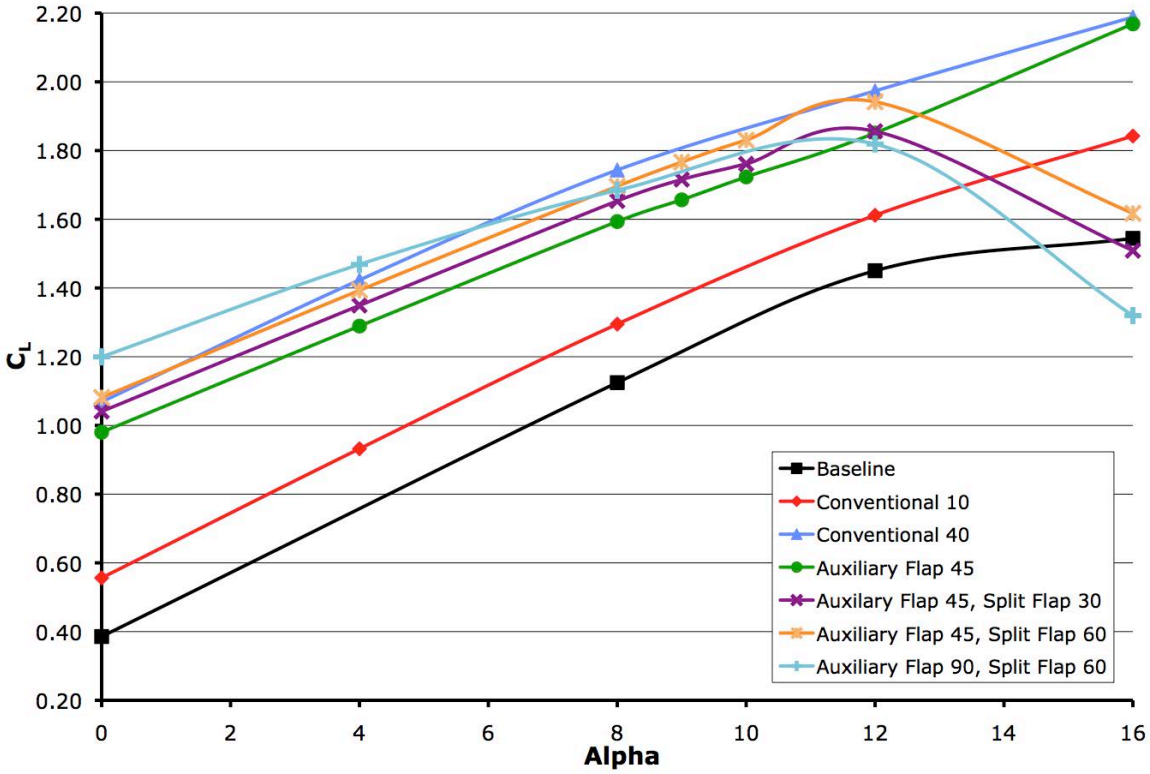

Figure B-2. Lift versus angle of attack (degrees) comparison.

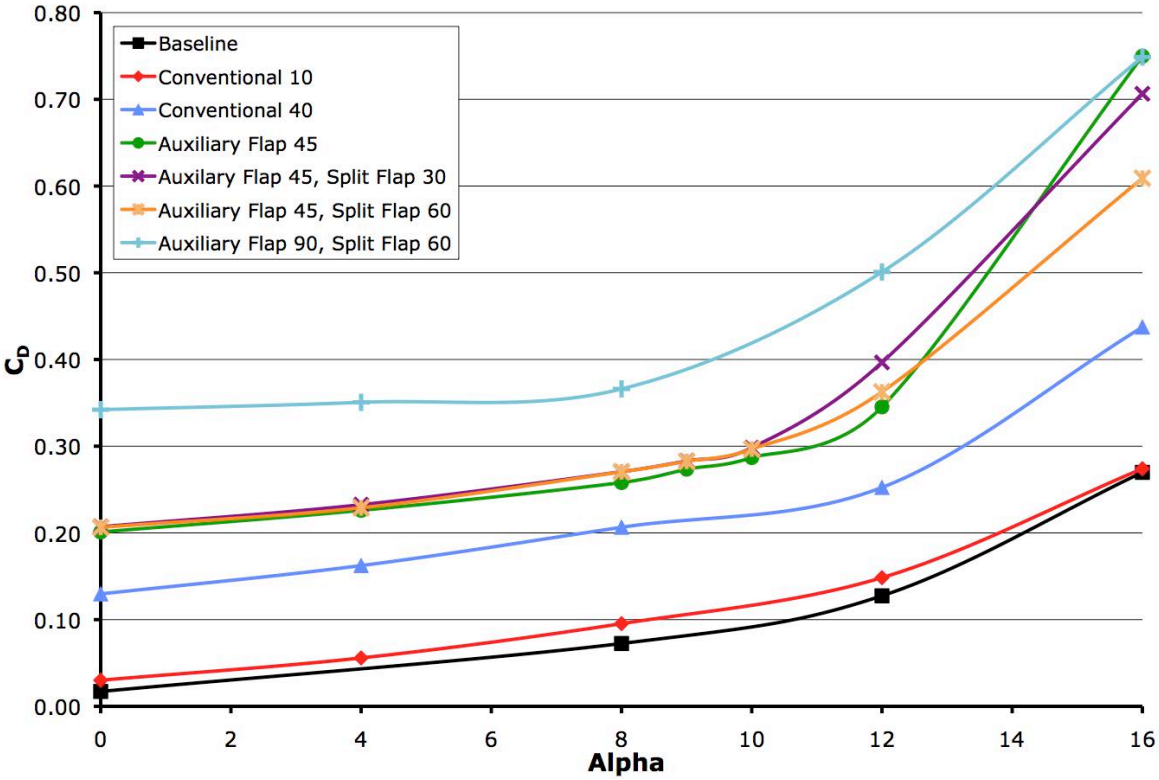

Figure B-3. Drag versus angle of attack (degrees) comparison.

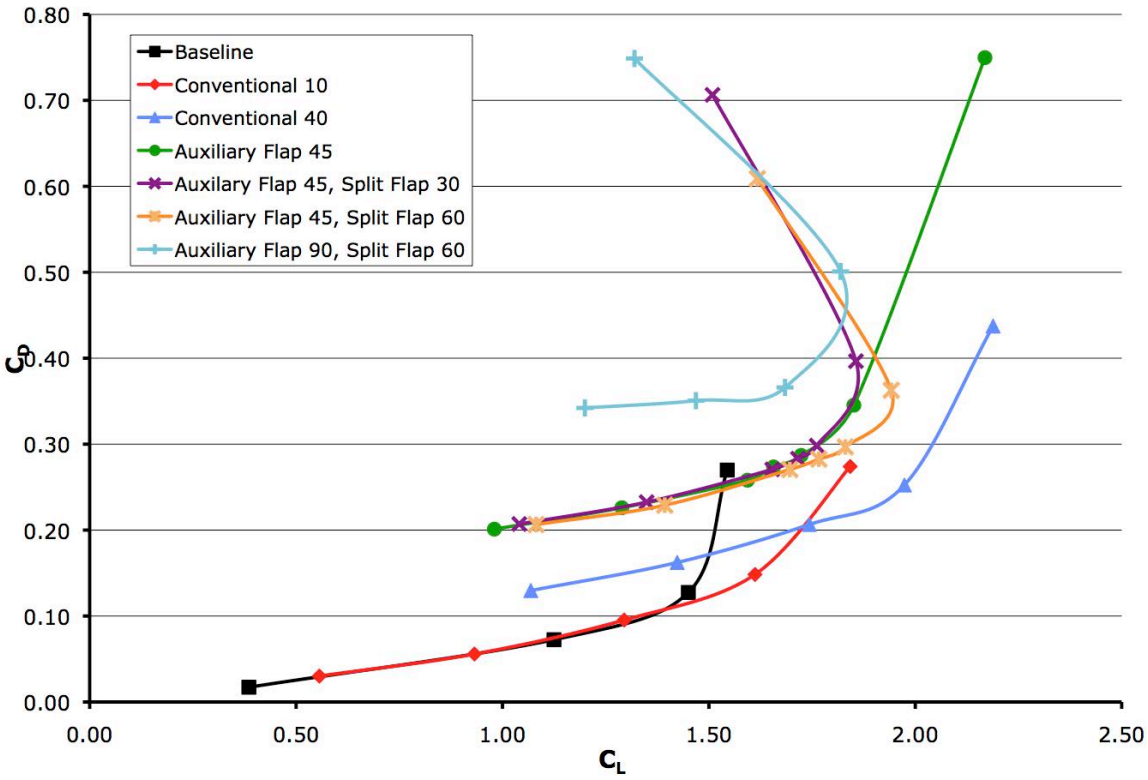

Figure B-4. Drag versus lift comparison.

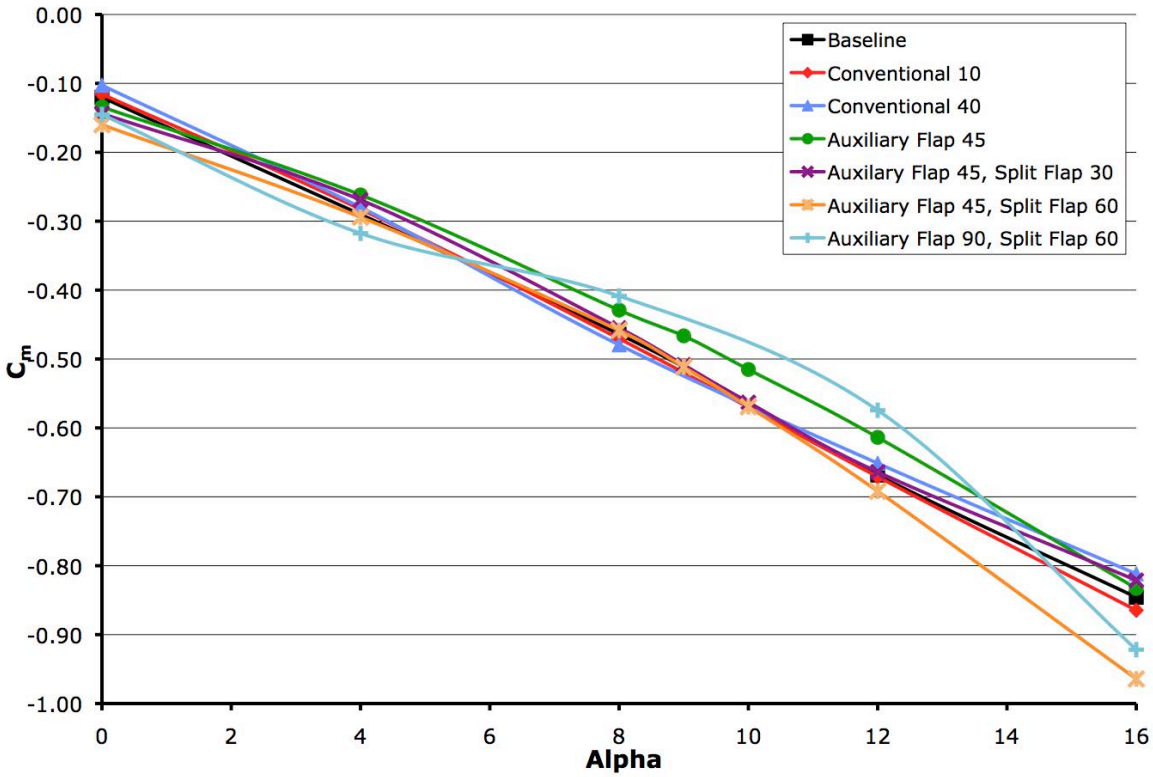

Figure B-5. Pitching moment comparison.

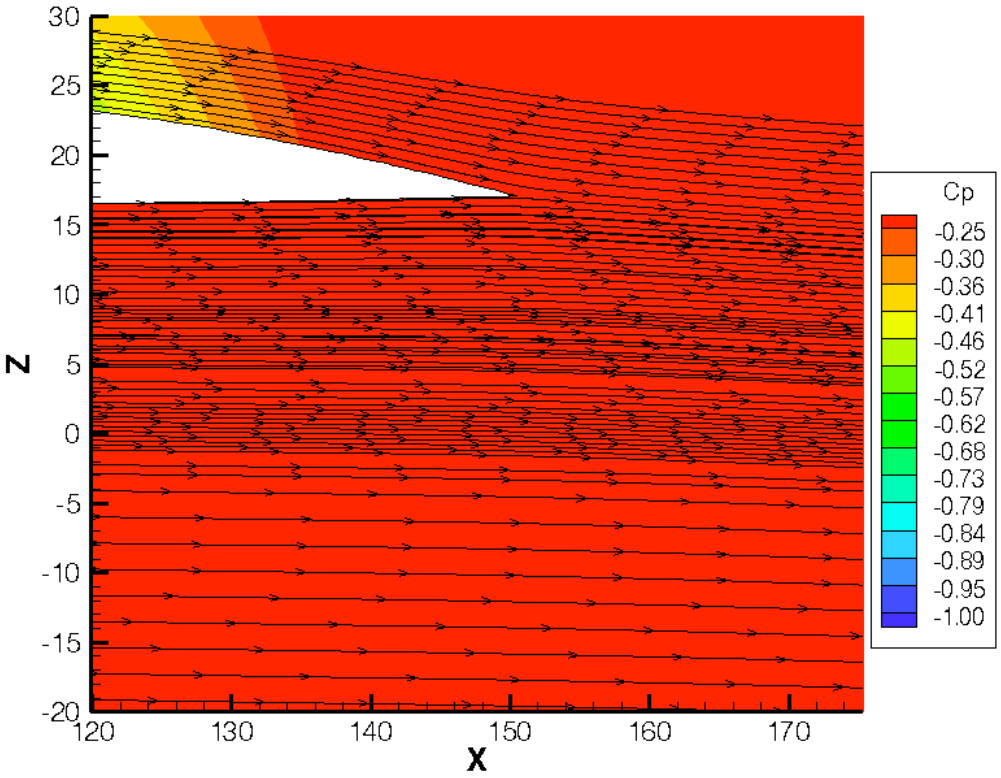

Figure B-6. Baseline wing at 0° angle of attack, 78 inches from center line of aircraft.

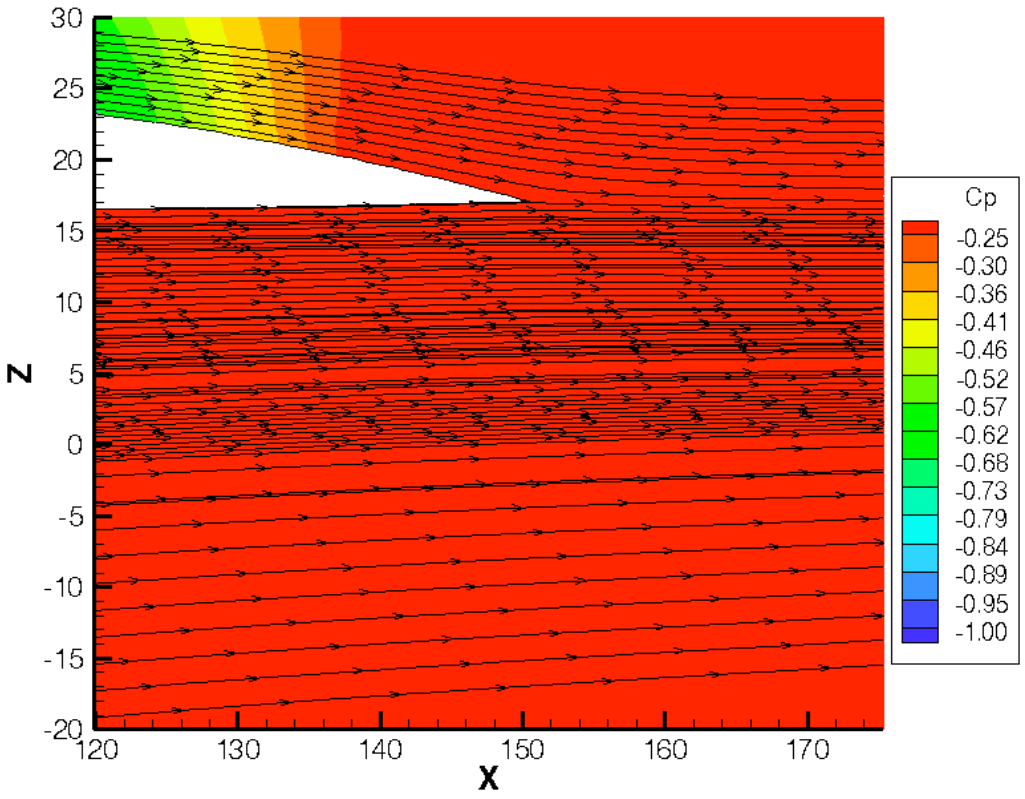

Figure B-7. Baseline wing at 8° angle of attack, 78 inches from center line of aircraft.

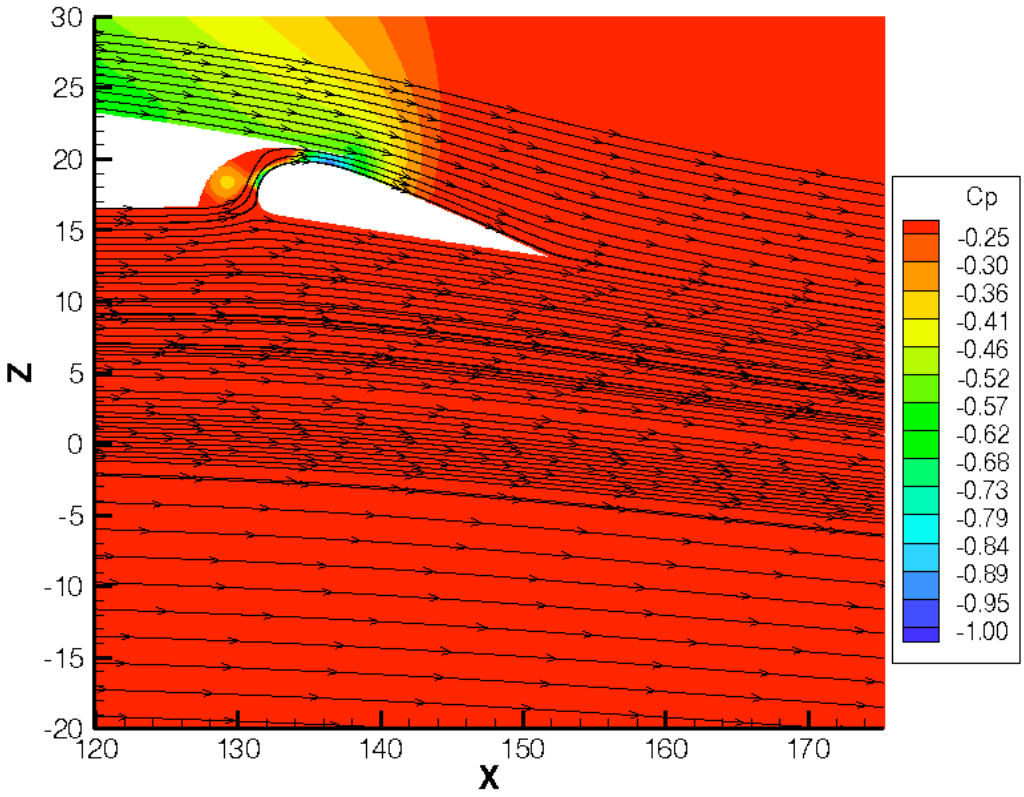

Figure B-8. Conventional flap at 10° (0° angle of attack), 78 inches from center line of aircraft.

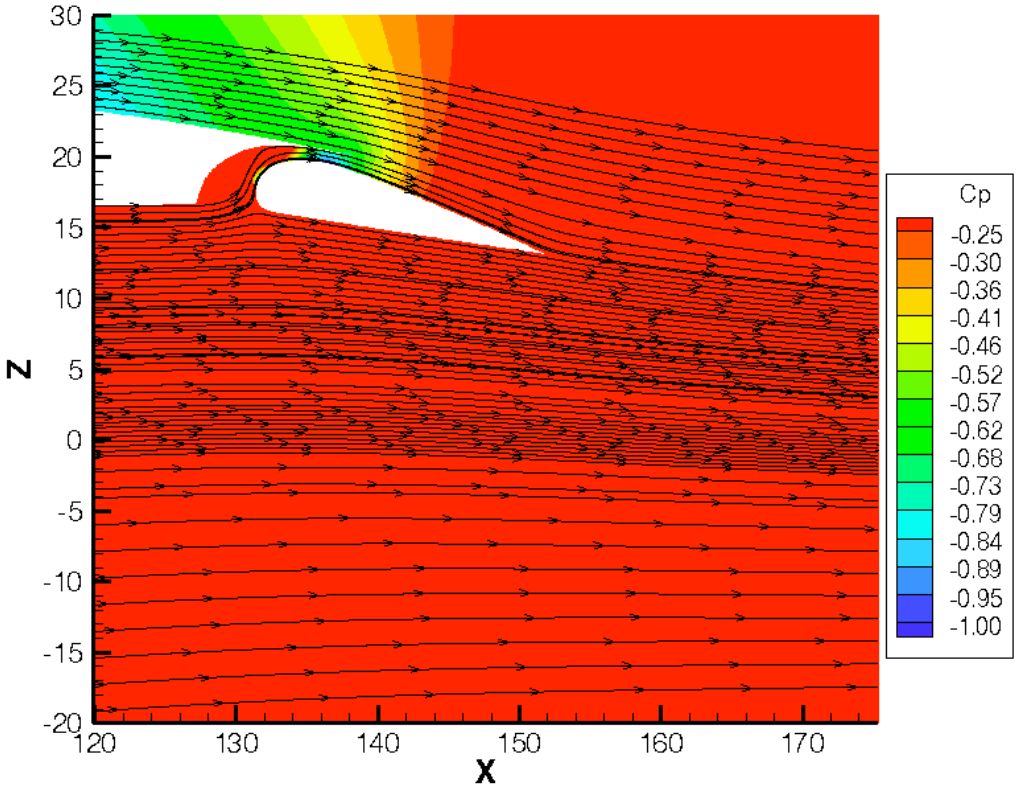

Figure B-9. Conventional flap at 10° (8° angle of attack), 78 inches from center line of aircraft.

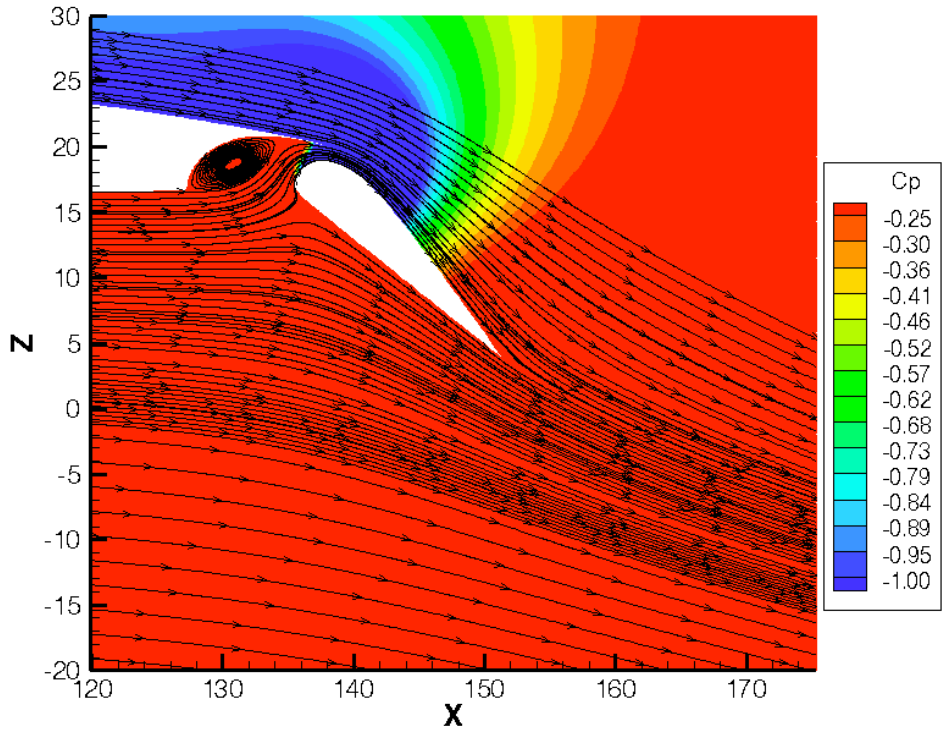

Figure B-10. Conventional flap at 40° (0° angle of attack), 78 inches from center line of aircraft.

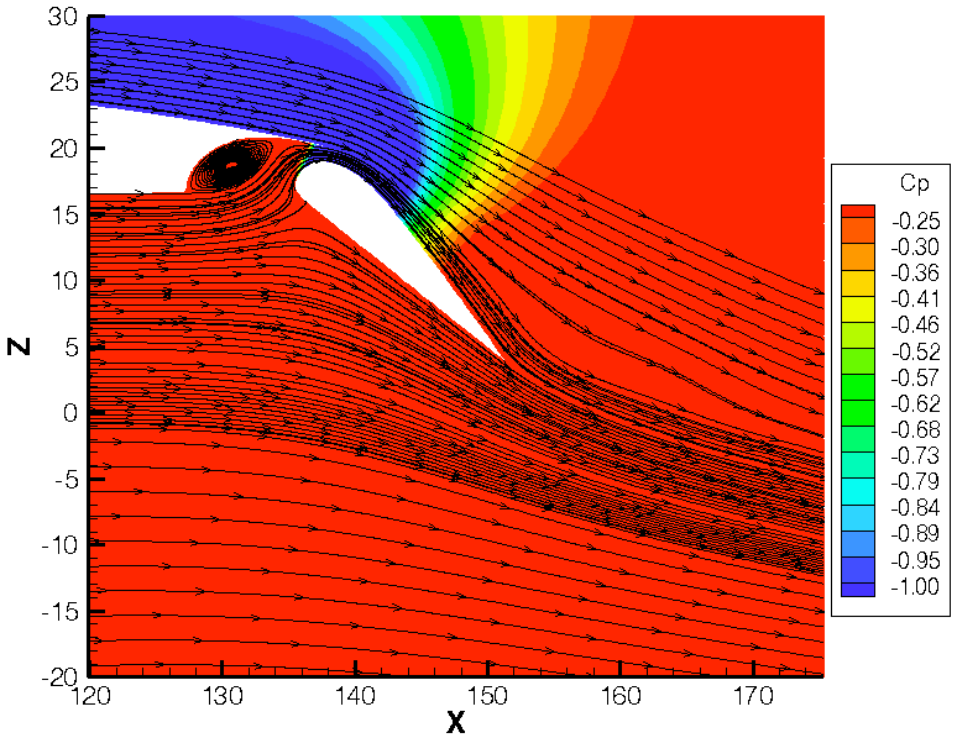

Figure B-11. Conventional flap at 40° (8° angle of attack), 78 inches from center line of aircraft.

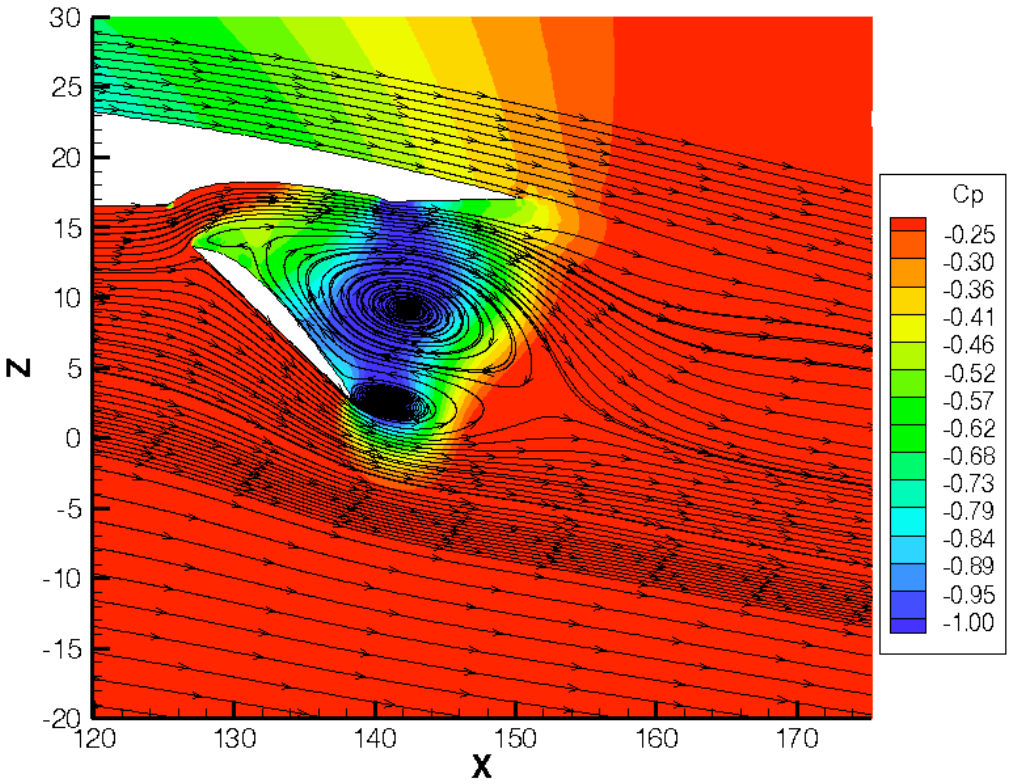

Figure B-12. Auxiliary flap at 45° (0° angle of attack), 78 inches from center line of aircraft.

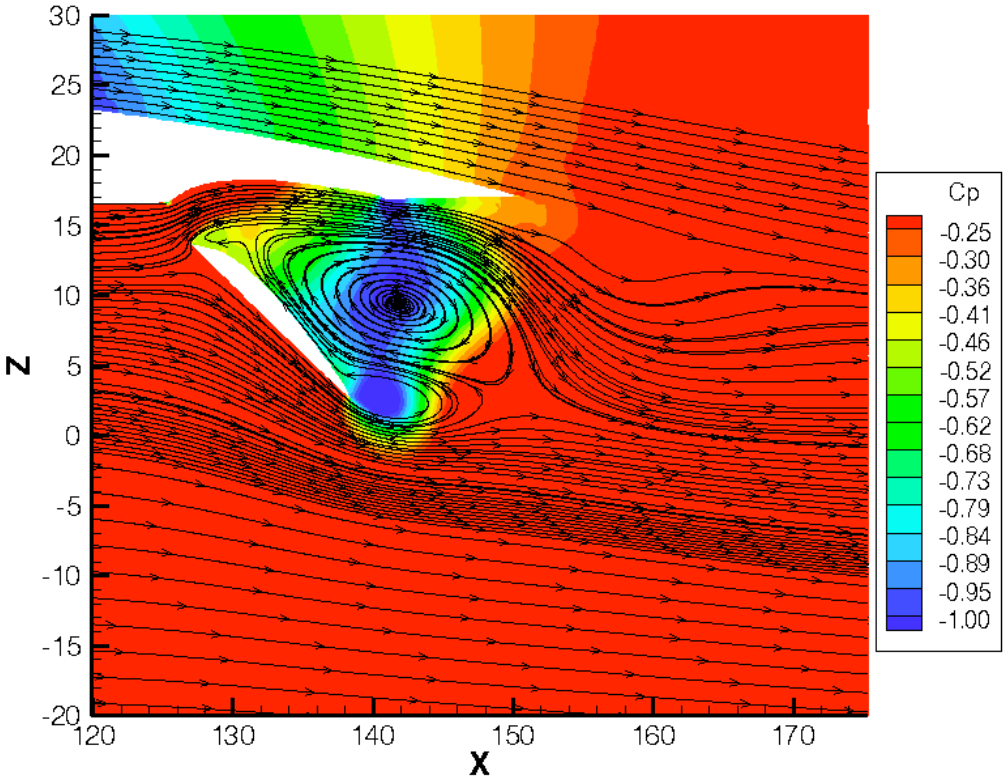

Figure B-13. Auxiliary flap at 45° (8° angle of attack), 78 inches from center line of aircraft.

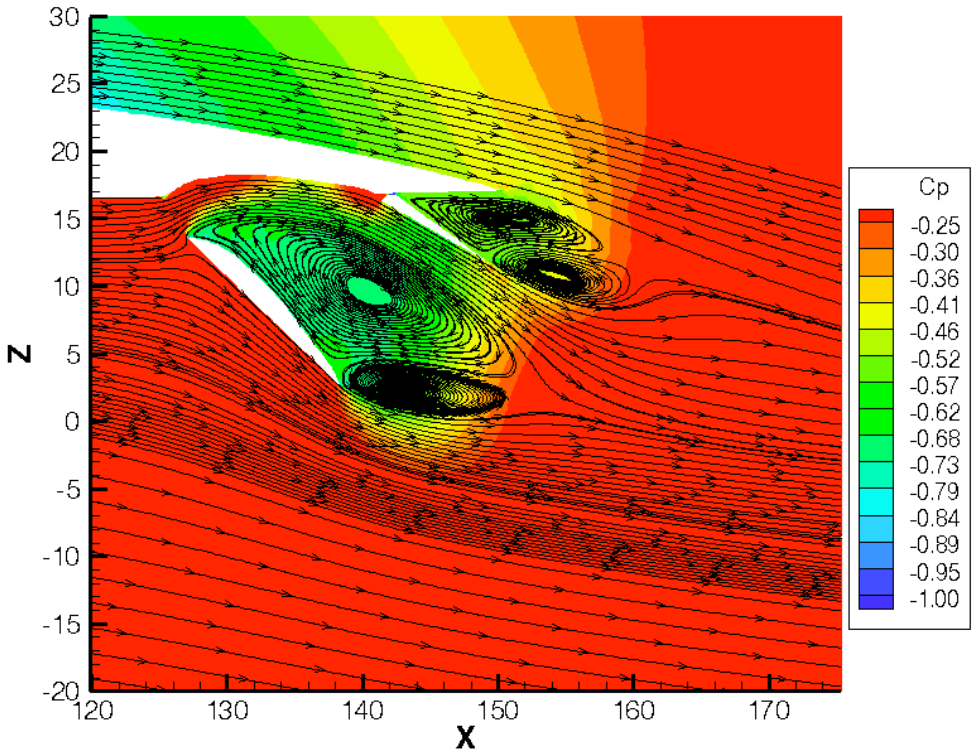

Figure B-14. Auxiliary flap at 45°, split flap at 30° (0° angle of attack), 78 inches from center line of aircraft.

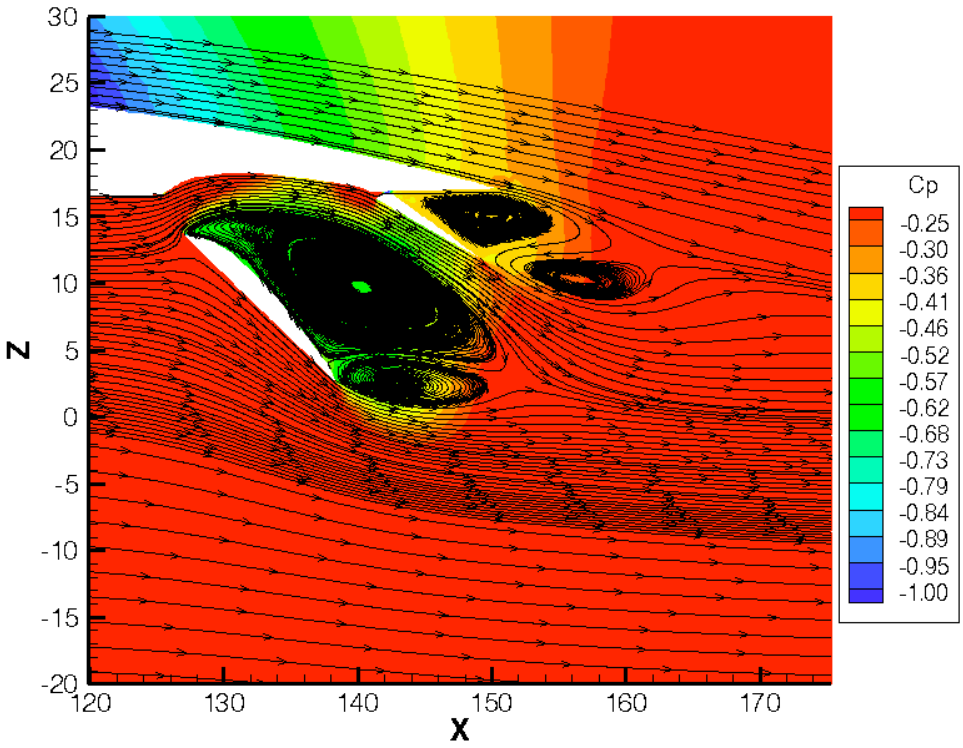

Figure B-15. Auxiliary flap at 45°, split flap at 30° (8° angle of attack), 78 inches from center line of aircraft.

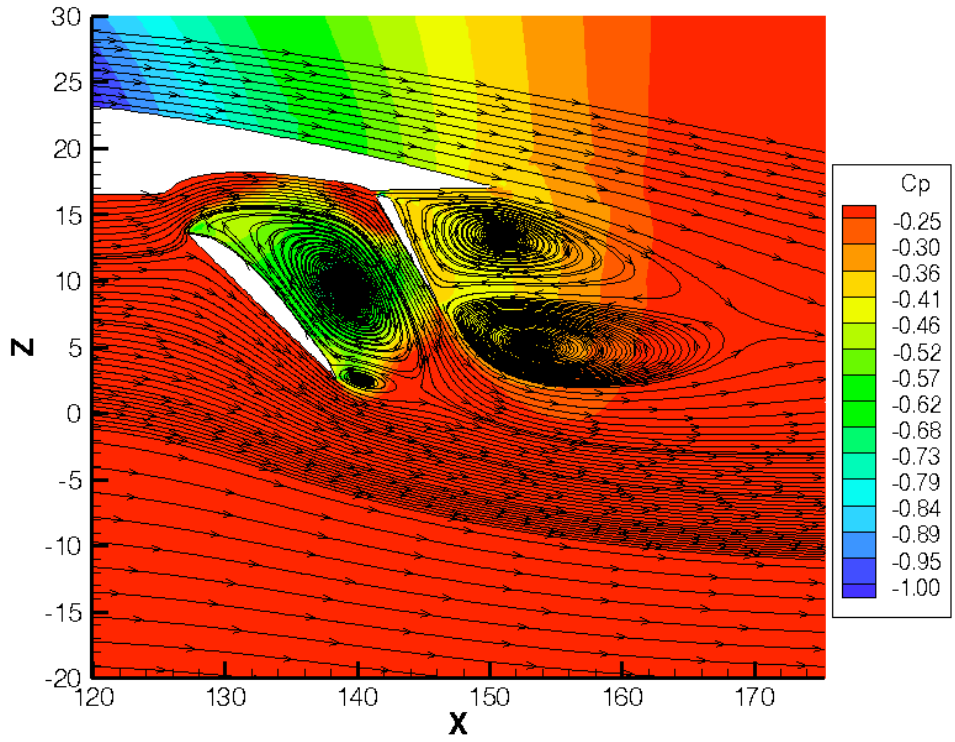

Figure B-16. Auxiliary flap at 45°, split flap at 60° (0° angle of attack), 78 inches from center line of aircraft.

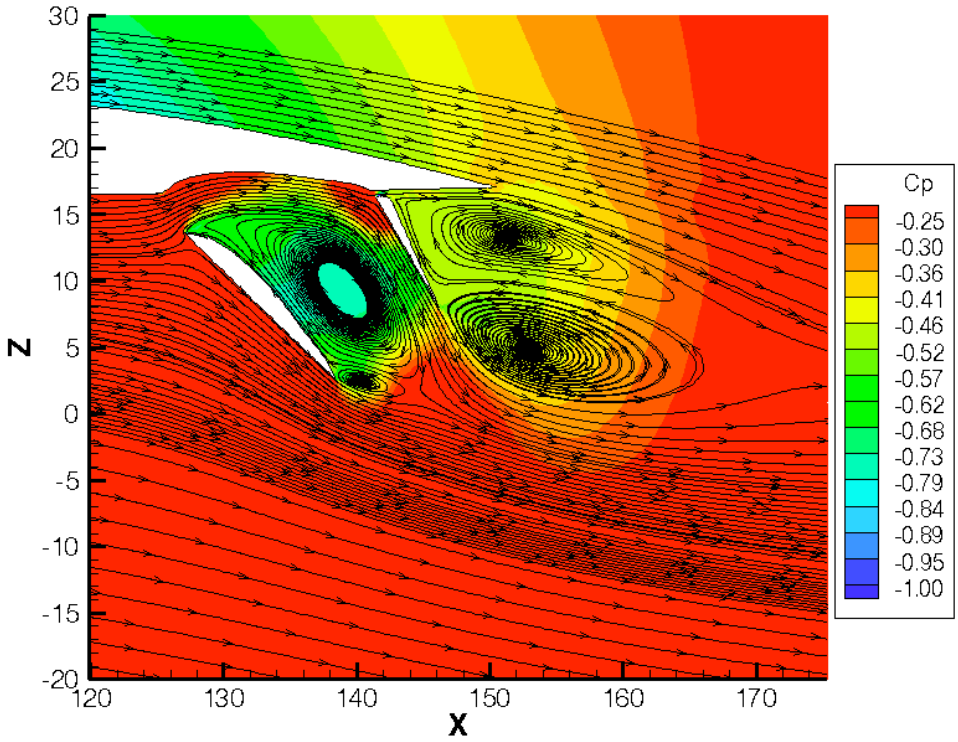

Figure B-17. Auxiliary flap at 45°, split flap at 60° (8° angle of attack), 78 inches from center line of aircraft.

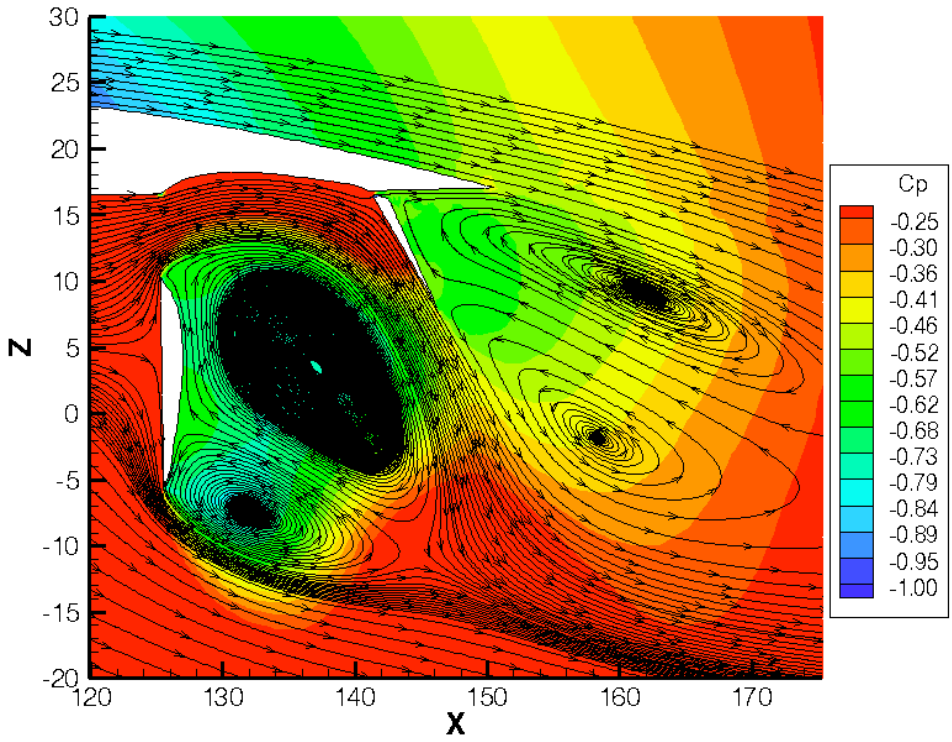

Figure B-18. Auxiliary flap at 90°, split flap at 60° (0° angle of attack), 78 inches from center line of aircraft.

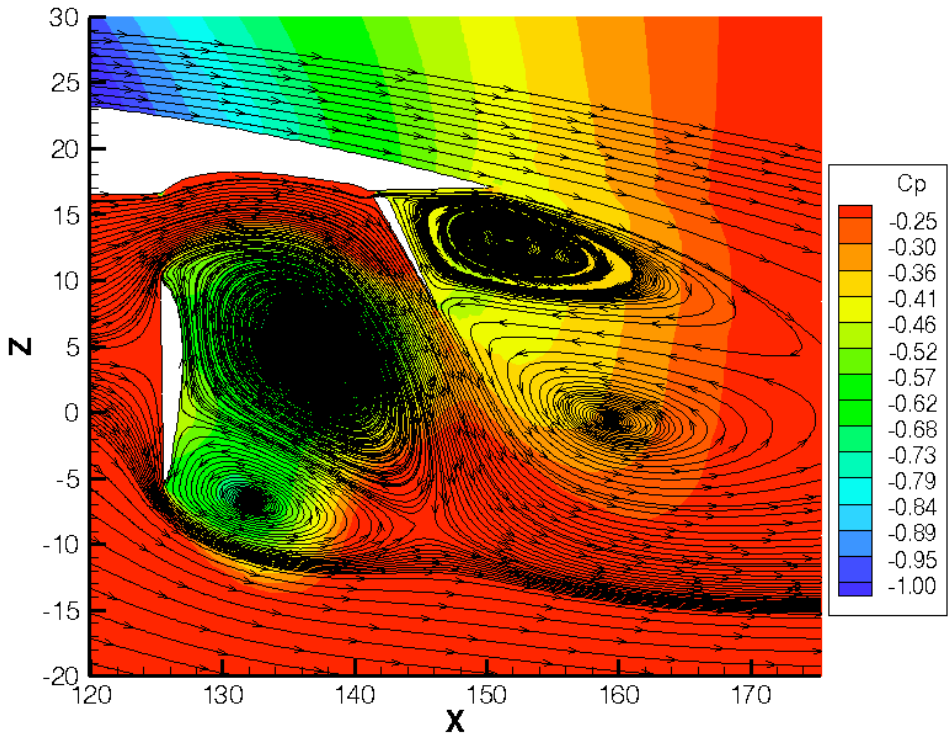

Figure B-19. Auxiliary flap at 90°, split flap at 60° (8° angle of attack), 78 inches from center line of aircraft.

Appendix C: Tuft Flow Visualization

Once the force and moment portion of the investigation was complete, tufts were affixed to the model as a simple surface flow visualization technique. Of particular interest were the surfaces of the auxiliary flap, split flap, and the side of the fuselage just below and aft of the main wing trailing edge. Photographs were taken for the angle of attack of 0°, 4°, 8°, 12° and 16°. Due to the unusual nature of the flap system, photographs were limited to ¾ rear viewing angles. Where possible, the views presented are

- inboard: rear ¾ view of the inboard trailing-edge flap system;
- outboard tip: rear ¾ view of the outboard trailing-edge flap system and the wing tip;
- fuselage: close to side view showing the tufted portion of the fuselage.

Table C-1 identifies the flap configuration and the corresponding angles of attack (α) at which the tuft images were taken. A sample of the nomenclature used to define the flap configuration is

Aux-In-45_Aux-Out-45_Split-60_Ail-0

This represents auxiliary flap inboard at 45°, auxiliary flap outboard at 45°, split flap at 60° and aileron at 0°.

Where the model surface is red or silver, the tufts are white. Where the model surface is white, the tufts are black.

It should be noted that the fuselage-view tuft photographs for the 60° split flap (figs. C-93–C-102) and the cruise wing (figs. C-103–C-115) all show the following:

Picture 2. This does not represent the actual surface flow, but rather the result of two individual tufts getting tangled.

Table C-1. Index to tuft flow visualization images.

Flap Configuration	Alpha	Appendix C Figure Number
Aux-In-45_Aux-Out-45_Split-60_Ail-0	0	1, 2, 3
	4	4, 5, 6
	8	7, 8, 9
	12	10, 11, 12
	16	13, 14, 15
	16	16, 17
Aux-In-45_Aux-Out-45_Split-0_Ail-0	0	18, 19, 20
	4	21, 22, 23
	8	24, 25, 26
	12	27, 28, 29
	16	30, 31, 32
Aux-In-0_Aux-Out-45_Split-60_Ail-0	0	33, 34, 35
	4	36, 37, 38
	8	39, 40, 41
	12	42, 43, 44
	16	45, 46, 47
Aux-In-0_Aux-Out-90_Split-60_Ail-0	0	48, 49, 50
	4	51, 52, 53
	8	54, 55, 56
	12	57, 58, 59
	16	60, 61, 62
Aux-In-90_Aux-Out-90_Split-60_Ail-0	0	63, 64, 65

	4	66, 67, 68
	8	69, 70, 71
	12	72, 73, 74
	16	75, 76, 77
Aux-In-90_Aux-Out-90_Split-0_Ail-0	0	78, 79, 80
	4	81, 82, 83
	8	84, 85, 86
	12	87, 88, 89
	16	90, 91, 92
Aux-In-0_Aux-Out-0_Split-60_Ail-0	0	93, 94
	4	95, 96
	8	97, 98
	12	99,100
	16	101, 102
Aux-In-0_Aux-Out-0_Split-0_Ail-0	0	103, 104, 105
	4	106, 107
	8	108, 109, 110
	12	111, 112, 113
	16	114, 115
LSS-In-45_LSS-Out-45_Split-60_Ail-0	0	116, 117, 118
	4	119, 120, 121, 122
	8	123, 124, 125, 126
	12	127, 128, 129

	16	130, 131, 132
LSS-In-45_LSS-Out-45_Split-0_Ail-0	0	133, 134, 135
	4	136, 137, 138
	8	139, 140, 141
	12	142, 143, 144
	16	145, 146, 147
LSS-In-0_LSS-Out-45_Split-0_Ail-0	0	148, 149, 150
	4	151, 152, 153
	8	154, 155, 156
	12	157, 158
	16	159, 160, 161
LSS-In-0_LSS-Out-45_Split-60_Ail-0	0	162, 163, 164
	4	165, 166
	8	167, 168, 169
	12	170, 171, 172
	16	173, 174, 175

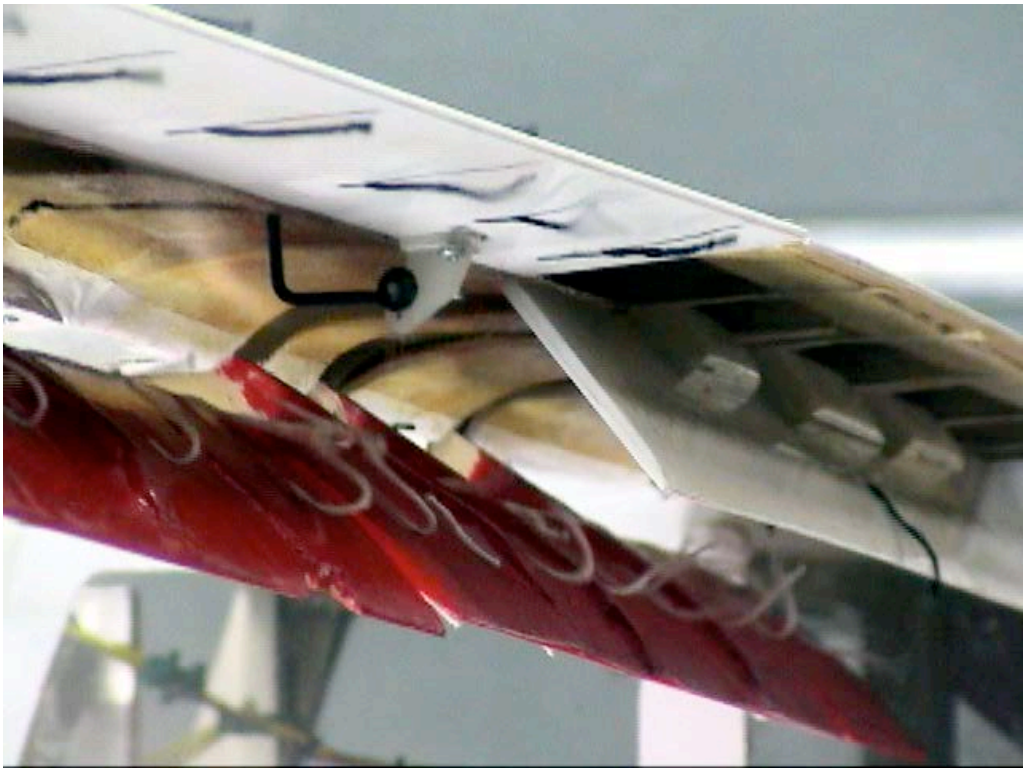

Figure C-1. Inboard view; Aux-In-45_Aux-Out-45_Split-60_Ail-0; α = 0°.

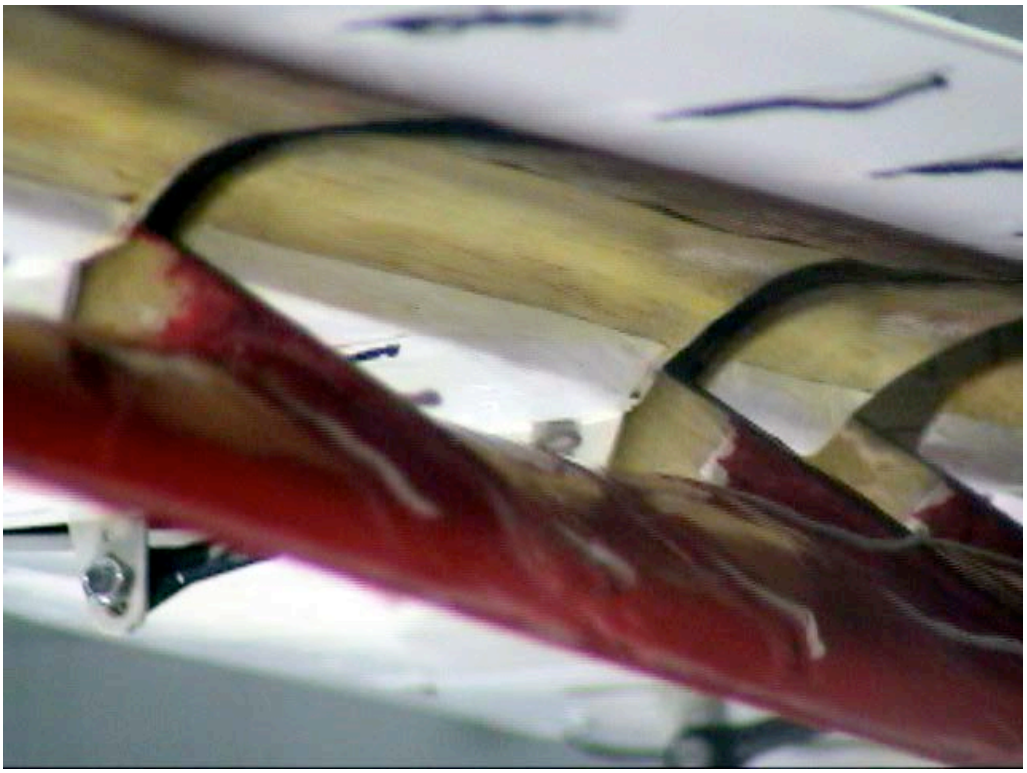

Figure C-2. Outboard tip view; Aux-In-45_Aux-Out-45_Split-60_Ail-0; α = 0°.

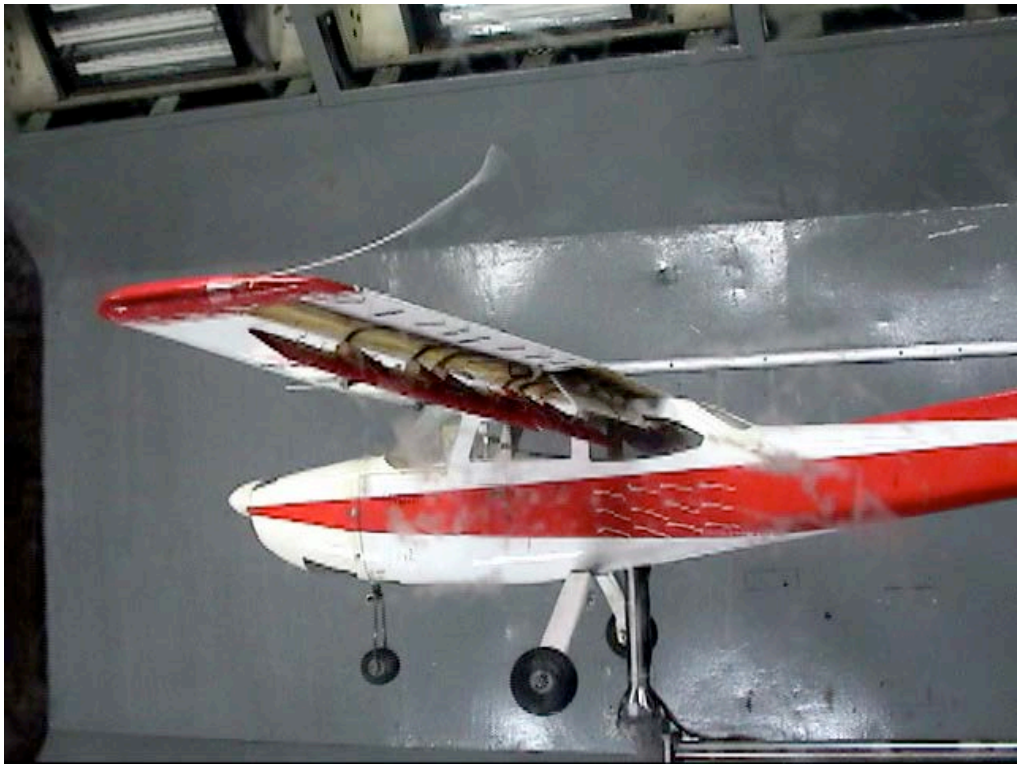

Figure C-3. Fuselage view; Aux-In-45_Aux-Out-45_Split-60_Ail-0; α = 0°.

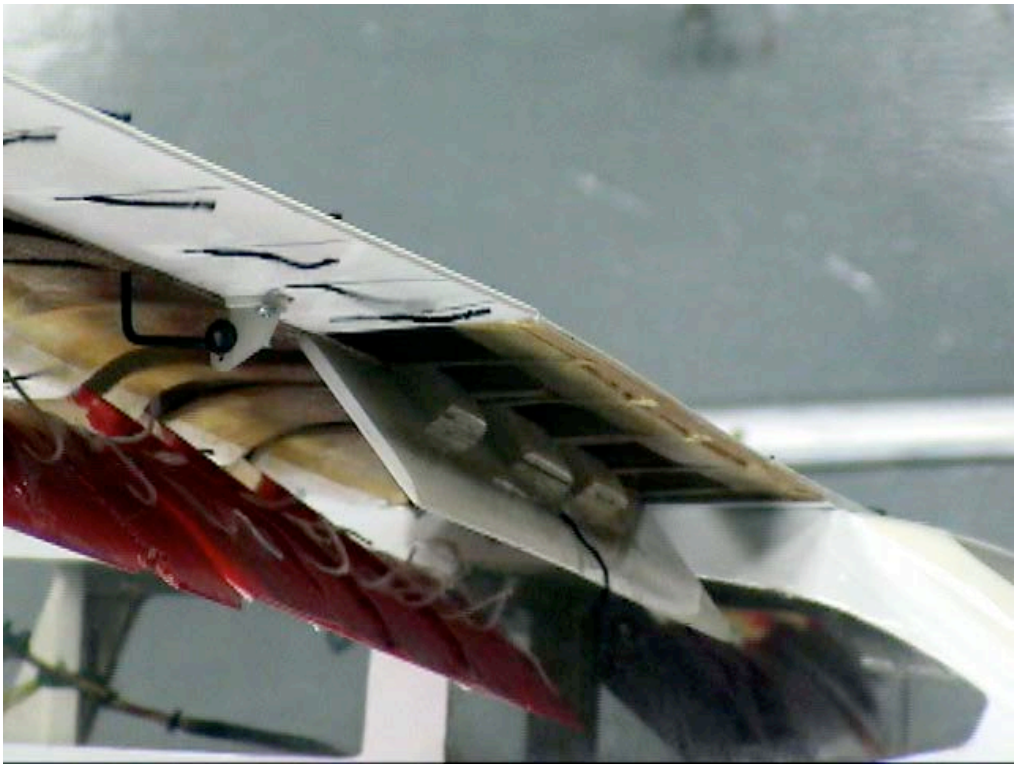

Figure C-4. Inboard view; Aux-In-45_Aux-Out-45_Split-60_Ail-0; α = 4°.

Figure C-5. Outboard tip view; Aux-In-45_Aux-Out-45_Split-60_Ail-0; α = 4°.

Figure C-6. Fuselage view; Aux-In-45_Aux-Out-45_Split-60_Ail-0; α = 4°.

Figure C-7. Inboard view; Aux-In-45_Aux-Out-45_Split-60_Ail-0; α = 8°.

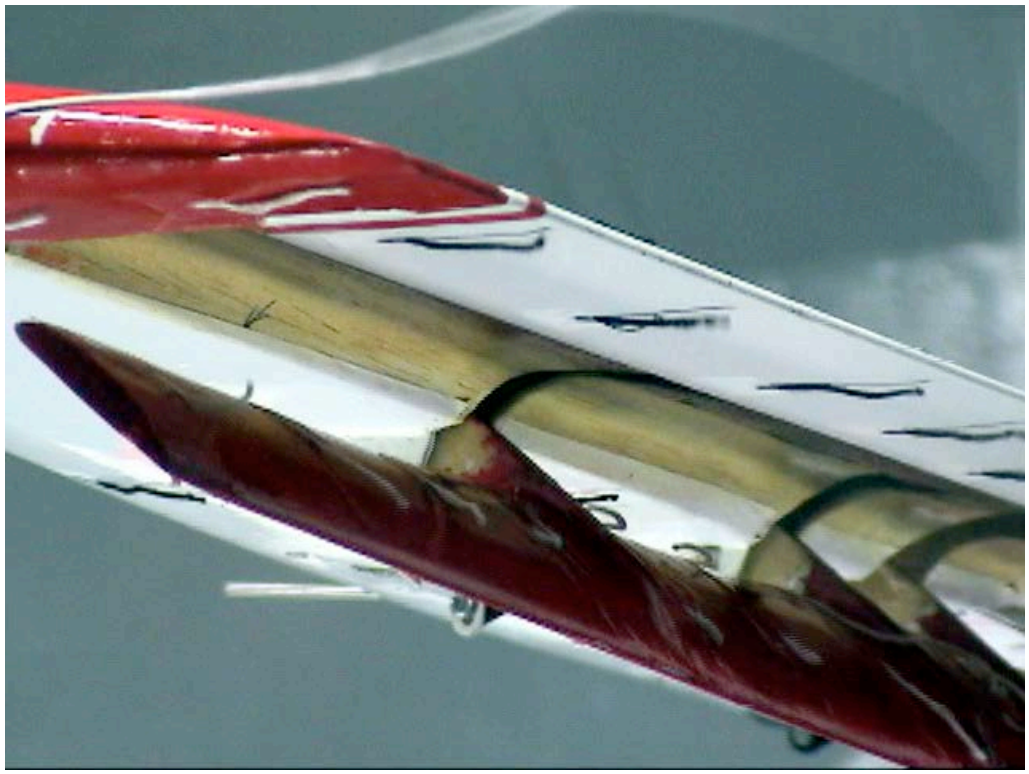

Figure C-8. Outboard tip view; Aux-In-45_Aux-Out-45_Split-60_Ail-0; α = 8°.

Figure C-9. Fuselage view; Aux-In-45_Aux-Out-45_Split-60_Ail-0; α = 8°.

Figure C-10. Inboard view; Aux-In-45_Aux-Out-45_Split-60_Ail-0; α = 12°.

Figure C-11. Outboard tip view; Aux-In-45_Aux-Out-45_Split-60_Ail-0; α = 12°.

Figure C-12. Fuselage view; Aux-In-45_Aux-Out-45_Split-60_Ail-0; α = 12°.

Figure C-13. Inboard view; Aux-In-45_Aux-Out-45_Split-60_Ail-0; α = 16°.

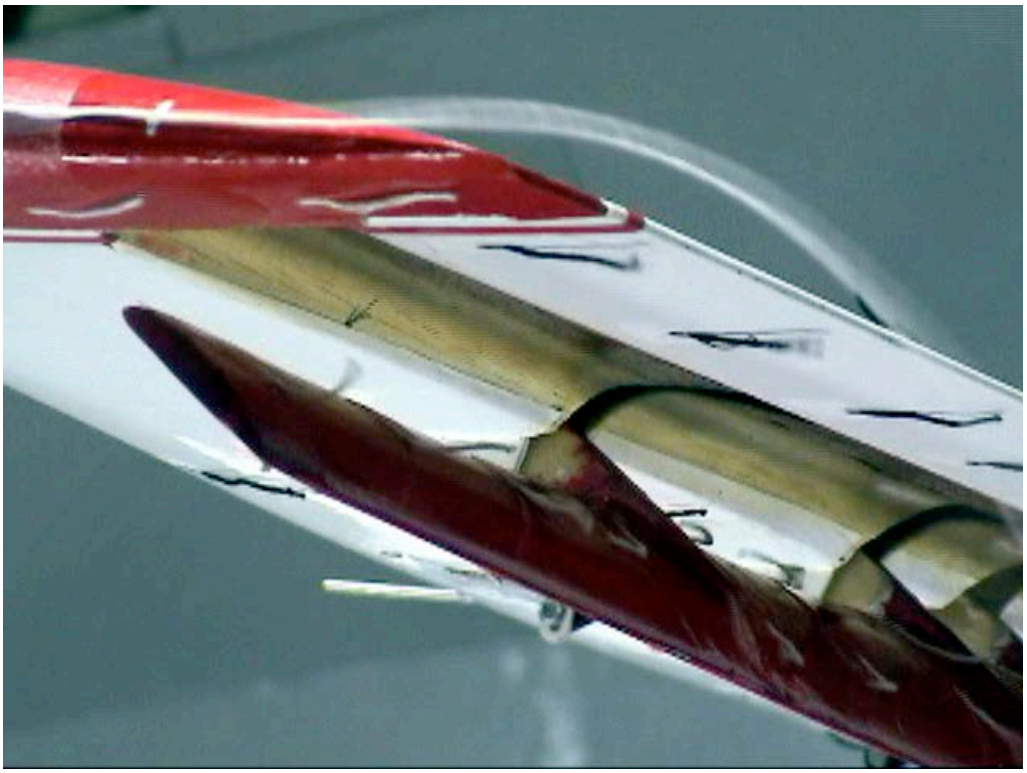

Figure C-14. Outboard tip view; Aux-In-45_Aux-Out-45_Split-60_Ail-0; α = 16°.

Figure C-15. Fuselage view; Aux-In-45_Aux-Out-45_Split-60_Ail-0; α = 16°.

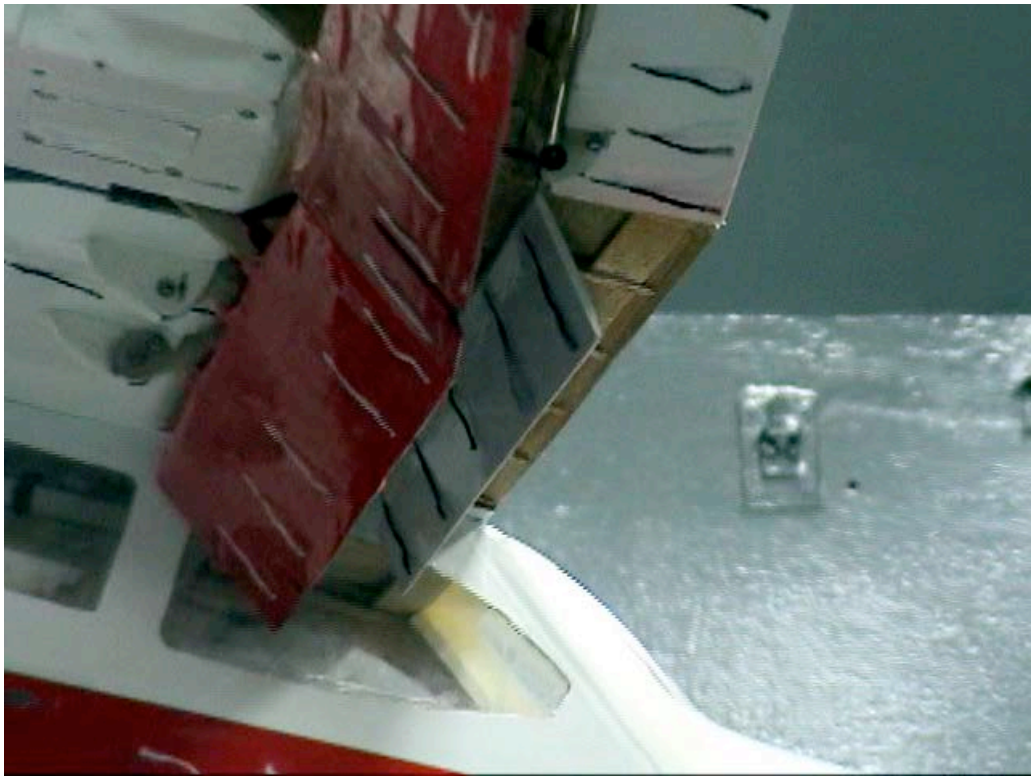

Figure C-16. Inboard lower surface view; Aux-In-45_Aux-Out-45_Split-60_Ail-0; α = 16°.

Figure C-17. Outboard lower surface view; Aux-In-45_Aux-Out-45_Split-60_Ail-0; α = 16°.

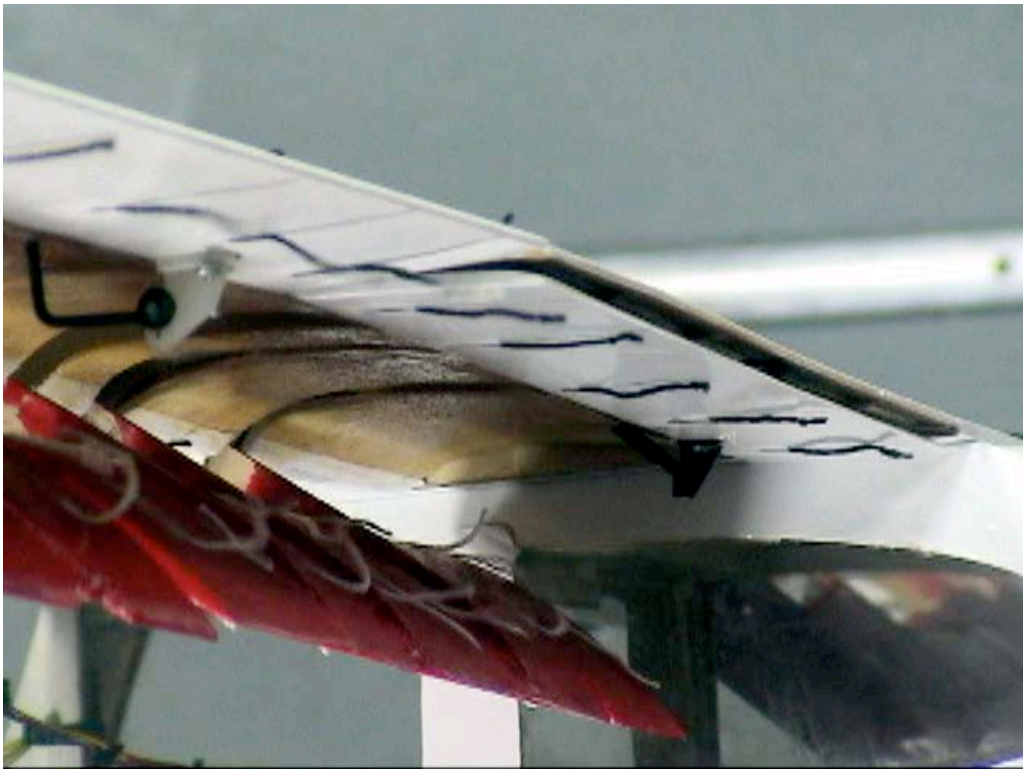

Figure C-18. Inboard view; Aux-In-45_Aux-Out-45_Split-0_Ail-0; α = 0°.

Figure C-19. Outboard tip view; Aux-In-45_Aux-Out-45_Split-0_Ail-0; α = 0°.

Figure C-20. Fuselage view; Aux-In-45_Aux-Out-45_Split-0_Ail-0; α = 0°.

Figure C-21. Inboard view; Aux-In-45_Aux-Out-45_Split-0_Ail-0; α = 4°.

Figure C-22. Outboard tip view; Aux-In-45_Aux-Out-45_Split-0_Ail-0; α = 4°.

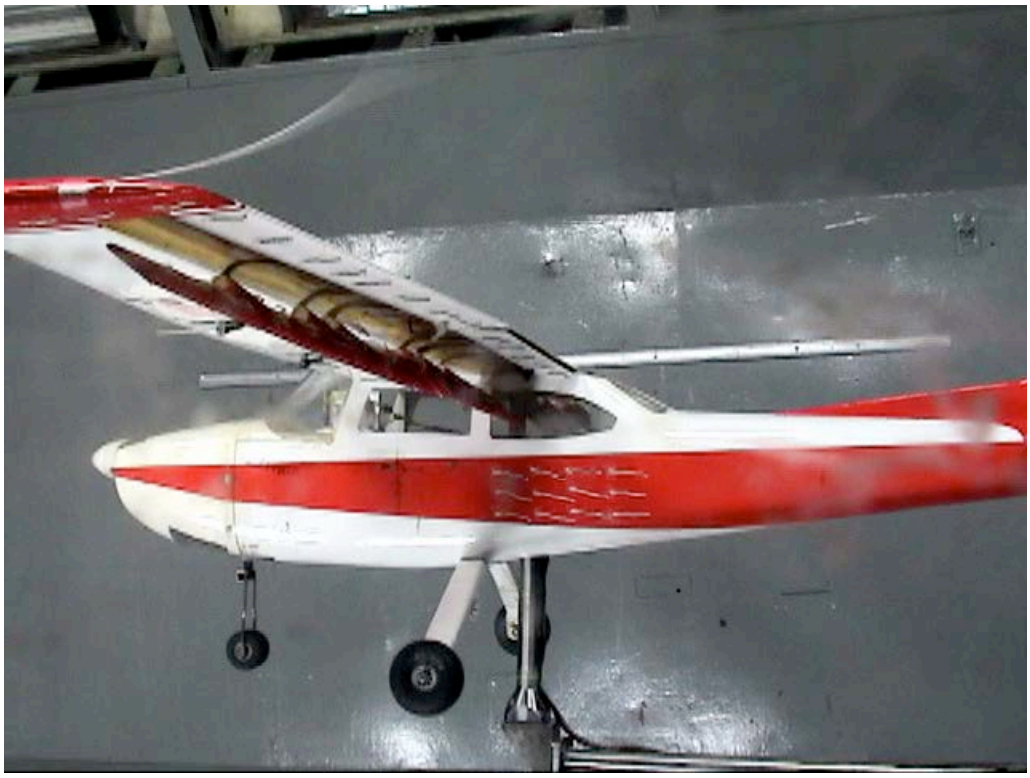

Figure C-23. Fuselage view; Aux-In-45_Aux-Out-45_Split-0_Ail-0; α = 4°.

Figure C-24. Inboard view; Aux-In-45_Aux-Out-45_Split-0_Ail-0; α = 8°.

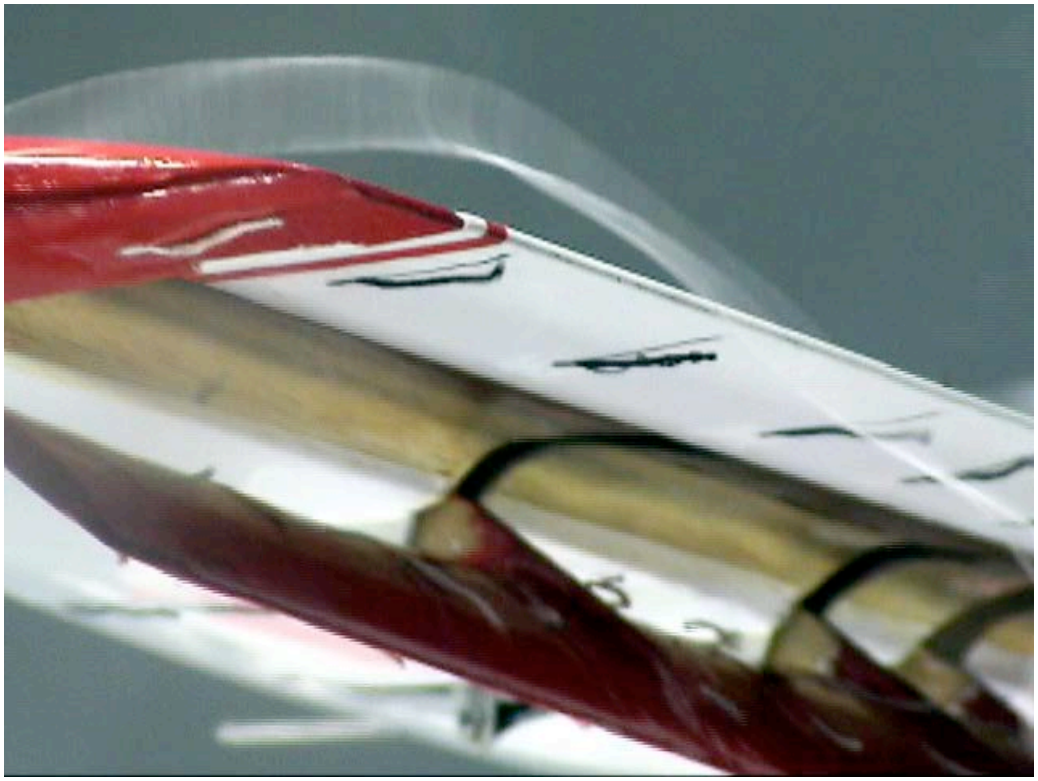

Figure C-25. Outboard tip view; Aux-In-45_Aux-Out-45_Split-0_Ail-0; α = 8°.

Figure C-26. Fuselage view; Aux-In-45_Aux-Out-45_Split-0_Ail-0; α = 8°.

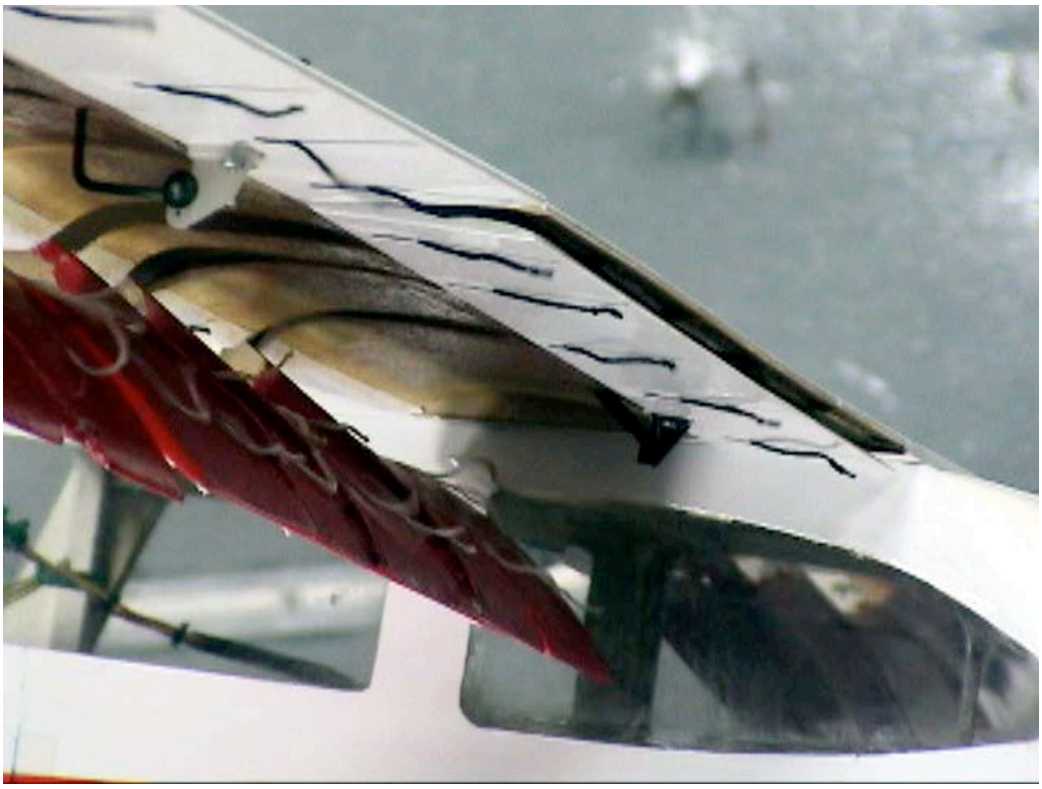

Figure C-27. Inboard view; Aux-In-45_Aux-Out-45_Split-0_Ail-0; α = 12°.

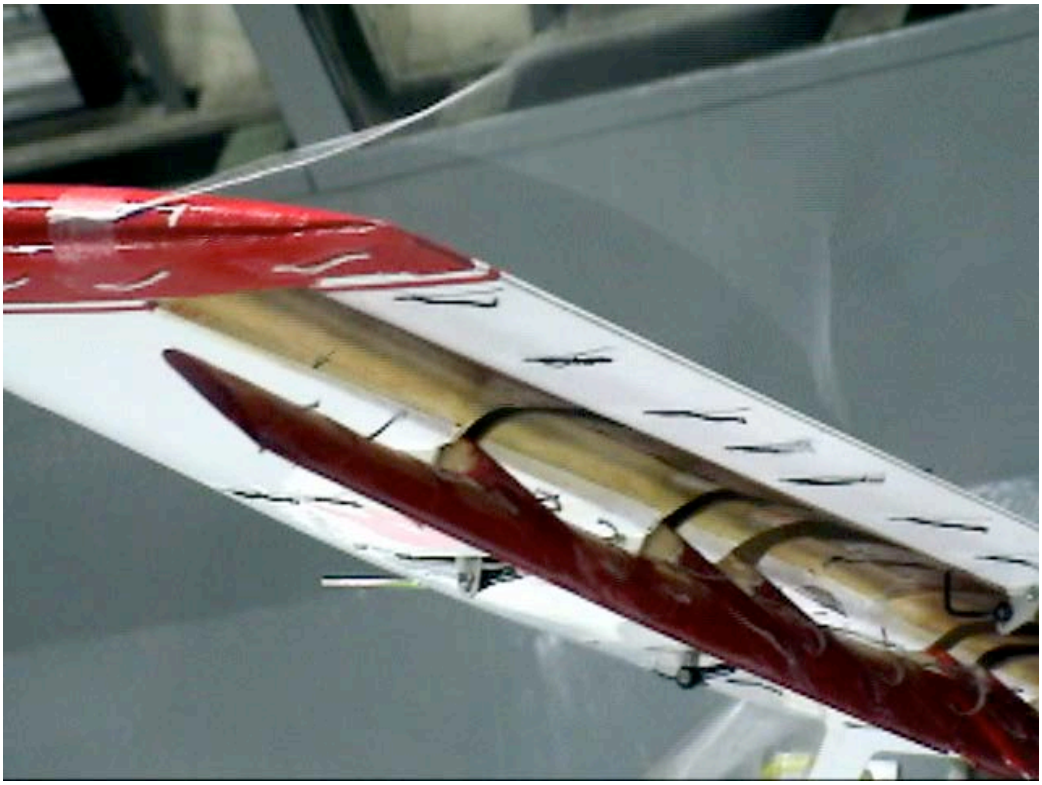

Figure C-28. Outboard tip view; Aux-In-45_Aux-Out-45_Split-0_Ail-0; α = 12°.

Figure C-29. Fuselage view; Aux-In-45_Aux-Out-45_Split-0_Ail-0; α = 12°.

Figure C-30. Inboard view; Aux-In-45_Aux-Out-45_Split-0_Ail-0; α = 16°.

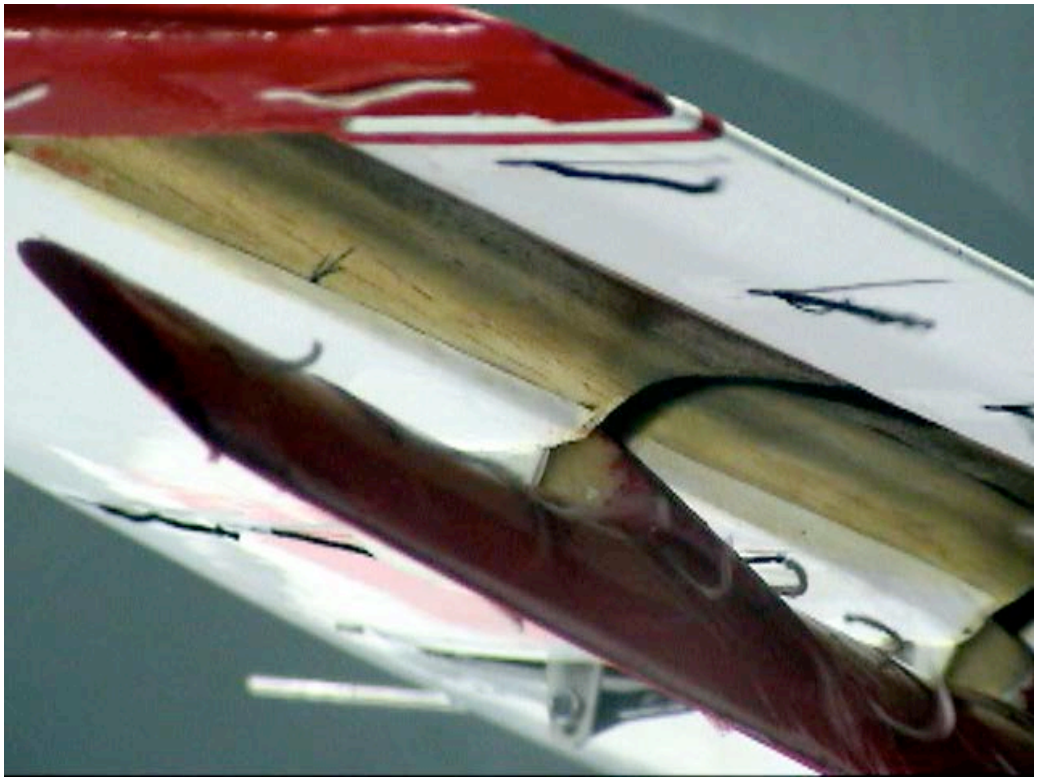

Figure C-31. Outboard tip view; Aux-In-45_Aux-Out-45_Split-0_Ail-0; α = 16°.

Figure C-32. Fuselage view; Aux-In-45_Aux-Out-45_Split-0_Ail-0; α = 16°.

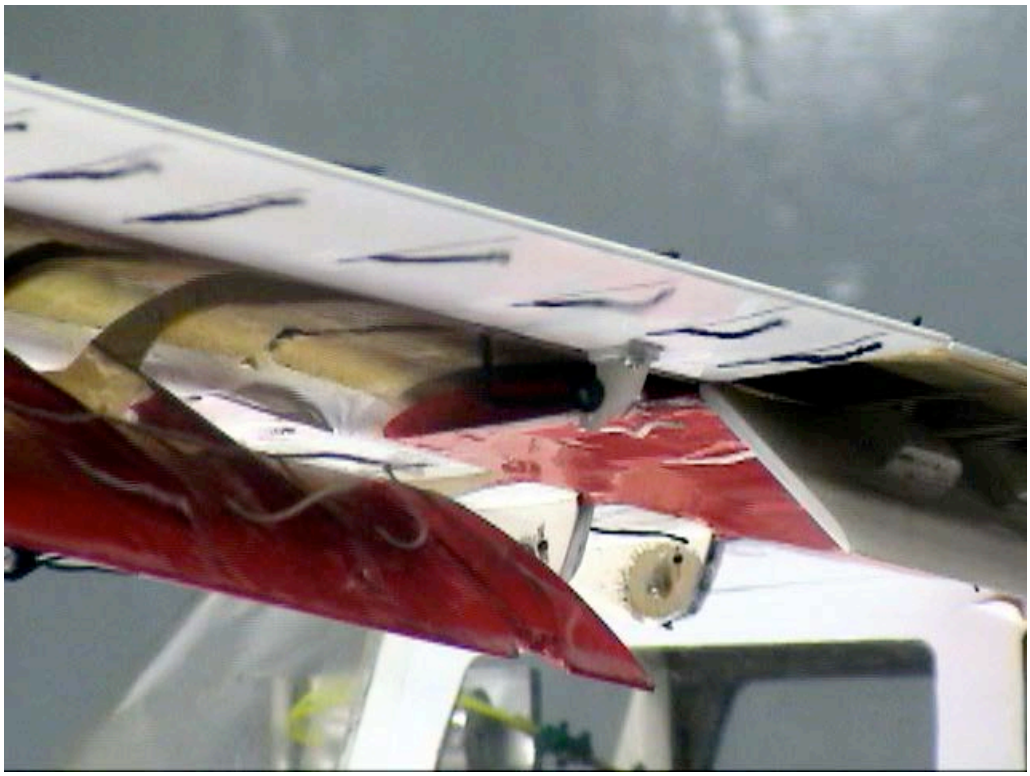

Figure C-33. Inboard view; Aux-In-0_Aux-Out-45_Split-60_Ail-0; α = 0°.

Figure C-34. Outboard tip view; Aux-In-0_Aux-Out-45_Split-60_Ail-0; α = 0°.

Figure C-35. Fuselage view; Aux-In-0_Aux-Out-45_Split-60_Ail-0; α = 0°.

Figure C-36. Inboard view; Aux-In-0_Aux-Out-45_Split-60_Ail-0; α = 4°.

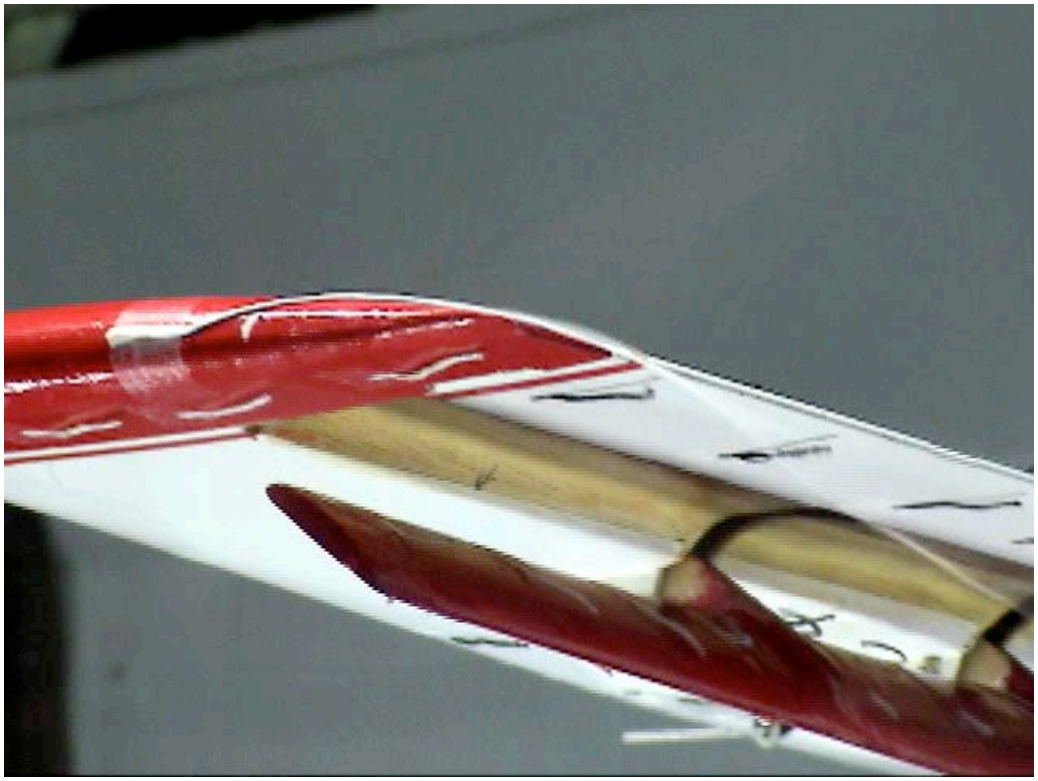

Figure C-37. Outboard tip view; Aux-In-0_Aux-Out-45_Split-60_Ail-0; α = 4°.

Figure C-38. Fuselage view; Aux-In-0_Aux-Out-45_Split-60_Ail-0; α = 4°.

Figure C-39. Inboard view; Aux-In-0_Aux-Out-45_Split-60_Ail-0; α = 8°.

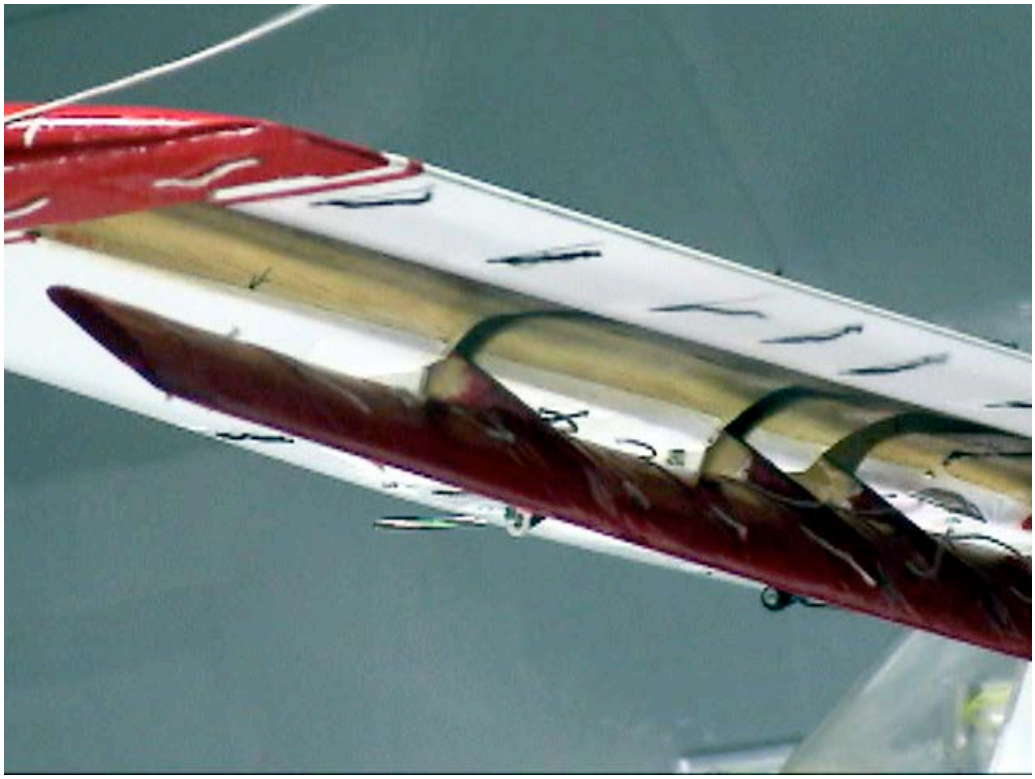

Figure C-40. Outboard tip view; Aux-In-0_Aux-Out-45_Split-60_Ail-0; α = 8°.

Figure C-41. Fuselage view; Aux-In-0_Aux-Out-45_Split-60_Ail-0; α = 8°.

Figure C-42. Inboard view; Aux-In-0_Aux-Out-45_Split-60_Ail-0; α = 12°.

Figure C-43. Outboard tip view; Aux-In-0_Aux-Out-45_Split-60_Ail-0; α = 12°.

Figure C-44. Fuselage view; Aux-In-0_Aux-Out-45_Split-60_Ail-0; α = 12°.

Figure C-45. Inboard view; Aux-In-0_Aux-Out-45_Split-60_Ail-0; α = 16°.

Figure C-46. Outboard tip view; Aux-In-0_Aux-Out-45_Split-60_Ail-0; α = 16°.

Figure C-47. Fuselage view; Aux-In-0_Aux-Out-45_Split-60_Ail-0; α = 16°.

Figure C-48. Inboard view; Aux-In-0_Aux-Out-90_Split-60_Ail-0; α = 0°.

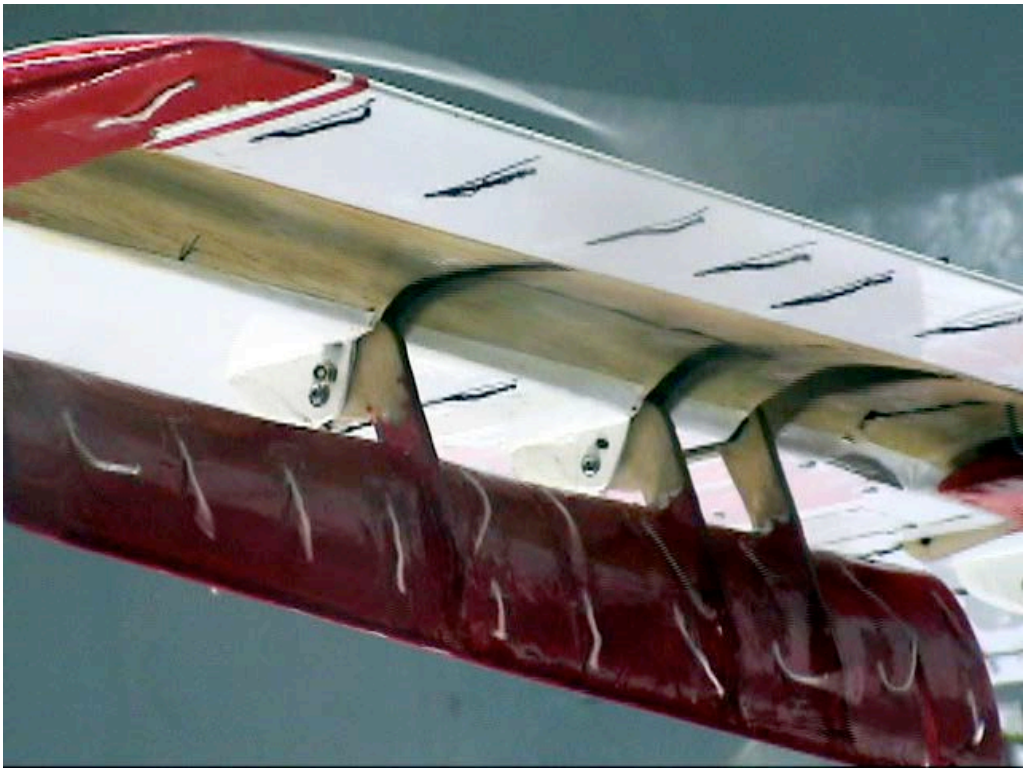

Figure C-49. Outboard tip view; Aux-In-0_Aux-Out-90_Split-60_Ail-0; α = 0°.

Figure C-50. Fuselage view; Aux-In-0_Aux-Out-90_Split-60_Ail-0; α = 0°.

Figure C-51. Inboard view; Aux-In-0_Aux-Out-90_Split-60_Ail-0; α = 4°.

Figure C-52. Outboard tip view; Aux-In-0_Aux-Out-90_Split-60_Ail-0; α = 4°.

Figure C-53. Fuselage view; Aux-In-0_Aux-Out-90_Split-60_Ail-0; α = 4°.

Figure C-54. Inboard view; Aux-In-0_Aux-Out-90_Split-60_Ail-0; α = 8°.

Figure C-55. Outboard tip view; Aux-In-0_Aux-Out-90_Split-60_Ail-0; α = 8°.

Figure C-56. Fuselage view; Aux-In-0_Aux-Out-90_Split-60_Ail-0; α = 8°.

Figure C-57. Inboard view; Aux-In-0_Aux-Out-90_Split-60_Ail-0; α = 12°.

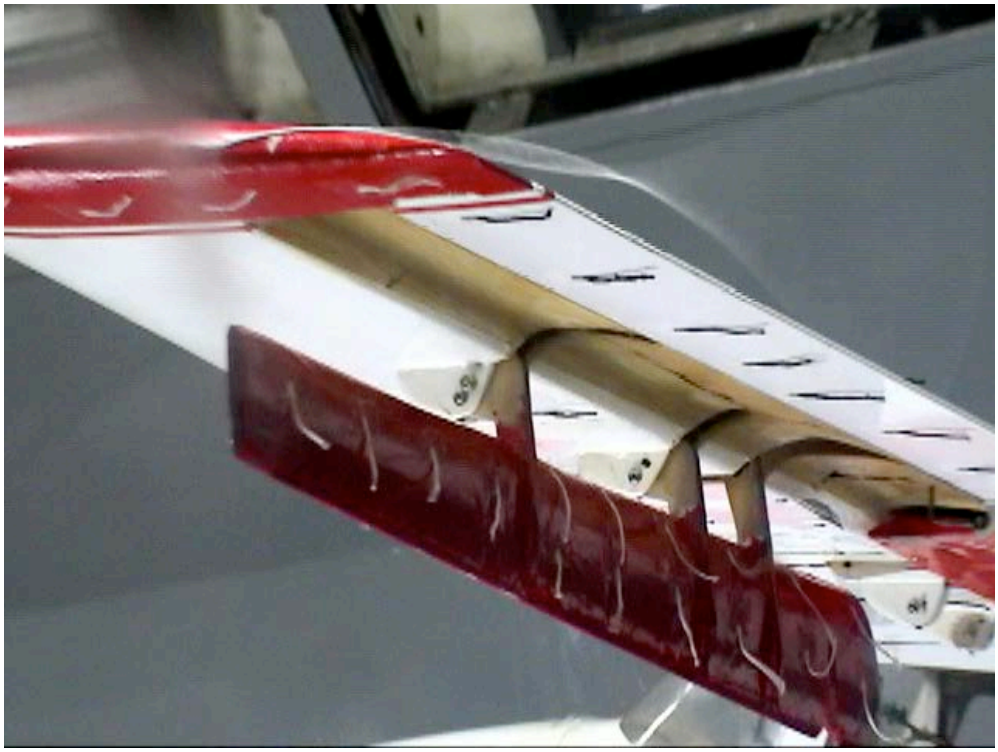

Figure C-58. Outboard tip view; Aux-In-0_Aux-Out-90_Split-60_Ail-0; α = 12°.

Figure C-59. Fuselage view; Aux-In-0_Aux-Out-90_Split-60_Ail-0; α = 12°.

Figure C-60. Inboard view; Aux-In-0_Aux-Out-90_Split-60_Ail-0; α = 16°.

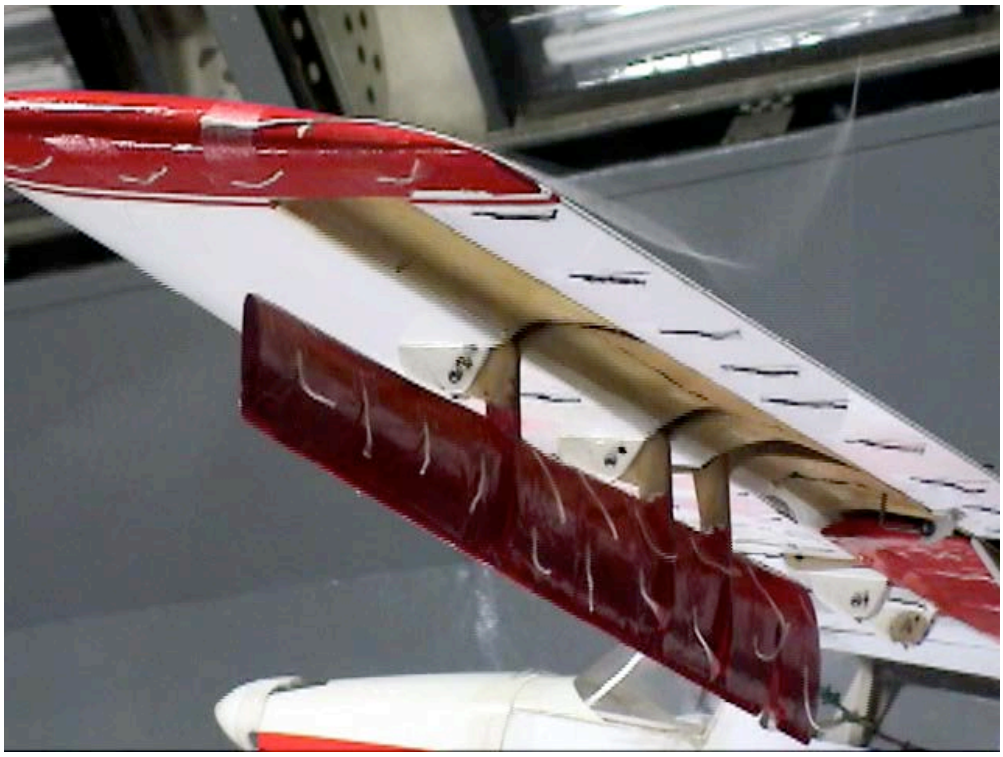

Figure C-61. Outboard tip view; Aux-In-0_Aux-Out-90_Split-60_Ail-0; α = 16°.

Figure C-62. Fuselage view; Aux-In-0_Aux-Out-90_Split-60_Ail-0; α = 16°.

Figure C-63. Inboard view; Aux-In-90_Aux-Out-90_Split-60_Ail-0; α = 0°.

Figure C-64. Outboard tip view; Aux-In-90_Aux-Out-90_Split-60_Ail-0; α = 0°.

Figure C-65. Fuselage view; Aux-In-90_Aux-Out-90_Split-60_Ail-0; α = 0°.

Figure C-66. Inboard view; Aux-In-90_Aux-Out-90_Split-60_Ail-0; α = 4°.

Figure C-67. Outboard tip view; Aux-In-90_Aux-Out-90_Split-60_Ail-0; α = 4°.

Figure C-68. Fuselage view; Aux-In-90_Aux-Out-90_Split-60_Ail-0; α = 4°.

Figure C-69. Inboard view; Aux-In-90_Aux-Out-90_Split-60_Ail-0; α = 8°.

Figure C-70. Outboard tip view; Aux-In-90_Aux-Out-90_Split-60_Ail-0; α = 8°.

Figure C-71. Fuselage view; Aux-In-90_Aux-Out-90_Split-60_Ail-0; α = 8°.

Figure C-72. Inboard view; Aux-In-90_Aux-Out-90_Split-60_Ail-0; α = 12°.

Figure C-73. Outboard tip view; Aux-In-90_Aux-Out-90_Split-60_Ail-0; α = 12°.

Figure C-74. Fuselage view; Aux-In-90_Aux-Out-90_Split-60_Ail-0; α = 12°.

Figure C-75. Inboard view; Aux-In-90_Aux-Out-90_Split-60_Ail-0; α = 16°.

Figure C-76. Outboard tip view; Aux-In-90_Aux-Out-90_Split-60_Ail-0; α = 16°.

Figure C-77. Fuselage view; Aux-In-90_Aux-Out-90_Split-60_Ail-0; α = 16°.

Figure C-78. Inboard view; Aux-In-90_Aux-Out-90_Split-0_Ail-0; α = 0°.

Figure C-79. Outboard tip view; Aux-In-90_Aux-Out-90_Split-0_Ail-0; α = 0°.

Figure C- 80. Fuselage view; Aux-In-90_Aux-Out-90_Split-0_Ail-0; α = 0°.

Figure C-81. Inboard view; Aux-In-90_Aux-Out-90_Split-0_Ail-0; α = 4°.

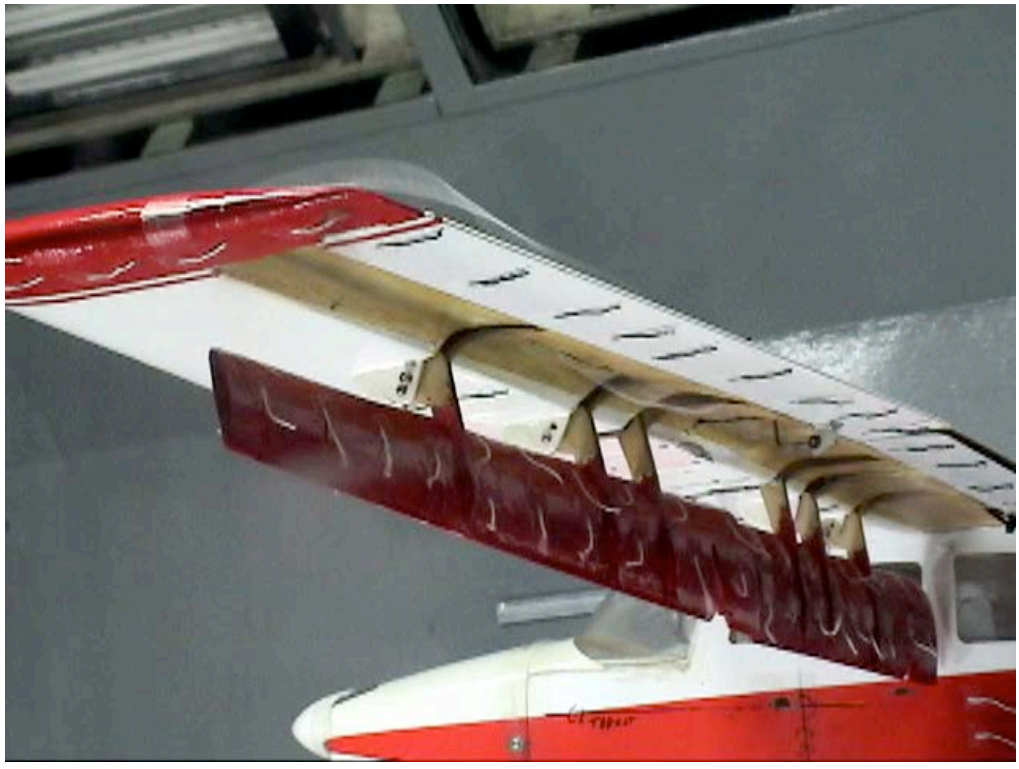

Figure C-82. Outboard tip view; Aux-In-90_Aux-Out-90_Split-0_Ail-0; α = 4°.

Figure C-83. Fuselage view; Aux-In-90_Aux-Out-90_Split-0_Ail-0; α = 4°.

Figure C-84. Inboard view; Aux-In-90_Aux-Out-90_Split-0_Ail-0; α = 8°.

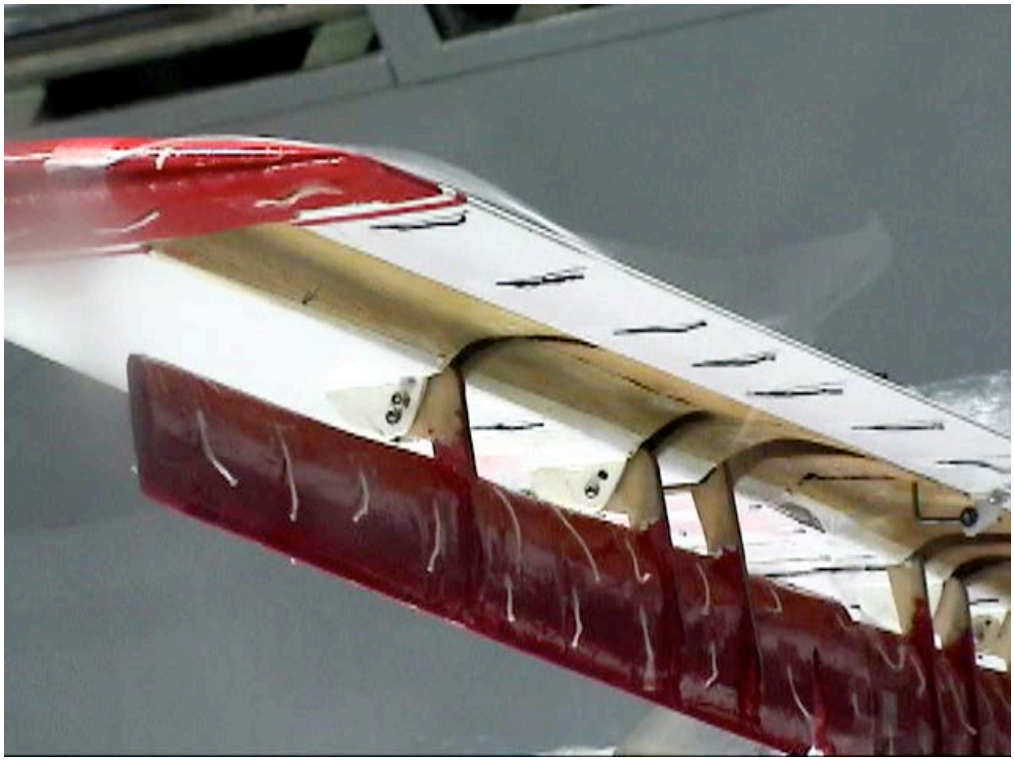

Figure C-85. Outboard tip view; Aux-In-90_Aux-Out-90_Split-0_Ail-0; α = 8°.

Figure C-86. Fuselage view; Aux-In-90_Aux-Out-90_Split-0_Ail-0; α = 8°.

Figure C-87. Inboard view; Aux-In-90_Aux-Out-90_Split-0_Ail-0; α = 12°.

Figure C-88. Outboard tip view; Aux-In-90_Aux-Out-90_Split-0_Ail-0; α = 12°.

Figure C-89. Fuselage view; Aux-In-90_Aux-Out-90_Split-0_Ail-0; α = 12°.

Figure C-90. Inboard view; Aux-In-90_Aux-Out-90_Split-0_Ail-0; α = 16°.

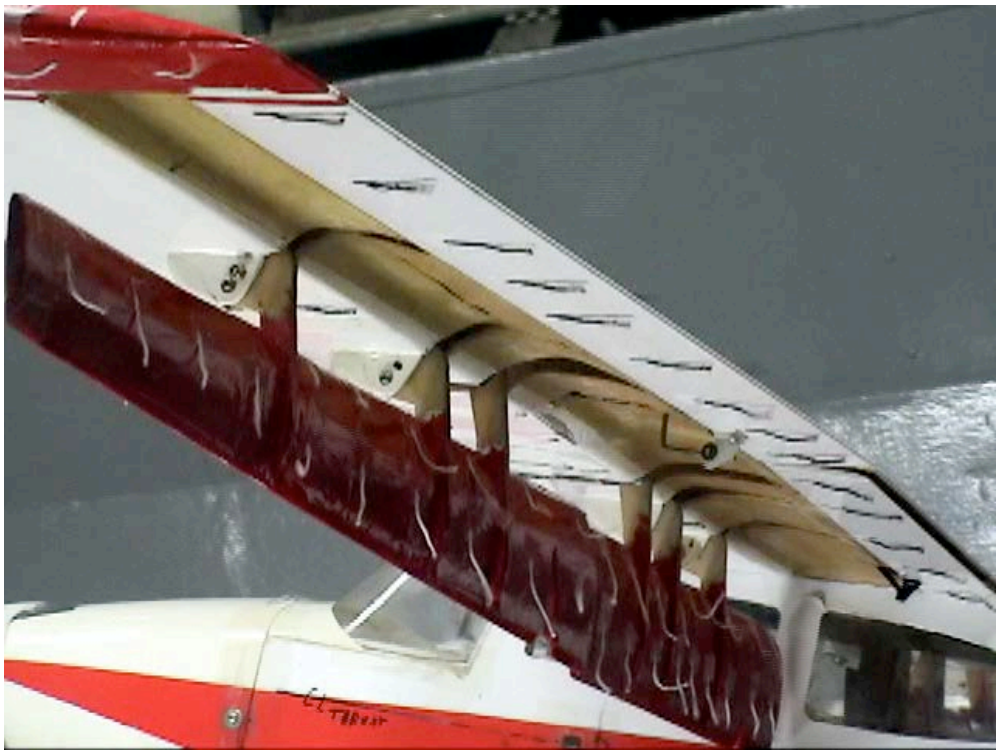

Figure C-91. Outboard tip view; Aux-In-90_Aux-Out-90_Split-0_Ail-0; α = 16°.

Figure C-92. Fuselage view; Aux-In-90_Aux-Out-90_Split-0_Ail-0; α = 16°.

Figure C-93. Inboard view; Aux-In-0_Aux-Out-0_Split-60_Ail-0; α = 0°.

Figure C-94. Fuselage view; Aux-In-0_Aux-Out-0_Split-60_Ail-0; α = 0°.

Figure C-95. Inboard view; Aux-In-0_Aux-Out-0_Split-60_Ail-0; α = 4°.

Figure C-96. Fuselage view; Aux-In-0_Aux-Out-0_Split-60_Ail-0; α = 4°.

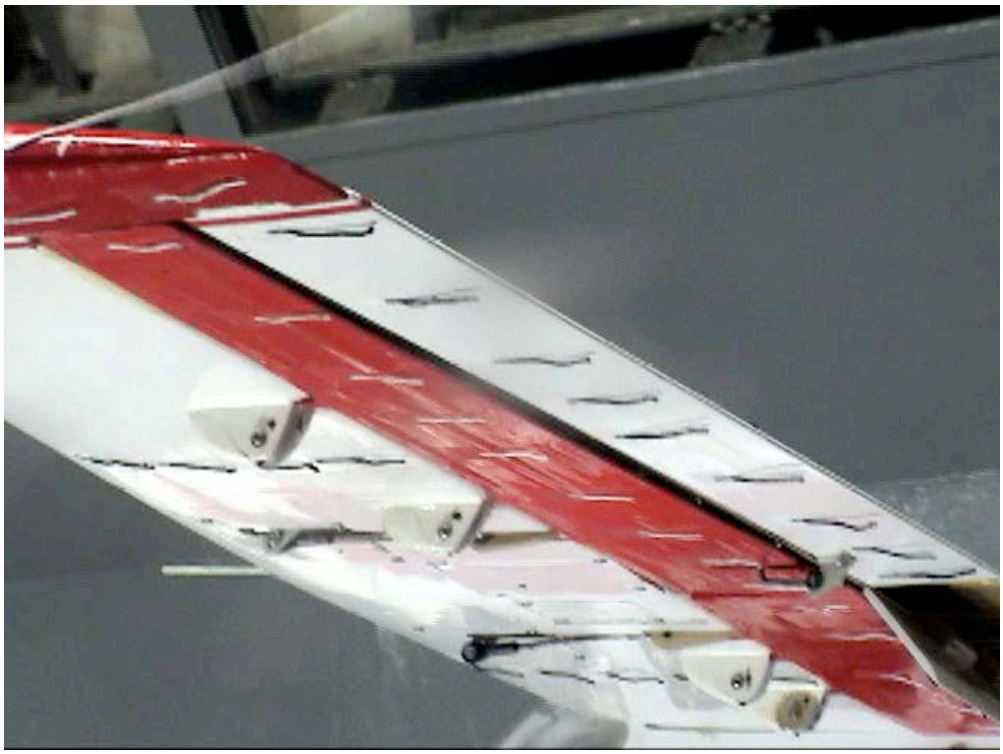

Figure C-97. Inboard view; Aux-In-0_Aux-Out-0_Split-60_Ail-0; α = 8°.

Figure C-98. Fuselage view; Aux-In-0_Aux-Out-0_Split-60_Ail-0; α = 8°.

Figure C-99. Inboard view; Aux-In-0_Aux-Out-0_Split-60_Ail-0; α = 12°.

Figure C-100. Fuselage view; Aux-In-0_Aux-Out-0_Split-60_Ail-0; α = 12°.

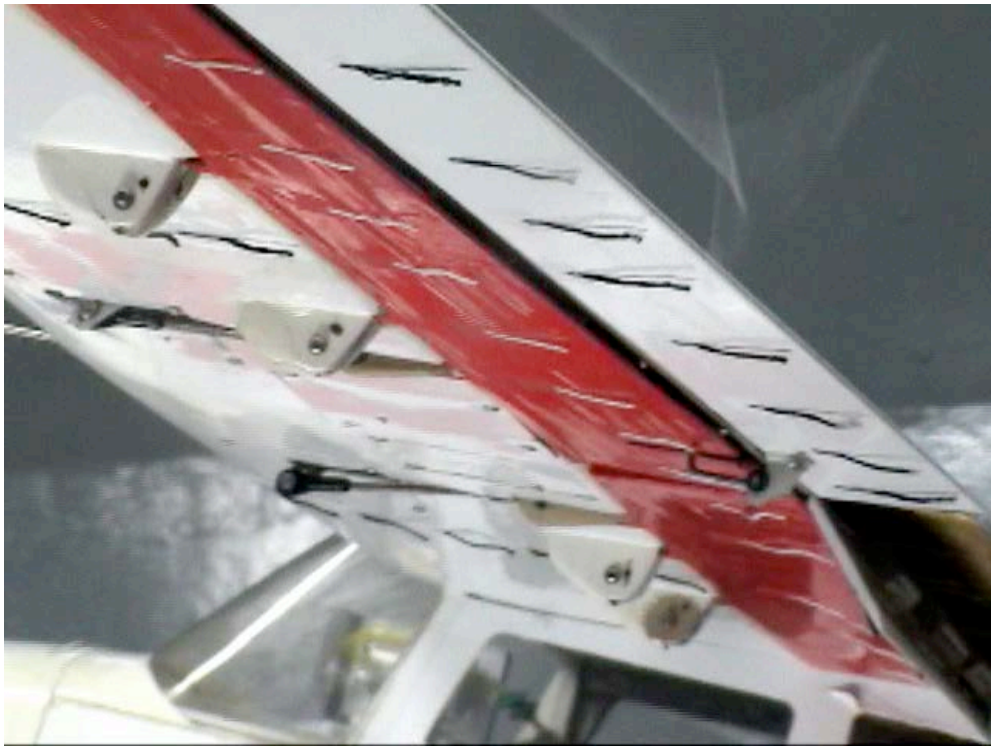

Figure C-101. Inboard view; Aux-In-0_Aux-Out-0_Split-60_Ail-0; α = 16°.

Figure C-102. Fuselage view; Aux-In-0_Aux-Out-0_Split-60_Ail-0; α = 16°.

Figure C-103. Inboard view; Aux-In-0_Aux-Out-0_Split-0_Ail-0; α = 0°.

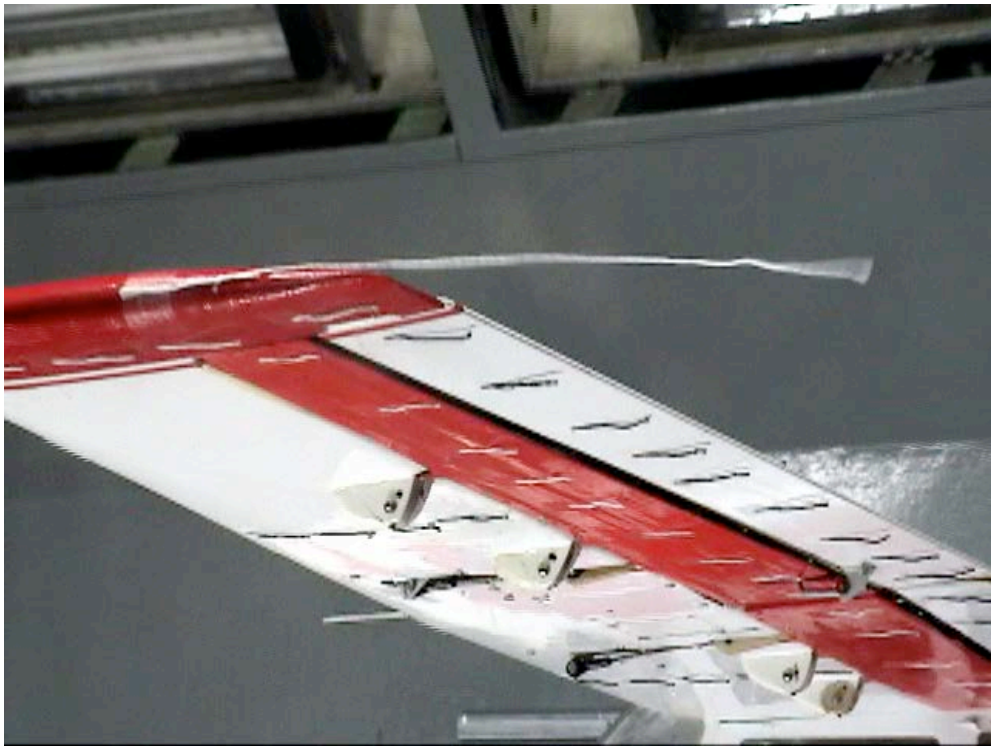

Figure C-104. Outboard tip view; Aux-In-0_Aux-Out-0_Split-0_Ail-0; α = 0°.

Figure C-105. Fuselage view; Aux-In-0_Aux-Out-0_Split-0_Ail-0; α = 0°.

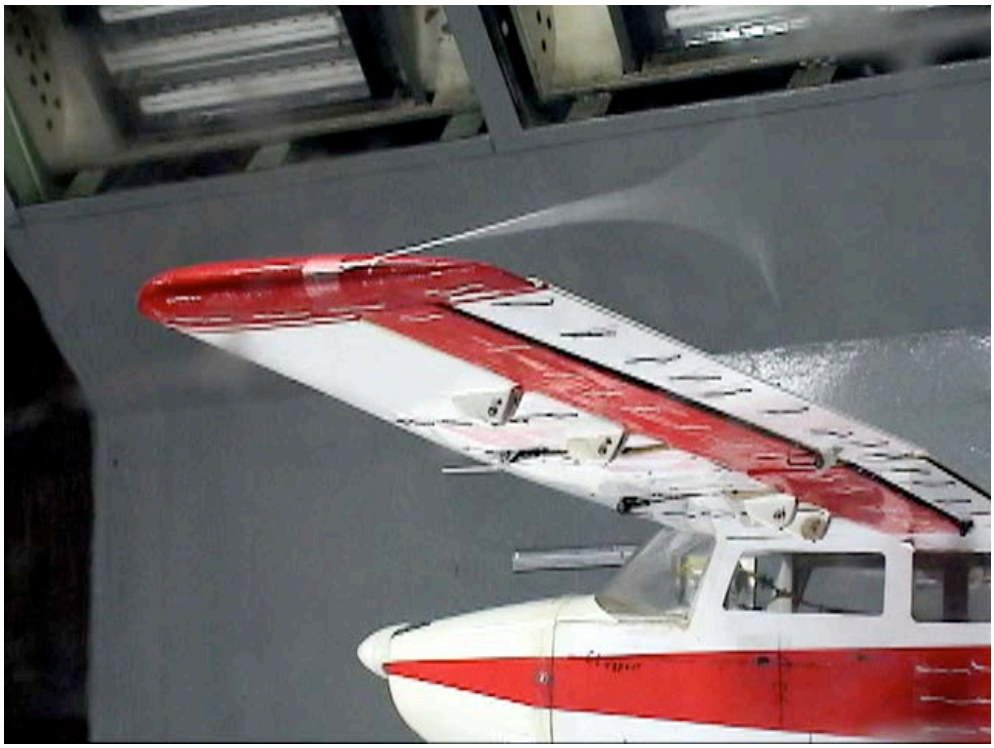

Figure C-106. Outboard tip view; Aux-In-0_Aux-Out-0_Split-0_Ail-0; α = 4°.

Figure C-107. Fuselage view; Aux-In-0_Aux-Out-0_Split-0_Ail-0; α = 4°.

Figure C-108. Inboard view; Aux-In-0_Aux-Out-0_Split-0_Ail-0; α = 8°.

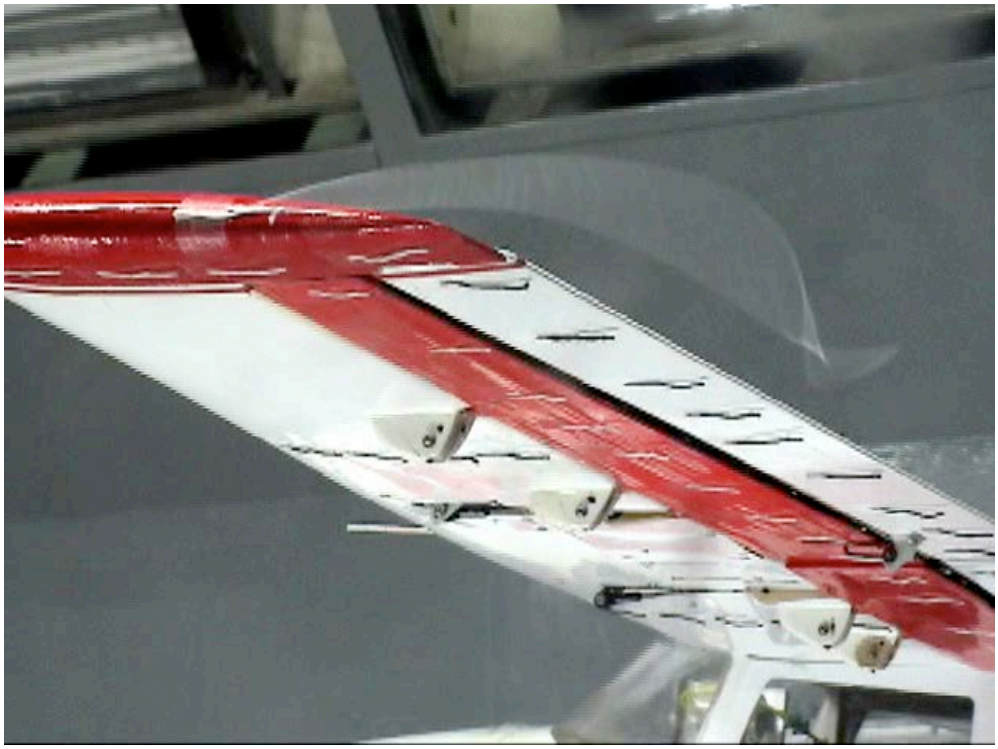

Figure C-109. Outboard tip view; Aux-In-0_Aux-Out-0_Split-0_Ail-0; α = 8°.

Figure C-110. Fuselage view; Aux-In-0_Aux-Out-0_Split-0_Ail-0; α = 8°.

Figure C-111. Inboard view; Aux-In-0_Aux-Out-0_Split-0_Ail-0; α = 12°.

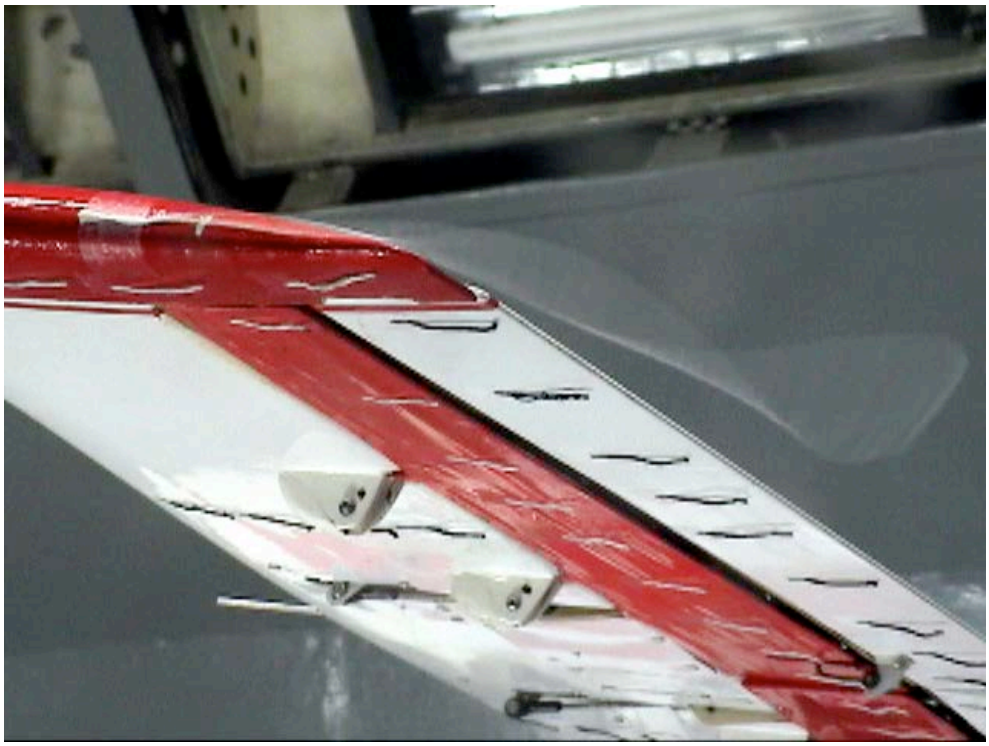

Figure C-112. Outboard tip view; Aux-In-0_Aux-Out-0_Split-0_Ail-0; α = 12°.

Figure C-113. Fuselage view; Aux-In-0_Aux-Out-0_Split-0_Ail-0; α = 12°.

Figure C-114. Inboard and fuselage views; Aux-In-0_Aux-Out-0_Split-0_Ail-0; α = 16°.

Figure C-115. Outboard tip view; Aux-In-0_Aux-Out-0_Split-0_Ail-0; α = 16°.

Figure C-116. Inboard view; LSS-In-45_LSS-Out-45_Split-60_Ail-0; α = 0°.

Figure C-117. Outboard tip view; LSS-In-45_LSS-Out-45_Split-60_Ail-0; α = 0°.

Figure C-118. Fuselage view; LSS-In-45_LSS-Out-45_Split-60_Ail-0; α = 0°.

Figure C-119. Inboard view; LSS-In-45_LSS-Out-45_Split-60_Ail-0; α = 4°.

Figure C-120. Outboard tip view; LSS-In-45_LSS-Out-45_Split-60_Ail-0; α = 4°.

Figure C-121. Mid-span view; LSS-In-45_LSS-Out-45_Split-60_Ail-0; α = 4°.

Figure C-122. Fuselage view; LSS-In-45_LSS-Out-45_Split-60_Ail-0; α = 4°.

Figure C-123. Inboard view; LSS-In-45_LSS-Out-45_Split-60_Ail-0; α = 8°.

Figure C-124. Mid-span view; LSS-In-45_LSS-Out-45_Split-60_Ail-0; α = 8°.

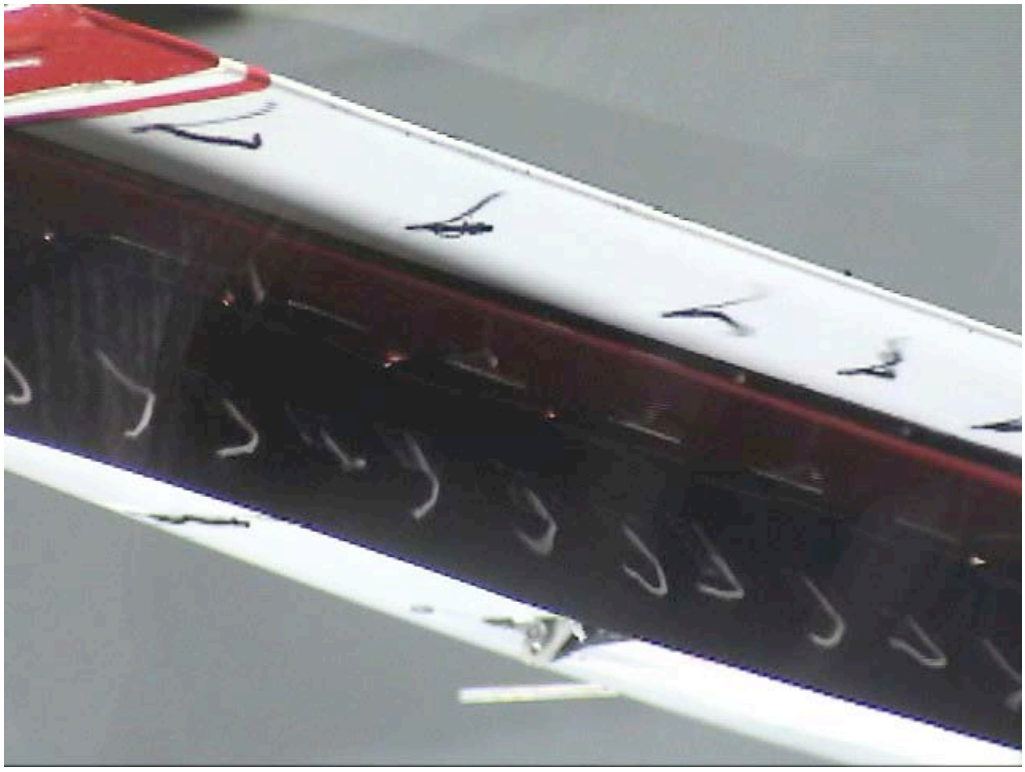

Figure C-125. Outboard tip view; LSS-In-45_LSS-Out-45_Split-60_Ail-0; α = 8°.

Figure C-126. Fuselage view; LSS-In-45_LSS-Out-45_Split-60_Ail-0; α = 8°.

Figure C-127. Inboard view; LSS-In-45_LSS-Out-45_Split-60_Ail-0; α = 12°.

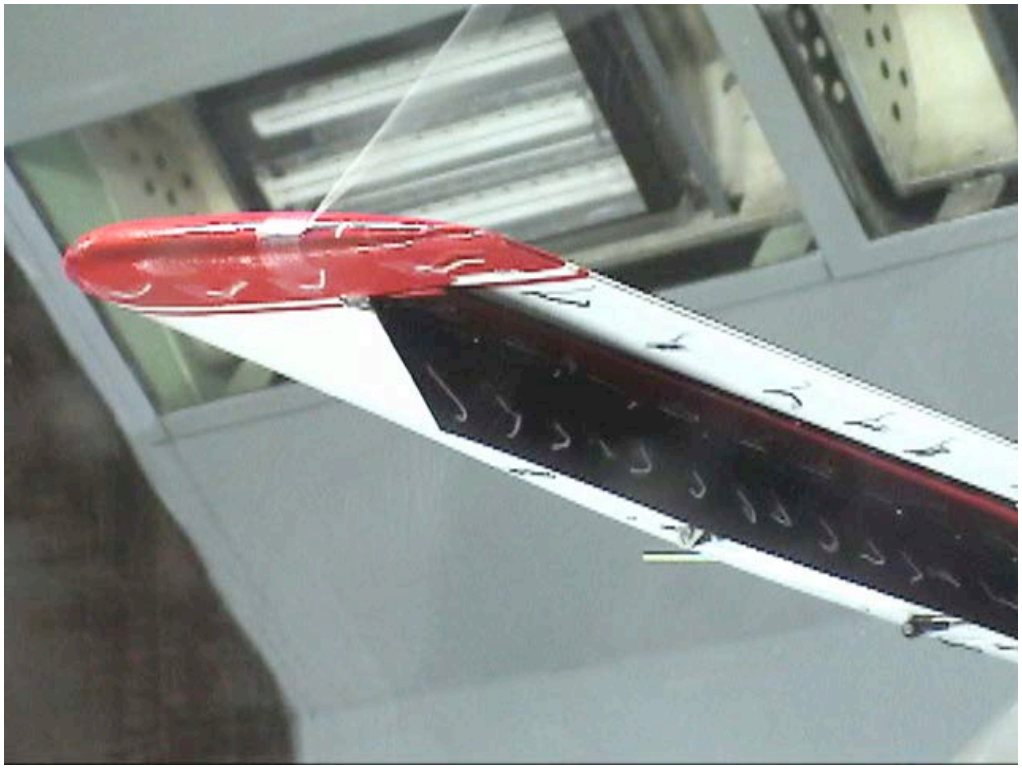

Figure C-128. Outboard tip view; LSS-In-45_LSS-Out-45_Split-60_Ail-0; α = 12°.

Figure C-129. Fuselage view; LSS-In-45_LSS-Out-45_Split-60_Ail-0; α = 12°.

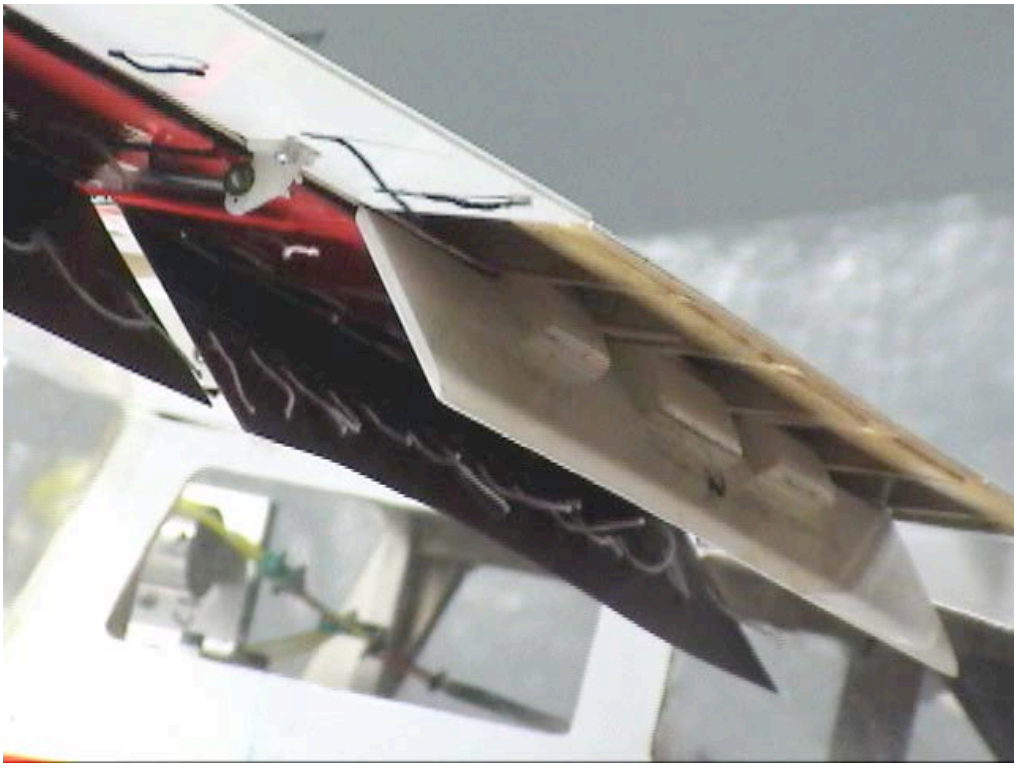

Figure C-130. Inboard view; LSS-In-45_LSS-Out-45_Split-60_Ail-0; α = 16°.

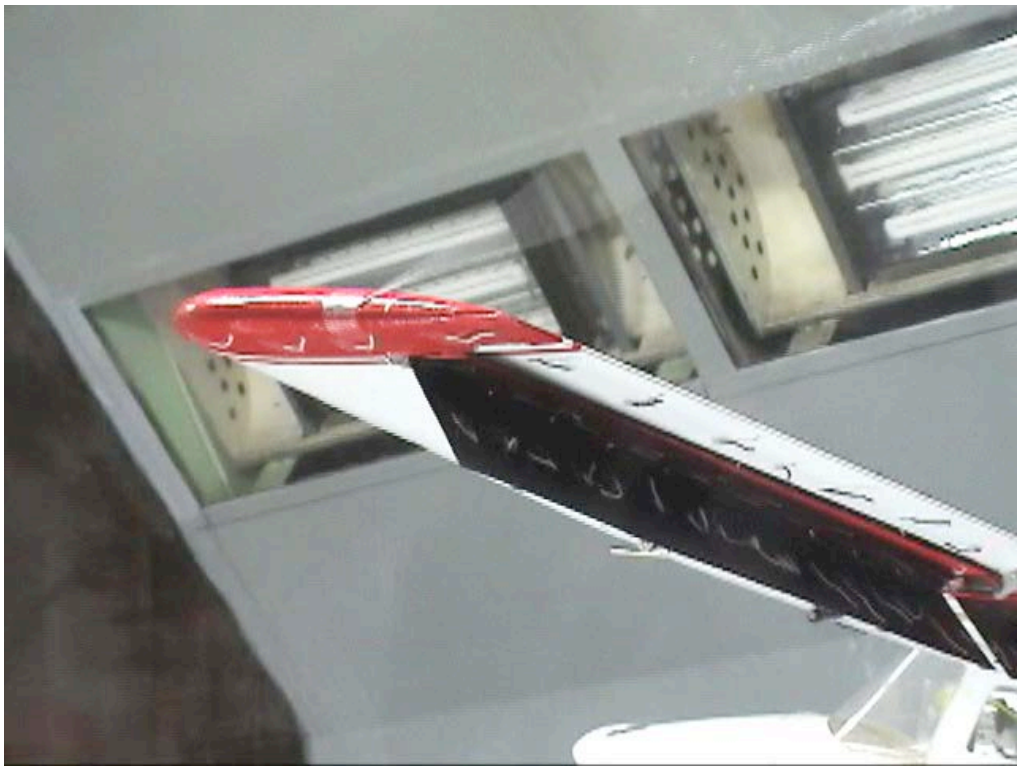

Figure C-131. Outboard tip view; LSS-In-45_LSS-Out-45_Split-60_Ail-0; α = 16°.

Figure C-132. Fuselage view; LSS-In-45_LSS-Out-45_Split-60_Ail-0; α = 16°.

Figure C-133. Inboard view; LSS-In-45_LSS-Out-45_Split-0_Ail-0; α = 0°.

Figure C-134. Outboard tip view; LSS-In-45_LSS-Out-45_Split-0_Ail-0; α = 0°.

Figure C-135. Fuselage view; LSS-In-45_LSS-Out-45_Split-0_Ail-0; α = 0°.

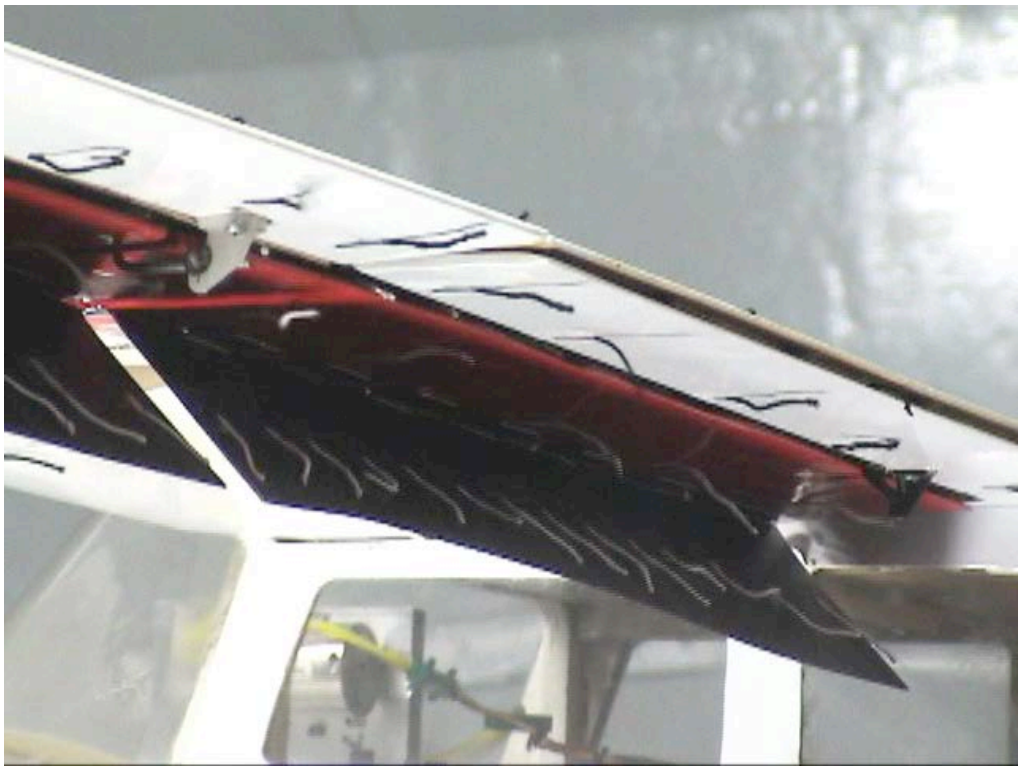

Figure C-136. Inboard view; LSS-In-45_LSS-Out-45_Split-0_Ail-0; α = 4°.

Figure C-137. Outboard tip view; LSS-In-45_LSS-Out-45_Split-0_Ail-0; α = 4°.

Figure C-138. Fuselage view; LSS-In-45_LSS-Out-45_Split-0_Ail-0; α = 4°.

Figure C-139. Inboard view; LSS-In-45_LSS-Out-45_Split-0_Ail-0; α = 8°.

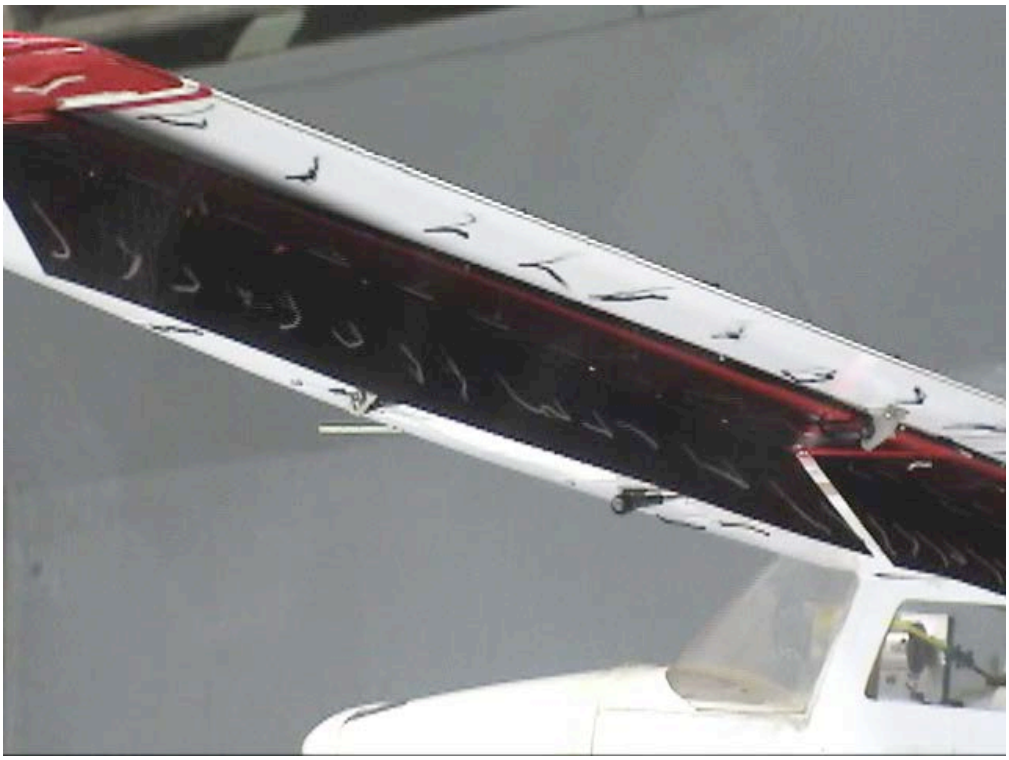

Figure C-140. Outboard tip view; LSS-In-45_LSS-Out-45_Split-0_Ail-0; α = 8°.

Figure C-141. Fuselage view; LSS-In-45_LSS-Out-45_Split-0_Ail-0; α = 8°.

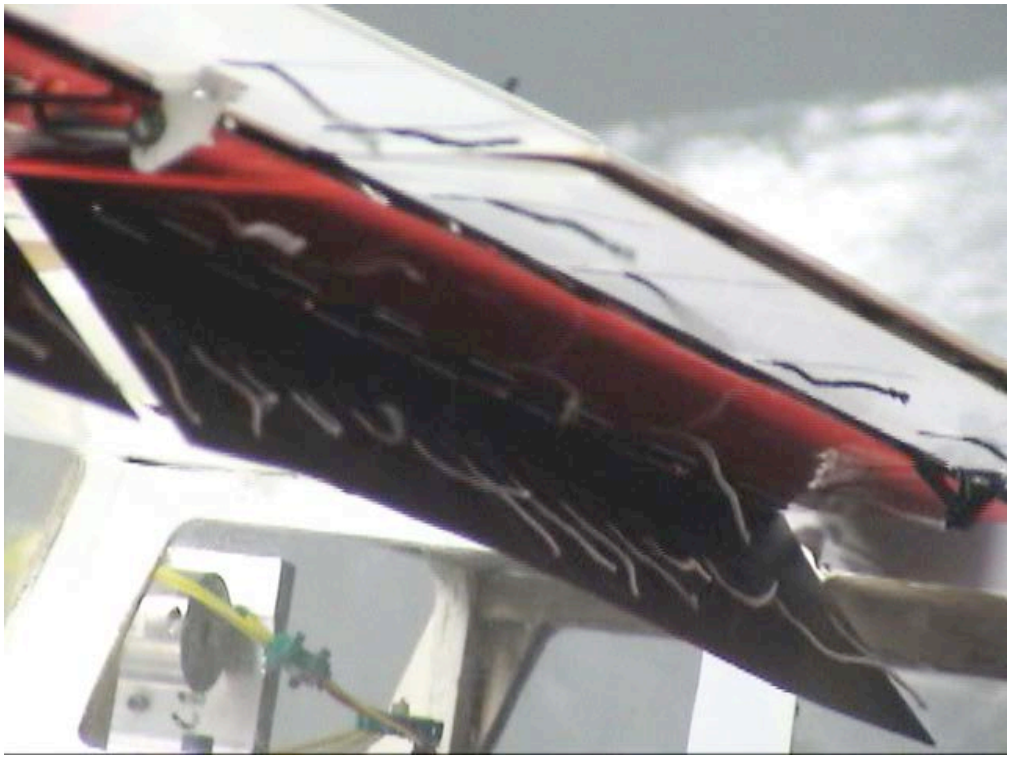

Figure C-142. Inboard view; LSS-In-45_LSS-Out-45_Split-0_Ail-0; α = 12°.

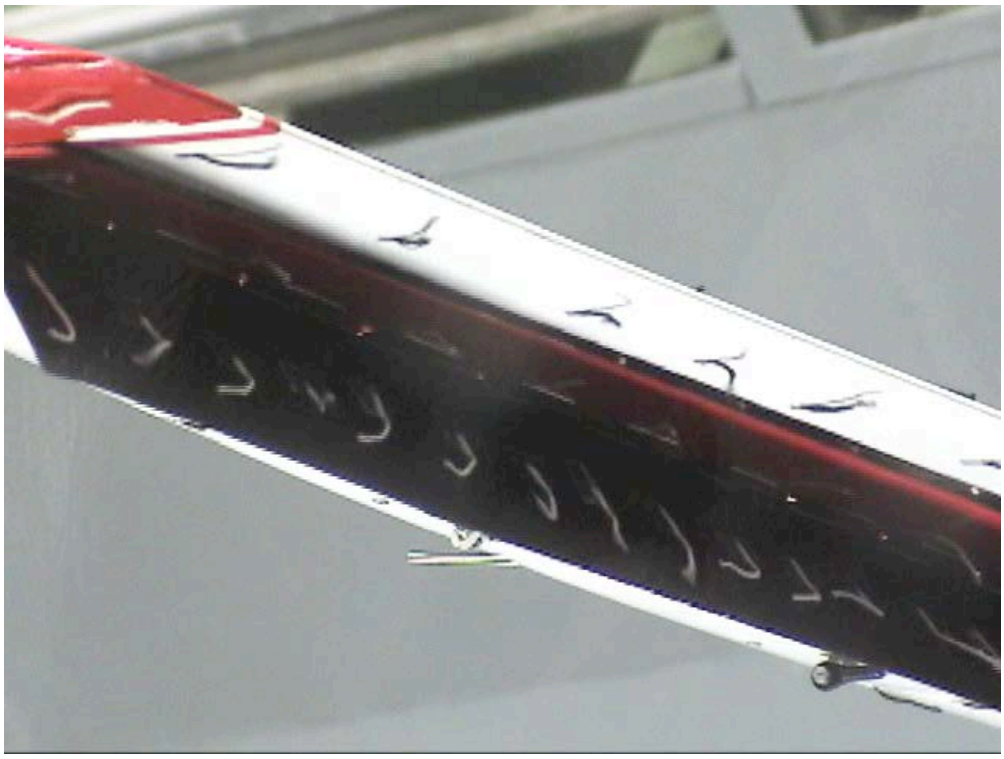

Figure C-143. Outboard tip view; LSS-In-45_LSS-Out-45_Split-0_Ail-0; α = 12°.

Figure C-144. Fuselage view; LSS-In-45_LSS-Out-45_Split-0_Ail-0; α = 12°.

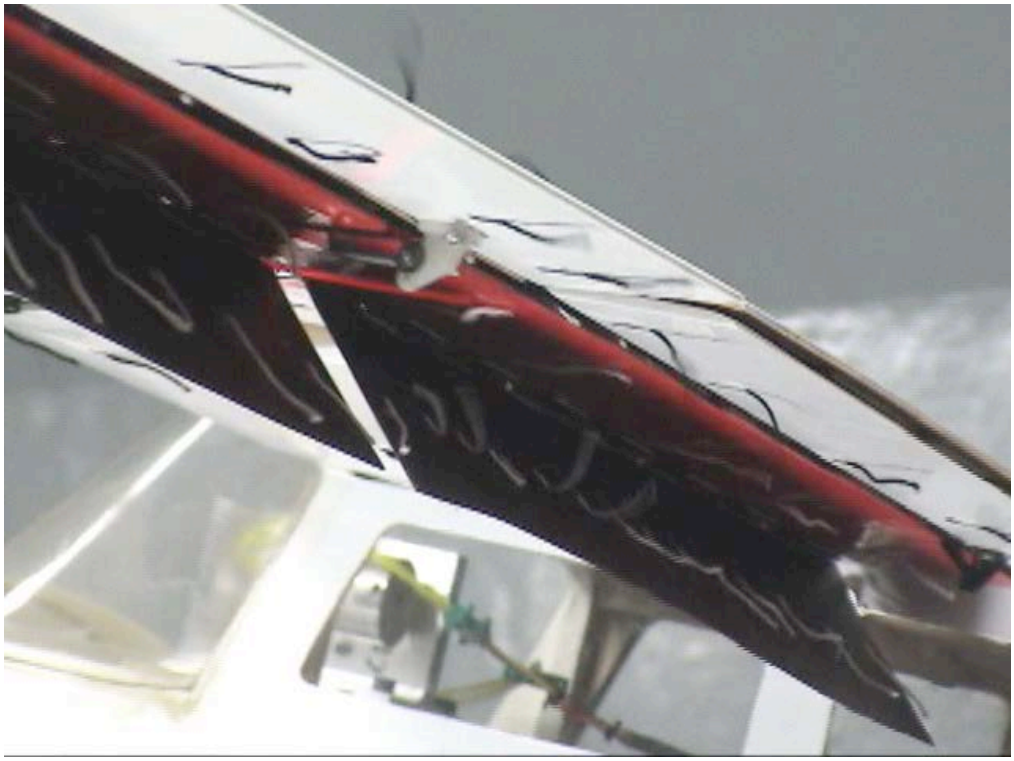

Figure C-145. Inboard view; LSS-In-45_LSS-Out-45_Split-0_Ail-0; α = 16°.

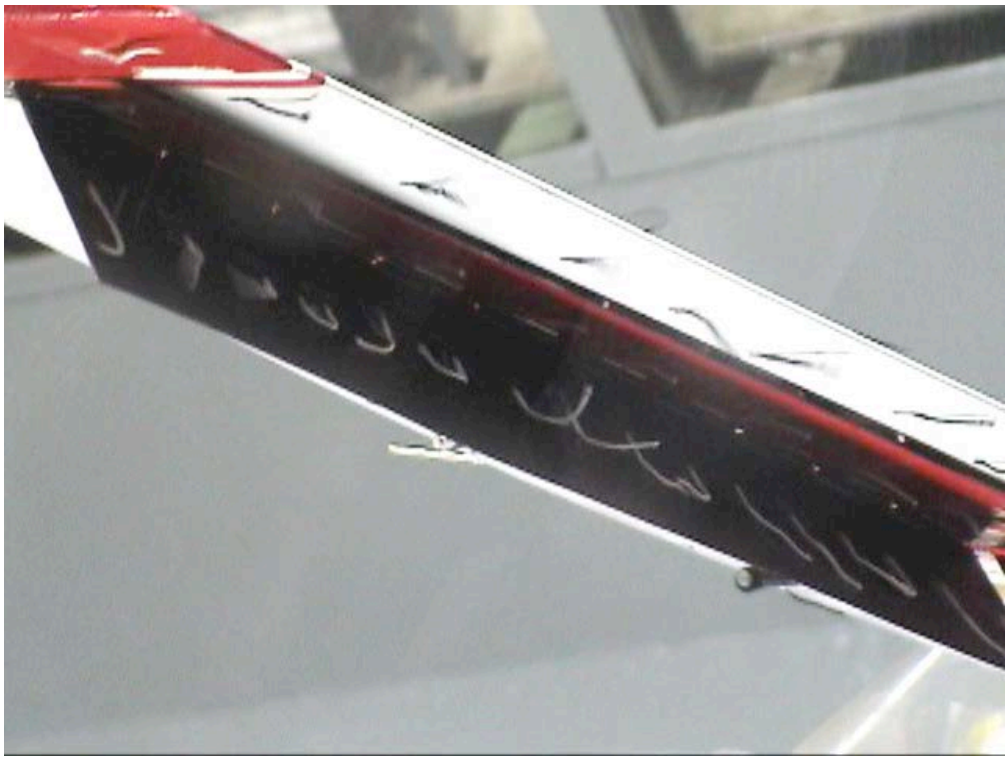

Figure C-146. Outboard tip view; LSS-In-45_LSS-Out-45_Split-0_Ail-0; α = 16°.

Figure C- 147. Fuselage view; LSS-In-45_LSS-Out-45_Split-0_Ail-0; α = 16°.

Figure C-148. Inboard view; LSS-In-0_LSS-Out-45_Split-0_Ail-0; α = 0°.

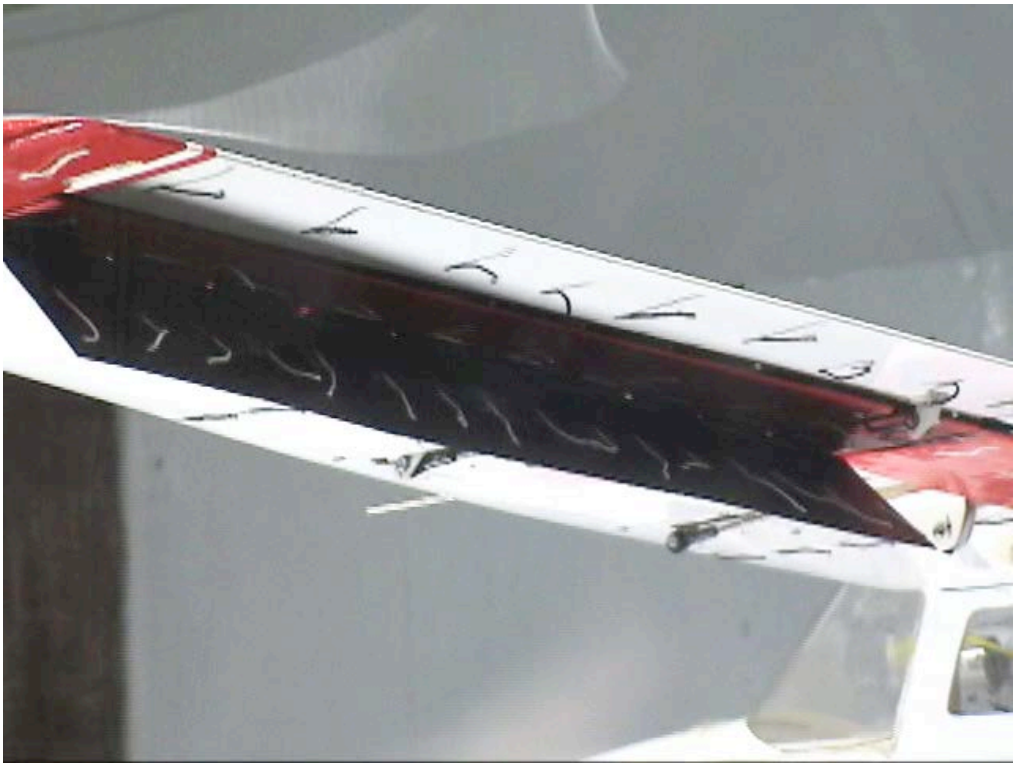

Figure C-149. Outboard tip view; LSS-In-0_LSS-Out-45_Split-0_Ail-0; α = 0°.

Figure C-150. Fuselage view; LSS-In-0_LSS-Out-45_Split-0_Ail-0; α = 0°.

Figure C-151. Inboard view; LSS-In-0_LSS-Out-45_Split-0_Ail-0; α = 4°.

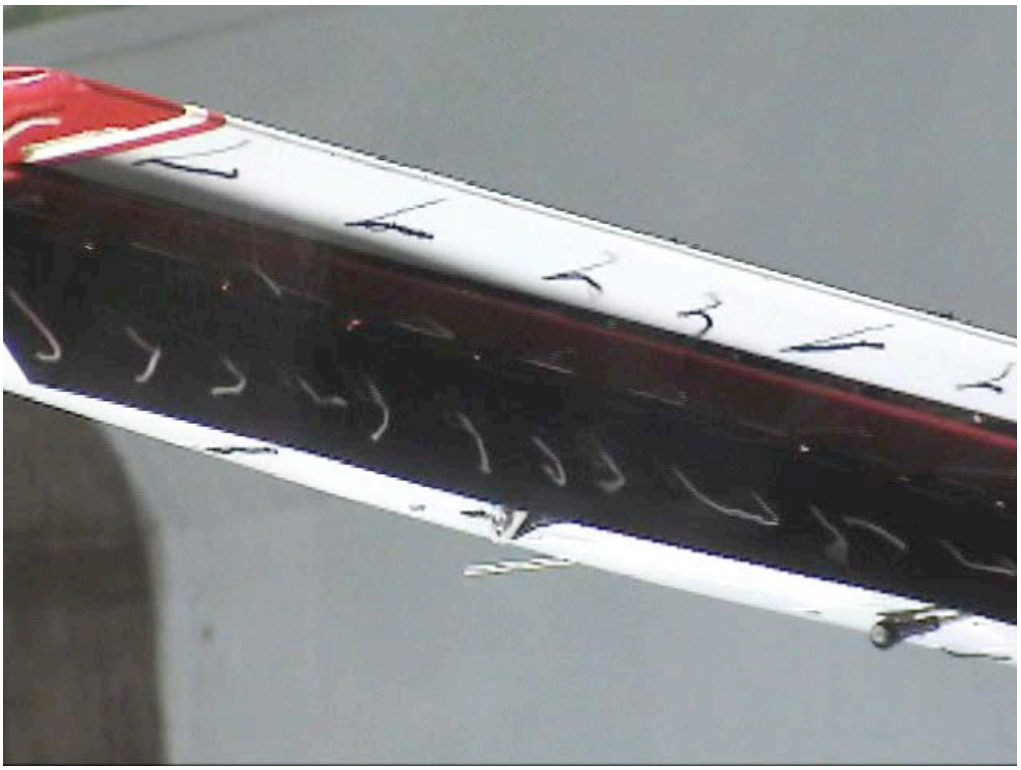

Figure C-152. Outboard tip view; LSS-In-0_LSS-Out-45_Split-0_Ail-0; α = 4°.

Figure C-153. Fuselage view; LSS-In-0_LSS-Out-45_Split-0_Ail-0; α = 4°.

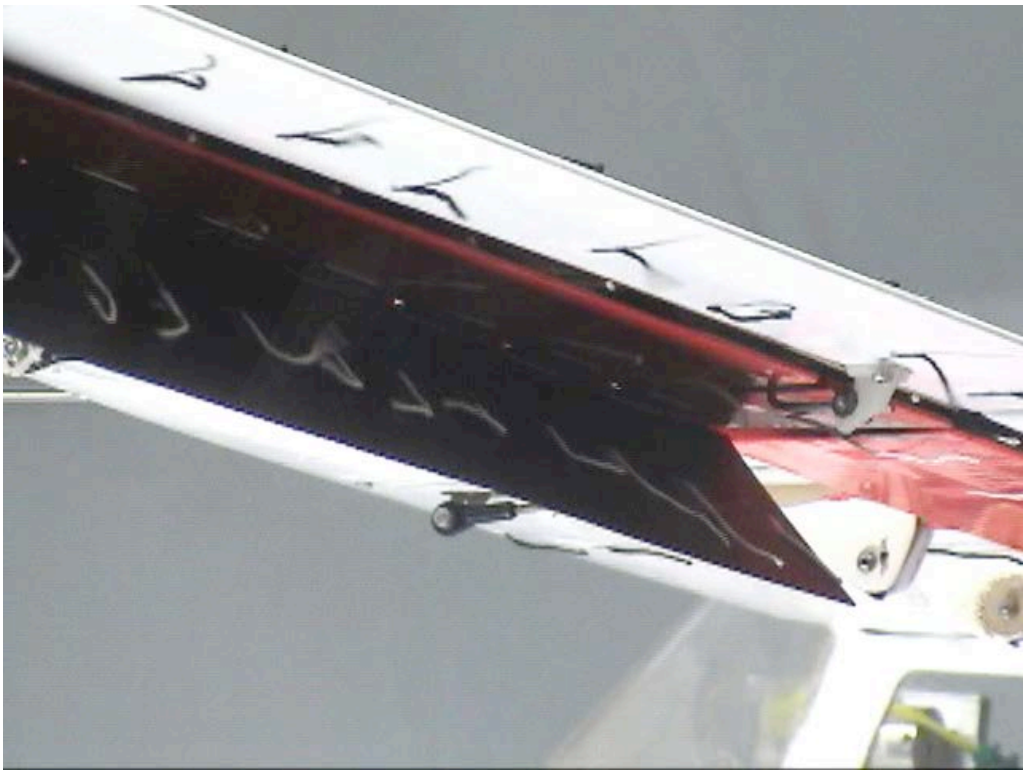

Figure C-154. Inboard view; LSS-In-0_LSS-Out-45_Split-0_Ail-0; α = 8°.

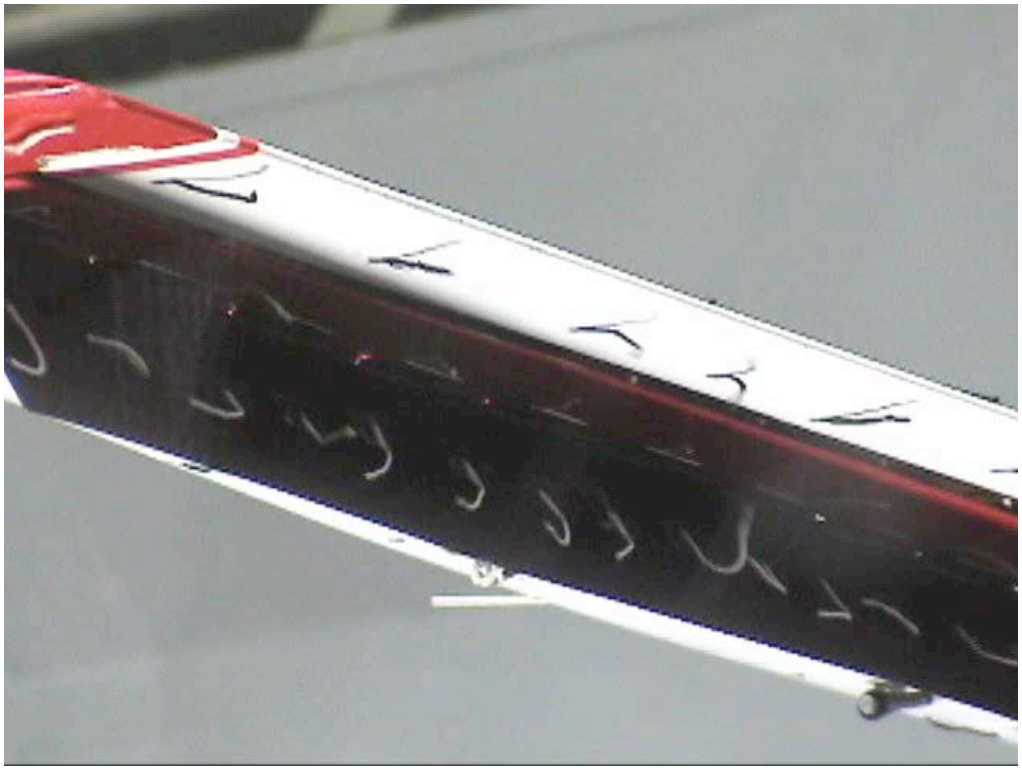

Figure C-155. Outboard tip view; LSS-In-0_LSS-Out-45_Split-0_Ail-0; α = 8°.

Figure C-156. Fuselage view; LSS-In-0_LSS-Out-45_Split-0_Ail-0; α = 8°.

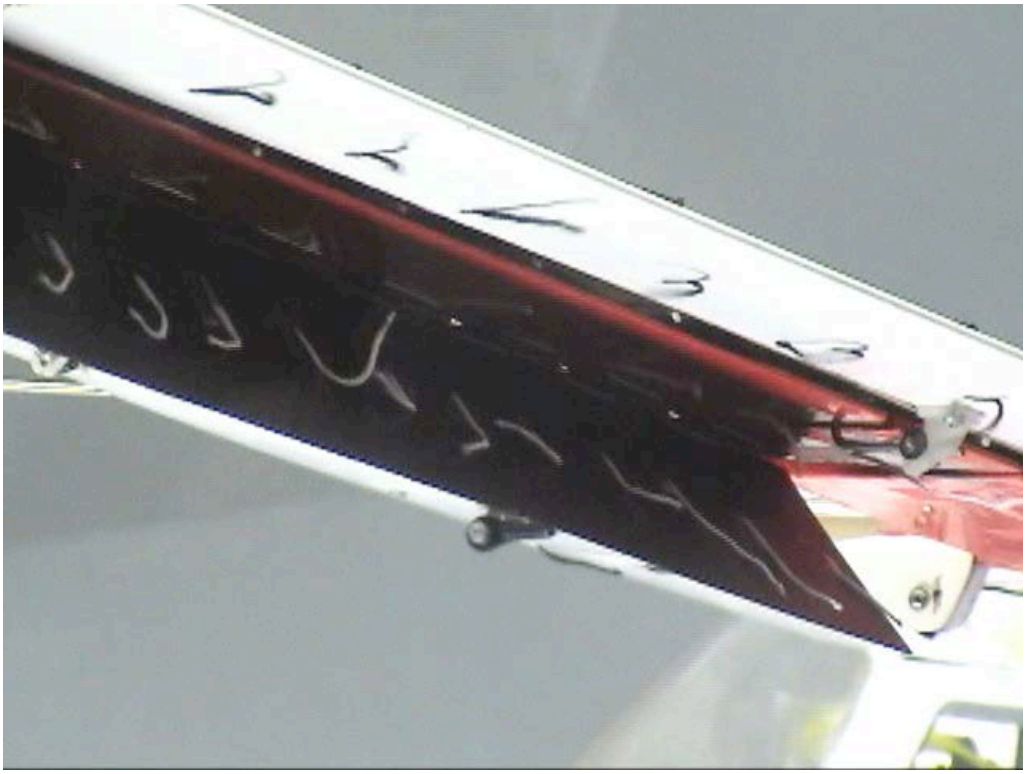

Figure C-157. Inboard view; LSS-In-0_LSS-Out-45_Split-0_Ail-0; α = 12°.

Figure C-158. Outboard tip view; LSS-In-0_LSS-Out-45_Split-0_Ail-0; α = 12°.

Figure C-159. Inboard view; LSS-In-0_LSS-Out-45_Split-0_Ail-0; α = 16°.

Figure C-160. Outboard tip view; LSS-In-0_LSS-Out-45_Split-0_Ail-0; α = 16°.

Figure C-161. Fuselage view; LSS-In-0_LSS-Out-45_Split-0_Ail-0; α = 16°.

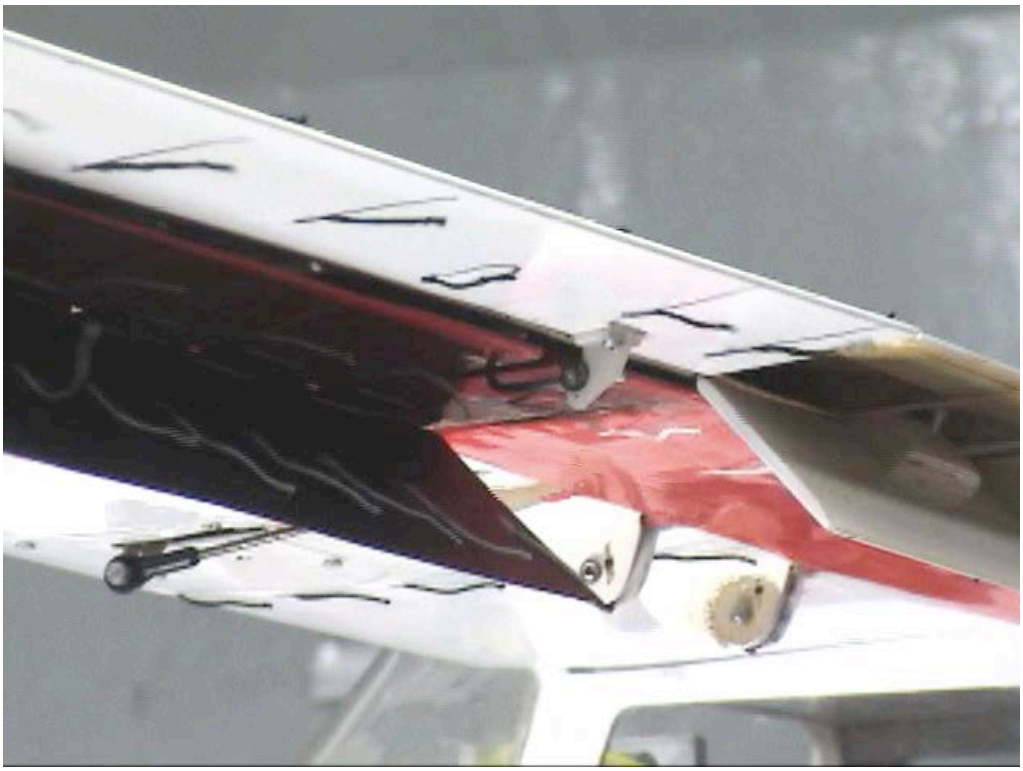

Figure C-162. Inboard view; LSS-In-0_LSS-Out-45_Split-60_Ail-0; α = 0°.

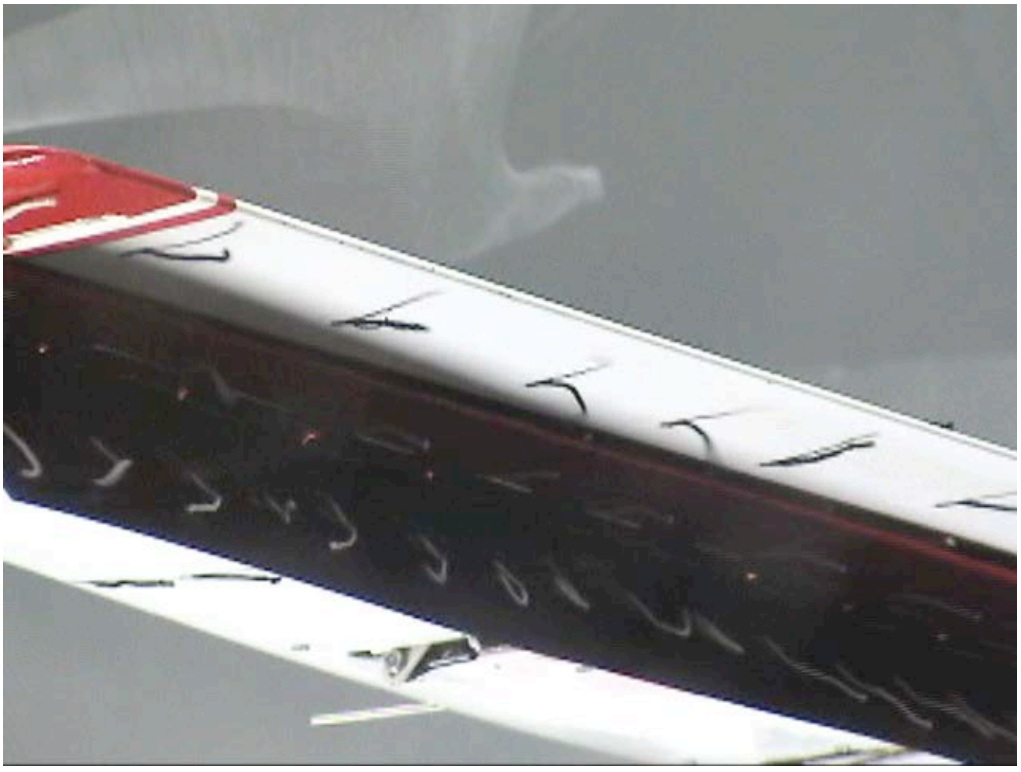

Figure C-163. Outboard tip view; LSS-In-0_LSS-Out-45_Split-60_Ail-0; α = 0°.

Figure C-164. Fuselage view; LSS-In-0_LSS-Out-45_Split-60_Ail-0; α = 0°.

Figure C-165. Inboard view; LSS-In-0_LSS-Out-45_Split-60_Ail-0; α = 4°.

Figure C-166. Fuselage view; LSS-In-0_LSS-Out-45_Split-60_Ail-0; α = 4°.

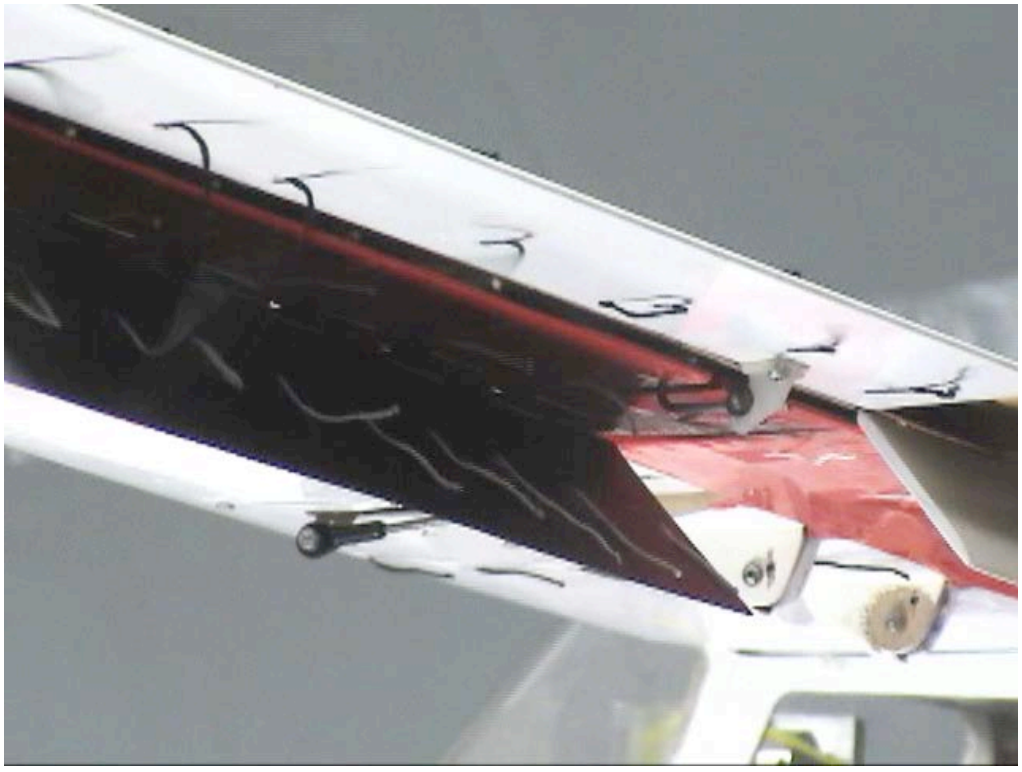

Figure C-167. Inboard view; LSS-In-0_LSS-Out-45_Split-60_Ail-0; α = 8°.

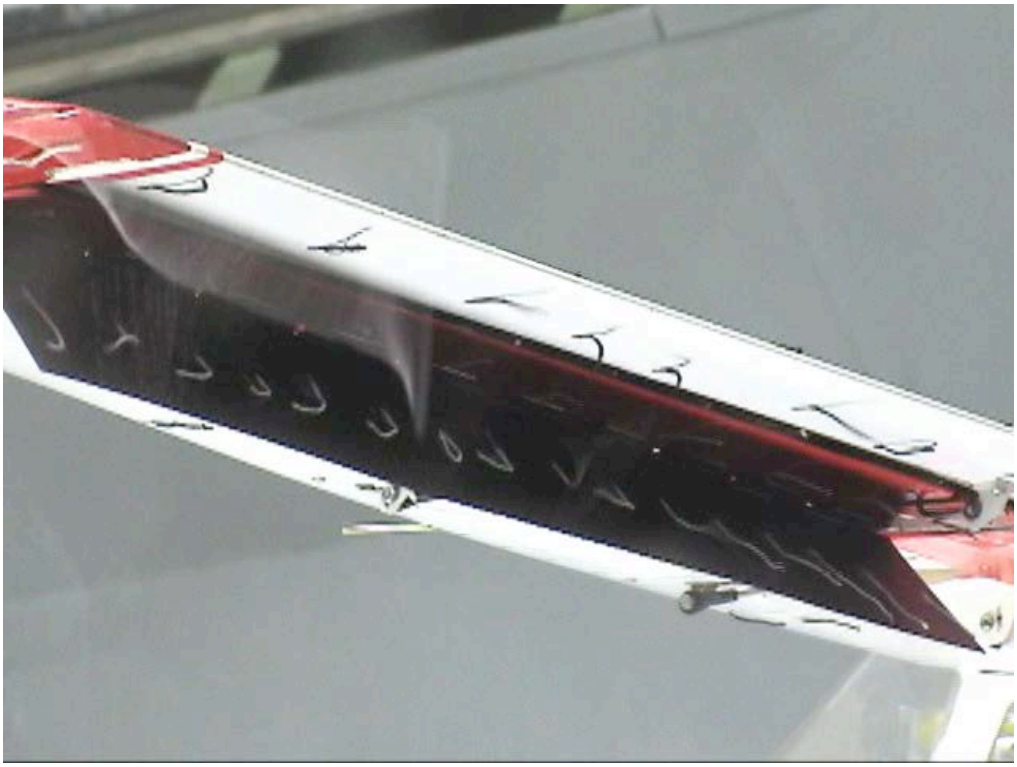

Figure C-168. Outboard tip view; LSS-In-0_LSS-Out-45_Split-60_Ail-0; α = 8°.

Figure C-169. Fuselage view; LSS-In-0_LSS-Out-45_Split-60_Ail-0; α = 8°.

Figure C-170. Inboard view; LSS-In-0_LSS-Out-45_Split-60_Ail-0; α = 12°.

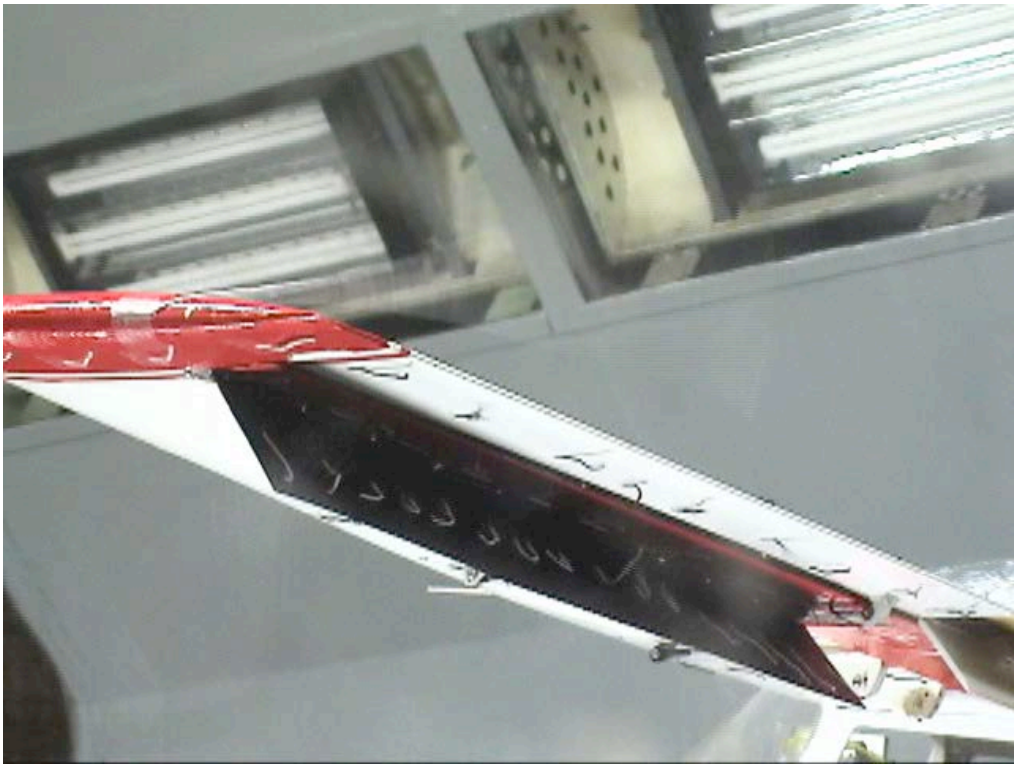

Figure C-171. Outboard tip view; LSS-In-0_LSS-Out-45_Split-60_Ail-0; α = 12°.

Figure C-172. Fuselage view; LSS-In-0_LSS-Out-45_Split-60_Ail-0; α = 12°.

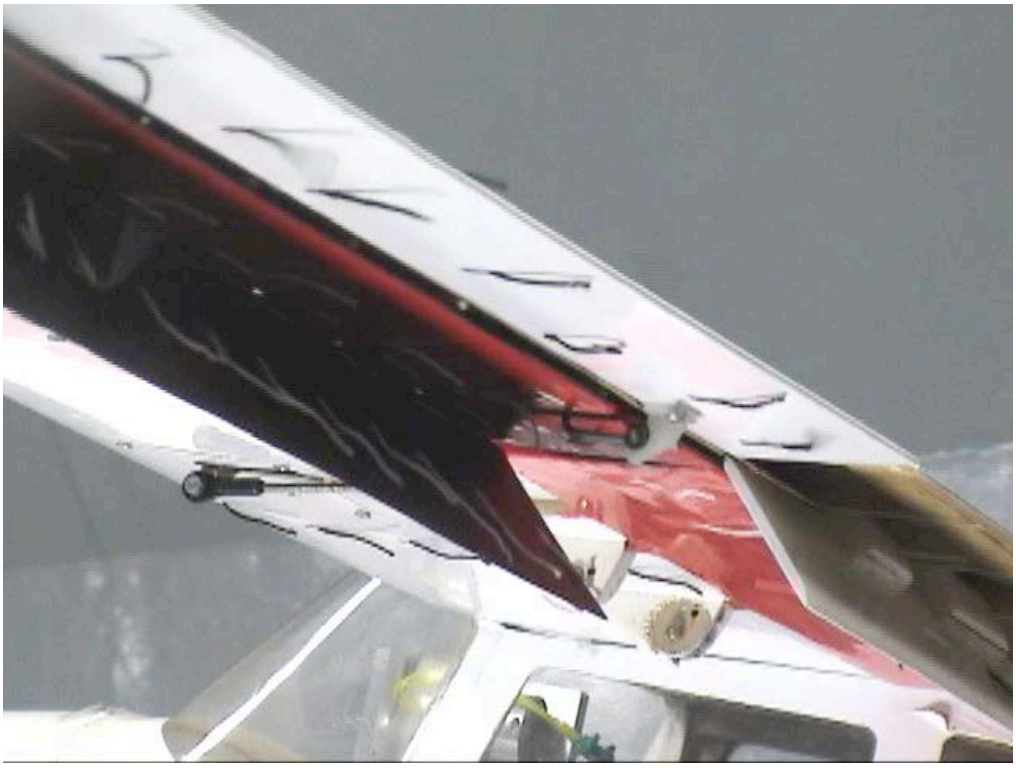

Figure C-173. Inboard view; LSS-In-0_LSS-Out-45_Split-60_Ail-0; α = 16°.

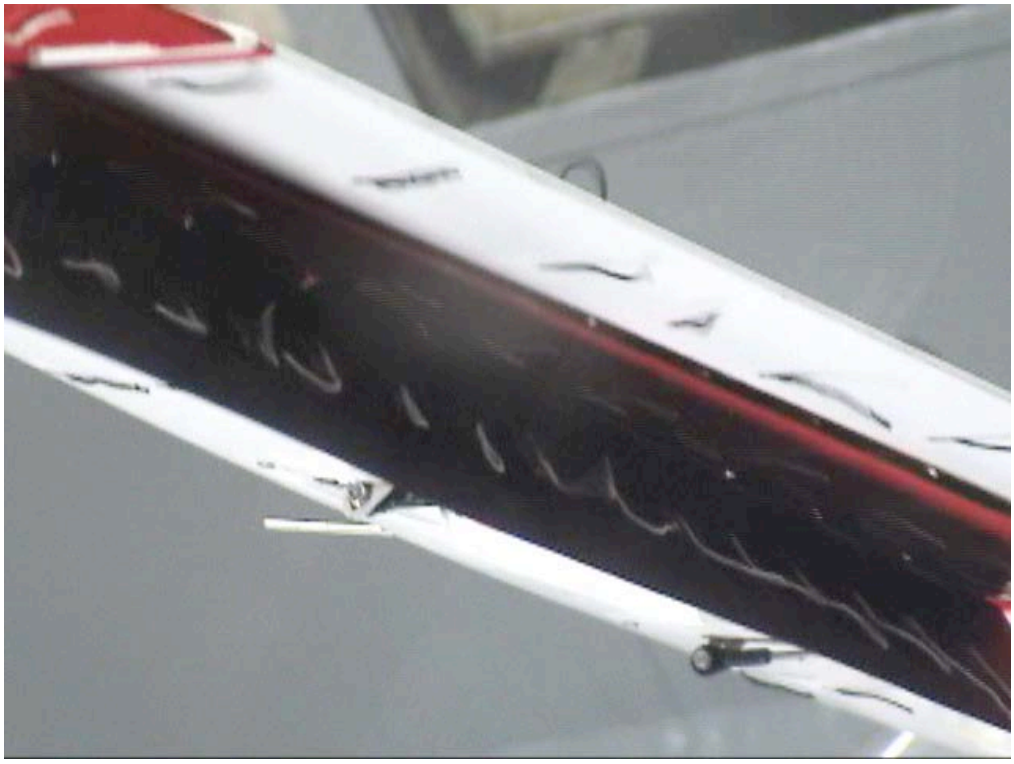

Figure C-174. Outboard tip view; LSS-In-0_LSS-Out-45_Split-60_Ail-0; α = 16°.

Figure C-175. Fuselage view; LSS-In-0_LSS-Out-45_Split-60_Ail-0; α = 16°.

REPORT DOCUMENTATION PAGE

Form Approved
OMB No. 0704-0188

1. REPORT DATE *(DD-MM-YYYY)*	2. REPORT TYPE	3. DATES COVERED *(From - To)*
01-07-2017	Technical Memorandum	

4. TITLE AND SUBTITLE

Assessment of a Conceptual Flap System Intended for Enhanced General Aviation Safety

5a. CONTRACT NUMBER

5b. GRANT NUMBER

5c. PROGRAM ELEMENT NUMBER

6. AUTHOR(S)

Campbell, Bryan A.; Carter, Melissa B.

5d. PROJECT NUMBER

5e. TASK NUMBER

5f. WORK UNIT NUMBER

561581.02.08.07.20.03

7. PERFORMING ORGANIZATION NAME(S) AND ADDRESS(ES)

NASA Langley Research Center
Hampton, VA 23681-2199

8. PERFORMING ORGANIZATION REPORT NUMBER

L-20030

9. SPONSORING/MONITORING AGENCY NAME(S) AND ADDRESS(ES)

National Aeronautics and Space Administration
Washington, DC 20546-0001

10. SPONSOR/MONITOR'S ACRONYM(S)

NASA

11. SPONSOR/MONITOR'S REPORT NUMBER(S)

NASA-TM-2017-219639

12. DISTRIBUTION/AVAILABILITY STATEMENT

Unclassified
Subject Category 03
Availability: NASA STI Program (757) 864-9658

13. SUPPLEMENTARY NOTES

14. ABSTRACT

A novel multi-element trailing-edge flap system for light general aviation airplanes was conceived for enhanced safety during normal and emergency landings. The system is designed to significantly reduce stall speed, and thus approach speed, with the goal of reducing maneuvering flight accidents and enhancing pilot survivability in the event of an accident. The research objectives were to assess the aerodynamic performance characteristics of the system and to evaluate the extent to which it provided both increased lift and increased drag required for the low-speed landing goal. The flap system was applied to a model of a light general aviation, high-wing trainer and tested in the Langley 12-Foot Low-Speed Wind Tunnel. Data were obtained for several device deflection angles, and component combinations at a dynamic pressure of 4 pounds per square foot. The force and moment data supports the achievement of the desired increase in lift with substantially increased drag, all at relatively shallow angles of attack. The levels of lift and drag can be varied through device deflection angles and inboard/outboard differential deflections. As such, it appears that this flap system may provide an enabling technology to allow steep, controllable glide slopes for safe rapid descent to landing with reduced stall speed.

15. SUBJECT TERMS

Conceptual Flap system; Flight accidents; General aviation safety; High-wing trainer; Higher-fidelity studies; Trailing-edge;

16. SECURITY CLASSIFICATION OF:			17. LIMITATION OF ABSTRACT	18. NUMBER OF PAGES	19a. NAME OF RESPONSIBLE PERSON
a. REPORT	b. ABSTRACT	c. THIS PAGE			STI Help Desk (email: help@sti.nasa.gov)
U	U	U	UU	244	19b. TELEPHONE NUMBER *(Include area code)* (757) 864-9658